THESE

pour obtenir le grade de

DOCTEUR DE L'UNIVERSITE JOSEPH FOURIER – GRENOBLE 1

Spécialité : PHYSIQUE

Présentée et soutenue publiquement par

Elias METRAL

Le 15 mars 1999

COUPLED LANDAU DAMPING OF TRANSVERSE COHERENT INSTABILITIES IN PARTICLE ACCELERATORS

Composition du jury :

Mme	**M. Rey-Campagnolle**	Présidente
MM.	**J. Le Duff**	
	J. M. Loiseaux	
	M. Martini	
	D. Möhl	
	F. Ruggiero	

ABSTRACT

The influence of linear coupling between the transverse planes of a circular accelerator on Landau damping of coherent instabilities is assessed using two typical frequency distributions (Lorentzian and “elliptical”). These spectra are limiting cases modeling distributions with and without important tails.

A general stability criterion is derived in both cases that includes the coupling strength (due to skew quadrupoles) and the tune distance from the difference resonances. It reveals the possibility of sharing the stabilising frequency spreads between the two planes. This can significantly improve the coherent beam stability, especially in cases where the situation is more critical in one plane. Another important observation is the fact that the influence of a large imaginary part in the beam-environment impedance, which normally requires a large frequency spread for Landau damping, can be compensated (at least in one plane) by a judicious choice of the coupling.

Experiments in the CERN-PS have been performed and the results confirm the general behaviour predicted by the theory. The mechanism of coupled Landau damping could therefore explain why a machine like the CERN-PS can be stabilised by tuning close to a coupling resonance and can be used to determine optimum values for the tune split and the linear coupling strength.

CONTENTS

FOREWORD

Particle accelerators are devices that handle the motion of charged particles by means of electromagnetic fields. Owing to the form of the Lorentz force, energy exchanges are governed by electric fields whereas magnetic fields are generally used to guide the particles along stable trajectories.

High-energy physics research has always been the driving force behind the development of particle accelerators. However, although very large new accelerators are being designed and built for high-energy physics, they represent only a small part of accelerator activity. Indeed, several thousand particle accelerators operating in many countries around the world, are now widely used in a variety of applications for applied physics, medicine, industrial processing, and possible utilisation in power engineering has been envisaged.[1-3]

At CERN and in many other high-energy physics laboratories, particle beams are used to probe the heart of matter and take us back to the beginning of time, the Big Bang. By accelerating particles to very high velocities and smashing them into targets, or into each other (in colliders), physicists can unravel the forces acting between them and produce new particles. This happens as matter turns into energy and back again following Einstein's equation, $E = mc^2$. The current description of matter and force particles is called the Standard Model, and although it has withstood experimental testing for over twenty years, it is known that it is incomplete and that it can only be a stepping stone to a better theory. It leaves too many questions unanswered. Why do particles have mass? Are the forces of nature just different aspects of the same thing? Is there really no antimatter left in the Universe? CERN is building a new accelerator, the Large Hadron Collider (LHC) which will probe deeper into matter than ever before to tackle these important questions. Due to switch on in 2005, it will ultimately collide beams of protons at an energy of 14 TeV. Beams of lead nuclei will also be accelerated, smashing together with a collision energy of 1150 TeV.[4]

The importance of accelerators in high-energy physics depends on the possibility of colliding two counter-rotating beams of relativistic particles, thus attaining high values of the centre-of-mass energy: however, the resulting luminosity, i.e. the number of events produced by the collisions, per second, for events with a cross section of one square centimeter, is low compared to that of fixed-target accelerators, since the density of particles in a fixed target is higher than the beam density.[5,6] Since a typical cross section for a high energy reaction is one nanobarn (1 nb = 10^{-33} cm^2), a luminosity $L = 10^{33}$ cm^{-2}s^{-1} only produces one such event per second. The figure that one quotes as luminosity is in general the peak luminosity of the machine (in cm^{-2}s^{-1}) which mostly interests machine designers. Luminosity integrated over a week, or one or several runs is what physicists are interested in; it is often measured in inverse picobarn (1 pb^{-1} = 10^{36} cm^{-2}). The nominal design value of LHC luminosity is $L = 10^{34}$ cm^{-2}s^{-1}, while the "ultimate" or so-called "beam-beam" limit (due to the interaction between the two counter-rotating beams) corresponds to $L = 2.5\ 10^{34}$ cm^{-2}s^{-1}.[7]

In order to obtain the maximum luminosity, one has to store the largest possible number of particles and to minimise the cross-section area of the beams. However, owing to collective effects, a system of many charged particles in interaction with its surroundings (e.g. the vacuum chamber walls) and with the other counter-rotating particle beam may become unstable when the number or the density of particles exceeds a threshold value. The importance of the subject of collective instabilities, which has been studied since the late 1950s, lies in the fact that it is one of the main

factors that determine the ultimate performance of the accelerator. The progress made in this field over the years is illustrated by the understanding and the cure of numerous collective instability mechanisms. Each accelerator, when pushed for performance, will encounter some intensity limit. After this limit is understood, and cured, a new limit emerges. The process repeats, and the result is the improved understanding and higher performance of the accelerator.[8]

The LHC will be built in the same tunnel as CERN's Large Electron Positron collider (LEP) and the proton (or lead ion) beams will be accelerated through the existing accelerator chain before being injected and accelerated in the LHC (Figure 1).

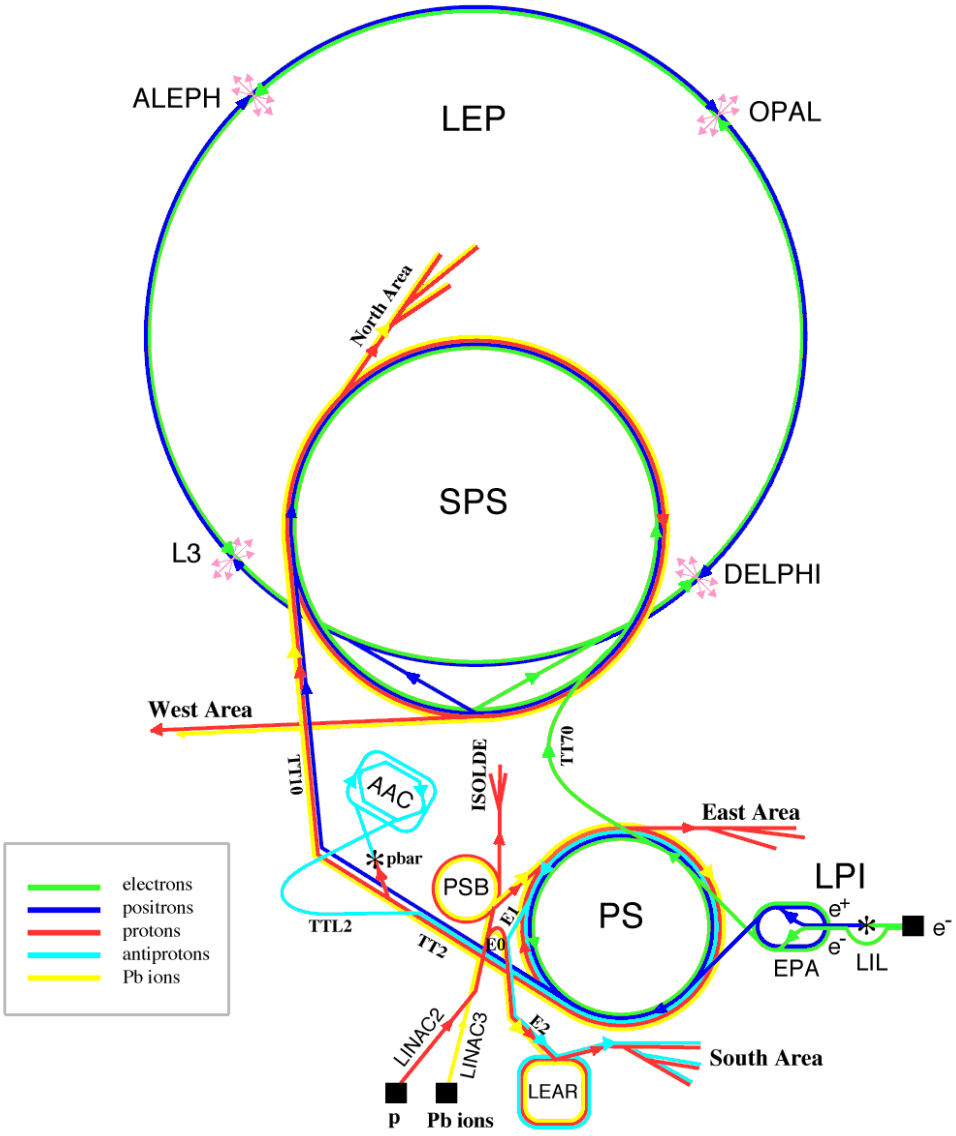

FIGURE 1 CERN accelerators in 1996.

The use of the Proton Synchrotron (PS), as part of the injection chain for the LHC, imposes strong constraints to achieve and preserve beams of high brightness, i.e. normalised transverse phase space density or intensity to emittance ratio (more than a factor 2, compared to the present performance, has to be gained).[7,9-12] Once the beam with the right brightness has been obtained the subsequent problem is how this brightness can be conserved. Space charge effects, imperfections of the beam optics,

injection and extraction errors can be very harmful particularly if the emittance is small. Moreover, instabilities of many kinds can also blow-up and even destroy the beam. In the PS, for example, the total emittance blow-up must be less than 20%. Such a tight emittance budget imposes a rigorous handling of all possible sources of blow-up along the injector chain.

The present work is directly related to the beam brightness conservation, and in particular to the damping of transverse collective instabilities. Starting from the observation that the PS (like many other high intensity accelerators and colliders) works best close to a "coupling resonance" (see Chapter 1), a theory of "coupled Landau damping" has been developed and applied to the PS. This theory extends the one-dimensional results of Landau damping of transverse coherent instabilities to include linear coupling between the transverse planes.

1 INTRODUCTION

In the design of an accelerator, one usually starts by considering the motion of a single particle. To describe the dynamics of a particle beam, one then regards the beam as a collection of noninteracting single particles moving in the environment (electric and magnetic fields of the various accelerator components) prescribed by the accelerator design. Intricate effects of linear and nonlinear dynamics can then be examined in detail.

At high intensity, forces acting between the particles have to be included. Then, in addition to the "single-particle phenomena", "collective effects" become important. An important class of collective effects is associated with coherent beam oscillations where, in the simplest case, all particles and hence the beam as a whole perform the same type of oscillation. This "coherent motion" of the particles adds to their "incoherent oscillation" which has random phases and thus does not lead to oscillation of the beam.

If a charged particle beam is locally displaced or "kicked" from the equilibrium path, it will start to make transverse coherent oscillations around this orbit. Due to these oscillations, the particles induce alternating image charges and currents in the vacuum chamber walls or any other structure surrounding the beam. These in turn create electromagnetic fields which act back on the oscillating beam, perturbing its motion. For relativistic beams these fields trail behind the emitting particles, which explains the name "wake fields". The concept of the wake field is a time domain description. The phenomenon can also be described in the frequency domain. In this case, "coupling impedances" are used, which are related to the wake functions through Fourier transformations. The descriptions of the wake forces in terms of wake functions in the time domain and in terms of coupling impedances in the frequency domain are two complementary descriptions of the same reality, and it is a matter of taste which approach to take.

Under unfavourable conditions (i.e. if there is an out of phase component of the forces, such as caused by the finite resistivity of the walls), the original oscillations may be reinforced. Their amplitude will then grow exponentially, i.e. the beam is unstable. The beam-surroundings interaction leads to an instability and a subsequent beam loss.

A beam can oscillate in many transverse "modes". Usually the most critical one for an instability and also the easiest to be detected, e.g. by a simple pair of electrostatic beam position "pick-up" electrodes, is the "dipolar mode", which corresponds to the case of a beam moving as a whole ("coherent", i.e. beam centre, motion). In other modes (quadrupolar mode, etc.), the beam centre remains stationary, but the particles around it move collectively. Only dipolar modes will be discussed in this manuscript.

Fortunately, stabilising mechanisms exist. Whenever the unwanted motion of the beam can be detected at an early stage of its growth by suitable detectors, active feedback damping can be applied. Furthermore, the coherent beam motion can be stabilised by the oscillation frequency spread of its particles: this stabilising mechanism is called "Landau damping". As concerns bunched beams, the main source of frequency spread comes from the non-linear nature of the restoring force (octupolar or higher order magnetic field) through the particle distribution in incoherent betatron amplitude. Maximisation of the "dynamic aperture" (largest oscillation amplitude which is still stable in the presence of non-linearities) and Landau damping of the collective instabilities are thus partly conflicting requirements.[13] On the one hand, the non-linearities of the "lattice" (arrangement of magnets in a beam transport channel or in a circular accelerator) must be minimised at large oscillation amplitudes to guarantee the

stability of the single-particle motion. On the other hand, a spread of the betatron frequencies is necessary to guarantee the stability of the collective motion of bunches of particles, which requires the introduction of non-linearities effective at small amplitudes. To a large extent the science of the accelerator physicist consists in playing with these two mechanisms to ensure the best possible performance of the machines.

In 1989, a coherent instability of the quadrupolar mode type driven by ions from the residual gas has been observed in the CERN-AA (Antiprotons Accumulator) and successfully cured by adjusting both "tunes" (numbers of horizontal and vertical betatron oscillations executed by particles travelling once around the machine circumference) close to 2.25.[14,15] In 1993, a single-bunch instability of the dipolar mode type driven by the resistive wall impedance has been observed in the CERN-PS (with the beam characteristics required for the LHC) and sometimes cured by adjusting both tunes close to 6.24.[16] These observations lead us to consider that coupling between the transverse planes together with tune separation might have a stabilising effect on collective instabilities. Furthermore, one family of 8 octupoles located at large vertical betatron function is used in the PS to suppress transverse coherent instabilities. The main stabilising effect is thus produced in the vertical plane, whereas instabilities always occur in the horizontal one. The idea is therefore to "transfer" Landau damping from the stable vertical to the unstable horizontal plane.

The energy exchange between the degrees of freedom of a multi-dimensional oscillator is a widespread phenomenon in physics. Strong coupling between the transverse planes of a particle beam leads to an "equi-partition" of the oscillation energy, including the "instability growth rates" in the case of coherent instability. The purpose of this paper is to show that, in the presence of a frequency spread, in addition to the exchange of energy, there can also be a partition of Landau damping for "optimum" coupling. This result could therefore be used to minimise the amount of external non-linearities required for Landau damping.

Chapter 2 is devoted to a review of the one-dimensional theory of transverse coherent instabilities and Landau damping for coasting beams. The influence of coupling on Landau damping is then assessed in Chapter 3 for both coasting (in Section 3.1) and bunched beams with particular wake fields (in Sections 3.2 and 3.3), using the single-particle equation formalism. This formalism allows us to discuss in a simple way rigid dipolar oscillations, or single-bunch head-tail modes for step-function (or resistive-wall) wakes. Introducing "equivalent" dispersion relation coefficients (which are the real betatron frequency shift and instability growth rate respectively, for a given mode, in the absence of both coupling and Landau damping), a generalised two-dimensional dispersion relation is derived, having the form of a product of two dispersion relations, one for the horizontal and the other for the vertical plane, equated to a coupling term (see Eqs. (3.12), (3.115) and (3.151)); when the latter vanishes, the known results on one-dimensional Landau damping are recovered. Entirely new stability criteria for the coherent motion of a beam in an accelerator with betatron coupling are obtained, using two typical (externally given) frequency distributions (Lorentzian, $\rho(f) \propto 1/(1+u^2)$ (see Eqs. (3.26) and (3.27)), and elliptical, $\rho(f) \propto \sqrt{1-u^2}$ where $u = (f - f_0)/\Delta f$ (see Eqs. (3.72) and (3.73))), knowing that Lorentzian and elliptical spectra are limiting cases and that realistic distributions are probably in between them. In the absence of tune spread, recent results on "chromaticity sharing" are also recovered (see Eqs. (3.159) and (3.161)). Considering octupolar non-linearities (and neglecting space-charge non-linearities), the two-dimensional dispersion relation is given by Eq. (3.164).

The main results of Chapter 3 are then rederived in Chapter 4 for bunched beams interacting with generic coupling impedances, using the Vlasov formalism, considering uncorrelated incoherent betatron amplitudes distributions and neglecting space-charge non-linearities. A perturbation treatment of the Vlasov equation, including both wake fields and linear coupling between the transverse planes is described. A general dispersion relation is derived, describing an eigenvalue problem (see Eq. (4.58)), which generalises Laclare's one-dimensional eigensystem.[17] A simplified two-dimensional dispersion relation (having the same form as in Chapter 3), where the coherent tune shifts are expressed in terms of effective impedances, is then derived, generalising the classical Sacherer's formula (see Eqs. (4.78) and (4.79)).[18]

Experiments performed in the CERN-PS are finally discussed in Chapters 5 and 6. The results of a calibration of the skew quadrupoles required to compensate and to control betatron coupling are reported in Chapter 5, while Chapter 6 summarises several machine experiments at fixed tune split and at fixed octupole strength. The results confirm the beneficial effect of coupling on Landau damping predicted by the theory, considering a Lorentzian distribution in the vertical plane.

2 REVIEW OF THE ONE-DIMENSIONAL THEORY OF TRANSVERSE COHERENT INSTABILITIES AND LANDAU DAMPING FOR COASTING BEAMS

Let us consider in this chapter the case of a coasting beam oscillating in the horizontal *x*-plane. When only the condition for stability is of interest, it can be assumed that the amplitudes of the oscillations are very small.[19] All pertinent equations can then be linearized. As a consequence, the superposition principle holds, and each frequency component can be investigated separately. In complex notation (using $j = \sqrt{-1}$ as the imaginary unit), a time (t) dependence of all perturbed quantities proportional to $e^{j\omega t}$, where the frequency ω may be a complex number, is assumed. If the imaginary part of ω is negative, an instability appears, and the instability growth rate is given by $-\mathrm{Im}(\omega)$.

In a circular machine, the oscillations must be periodic with the machine circumference. If the average position along the beam is described by the azimuthal angle $\vartheta = s / R$, where s is the azimuthal coordinate and R is the average radius of the machine, all the perturbations will be proportional to $e^{-jn_x\vartheta}$, where the "closing condition" requires that n_x be an integer, called the horizontal "azimuthal mode number".

Usually it is possible to ignore the major curvature of the machine, which is always very large compared to the transverse beam and vacuum chamber dimensions in synchrotrons or storage rings. A straight beam in a straight chamber, periodic with the machine circumference is then considered. If z is used as the longitudinal coordinate, the oscillations will finally be proportional to $e^{j(\omega t - k_x z)}$ where $k_x = n_x / R$ is the horizontal "wave number".

Once the transverse motions of the particles in the beam have been specified, the electromagnetic fields caused by them can be found (in principle) by solving Maxwell's equations with the proper boundary conditions. From the field components, the Lorentz force acting on a particle of unit charge $\vec{F} = e\left(\vec{E} + \vec{v} \times \vec{B}\right)$ is then calculated. For dipolar modes, the force is averaged over the beam cross-section. The transverse coupling impedance is directly proportional to this averaged force and will be defined later on in Section 2.1.

In the following, the influence of both the electromagnetic fields induced by the beam and Landau damping on the dipolar motion of an oscillating beam will be reviewed. The conceptually simple method that starts from the equation of motion of a test particle *i*, from which the beam motion is obtained by integration over suitable distributions, is adopted in this chapter. A more rigorous method which calculates directly the evolution of a distribution of particles with the Vlasov equation will be described later on in Chapter 4 for bunched beams.

2.1 Single-particle equation of motion

The effects of interest are integrated over complete turns in the machine. A theory built on the "smooth or weak approximation"[20,21] for the single-particle unperturbed betatron motion seems therefore reasonable. The horizontal oscillation of the *i*th particle in the external focusing field of an accelerator or storage ring is described by the betatron frequency $Q_{0x,i}\,\Omega_i$, where $Q_{0x,i}$ is the horizontal "incoherent" (single-particle) tune and Ω_i is the revolution frequency of the particle (see Appendix

A). The influence of the electromagnetic fields generated by the beam is described by the Lorentz force component in the direction of oscillation $F_{x,i}$ divided by the particle mass γm_0,

$$\ddot{x}_i + Q_{0x,i}^2 \Omega_i^2 x_i = \frac{F_{x,i}}{\gamma m_0}, \tag{2.1}$$

where x_i is the horizontal betatron coordinate and where a point denotes the derivative with respect to time. Depending on which contributions to $F_{x,i}$ are considered, the analysis develops towards self (or direct) fields (leading to an incoherent tune shift, dominant at low energy), local image fields (incoherent and coherent tune shifts) or wake fields (transverse coherent instabilities).[22] The function $F_{x,i}$ can be expanded to first order in terms of the test particle's motion x_i and the average beam position $\bar{x}$ to give

$$F_{x,i} = \left(\frac{\partial F_{x,i}}{\partial x_i} \right)_{\bar{x}=0} x_i + \left(\frac{\partial F_{x,i}}{\partial \bar{x}} \right)_{x_i=0} \bar{x}. \tag{2.2}$$

When $\bar{x}(t) = 0$, the beam and its associated fields are static and $\partial F_{x,i} / \partial x_i$ is a real constant. The first term in the right-hand side (r.h.s) of Eq. (2.2) can be assimilated into the left-hand side (l.h.s) of Eq. (2.1) as an additional focusing term and leads to an incoherent tune shift. The new (incoherent) tune of the test particle is $Q_{x,i} = Q_{0x,i} + \Delta Q_{inc,x}$, so that for small tune shifts,

$$Q_{x,i}^2 \approx Q_{0x,i}^2 + 2 Q_{0x,i} \Delta Q_{inc,x}, \tag{2.3}$$

where

$$\Delta Q_{inc,x} = -\frac{1}{2 Q_{0x,i} \Omega_i^2 \gamma m_0} \left(\frac{\partial F_{x,i}}{\partial x_i} \right)_{\bar{x}=0}. \tag{2.4}$$

In this linear approximation, $\bar{x}$ needs not in fact be zero, but only constant in time, i.e. a static closed orbit distortion does not affect $\Delta Q_{inc,x}$. When $\dot{\bar{x}} \neq 0$, the beam and its associated fields are time varying and $\partial F_{x,i} / \partial \bar{x}$ (for $x_i = 0$) is in general complex, i.e. in addition to the real local image a phase factor appears to account for local resistive wall effects and the wake fields left by other particles at other azimuthal positions in the accelerator. If only the real part is considered, this leads to local image fields. The inclusion of the imaginary part leads to complex coupling impedances (coherent instabilities). The coherent motion can be solved by choosing $x_i = \bar{x}$ in Eqs. (2.1) and (2.2). This leads to a coherent tune shift, which is related to the average motion of the whole beam and can be written in the same way as the incoherent tune shift,

$$\Delta Q_{coh,x} = -\frac{1}{2 Q_{0x,i} \Omega_i^2 \gamma m_0} \left[\left(\frac{\partial F_{x,i}}{\partial x_i} \right)_{\bar{x}=0} + \left(\frac{\partial F_{x,i}}{\partial \bar{x}} \right)_{x_i=0} \right]. \tag{2.5}$$

Taking into account the external focusing forces, the coherent and incoherent space-charge forces, the equation of motion (2.1) of a test particle *i* can thus be written as

$$\ddot{x}_i + \Omega_i^2 \left(Q_{0x,i}^2 + 2 Q_{0x,i}\, \Delta Q_{inc,x} \right) x_i = -2 \Omega_i^2\, Q_{0x,i} \left(\Delta Q_{coh,x} - \Delta Q_{inc,x} \right) \bar{x}. \qquad (2.6)$$

Here, all the terms given by the motion of the beam centre $\bar{x}$ have been combined on the r.h.s of the equation, treating them as "driving terms". Furthermore, the coherent and incoherent (Laslett) tune shifts, $\Delta Q_{coh,x}$ and $\Delta Q_{inc,x}$, are generalised to include wake fields (due to resistivity, cross-sectional variations, etc.) for the oscillation mode number under consideration. The relation between the generalised Laslett tune shifts and the horizontal coupling impedance is given by[23]

$$Z_x(\omega) = \frac{j}{e \beta I \Delta_x} \int_0^{2\pi R} \overline{F}_{x,i}\, ds = -j \frac{2 \pi R \gamma m_0}{e \beta I} 2 \Omega_i^2\, Q_{0x,i} \left(\Delta Q_{coh,x} - \Delta Q_{inc,x} \right)_{(\omega)}, \quad (2.7)$$

where e is the elementary charge, β is the relativistic velocity factor, I is the circulating beam current, $\Delta_x e^{j\omega t}$ describes the horizontal beam oscillations and $\overline{F}_{x,i}\, e^{j\omega t}$ is the average, over the beam cross section, of the horizontal force exerted on the *i*th particle.

2.2 Dispersion relation considering an externally given beam frequency spectrum

In an accelerator, the spread in betatron frequency $\omega_{x,i} = Q_{x,i}\, \Omega_i$ of the beam comes from several sources. A dependence of the betatron frequency on the energy of the particle, together with an energy spread in the beam, leads to a spread in $\omega_{x,i}$. Non-linearities in the focusing system (octupoles) and space-charge non-linearities cause a dependence of $\omega_{x,i}$ on the particle's transverse betatron amplitudes. A spread in betatron amplitudes then leads also to a spread in $\omega_{x,i}$. The revolution frequency Ω_i, the tune $Q_{0x,i}$ and the incoherent tune shift $\Delta Q_{inc,x}$ can be written as follows[24]

$$\Omega_i(p_i) = \Omega_0 \left(1 - \eta \frac{\Delta p_i}{p_0} \right), \qquad (2.8)$$

$$Q_{0x,i}(\hat{x}_i, \hat{y}_i, p_i) = Q_{0x0} \left(1 + \xi_x \frac{\Delta p_i}{p_0} \right) + \frac{\partial Q_{0x,i}}{\partial \hat{x}_i^2} \hat{x}_i^2 + \frac{\partial Q_{0x,i}}{\partial \hat{y}_i^2} \hat{y}_i^2, \qquad (2.9)$$

$$\Delta Q_{inc,x}(\hat{x}_i, \hat{y}_i, p_i) = \Delta Q_{inc,x0} + \frac{\partial \Delta Q_{inc,x}}{\partial p_i} \Delta p_i + \frac{\partial \Delta Q_{inc,x}}{\partial \hat{x}_i^2} \hat{x}_i^2 + \frac{\partial \Delta Q_{inc,x}}{\partial \hat{y}_i^2} \hat{y}_i^2, \quad (2.10)$$

neglecting the dependence of Ω_i on the transverse betatron amplitudes and retaining terms up to the octupole moment. Here, p_i is the particle momentum, p_0 is the ideal momentum corresponding to a particle travelling on the design orbit, $\Delta p_i = p_i - p_0$, $\hat{x}_i$ and $\hat{y}_i$ are the horizontal and vertical amplitudes of the incoherent betatron oscillations

(solutions of the homogeneous equations of motion). Furthermore, η is the slippage (or off-momentum) factor and ξ_x is the horizontal chromaticity, which are defined by

$$\eta = \frac{1}{\gamma_{tr}^2} - \frac{1}{\gamma^2} = -\frac{d\,\Omega_i}{dp_i}\frac{p_i}{\Omega_i}, \qquad \xi_x = \frac{d\,Q_{0x,i}}{dp_i}\frac{p_i}{Q_{0x,i}}. \tag{2.11}$$

In the following, for simplicity until Section 2.5, the revolution frequency will be supposed to be the same for all the particles, i.e. $\Omega_i = \Omega_0$, and a spread in betatron frequency specified by an externally given beam frequency distribution will be assumed.

Suppose that at time $t = 0$ a perturbation is imposed on the beam so that each azimuthal slice is displaced transversally by an amount $\bar{x}(t=0,\vartheta)$. This pattern $\bar{x}(t=0,\vartheta)$ is necessarily closed around the circumference and therefore can be decomposed into a Fourier series[25]

$$\bar{x}(t=0,\vartheta) = \sum_{n_x=-\infty}^{n_x=+\infty} \overline{X}_{n_x} e^{-j n_x \vartheta}, \tag{2.12}$$

so that it is only necessary to consider the evolution of a single sinusoidal wave n_x. The betatron oscillation of the beam centre which was at azimuth $\vartheta_{c,0}$ at time $t = 0$ is then given by

$$\bar{x}(t,\vartheta_{c,0}) = \overline{X}\, e^{j(\omega_c t - n_x \vartheta_{c,0})}, \tag{2.13}$$

where $\omega_c = Q_c\,\Omega_0$ is the coherent betatron frequency, and $\overline{X}_{n_x}$ has been written $\overline{X}$ for simplicity. Since the azimuth ϑ after a time t is given by $\vartheta = \vartheta_{c,0} + \Omega_0 t$, the position of the whole beam in azimuth and time can be described as follows

$$\bar{x}(t,\vartheta) = \overline{X}\, e^{j[(n_x+Q_c)\Omega_0 t - n_x \vartheta]}. \tag{2.14}$$

This leads to the relation between the coherent tune Q_c and the local collective frequency ω (frequency observed at a fixed azimuth ϑ)

$$\omega = (n_x + Q_c)\,\Omega_0. \tag{2.15}$$

With this formula it is easy to see that the initial wave pattern rotates with an angular velocity $\omega_{n_x} = \omega / n_x = (1 + Q_c / n_x)\,\Omega_0$. Thus different wave patterns rotate at different velocities; for positive values of n_x the angular velocity of the wave is larger than the velocity of the particles, whereas for negative values of n_x the wave travels slower than the particles. For this reason, the waves associated with positive orbital harmonics are called “fast waves”, and those associated with negative orbital harmonics are called “slow waves”. A small subset of the slow waves travel backwards with

respect to the particles: these are associated with orbital harmonics of order $n_x < 0$ such that $|n_x| < Q_c$. Although a snapshot of the whole beam at a given time reveals exactly the same pattern for waves of opposite harmonic number n_x and $-n_x$, these waves are of fundamentally different nature. Wake fields laid on by a fast wave in the surrounding structure exert a force on the particles which has the right phase to produce a damping of the betatron wave. On the contrary, a slow wave generates wake fields which are capable of increasing the amplitude of the wave, leading to an instability. Backward waves cannot lead to instabilities.

The influence of the wake fields can be calculated either in the laboratory or in a moving-frame that goes around with the particle. In the present case, the second (hydrodynamic) view is adopted. Then, the derivative in Eq. (2.6) has to be taken along the orbit of the particles, i.e. $d/dt = \partial/\partial t + \dot{\vartheta}\partial/\partial\vartheta = j(\omega - n_x \Omega_0)$. The steady-state solution of the test particle has the same t and ϑ dependence as the driving term $\bar{x}$. We then look for a particular solution of the form

$$x_i = X_i e^{j(\omega t - n_x \vartheta)}. \tag{2.16}$$

Substituting Eq. (2.16) into Eq. (2.6), yields

$$X_i = -\frac{je\beta I Z_x}{2\pi R\gamma m_0}\left[\frac{\bar{X}}{\omega_{x,i}^2 - (\omega - n_x \Omega_0)^2}\right]. \tag{2.17}$$

In the absence of interaction, the continuous beam oscillates transversally on its azimuthal mode n_x; there are n_x wave lengths around the machine and the only coherent spectral line is at $\omega = (n_x + Q_{x0})\Omega_0$, where $Q_{x0} = \omega_{x0}/\Omega_0$ is the horizontal coherent tune in the absence of interaction.

In the presence of beam-surroundings interaction, which is treated as a perturbation, the mode frequency shift is always small compared to the unperturbed frequency. Furthermore, the frequency spread is also always much smaller than the unperturbed frequency. The following approximation can thus be made

$$\omega_{x,i}^2 - (\omega - n_x \Omega_0)^2 \approx 2\omega_{x0}\left[\omega_{x,i} - (\omega - n_x \Omega_0)\right]. \tag{2.18}$$

Substituting Eq. (2.18) into Eq. (2.17) yields

$$X_i = -\frac{je\beta I Z_x}{2\omega_{x0}\, 2\pi R\gamma m_0}\left[\frac{\bar{X}}{\omega_{x,i} - (\omega - n_x \Omega_0)}\right]. \tag{2.19}$$

If one multiplies X_i by the distribution function that influences the betatron frequency $\omega_{x,i}$ and integrates, the displacement of the beam centre $\bar{X}$ should be obtained. Suppose the ensemble of particles has a spectrum with the distribution function $\rho_x(\omega_{x,i})$, which is normalised to unity

$$\int_{-\infty}^{+\infty} \rho_x\left(\omega_{x,i}\right) d\omega_{x,i} = 1. \tag{2.20}$$

Then

$$\overline{X} = \int_{-\infty}^{+\infty} \rho_x\left(\omega_{x,i}\right) X_i \, d\omega_{x,i} \tag{2.21}$$

leads to the self-consistency relation

$$1 = \frac{j e \beta \, I Z_x}{2\omega_{x0} \, 2\pi R \gamma m_0} \int_{-\infty}^{+\infty} \frac{\rho_x\left(\omega_{x,i}\right) d\omega_{x,i}}{\omega - \left(n_x + Q_{x,i}\right)\Omega_0}. \tag{2.22}$$

This expression constitutes a "dispersion relation", since it specifies the dependence of the oscillation frequency ω on the wave number $k_x = n_x / R$. Substituting Eq. (2.15) into Eq. (2.22) yields

$$\left(\int_{-\infty}^{+\infty} \frac{\rho_x\left(\omega_{x,i}\right) d\omega_{x,i}}{\omega_c - \omega_{x,i}} \right)^{-1} = \frac{j e \beta \, I Z_x}{2\omega_{x0} \, 2\pi R \gamma m_0}, \tag{2.23}$$

remembering that Z_x has to be evaluated at the mode frequency $\omega = \left(n_x + Q_c\right)\Omega_0$. This equation can be simplified for beam stability discussions and written as

$$\left(\int_{-\infty}^{+\infty} \frac{\rho_x\left(\omega_{x,i}\right) d\omega_{x,i}}{\omega_c - \omega_{x,i}} \right)^{-1} = U_x - jV_x, \tag{2.24}$$

where U_x [a] and V_x are the "dispersion relation coefficients" of Laslett, Neil and Sessler,[26] which are related to the coupling impedance by (see Eqs. (2.23) and (2.24))[19,23,27]

$$\left(U_x - jV_x\right)_{(\omega)} = \frac{j e \beta I Z_x(\omega)}{2\omega_{x0} \, 2\pi R \gamma m_0}. \tag{2.25}$$

Therefore, in the absence of a frequency spread, U_x is the real frequency shift and V_x is the instability growth rate.

If the driving frequency ω_c belongs to the betatron frequency spread, then Eq. (2.24) contains a singularity at $\omega_{x,i} = \omega_c$. This leads us to the important concept of Landau damping, which will be reviewed in the next section.

2.3 Physical origin of Landau damping

Landau damping is a general process that arises when one considers a whole collection of particles or other systems which have a spectrum of resonant frequencies, and interact in some way.[8,28-33] In accelerators we are usually concerned with an interaction of a kind that may make the beam unstable (wake fields), and we want to find out whether or not (and how) the spread of resonant frequencies will stabilise it.

[a] Sometimes $U + V$ is written in place of U as used here.

If the particles have a spread in their natural frequencies, the motion of the particles can lose its coherency. In order to understand the physical origin of this effect, let us first consider a simple harmonic oscillator i which oscillates in the x-direction with a natural frequency $\omega_{x,i}$.[8] Let this oscillator be driven, starting at time $t = 0$, by a sinusoidal force of frequency ω_c. The equation of motion is

$$\ddot{x}_i + \omega_{x,i}^2 \, x_i = f \cos(\omega_c t), \tag{2.26}$$

with the initial conditions $x_i(0) = 0$ and $\dot{x}_i(0) = 0$. The solution of Eq. (2.26) is

$$x_i(t > 0) = -\frac{f}{\omega_c^2 - \omega_{x,i}^2}\left[\cos(\omega_c t) - \cos(\omega_{x,i} t)\right]. \tag{2.27}$$

In Eq. (2.27), the $\cos(\omega_c t)$ term gives the main term responding to the driving force; the $\cos(\omega_{x,i} t)$ term comes from matching the initial conditions. Thanks to the initial conditions term, Eq. (2.27) is well behaved at $\omega_{x,i} = \omega_c$. Following a treatment by Hereward,[29] Eq. (2.27) is the starting point for the Landau damping analysis.

Consider now an ensemble of oscillators (each oscillator represents a single particle in the beam) which do not interact with each other and have a spectrum of natural frequency $\omega_{x,i}$ with a distribution $\rho_x(\omega_{x,i})$ normalised to unity. As assumed in Section 2.2, the origin of the betatron frequency spread is not specified: an externally given beam frequency spectrum is supposed. Now starting at time $t = 0$, subject this ensemble of particles to the driving force $f \cos(\omega_c t)$ with all particles starting with initial conditions $x_i(0) = 0$ and $\dot{x}_i(0) = 0$. We are interested in the ensemble average of the response, which is given by superposition by

$$\bar{x}(t) = -\frac{f}{2\omega_{x0}} \int_{-\infty}^{+\infty} \frac{1}{\omega_c - \omega_{x,i}} \left[\cos(\omega_c t) - \cos(\omega_{x,i} t)\right] \rho_x(\omega_{x,i}) \, d\omega_{x,i}. \tag{2.28}$$

Here, for simplicity, a narrow beam spectrum around a frequency ω_{x0} has been assumed (as in Section 2.2 since it is the case of practical interest), as well as a driving frequency near the spectrum, i.e. $\omega_c \approx \omega_{x0}$. Changing variable from $\omega_{x,i}$ to $u = \omega_{x,i} - \omega_c$ leads to

$$\begin{aligned}
\bar{x}(t) &= \frac{f}{2\omega_{x0}} \int_{-\infty}^{+\infty} \left[\cos(\omega_c t) - \cos(\omega_c t + u t)\right] \frac{\rho_x(u + \omega_c)}{u} \, du \\
&= \frac{f}{2\omega_{x0}} \left[\cos(\omega_c t) \int_{-\infty}^{+\infty} \left[1 - \cos(u t)\right] \frac{\rho_x(u + \omega_c)}{u} \, du + \sin(\omega_c t) \int_{-\infty}^{+\infty} \sin(u t) \, \frac{\rho_x(u + \omega_c)}{u} \, du \right].
\end{aligned} \tag{2.29}$$

In Eq. (2.29), all integrals are well behaved at $u = 0$. Observing that

$$\lim_{t \to +\infty} \frac{\sin(u t)}{u} = \pi \delta(u),$$

(2.30)

$$\lim_{t\to+\infty}\frac{1-\cos(ut)}{u}=\text{P.V.}\left(\frac{1}{u}\right),$$

where P.V. stands for principal value and $\delta(\ )$ for the Dirac function, we see that the time-dependent coefficients of the $\cos(\omega_c t)$ and $\sin(\omega_c t)$ terms in Eq. (2.29) approach well-behaved limits when $t\to+\infty$. If we are not interested in the transient effects immediately following the onset of the driving force, we may substitute Eqs. (2.30) into Eq. (2.29) and obtain

$$\bar{x}(t)=\frac{f}{2\omega_{x0}}\left[\cos(\omega_c t)\,\text{P.V.}\int_{-\infty}^{+\infty}\frac{\rho_x(\omega_{x,i})}{\omega_{x,i}-\omega_c}\,d\omega_{x,i}+\pi\,\rho_x(\omega_c)\sin(\omega_c t)\right]. \quad (2.31)$$

The sign of the $\cos(\omega_c t)$ term relative to the driving force depends on the sign of $\text{P.V.}\int_{-\infty}^{+\infty}d\omega_{x,i}\,\rho_x(\omega_{x,i})/(\omega_{x,i}-\omega_c)$. Generally, this term is approximately given by $1/(\omega_{x,i}-\omega_c)$ outside the spectrum and crosses through zero somewhere inside the spectrum. A system is referred to as "capacitive" or "inductive" based on whether its sign is positive or negative.

The $\sin(\omega_c t)$ term has a definite sign relative to the driving force, because $\rho_x(\omega_c)$ is always positive. In particular, $\dot{\bar{x}}$ is always in phase with the force, indicating work is being done on the system. The system always reacts to the force "resistively".

The Landau damping effect is to be distinguish from a "decoherence (also called phase-mixing, or filamentation) effect" that occurs when the beam has nonzero initial conditions. Had we included an initial condition $x_i(0)=x_{i,0}$ and $\dot{x}_i(0)=\dot{x}_{i,0}$, we would have introduced two additional terms into the ensemble response, which do not participate in the dynamic interaction of the beam particles and are not interesting for our purposes here. In this decoherence effect, individual particles continue to execute oscillations of constant amplitude, but the total beam response $\bar{x}$ decreases with time.

As mentioned above, work is continuously being done on the system. However, the amplitude of $\bar{x}$, as given in Eq. (2.31), does not increase with time. Where did the energy go? To investigate this, let us identify the energy of a particle as the square of its oscillation amplitude. First let us rewrite Eq. (2.27) in the following form

$$x_i(t>0)=\frac{f}{2\omega_{x0}}\sin(\omega_{x0}t)\,\frac{\sin\left[(\omega_c-\omega_{x,i})t/2\right]}{(\omega_c-\omega_{x,i})/2}. \quad (2.32)$$

The amplitude of the particle is given by the slowly varying envelope

$$\text{A}_{x,i}=\frac{f}{\omega_{x0}(\omega_c-\omega_{x,i})}\sin\left[\frac{(\omega_c-\omega_{x,i})t}{2}\right]. \quad (2.33)$$

This leads to a total oscillation energy of

$$\begin{aligned} \mathrm{E}_x &= N \int_{-\infty}^{+\infty} \rho_x\left(\omega_{x,i}\right) d\omega_{x,i} \left\{ \frac{f}{\omega_{x0}\left(\omega_c - \omega_{x,i}\right)} \sin\left[\frac{\left(\omega_c - \omega_{x,i}\right) t}{2} \right] \right\}^2 \\ &= \frac{N f^2}{\omega_{x0}^2} \int_{-\infty}^{+\infty} \rho_x\left(u + \omega_c\right) du \, \frac{\sin^2\left(u t/2\right)}{u^2}, \end{aligned} \tag{2.34}$$

where N is the total number of particles in the beam. Observing that

$$\lim_{t \to +\infty} \frac{\sin^2\left(u t/2\right)}{u^2} = \frac{\pi t}{2} \delta\left(u\right), \tag{2.35}$$

Eq. (2.34) then reads

$$\mathrm{E}_x = \frac{\pi N f^2}{2\omega_{x0}^2} \rho_x\left(\omega_c\right) t. \tag{2.36}$$

The system therefore absorbs energy from the driving force indefinitely while holding the ensemble beam response within bounds.

An analogy occurs in the decoherence behavior, where the single particle energies and thus the total beam energy are constant in time, but the ensemble signal $\bar{x}$ decreases with time.

The stored energy (Eq. (2.36)) is incoherent in the sense that the energy is contained in the individual particles, but it is not to be regarded as heat in the system. This is because the stored energy is not distributed more or less uniformly in all particles, but is selectively stored in particles with continuously narrowing range of frequencies around the driving frequency. Observe two particles $\omega_{x,i} = \omega_c$ and $\omega_{x,i} \neq \omega_c$ (Figure 2). At the beginning, they oscillate "coherently" (same amplitude and same phase). However, after a while the particle with $\omega_{x,i} = \omega_c$, being resonantly driven, continues to increase in amplitude as t increases, whereas the other particle with $\omega_{x,i} \neq \omega_c$ realises that its frequency is not the same as the driving one and the "beating" phenomenon is observed for this particle.

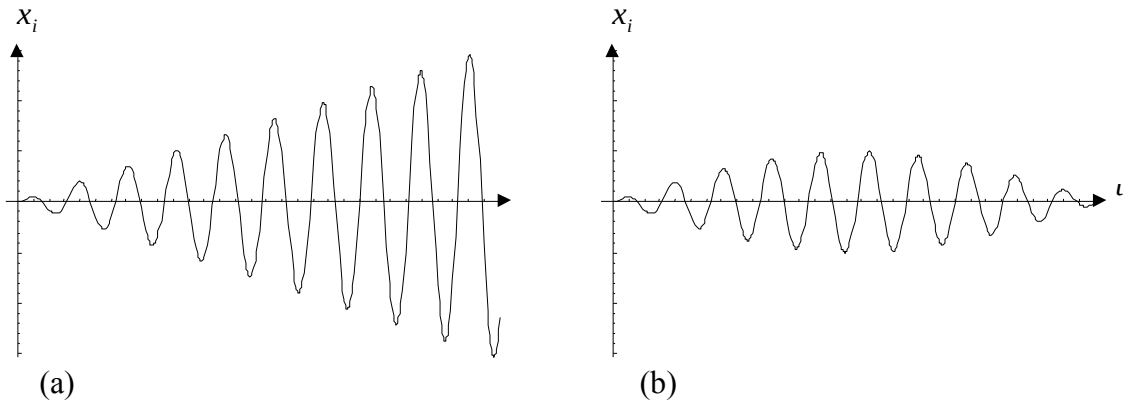

FIGURE 2 Shape of the single-particle response $x_i(t)$ to the sinusoidal driving force $f\cos\left(\omega_c t\right)$. (a) $\omega_{x,i} = \omega_c$ (resonance). (b) $\omega_{x,i} \neq \omega_c$ (beating oscillations).

The particle with $\omega_{x,i} \neq \omega_c$ is considered off-coherence when $\sin\left[\left(\omega_c - \omega_{x,i}\right) t \,/\, 2\right]$ is maximum, i.e. after the time approximately $\bar{t} = \pi / \left|\omega_c - \omega_{x,i}\right|$, and at time $2\bar{t}$, the

particle returns all its energy back to the driving force in a beating process. One can also say that, if one considers the phenomenon for a time t, only the particles with $\left|\omega_c - \omega_{x,i}\right| < \pi/t$ still oscillate coherently. All the others are "beating". It is mainly those particles with $\left|\omega_c - \omega_{x,i}\right| < \pi/t$ that contribute to the $\sin(\omega_c t)$ response of Eq. (2.31), and those particles with $\left|\omega_c - \omega_{x,i}\right| > \pi/t$ that contribute to the $\cos(\omega_c t)$ response. Since the number of particles with $\left|\omega_c - \omega_{x,i}\right| < \pi/t$ decreases with time as $1/t$ while their amplitude increases as t, the net $\sin(\omega_c t)$ contribution to $\bar{x}$ is constant with time.

Having demonstrated the detailed treatment of the initial conditions, the apparent singularities, and the out-of-phase beam responses, we are now ready to introduce a mathematical trick which bypasses most of these subtleties and makes the analysis much more concise. It turns out that one can "derive" the same result by venturing with the complex notation. In this case, the driving force is written $f e^{j\omega_c t}$ and the single-particle motion gives the total beam response

$$\bar{x} = -\frac{f e^{j\omega_c t}}{2\omega_{x0}} \int_{-\infty}^{+\infty} \frac{1}{\omega_c - \omega_{x,i}} \rho_x(\omega_{x,i})\, d\omega_{x,i}\,. \tag{2.37}$$

If one considers the integration along the real axis of the $\omega_{x,i}-$plane, but moves the pole at $\omega_{x,i} = \omega_c$ down by an infinitesimal amount ε,

$$\omega_c \rightarrow \omega_c - j\varepsilon, \tag{2.38}$$

the integral in Eq. (2.37) has then no singularity and the following result is obtained

$$\bar{x} = \frac{f e^{j\omega_c t}}{2\omega_{x0}} \left[-\text{P.V.} \int_{-\infty}^{+\infty} \frac{\rho_x(\omega_{x,i})}{\omega_c - \omega_{x,i}}\, d\omega_{x,i} - j\pi\rho_x(\omega_c) \right]. \tag{2.39}$$

The connection (2.38) has the physical meaning of considering a force that has a time dependence of $e^{j\omega_c t + \varepsilon t}$, i.e. a force that grows with time at an infinitesimal rate. This means the driving force has not been in existence since $t = -\infty$, which has the same effect as introducing explicit initial conditions as far as removing the singularity is concerned.

2.4 Landau damping of collective instabilities

Results obtained in the previous section, when applied to circular accelerators, lead to Landau damping of collective instabilities. To demonstrate this, let us come back to the coasting beam case of Section 2.2 where Eq. (2.24) has to be solved. The r.h.s of Eq. (2.24) contains information about the beam intensity and the impedance. The l.h.s contains information about the beam frequency spectrum. Calculation of the r.h.s is straightforward. For a given impedance, one only needs to calculate the complex mode frequency shift $\omega_c - \omega_{x0} = U_x - jV_x$, in the absence of Landau damping. Without frequency spread, the condition for the beam to be stable is thus simply $V_x \leq 0$.

Once its r.h.s is obtained, Eq. (2.24) can in principle be used to determine the coherent betatron frequency ω_c in the presence of Landau damping when the beam is at the edge of instability. However, the exact value of ω_c is not a very useful piece of information. The more useful question to ask is under what conditions the beam becomes unstable regardless of the exact value of ω_c under these conditions, and Eq. (2.24) can be used in a reversed manner to address this question. To do so, one considers the real parameter $\omega_c - \omega_{x0}$ (stability limit) and observes the locus traced out in the complex $D-$plane as $\omega_c - \omega_{x0}$ is scanned form $-\infty$ to $+\infty$, where D is the l.h.s of Eq. (2.24),

$$D = \left(\int_{-\infty}^{+\infty} \frac{\rho_x\left(\omega_{x,i}\right) d\omega_{x,i}}{\omega_c - \omega_{x,i}} \right)^{-1}. \tag{2.40}$$

This locus defines a "stability boundary diagram".[8,34-36] The r.h.s of Eq. (2.24), a complex quantity, is then plotted in the complex $D-$plane as a single point. If this point lies on the lotus, it means the solution of ω_c for Eq. (2.24) is real, and this $\omega_c - \omega_{x0}$ is such that the beam is just at the edge of instability. If it lies on the inside of the lotus (the side which contains the origin of the $D-$plane), the beam is stable. If it lies on the outside of the lotus, the beam is unstable.

In case of the $\delta-$function spectrum, which is the case without Landau damping (no frequency spread), the stability region reduces to the condition $V_x \le 0$. A spread in the natural frequencies leads to larger regions of stability, as we will see in the following, and thus helps stabilise the beam against collective instabilities, demonstrating the Landau damping mechanism.

The dispersion relation is particularly simple for the Lorentzian spectrum (Figure 3). In this case the distribution function centred at ω_{x0} is written as[8]

$$\rho_x\left(\omega_{x,i}\right) = \frac{\delta\omega_x}{\pi}\left[\left(\omega_{x,i} - \omega_{x0}\right)^2 + \delta\omega_x^2\right]^{-1}, \tag{2.41}$$

where $\delta\omega_x$ is the half width at half maximum of the spectrum.

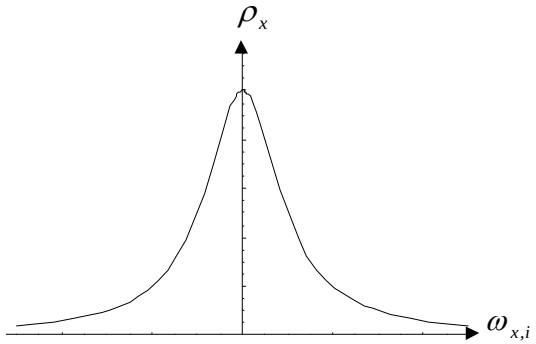

FIGURE 3 Shape of the Lorentzian spectrum.

The corresponding dispersion integral is given by[8]

$$\int_{-\infty}^{+\infty} \frac{\rho_x(\omega_{x,i})\, d\omega_{x,i}}{\omega_c - \omega_{x,i}} = \frac{1}{\omega_c - \omega_{x0} - j\,\delta\omega_x}. \tag{2.42}$$

Substituting Eq. (2.42) into Eq. (2.24) leads to

$$\omega_c = \omega_{x0} + U_x + j(\delta\omega_x - V_x). \tag{2.43}$$

The stability condition $\mathrm{Im}(\omega_c) \geq 0$ therefore becomes

$$\delta\omega_x \geq V_x. \tag{2.44}$$

This means that the stability is obtained when the frequency spread is greater than the instability growth rate in the absence of Landau damping. The stability boundary diagram is represented in Figure 4.

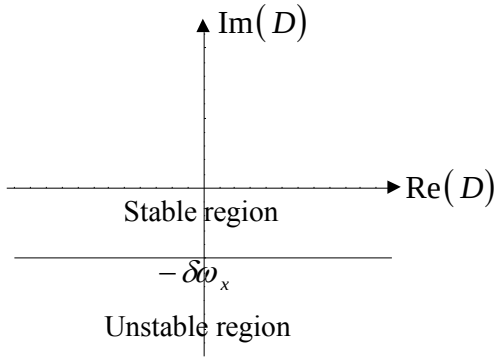

FIGURE 4 Stability boundary diagram for the Lorentzian spectrum in the complex $D-$plane.

The fact that the stable region is always enlarged by the frequency spread can be traced back to the fact that $\rho_x(\omega_c)$ is always positive (see Eq. (2.39)). As pointed out in Section 2.3, this in turn comes from the fact that the beam continues to absorb energy from the driving force without having to let $\bar{x}$ grow.

The larger the frequency spread, the stronger the Landau damping. Also, for a given spread, the effectiveness of Landau damping is different for different spectral shapes. The Lorentzian spectrum, having a long distribution tail, is very effective; spectra with cutoff tails tend to be less effective, while the $\delta-$function spectrum, of course, is not effective at all. Sharp edges in a spectral shape are reflected in sharp edges in the stability boundary.

The Lorentzian distribution describes the stabilising mechanism of Landau damping in a simple way, but neglects an important point. The real part of the complex mode frequency shift, U_x, is not taken into account in the stability criterion because of its infinite tails. However, realistic distributions have finite tails and for distributions without important tails, Landau damping is prevented when the shift $|U_x|$ (with $|U_x| >> |V_x|$ at low energy) is larger than the frequency spread $\Delta\omega_x$. This is explained by the large detuning which shifts the coherent frequency $\omega_{x0} + U_x$ to a value outside the spectrum $\omega_{x0} \pm \Delta\omega_x$. This kills Landau damping since they are no individual particles which can couple to the coherent response.

For practical accelerator operations, there may be approximate information on the value of the frequency spread, but not enough detailed information on the shape of the frequency spectrum; or there may be only a need of a rough estimate of whether the collective instability is Landau damped. For those purposes, a simplified stability criterion derived using the elliptical spectrum (Figure 5) is introduced, knowing that Lorentzian and elliptical spectra are limiting cases and that realistic distributions are probably between them.[8,34-36] In this case, the distribution function is defined by[8]

$$\rho_x\left(\omega_{x,i}\right)=\begin{cases}\dfrac{2}{\pi\,\Delta\omega_x^2}\sqrt{\Delta\omega_x^2-\left(\omega_{x,i}-\omega_{x0}\right)^2} & , \quad \left|\omega_{x,i}-\omega_{x0}\right|\le\Delta\omega_x \\ 0 & , \quad \left|\omega_{x,i}-\omega_{x0}\right|>\Delta\omega_x\end{cases}. \tag{2.45}$$

Here, $\Delta\omega_x$ is the half width at the bottom of the distribution.

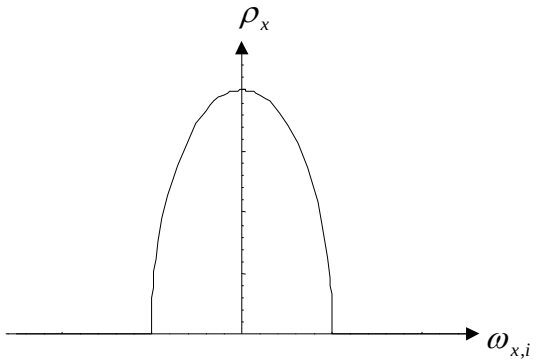

FIGURE 5 Shape of the elliptical spectrum.

The corresponding dispersion integral is given by[8]

$$\int_{-\infty}^{+\infty}\frac{\rho_x\left(\omega_{x,i}\right)d\omega_{x,i}}{\omega_c-\omega_{x,i}}=2\left[\,\omega_c-\omega_{x0}-j\sqrt{\Delta\omega_x^2-\left(\omega_c-\omega_{x0}\right)^2}\,\right]^{-1}, \tag{2.46}$$

with

$$\begin{aligned}-j\sqrt{\Delta\omega_x^2-\left(\omega_c-\omega_{x0}\right)^2}&=\sqrt{\left(\omega_c-\omega_{x0}\right)^2-\Delta\omega_x^2} \quad \text{for} \quad \omega_c>\omega_{x0}+\Delta\omega_x\,, \\ -j\sqrt{\Delta\omega_x^2-\left(\omega_c-\omega_{x0}\right)^2}&=-\sqrt{\left(\omega_c-\omega_{x0}\right)^2-\Delta\omega_x^2} \quad \text{for} \quad \omega_c<\omega_{x0}-\Delta\omega_x\,.\end{aligned} \tag{2.47}$$

Substituting Eq. (2.46) into Eq. (2.24) leads to

$$\omega_c-\omega_{x0}-2U_x-j\left[\sqrt{\Delta\omega_x^2-\left(\omega_c-\omega_{x0}\right)^2}-2V_x\right]=0. \tag{2.48}$$

By squaring of Eq. (2.48) and rearranging terms, we obtain

$$\omega_c=\omega_{x0}+U_x\frac{\Delta\omega_x^2+4\left(U_x^2+V_x^2\right)}{4\left(U_x^2+V_x^2\right)}+jV_x\frac{\Delta\omega_x^2-4\left(U_x^2+V_x^2\right)}{4\left(U_x^2+V_x^2\right)}. \tag{2.49}$$

The simplified stability criterion is finally written (for $V_x > 0$, i.e. for the case of an unstable beam in the absence of a frequency spread) as

$$\Delta\omega_x \geq 2\left|U_x - jV_x\right|, \tag{2.50}$$

which thus leads to a semi-circular range of stability in the $D-$plane (Figure 6).

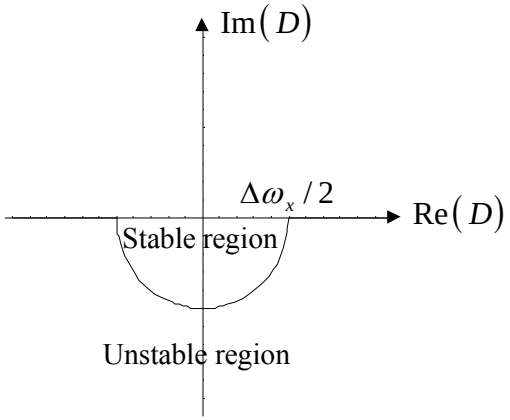

FIGURE 6 Stability boundary diagram for the elliptical spectrum in the complex $D-$plane.

A fair comparison of two spectral shapes can be made when they have the same half width at half maximum $\Delta\omega^x_{\mathrm{HWHH}}$. For the Lorentzian spectrum, $\Delta\omega^x_{\mathrm{HWHH}} = \delta\omega_x$, but for the elliptical spectrum, $\Delta\omega^x_{\mathrm{HWHH}} = \left(\sqrt{3}/2\right)\Delta\omega_x$. The simplified stability criterion can therefore be written

$$\Delta\omega^x_{\mathrm{HWHH}} \geq \sqrt{3}\left|U_x - jV_x\right|. \tag{2.51}$$

Although the exact stability condition depends on details of the spectrum, Eq. (2.51) is an important result which takes into account both contributions of U_x and V_x. It says that if the real mode frequency shift or growth rate, calculated without Landau damping, is larger than $\Delta\omega^x_{\mathrm{HWHH}}/\sqrt{3}$, Landau damping most likely will not rescue the beam from instability.

2.5 Dispersion relation considering external non-linearities

The origins of the frequency spread that leads to Landau damping have been specified in Section 2.2 (see Eqs. (2.8), (2.9) and (2.10)) but have not been taken into account till now. The case where the frequency spread comes from the longitudinal momentum spread of the beam is straightforward (for a coasting beam), because the longitudinal momentum is a constant, which just affects the coefficients in the equations of motion of the transverse oscillations, and hence their frequencies. It can be dealt with the same method as in the previous sections. The same result applies also if one considers a tune spread that is due to a non-linearity in the other plane, $Q_{x,i}\left(\hat{y}_i\right)$. However, this result is no longer valid if the non-linearity is in the plane of coherent motion, $Q_{x,i}\left(\hat{x}_i\right)$.[37] In this case, the steady-state is more involved because the coherent motion is then a small addition to the large incoherent amplitudes that make the

frequency spread, and it is inconsistent to assume that it can be treated as a linear superposition. One needs to consider "second order" non-linear terms and one finds then that the dispersion integral does not contain the distribution function but its derivative times $\hat{x}_i^2$. This is easier to show starting from the Vlasov equation,[26,32] as we will see in Chapter 4. However, in this section, the single-particle equation formalism will be used to review the result obtained by Hereward.[37]

Let us thus proceed to include the frequency spread due to a non-linearity in the external focusing, in the plane of coherent motion only. In this case, the steady-state response of the l.h.s of Eq. (2.6) to the driving force of the r.h.s, which can be written as $2\omega_{x0}\left(-U_x + jV_x\right)\bar{x}$, is more involved than the simple-minded response given by Eq. (2.17). To first order in the amplitude dependence $\omega_{x,i}\left(\hat{x}_i\right)$, namely for $K_x = \left(d\omega_{x,i}/d\hat{x}_i\right)/\left(\omega_{x,i}/\hat{x}_i\right) << 1$, one has

$$X_i = \left[\left(1-\frac{K_x}{2}\right)\frac{1}{\omega_{x,i}^2\left(\hat{x}_i\right)-\left(\omega-n_x\,\Omega_0\right)^2} - \frac{K_x}{2}\,\frac{\omega_{x,i}^2\left(\hat{x}_i\right)+\left(\omega-n_x\,\Omega_0\right)^2}{\left[\omega_{x,i}^2\left(\hat{x}_i\right)-\left(\omega-n_x\,\Omega_0\right)^2\right]^2}\right]\times \tag{2.52}$$
$$2\omega_{x0}\left(-U_x + jV_x\right)\bar{X}\,.$$

If $K_x = 0$, Eq. (2.17) is recovered. Let the density of the phase space $\left(x, \dot{x}\right)$ be given by $\rho_x\left(\hat{x}_i\right)$. The unperturbed oscillation of the *i*th particle describes an ellipse in the phase space, whose area is $\pi\,\hat{x}_i^2\,\omega_{x,i}\left(\hat{x}_i\right)$. The number of particles present is then

$$\begin{aligned} N &= \int_0^{+\infty} \rho_x\left(\hat{x}_i\right)\, d\left[\pi\,\hat{x}_i^2\,\omega_{x,i}\left(\hat{x}_i\right)\right] \\ &= \int_0^{+\infty}\left(1+\frac{K_x}{2}\right)\omega_{x,i}\left(\hat{x}_i\right)\,\rho_x\left(\hat{x}_i\right)\,2\pi\,\hat{x}_i\,d\hat{x}_i\,. \end{aligned} \tag{2.53}$$

This yields the averaged response

$$\bar{X} = \frac{1}{N}\int_0^{+\infty} X_i\,\rho_x\left(\hat{x}_i\right)\,d\left[\pi\,\hat{x}_i^2\,\omega_{x,i}\left(\hat{x}_i\right)\right]. \tag{2.54}$$

Using the fact that

$$\begin{aligned} &\left\{\frac{\omega_{x,i}\left(\hat{x}_i\right)}{\omega_{x,i}^2\left(\hat{x}_i\right)-\left(\omega-n_x\,\Omega_0\right)^2} - \frac{K_x}{2}\,\frac{\omega_{x,i}\left(\hat{x}_i\right)\left[\omega_{x,i}^2\left(\hat{x}_i\right)+\left(\omega-n_x\,\Omega_0\right)^2\right]}{\left[\omega_{x,i}^2\left(\hat{x}_i\right)-\left(\omega-n_x\,\Omega_0\right)^2\right]^2}\right\} 2\,\hat{x}_i \\ &= \frac{d}{d\hat{x}_i}\left[\frac{\omega_{x,i}\left(\hat{x}_i\right)\,\hat{x}_i^2}{\omega_{x,i}^2\left(\hat{x}_i\right)-\left(\omega-n_x\,\Omega_0\right)^2}\right], \end{aligned} \tag{2.55}$$

the following dispersion relation is obtained

$$\left[-\frac{\pi}{N}\int_0^{+\infty}\rho_x'\left(\hat{x}_i\right)\,\frac{\omega_{x,i}\left(\hat{x}_i\right)\,\hat{x}_i^2}{\omega_{x,i}^2\left(\hat{x}_i\right)-\left(\omega-n_x\,\Omega_0\right)^2}\,d\hat{x}_i\right]^{-1} = 2\omega_{x0}\left(-U_x + jV_x\right). \tag{2.56}$$

Here, an integration by parts has been used, assuming $\hat{x}_i^2\,\rho_x(\hat{x}_i)$ is zero at the limits $\hat{x}_i = 0$ and $\hat{x}_i = +\infty$. It is found that the derivative $\rho'_x(\hat{x}_i)$, not $\rho_x(\hat{x}_i)$, is the weighting function inside the dispersion integral: regions of uniform density contribute nothing. If instead of the distribution $\rho_x(\hat{x}_i)$, we choose the distribution function $h_x(\hat{x}_i)$ normalised as

$$\int_0^{+\infty} h_x(\hat{x}_i)\,\hat{x}_i\,d\hat{x}_i = 1, \tag{2.57}$$

then neglecting the $\hat{x}_i$-dependence of $\omega_{x,i}$ in the numerator of the dispersion integral and making the approximation of Eq. (2.18), Eq. (2.56) can be written as

$$\left[\int_0^{+\infty} \frac{1}{\omega - \left[n_x + Q_{x,i}(\hat{x}_i)\right]\Omega_0}\left(-\frac{h'_x(\hat{x}_i)\,\hat{x}_i^2}{2}\right)d\hat{x}_i\right]^{-1} = U_x - j\,V_x\,. \tag{2.58}$$

The function $h_x(\hat{x}_i)$ is related to $\rho_x(\hat{x}_i)$ by $h'_x(\hat{x}_i) = 2\,\omega_{x0}\,\frac{\pi}{N}\,\rho'_x(\hat{x}_i)$.

2.6 Dispersion relation considering both non-linear space-charge forces and octupoles

Let us call $h_y(\hat{y}_i)$ and $g(p_i)$ the distribution functions of the incoherent vertical amplitudes and momenta of the particles. Taking the three distributions as uncorrelated, choosing the normalisations

$$\int_0^{+\infty} h_y(\hat{y}_i)\,\hat{y}_i\,d\hat{y}_i = 1, \qquad \int_0^{+\infty} g(p_i)\,dp_i = 1, \tag{2.59}$$

and noting that $\overline{X} = \iiint X_i\,h_x(\hat{x}_i)h_y(\hat{y}_i)g(p_i)\hat{x}_i\,d\hat{x}_i\,\hat{y}_i\,d\hat{y}_i\,dp_i$, the dispersion relation (2.58) becomes[23]

$$\left[\iiint \frac{(U_x - jV_x)_{(\hat{x}_i,\hat{y}_i,p_i)}}{\omega - \left[n_x + Q_{x,i}(\hat{x}_i,\hat{y}_i,p_i)\right]\Omega_i(p_i)}\left(-\frac{h'_x(\hat{x}_i)\,\hat{x}_i^2}{2}\right)h_y(\hat{y}_i)\hat{y}_i\,g(p_i)d\hat{x}_i\,d\hat{y}_i\,dp_i\right]^{-1} = 1. \tag{2.60}$$

From Eq. (2.60), it is found that the combined effect of external (octupoles) and space-charge non-linearities can considerably enhance the stability conditions, and that the spreads from both transverse directions are important.[23,24] The spread of the incoherent tune shift alone has no stabilising effect on the dipolar type of instabilities. If, however, external non-linearities, e.g. octupolar lenses, are included, then the incoherent tune spread can also become effective for Landau damping. It is then important to choose the "right" sign of excitation of the octupolar lenses so that they add to the internal tune spread. Roughly speaking, the external spread required for stability is about 2 times smaller with the good sign or 2 times greater with the bad sign than without taking into account non-linear space-charge forces.

In the following of this paper, the coupling impedances will be supposed to be the same for all the particles (space-charge non-linearities are thus not treated).

3 COUPLED LANDAU DAMPING USING THE SINGLE-PARTICLE EQUATION FORMALISM

The influence of coupling on Landau damping is assessed in this chapter for both coasting (in Section 3.1) and bunched beams with particular wake fields (in Sections 3.2 and 3.3), using the single-particle equation formalism. This formalism allows us to discuss in a simple way rigid dipolar oscillations, or single-bunch head-tail modes for step-function (or resistive-wall) wakes, while the Vlasov formalism presented in Chapter 4 can be used to generalise the results to higher order head-tail modes for bunched beams and general wakes.

Introducing "equivalent" dispersion relation coefficients (which are the real betatron frequency shift and instability growth rate respectively, for a given mode, in the absence of both coupling and Landau damping), a generalised two-dimensional dispersion relation is derived, having the form of a product of two dispersion relations, one for the horizontal and the other for the vertical plane, equated to a coupling term (see Eqs. (3.12), (3.115) and (3.151)); when the latter vanishes, the known results on one-dimensional Landau damping are recovered. Entirely new stability criteria for the coherent motion of a beam in an accelerator with betatron coupling are obtained, using two typical (externally given) frequency distributions (Lorentzian, $\rho(f) \propto 1/(1+u^2)$ (see Eqs. (3.26) and (3.27)), and elliptical, $\rho(f) \propto \sqrt{1-u^2}$ where $u = (f - f_0)/\Delta f$ (see Eqs. (3.72) and (3.73))), knowing that Lorentzian and elliptical spectra are limiting cases and that realistic distributions are probably in between them. In the absence of tune spread, recent results on "chromaticity sharing" are also recovered (see Eqs. (3.159) and (3.161)). Considering octupolar non-linearities (and neglecting space-charge non-linearities), the two-dimensional dispersion relation is given by Eq. (3.164).

3.1 Coasting beams

3.1.1 Equations of motion

Four types of forces are taken into account in writing the equations of betatron motion of a test particle *i*:[38]

1) the external focusing forces that depend on the horizontal deviation x_i (the vertical deviation y_i) of the particle from a fixed reference (e.g. the centre of the chamber). The corresponding tune is $Q_{0x,i}$ ($Q_{0y,i}$);
2) the coherent space-charge forces that depend on the deviation $\bar{x}$ ($\bar{y}$) of the beam centre from the centre of the chamber. The corresponding (generalised) tune shift is $\Delta Q_{coh,x}$ ($\Delta Q_{coh,y}$);
3) the incoherent space-charge forces that depend on the deviation $x_i - \bar{x}$ ($y_i - \bar{y}$) of the particle from the beam centre. The corresponding (generalised) tune shift is $\Delta Q_{inc,x}$ ($\Delta Q_{inc,y}$);
4) the coupling forces, represented by the normalised skew gradient $\underline{K}_i = (e/p_i)(\partial B_{x,i}/\partial x_i)$, that make the vertical (horizontal) deviation appear in the horizontal (vertical) equation of motion of the particle.[21] Here, $B_{x,i}$ is the horizontal magnetic field at the position of the *i*th particle. Coupling of the horizontal and vertical oscillations is a parameter of prime importance for the ring operation and for the performance. It can cause for example, emittance blow-up, resonance excitation and tune shifts. In high energy accelerators there are two

sources of linear coupling insofar as single-particle motion is concerned: skew quadrupolar fields, and occasionally, solenoidal fields. Even in the absence of "normal" skew quadrupoles and solenoids, there always exists a certain amount of linear coupling due to alignment errors of the regular quadrupoles. This yields

$$\begin{aligned}
&\ddot{x}_i + \Omega_i^2\left(Q_{0x,i}^2 + 2Q_{0x,i}\,\Delta Q_{inc,x}\right)x_i = -2\Omega_i^2\,Q_{0x,i}\left(\Delta Q_{coh,x} - \Delta Q_{inc,x}\right)\bar{x} + \underline{K}_i\,R_i^2\,\Omega_i^2\,y_i\,,\\
&\ddot{y}_i + \Omega_i^2\left(Q_{0y,i}^2 + 2Q_{0y,i}\,\Delta Q_{inc,y}\right)y_i = -2\Omega_i^2\,Q_{0y,i}\left(\Delta Q_{coh,y} - \Delta Q_{inc,y}\right)\bar{y} + \underline{K}_i\,R_i^2\,\Omega_i^2\,x_i\,.
\end{aligned} \tag{3.1}$$

Using the normalised (Courant-Snyder) coordinates and angle, given by[21]

$$\begin{aligned}
&\eta_i = x_i\,\beta_{0x,i}^{-1/2}(s), \qquad\qquad \zeta_i = y_i\,\beta_{0y,i}^{-1/2}(s),\\
&\phi_i = Q_{0x,i}^{-1}\int_0^s \beta_{0x,i}^{-1}(t)\,dt \approx Q_{0y,i}^{-1}\int_0^s \beta_{0y,i}^{-1}(t)\,dt,
\end{aligned} \tag{3.2}$$

the equations of motion (3.1) can be rewritten

$$\begin{aligned}
&\frac{d^2\eta_i}{d\phi_i^2} + Q_{x,i}^2\,\eta_i = \beta_{0x,i}^{3/2}\,\beta_{0y,i}^{1/2}\,Q_{0x,i}^2\,\underline{K}_i\,\zeta_i - \left(\Delta Q_{coh,x} - \Delta Q_{inc,x}\right)\frac{2\,Q_{0x,i}^3\,\beta_{0x,i}^2}{R_i^2}\,\bar{\eta}\,,\\
&\frac{d^2\zeta_i}{d\phi_i^2} + Q_{y,i}^2\,\zeta_i = \beta_{0y,i}^{3/2}\,\beta_{0x,i}^{1/2}\,Q_{0y,i}^2\,\underline{K}_i\,\eta_i - \left(\Delta Q_{coh,y} - \Delta Q_{inc,y}\right)\frac{2Q_{0y,i}^3\,\beta_{0y,i}^2}{R_i^2}\,\bar{\zeta}\,.
\end{aligned} \tag{3.3}$$

Here, $Q_{x,i} = Q_{0x,i} + \Delta Q_{inc,x}$ and $Q_{y,i} = Q_{0y,i} + \Delta Q_{inc,y}$ are the new incoherent tunes, $\bar{\eta}$ and $\bar{\zeta}$ are the normalised coordinates of the beam centre. The betatron functions are given by $\beta_{0x,i} \approx R_i / Q_{0x,i} \approx R/Q_{0x0}$ and $\beta_{0y,i} \approx R_i / Q_{0y,i} \approx R/Q_{0y0}$ in the smooth approximation (with Q_{0x0} and Q_{0y0} the averages of the incoherent tunes). Replacing the revolution frequency Ω_i by its average value Ω_0 ($\phi_i = \Omega_0\,t = \phi$ in the smooth approximation), the orbit radius R_i by its average value R, and supposing that the skew gradient is the same for all the particles, i.e. $\underline{K}_i = \underline{K}_0$, the equations of motion can be finally written as

$$\begin{aligned}
&\frac{d^2\eta_i}{d\phi^2} + Q_{x,i}^2\,\eta_i = -j\,\frac{e\,\beta\,I\,Z_x}{2\pi\,R\,m_0\,\gamma\,\Omega_0^2}\,\bar{\eta} + R^2\left(\frac{Q_{0x0}}{Q_{0y0}}\right)^{1/2}\underline{K}_0\,\zeta_i\,,\\
&\frac{d^2\zeta_i}{d\phi^2} + Q_{y,i}^2\,\zeta_i = -j\,\frac{e\,\beta\,I\,Z_y}{2\pi\,R\,m_0\,\gamma\,\Omega_0^2}\,\bar{\zeta} + R^2\left(\frac{Q_{0y0}}{Q_{0x0}}\right)^{1/2}\underline{K}_0\,\eta_i\,.
\end{aligned} \tag{3.4}$$

3.1.2 Two-dimensional dispersion relation

In the following, transverse betatron frequency spreads specified by externally given beam frequency spectra are assumed. The ensemble of particles has spectra with the distribution functions $\rho_x(\omega_{x,i})$ and $\rho_y(\omega_{y,i})$ which are supposed to be

uncorrelated and normalised to unity (see Eq. (2.20)). The betatron frequencies are given by $\omega_{x,i} = \Omega_0 Q_{x,i}$ and $\omega_{y,i} = \Omega_0 Q_{y,i}$. Moreover, in a circular machine, linear coupling is periodic in ϕ with period 2π, and thus can be expanded into Fourier series[21]

$$\underline{K}_0(\phi) = \sum_{l=-\infty}^{l=+\infty} \hat{\underline{K}}_0(l)\, e^{jl\phi}, \tag{3.5}$$

with

$$\hat{\underline{K}}_0(l) = \frac{1}{2\pi} \int_0^{2\pi} \underline{K}_0(\phi)\, e^{-jl\phi}\, d\phi. \tag{3.6}$$

Considering only the dominant Fourier component of the coupling (l) and following the standard procedure of identifying normal mode frequencies, yields particular solutions of the form

$$\eta_i = \mathrm{H}_i\, e^{jQ_c\phi}, \qquad \zeta_i = \mathrm{Z}_i\, e^{j(Q_c - l)\phi}, \tag{3.7}$$

where Q_c is the coherent tune to be determined. Substituting Eqs. (3.7) into Eqs. (3.4) yields

$$\begin{aligned} \mathrm{H}_i &= \frac{1}{Q_{x,i}^2 - Q_c^2}\left[R^2 \left(\frac{Q_{0x0}}{Q_{0y0}}\right)^{1/2} \hat{\underline{K}}_0(l)\, \mathrm{Z}_i + \frac{2\omega_{x0}}{\Omega_0^2}\left(-U_x + jV_x\right)\overline{\mathrm{H}}\right], \\ \mathrm{Z}_i &= \frac{1}{Q_{y,i}^2 - (Q_c - l)^2}\left[R^2 \left(\frac{Q_{0y0}}{Q_{0x0}}\right)^{1/2} \hat{\underline{K}}_0(-l)\, \mathrm{H}_i + \frac{2\omega_{y0}}{\Omega_0^2}\left(-U_y + jV_y\right)\overline{\mathrm{Z}}\right], \end{aligned} \tag{3.8}$$

where $U_{x,y}$ and $V_{x,y}$ are defined by Eq. (2.25). Integrating the first equation of Eqs. (3.8) over the spectrum $\rho_x(\omega_{x,i})$ yields

$$\overline{\mathrm{H}} = \left[R^2 \left(\frac{Q_{0x0}}{Q_{0y0}}\right)^{1/2} \hat{\underline{K}}_0(l)\, \mathrm{Z}_i + \frac{2\omega_{x0}}{\Omega_0^2}\left(-U_x + jV_x\right)\overline{\mathrm{H}}\right] \int_{-\infty}^{+\infty} \frac{\rho_x(\omega_{x,i})\, d\omega_{x,i}}{\frac{\omega_{x,i}^2}{\Omega_0^2} - Q_c^2}. \tag{3.9}$$

Integrating now Eq. (3.9) over the spectrum $\rho_y(\omega_{y,i})$ yields

$$\overline{\mathrm{H}} = \left[R^2 \left(\frac{Q_{0x0}}{Q_{0y0}}\right)^{1/2} \hat{\underline{K}}_0(l)\, \overline{\mathrm{Z}} + \frac{2\omega_{x0}}{\Omega_0^2}\left(-U_x + jV_x\right)\overline{\mathrm{H}}\right] \int_{-\infty}^{+\infty} \frac{\rho_x(\omega_{x,i})\, d\omega_{x,i}}{\frac{\omega_{x,i}^2}{\Omega_0^2} - Q_c^2}. \tag{3.10}$$

With the second equation of Eqs. (3.8), a similar result is obtained after integration over the spectra $\rho_y(\omega_{y,i})$ and $\rho_x(\omega_{x,i})$,

$$\overline{Z} = \left[R^2 \left(\frac{Q_{0y0}}{Q_{0x0}} \right)^{1/2} \underline{\hat{K}}_0(-l)\, \overline{\mathrm{H}} + \frac{2\omega_{y0}}{\Omega_0^2} \left(-U_y + jV_y \right) \overline{Z} \right] \int_{-\infty}^{+\infty} \frac{\rho_y(\omega_{y,i})\, d\omega_{y,i}}{\frac{\omega_{y,i}^2}{\Omega_0^2} - (Q_c - l)^2}. \quad (3.11)$$

Equating the terms $\overline{\mathrm{H}} / \overline{Z}$ of Eqs. (3.10) and (3.11), the two-dimensional dispersion relation in the coherent betatron frequency $\omega_c = \Omega_0 Q_c$ is then obtained

$$\begin{aligned} &\left[\left(\int_{-\infty}^{+\infty} \frac{\rho_x(\omega_{x,i})\, d\omega_{x,i}}{\omega_c - \omega_{x,i}} \right)^{-1} - U_x + jV_x \right] \times \\ &\left[\left(\int_{-\infty}^{+\infty} \frac{\rho_y(\omega_{y,i})\, d\omega_{y,i}}{\omega_c - l\Omega_0 - \omega_{y,i}} \right)^{-1} - U_y + jV_y \right] = \frac{\left| \underline{\hat{K}}_0(l) \right|^2 R^4 \Omega_0^4}{4\, \omega_{x0}\, \omega_{y0}}, \end{aligned} \quad (3.12)$$

making the usual assumptions $\omega_{x,i} \approx \omega_c \approx \omega_{x0}$ and $\omega_{y,i} \approx \omega_c - l\Omega_0 \approx \omega_{y0}$, where $\omega_{x0} = \Omega_0 Q_{x0}$ and $\omega_{y0} = \Omega_0 Q_{y0}$ are the centres of the distributions. Here, the wake field terms must be evaluated at the local collective frequencies, given approximately by

$$\omega_1 \approx (n_x + Q_{x0})\, \Omega_0, \qquad \omega_2 \approx (n_y + Q_{y0})\, \Omega_0, \quad (3.13)$$

where $n_{x,y}$ are the transverse azimuthal mode numbers related by $n_x = n_y - l$.

Using the same approximations as previously, the results (3.12) and (3.13) can also be obtained from Eqs. (3.1), as follows. Assume that the beam centre oscillates harmonically in time and space with (see Eqs. (2.14) and (2.15))

$$\bar{x} = \overline{X}\, e^{j(\omega t - n_x \vartheta)}, \qquad \bar{y} = \overline{Y}\, e^{j(\omega t - n_y \vartheta)}. \quad (3.14)$$

In a circular machine, linear coupling is periodic in the azimuthal angle ϑ with period 2π, and thus can be expanded into Fourier series

$$\underline{K}_0(\vartheta) = \sum_{l=-\infty}^{l=+\infty} \underline{\hat{K}}_0(l)\, e^{jl\vartheta}, \quad (3.15)$$

with

$$\underline{\hat{K}}_0(l) = \frac{1}{2\pi} \int_0^{2\pi} \underline{K}_0(\vartheta)\, e^{-jl\vartheta}\, d\vartheta. \quad (3.16)$$

The steady-state solutions of the test particle have the same t and ϑ dependence as the driving terms

$$x_i = X_i\, e^{j(\omega t - n_x \vartheta)}, \qquad y_i = Y_i\, e^{j(\omega t - n_y \vartheta)}. \quad (3.17)$$

Considering only the dominant Fourier component of the coupling (l) and using the hydrodynamic view, yields the relation between the azimuthal mode numbers, $n_x = n_y - l$, and the two-dimensional dispersion relation in the mode frequency ω

$$\left[\left(\int_{-\infty}^{+\infty}\frac{\rho_x\left(\omega_{x,i}\right)d\omega_{x,i}}{\omega-\left(n_x+Q_{x,i}\right)\Omega_0}\right)^{-1}-U_x+jV_x\right]\times$$
$$\left[\left(\int_{-\infty}^{+\infty}\frac{\rho_y\left(\omega_{y,i}\right)d\omega_{y,i}}{\omega-\left(n_y+Q_{y,i}\right)\Omega_0}\right)^{-1}-U_y+jV_y\right]=\frac{\left|\underline{\hat{K}}_0(l)\right|^2R^4\Omega_0^4}{4\,\omega_{x0}\,\omega_{y0}}. \tag{3.18}$$

Using the fact that the mode frequency ω is related to the coherent betatron frequency by $\omega=\left(n_x+Q_c\right)\Omega_0=\left(n_y+Q_c-l\right)\Omega_0$, Eq. (3.12) is recovered. Near the coupling resonance $Q_h-Q_v=l$, the local collective frequencies in the wake field terms can be approximated by Eq. (3.13).

3.1.3 Stability criterion for Lorentzian spectra

In this case, the horizontal distribution function and dispersion integral are given by Eqs. (2.41) and (2.42) respectively. Similar equations are obtained for the vertical plane replacing x by y and ω_c by $\omega_c-l\Omega_0$, which yields for the vertical dispersion integral

$$\int_{-\infty}^{+\infty}\frac{\rho_y\left(\omega_{y,i}\right)d\omega_{y,i}}{\omega_c-l\Omega_0-\omega_{y,i}}=\frac{1}{\omega_c-l\Omega_0-\omega_{y0}-j\,\delta\omega_y}. \tag{3.19}$$

Substituting Eqs. (2.42) and (3.19) into Eq. (3.12), the dispersion relation becomes

$$\left[\omega_c-\omega_{x0}-U_x-j\left(\delta\omega_x-V_x\right)\right]\times$$
$$\left[\omega_c-\omega_{y0}-l\Omega_0-U_y-j\left(\delta\omega_y-V_y\right)\right]=\frac{\left|\underline{\hat{K}}_0(l)\right|^2R^4\Omega_0^4}{4\,\omega_{x0}\,\omega_{y0}}. \tag{3.20}$$

The dispersion equation has two solutions for ω_c which describe the two coherent oscillation modes of the coupled system. Coherent motions of the form $e^{j\omega_c t}$ are considered; therefore, for each solution ω_c, $\mathrm{Re}\left(\omega_c\right)$ describes the coherent oscillation frequency and $-\mathrm{Im}\left(\omega_c\right)$ is the instability growth rate. Thus, to be stable, a coherent oscillation mode must satisfy $\mathrm{Im}\left(\omega_c\right)\geq 0$.

The imaginary parts of the two coherent oscillation frequencies are given by

$$\mathrm{Im}\left(\omega_{c1,2}\right)=\left(\delta\omega_{x,y}-V_{x,y}\right)\pm\frac{\left(\delta\omega_y-V_y-\delta\omega_x+V_x\right)}{2}C\left(a,\delta\right). \tag{3.21}$$

Here, $C\left(a,\delta\right)$ is a normalised coupling (or sharing) function given by

$$C\left(a,\delta\right)=1-\frac{1}{\sqrt{2}}\sqrt{1-4a^2-\delta^2+\sqrt{\left(-1+4a^2+\delta^2\right)^2+4\delta^2}}\,, \tag{3.22}$$

with

$$a = \frac{\left|\hat{\underline{K}}_0(l)\right| R^2 \Omega_0^2}{2\sqrt{\omega_{x0}\,\omega_{y0}}\left|\delta\omega_y - V_y - \delta\omega_x + V_x\right|}, \qquad \delta = \frac{\Omega_0 \left|Q_h - Q_v - l\right|}{\left|\delta\omega_y - V_y - \delta\omega_x + V_x\right|}, \quad (3.23)$$

where

$$Q_{h,v} = \left(\omega_{x0,y0} + U_{x,y}\right)/\Omega_0 \quad (3.24)$$

are the horizontal and vertical coherent tunes in the presence of wake fields ($U_{x,y}$), but in the absence of coupling.

Three plots of $C(a)$ are represented in Figure 7 for $\delta = 1$, $\delta = 0.25$ and $\delta = 0$.

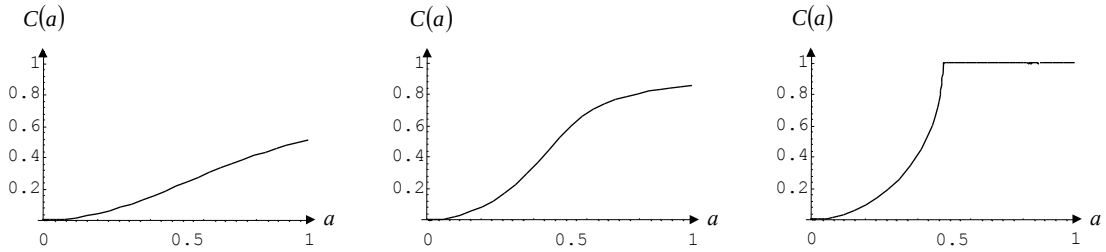

FIGURE 7 Sharing function $C(a)$ for: (a) $\delta = 1$; (b) $\delta = 0.25$; (c) $\delta = 0$.

Whatever the value of δ, the sharing function varies between $C = 0$ and $C = 1$. However, the rate at which $C(a)$ grows increases when δ decreases. The smaller the tune separation, the easier the sharing. The sharing ratio can be chosen by adjusting the tune split and/or the coupling strength.

For $C = 0$ (no coupling), transverse stability in the horizontal and vertical planes requires (see Eq. (2.44))

$$\delta\omega_x \geq V_x, \qquad \delta\omega_y \geq V_y. \quad (3.25)$$

For $C = 1$ (full coupling), by virtue of Eq. (3.21), these two criteria reduce into the stability criterion

$$\delta\omega_x + \delta\omega_y \geq V_x + V_y. \quad (3.26)$$

Equation (3.26) shows the beneficial effect of coupling. Even in the absence of a frequency spread in one plane, a coherent instability can be damped thanks to the other plane: Landau damping is transferred from the stable to the unstable plane. In the case of full coupling, each plane has the mean transverse betatron frequency spread $(\delta\omega_x + \delta\omega_y)/2$ to damp the instability represented by the mean instability growth rate $(V_x + V_y)/2$. When the transverse tune spreads are equal, there is no re-distribution of Landau damping but there still is a sharing of the growth rates. Therefore, the beam can be stabilised provided that $\delta\omega_x = \delta\omega_y \geq (V_x + V_y)/2$. The result of coupling is thus a transfer of Landau damping from the stable to the unstable plane and at the same time a transfer of the instability growth rate from the unstable to the stable plane up to a perfect sharing of both damping and growth. It can be seen from Eq. (3.26), that if the two planes are stable without coupling, then they remain stable with full coupling. In

the same way, if both planes are unstable without coupling, they remain unstable with full coupling.

Consider the interesting case of one unstable transverse plane in the absence of coupling. If the necessary condition of Eq. (3.26) is fulfilled, then it is possible to stabilise the beam in the two planes by choosing a pair (a,δ) that satisfies $\mathrm{Im}(\omega_{c1,2}) \geq 0$ (see Eq. (3.21)). The stabilising values of the modulus of the Fourier coefficient of the skew gradient are given by

$$\left|\underline{\hat{K}}_0(l)\right| \geq \frac{2\left[-Q_{x0}\,Q_{y0}\left(\delta\omega_x - V_x\right)\left(\delta\omega_y - V_y\right)\right]^{1/2}}{R^2\,\Omega_0} \times \frac{\left[\left(\delta\omega_x + \delta\omega_y - V_x - V_y\right)^2 + \Omega_0^2\left(Q_h - Q_v - l\right)^2\right]^{1/2}}{\delta\omega_x + \delta\omega_y - V_x - V_y}. \tag{3.27}$$

The plot of the stability boundary (given by the equal sign in Eq. (3.27)) is a symmetric curve with respect to the vertical axis (Figure 8). It exhibits one stability region for the modulus of the Fourier component of the skew gradient and the tune split $Q_h - Q_v - l$.

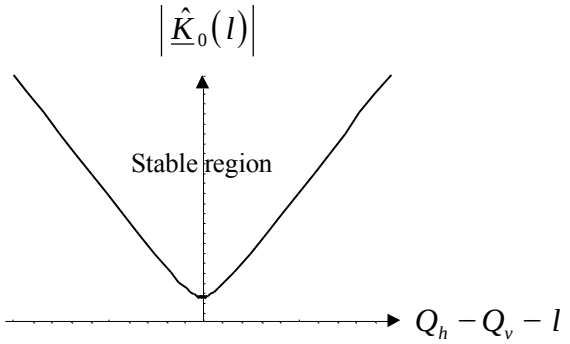

FIGURE 8 Shape of stability boundary in the plane $\left|\underline{\hat{K}}_0(l)\right|$ vs. $Q_h - Q_v - l$.

3.1.4 Stability criterion for elliptical spectra

Due to its infinite tails, the Lorentzian frequency distribution tends to underestimate two important points. The first is the effect of the real betatron frequency shift. The importance of U emerges already in the uncoupled case and has been discussed in Section 2.4.

As a second point, which is in fact closely related to the first, it will be found that too strong coupling can be detrimental and may shift the coherent frequency outside the spectrum and thus again prevent Landau damping. To study these two effects, consider elliptical spectra, from which the simplified one-dimensional stability criterion is derived.

In this case, the horizontal distribution function and dispersion integral are given by Eqs. (2.45) and (2.46) respectively. Similar equations are obtained for the vertical plane replacing x by y and ω_c by $\omega_c - l\Omega_0$, which yields for the vertical dispersion integral

$$\int_{-\infty}^{+\infty} \frac{\rho_y(\omega_{y,i})\,d\omega_{y,i}}{\omega_c - l\Omega_0 - \omega_{y,i}} = 2\left[\,\omega_c - \omega_{y0} - l\Omega_0 - j\sqrt{\Delta\omega_y^2 - \left(\omega_c - \omega_{y0} - l\Omega_0\right)^2}\,\right]^{-1}, \tag{3.28}$$

with the conditions of Eqs. (2.47) for both planes. Substituting Eqs. (2.46) and (3.28) into Eq. (3.12), the dispersion relation becomes

$$\left\{\omega_c-\omega_{x0}-2U_x-j\left[\sqrt{\Delta\omega_x^2-\left(\omega_c-\omega_{x0}\right)^2}-2V_x\right]\right\}\times$$

$$\left\{\omega_c-\omega_{y0}-l\Omega_0-2U_y-j\left[\sqrt{\Delta\omega_y^2-\left(\omega_c-\omega_{y0}-l\Omega_0\right)^2}-2V_y\right]\right\}=\frac{\left|\underline{\hat{K}}_0(l)\right|^2R^4\Omega_0^4}{\omega_{x0}\,\omega_{y0}}. \tag{3.29}$$

This equation seems to be difficult to solve in the general case. Therefore, in the following, the case of an unstable horizontal and a stable vertical plane in the absence of coupling is considered and different limiting cases are investigated, in order to find out an approximate general stability criterion, which is given in Section 3.1.4.5.[39]

3.1.4.1 No horizontal tune spread and no vertical wake field

In this case, $\Delta\omega_x=0$ and $U_y=V_y=0$, the dispersion relation is written as

$$\left[\omega_c-\omega_{x0}-U_x+jV_x\right]\times$$

$$\left[\omega_c-\omega_{y0}-l\Omega_0-j\sqrt{\Delta\omega_y^2-\left(\omega_c-\omega_{y0}-l\Omega_0\right)^2}\right]=\frac{\left|\underline{\hat{K}}_0(l)\right|^2R^4\Omega_0^4}{2\,\omega_{x0}\,\omega_{y0}}. \tag{3.30}$$

Let's define the parameter

$$\kappa=\frac{\left|\underline{\hat{K}}_0(l)\right|^2R^4\Omega_0^4}{\Delta\omega_y^2\,\omega_{x0}\,\omega_{y0}}. \tag{3.31}$$

For $\kappa=1$, Eq. (3.30) has only one solution given by

$$\omega_c=\omega_{x0}+U_x-jV_x-\frac{\Delta\omega_y^2}{4}\frac{\left(\omega_{y0}+l\Omega_0-\omega_{x0}-U_x-jV_x\right)}{\left(\omega_{y0}+l\Omega_0-\omega_{x0}-U_x\right)^2+V_x^2}. \tag{3.32}$$

A stability criterion is deduced

$$\Delta\omega_y\geq 2\sqrt{\Omega_0^2\left(Q_h-Q_v-l\right)^2+V_x^2}\,, \tag{3.33}$$

where Eq. (3.24) has been used. This is a very simple and interesting result that reveals several things. Firstly, it demonstrates the sharing of Landau damping from the stable vertical to the unstable horizontal plane, relating the vertical spread to the horizontal impedance. Secondly, when $Q_{x0}-Q_{y0}-l=0$, the same criterion as in the case of uncoupled planes is found. Thirdly, Eq. (3.33) exhibits another important feature of the coupling: the possible cancellation of the effect of U_x. Indeed, adjusting conveniently the tune separation, i.e. on the resonance $Q_h-Q_v-l=0$, the stability criterion becomes

$$\Delta\omega_y\geq 2V_x\,, \tag{3.34}$$

which resembles the criterion obtained with the Lorentzian spectrum.

For $\kappa \neq 1$, Eq. (3.30) can be written in a way similar to the Lorentzian equation (see Eq. (3.20))

$$\begin{aligned}&\left[\omega_c - \omega_{x0} - U_x + jV_x\right]\times \\ &\left[\omega_c + \frac{U_x + \omega_{x0} - \kappa\left(\omega_{y0} + l\Omega_0\right)}{\kappa - 1} - j\frac{V_x}{\kappa - 1}\right] = \frac{\left|\underline{\hat{K}}_0(l)\right|^2 R^4 \Omega_0^4}{4\,\omega_{x0}\,\omega_{y0}}\left(\frac{\kappa}{\kappa - 1}\right).\end{aligned} \tag{3.35}$$

The necessary condition for stability, equivalent to Eq. (3.26) in the Lorentzian case, reads here

$$-V_x + \frac{V_x}{\kappa - 1} \geq 0, \tag{3.36}$$

which leads to the inequalities

$$1 \leq \kappa \leq 2. \tag{3.37}$$

By analogy with the Lorentzian case, the imaginary parts of the two coherent oscillation frequencies are given by

$$\begin{aligned}\mathrm{Im}\left(\omega_{c1}\right) &= -V_x + \frac{V_x\,\kappa}{2\left(\kappa - 1\right)} C\left(a', \delta'\right), \\ \mathrm{Im}\left(\omega_{c2}\right) &= \frac{V_x}{\kappa - 1} - \frac{V_x\,\kappa}{2\left(\kappa - 1\right)} C\left(a', \delta'\right).\end{aligned} \tag{3.38}$$

Here, $C\left(a', \delta'\right)$ is the sharing function, defined in Eq. (3.22), with

$$a' = \frac{\Delta\omega_y}{2V_x}\sqrt{\kappa - 1}, \qquad \delta' = \frac{\Omega_0\left|Q_h - Q_v - l\right|}{V_x}\left(\frac{\kappa - 1}{\kappa}\right). \tag{3.39}$$

The stability condition $\mathrm{Im}\left(\omega_{c1}\right) \geq 0$ yields

$$\left|Q_h - Q_v - l\right| \leq \frac{1}{\Omega_0}\left(\frac{\Delta\omega_y^2}{4}\kappa^2 - \Delta\omega_y^2\,\kappa + \Delta\omega_y^2 - V_x^2 + \frac{4V_x^2}{\kappa} - \frac{4V_x^2}{\kappa^2}\right)^{1/2}. \tag{3.40}$$

The stability boundary relates the coherent tune separation to the linear coupling strength. If $\Delta\omega_y < V_x$, then it is impossible to stabilise the beam by coupled Landau damping (see Eq. (3.38)): there is not enough Landau damping which can be transferred to the unstable plane. The minimum frequency spread that can stabilise the beam is $\Delta\omega_y = V_x$. In this case, there is only one condition for stability which is $Q_h - Q_v - l = 0$ and $\kappa = 2$. If $\Delta\omega_y > V_x$, we can plot the curve describing the stability boundary (given by the equal sign in Eq. (3.40)), which takes different forms according to the value of $\Delta\omega_y$. For example, in the case where $\Delta\omega_y = 2V_x$, the absolute value of

the tune separation $\left|Q_h - Q_v - l\right|$ vs. normalised coupling strength κ is represented in Figure 9.

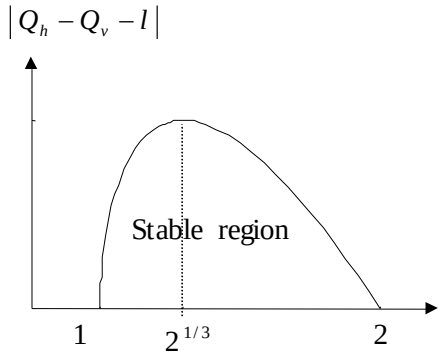

FIGURE 9 Absolute value of the coherent tune separation $\left|Q_h - Q_v - l\right|$ at the stability boundary vs. normalised coupling strength κ, for $\Delta\omega_y = 2V_x$.

One can conclude from Figure 9 that below and above certain values of coupling κ, stabilisation is impossible whereas for intermediate values stabilisation is possible even with some tune split $\left|Q_h - Q_v - l\right|$. If the coupling is too small, there is not enough Landau damping transferred to the unstable plane. If the coupling is too large, the coherent frequencies fall outside the incoherent frequency spreads and Landau damping can't exist. The "optimum" coupling κ leads to the maximum of tune split tolerable for stability. It is obtained for $\kappa = 2^{1/3}$ and the corresponding maximum tune split is $\left|Q_h - Q_v - l\right|_{\max} = \left(\sqrt{3}V_x/\Omega_0\right)\sqrt{1+2^{2/3}\left(1-2^{2/3}\right)}$.

3.1.4.2 No horizontal tune spread

In the absence of horizontal tune spread, $\Delta\omega_x = 0$, but $U_{x,y}$, $V_{x,y} > 0$ and $\Delta\omega_y$ finite, the dispersion relation writes

$$\left[\omega_c - \omega_{x0} - U_x + j\,V_x\right]\times$$
$$\left\{\omega_c - \omega_{y0} - l\Omega_0 - 2U_y - j\left[\sqrt{\Delta\omega_y^2 - \left(\omega_c - \omega_{y0} - l\Omega_0\right)^2} - 2V_y\right]\right\} = \frac{\left|\underline{\hat{K}}_0(l)\right|^2 R^4\,\Omega_0^4}{2\,\omega_{x0}\,\omega_{y0}}. \tag{3.41}$$

Putting ω_c real in Eq. (3.41) and equating the real and imaginary parts separately, yields the conditions at the stability limit,

$$\left(\omega_c - \omega_{x0} - U_x\right)\left(\omega_c - \omega_{y0} - l\Omega_0 - 2U_y\right)$$
$$-V_x\left[2V_y - \sqrt{\Delta\omega_y^2 - \left(\omega_c - \omega_{y0} - l\Omega_0\right)^2}\right] = \frac{\left|\underline{\hat{K}}_0(l)\right|^2 R^4\,\Omega_0^4}{2\,\omega_{x0}\,\omega_{y0}}, \tag{3.42}$$

$$V_x\left(\omega_c - \omega_{y0} - l\Omega_0 - 2U_y\right)$$
$$+\left[2V_y - \sqrt{\Delta\omega_y^2 - \left(\omega_c - \omega_{y0} - l\Omega_0\right)^2}\right]\left(\omega_c - \omega_{x0} - U_x\right) = 0. \tag{3.43}$$

Let's consider the case where

$$\omega_{x0} + U_x = \omega_{y0} + l\,\Omega_0 + 2U_y\,. \tag{3.44}$$

This choice will be justified at the end of this section. Then Eq. (3.43) is verified if

$$\omega_c = \omega_{x0} + U_x\,, \tag{3.45}$$

or

$$\sqrt{\Delta\omega_y^2 - \left(\omega_c - \omega_{y0} - l\,\Omega_0\right)^2} \;= V_x + 2V_y\,. \tag{3.46}$$

If Eq. (3.45) is fulfilled then Eq. (3.42) becomes

$$\frac{\left|\underline{\hat{K}}_0(l)\right|^2 R^4\,\Omega_0^4}{2\;\omega_{x0}\;\omega_{y0}} = V_x\left[\;\sqrt{\Delta\omega_y^2 - \left(\omega_c - \omega_{y0} - l\,\Omega_0\right)^2}\;\; - 2V_y\right]. \tag{3.47}$$

If Eq. (3.46) is verified then

$$\left(\omega_c - \omega_{y0} - l\,\Omega_0\right)^2 = \Delta\omega_y^2 - \left(V_x + 2V_y\right)^2. \tag{3.48}$$

Besides Eq. (3.42) yields

$$\left(\omega_c - \omega_{x0} - U_x\right)^2 = \frac{\left|\underline{\hat{K}}_0(l)\right|^2 R^4\,\Omega_0^4}{2\;\omega_{x0}\,\omega_{y0}} - V_x^2\,. \tag{3.49}$$

From Eqs. (3.44), (3.48) and (3.49), the solution ω_c can be obtained

$$\omega_c = \omega_{y0} + l\,\Omega_0 + U_y + \frac{1}{4U_y}\left(\;\Delta\omega_y^2 - \left(V_x + 2V_y\right)^2 - \frac{\left|\underline{\hat{K}}_0(l)\right|^2 R^4\,\Omega_0^4}{2\;\omega_{x0}\,\omega_{y0}} + V_x^2\right). \tag{3.50}$$

Equating $\left(\omega_c - \omega_{y0} - l\,\Omega_0\right)^2$ in Eqs. (3.50) and (3.48) gives a second order equation in $\Delta\omega_y^2 - \left(V_x + 2V_y\right)^2$. This can be solved in $\Delta\omega_y^2$,

$$\Delta\omega_y^2 = 4U_y^2 + 4V_y^2 + 4V_x V_y + \frac{\left|\underline{\hat{K}}_0(l)\right|^2 R^4\,\Omega_0^4}{2\;\omega_{x0}\,\omega_{y0}} \pm 4U_y\left(\frac{\left|\underline{\hat{K}}_0(l)\right|^2 R^4\,\Omega_0^4}{2\;\omega_{x0}\,\omega_{y0}} - V_x^2\right)^{1/2}. \tag{3.51}$$

Using Eq. (3.47), the following equation is obtained

$$\begin{aligned}\Delta\omega_y^2 &= 4U_y^2 + 4V_y^2 + 4V_x V_y + V_x\left(\sqrt{\Delta\omega_y^2 - 4U_y^2} - 2V_y\right)\\ &\pm 4U_y\left[V_x\left(\sqrt{\Delta\omega_y^2 - 4U_y^2} - 2V_y\right) - V_x^2\right]^{1/2},\end{aligned} \tag{3.52}$$

which can be rewritten

$$\left(\Delta\omega_y^2 - 4U_y^2\right)^2 - 2V_x\left(\Delta\omega_y^2 - 4U_y^2\right)^{3/2} + \left[V_x^2 - 4V_y\left(V_x + 2V_y\right)\right]\left(\Delta\omega_y^2 - 4U_y^2\right)$$
$$+ 4V_x\left[V_y\left(V_x + 2V_y\right) - 4U_y^2\right]\left(\Delta\omega_y^2 - 4U_y^2\right)^{1/2} + 4V_y^2\left(V_x + 2V_y\right)^2 + 16\,U_y^2 V_x\left(V_x + 2V_y\right) = 0. \tag{3.53}$$

One has to solve this equation to find the two-dimensional criterion for $\Delta\omega_y$. Let's consider the practical case where $|U| >> V$, then the stability criterion reduces approximately to

$$\Delta\omega_y \geq \sqrt{4U_y^2 + (16\,V_x U_y^2)^{2/3}}\,. \tag{3.54}$$

This criterion is very close to the one-dimensional vertical one (see Eq. (2.50) replacing x by y) but with the important difference that it guarantees stability also for the horizontal plane. Since $|U| >> V$, a rough criterion is therefore just

$$\Delta\omega_y \geq 2\,|U_y|. \tag{3.55}$$

This is a very simple and interesting result which shows all the effectiveness of coupling in machines where $|U| >> V$. At one dimension, one has to compensate U and V, i.e. one has to satisfy Eq. (2.50) for both planes separately. If one uses coupled Landau damping, the main part of the job, the cancellation of the effect of U_x, is done by coupling. Then it roughly remains to Landau damp V_x. Loosely speaking, one plane is thus stabilised by Landau damping and the other one is stabilised by coupling.

Let's come now back to Eq. (3.44). For the particular case treated in this section, the horizontal real coherent betatron frequency in the absence of coupling is

$$\omega_h = \omega_{x0} + U_x\,, \tag{3.56}$$

but the vertical one is

$$\omega_v = \omega_{y0} + l\,\Omega_0 + U_y\left[\Delta\omega_y^2 + 4\left(U_y^2 + V_y^2\right)\right] \,/\, \left[4\left(U_y^2 + V_y^2\right)\right]. \tag{3.57}$$

Therefore, Eq. (3.44) represents the resonance $Q_h - Q_v - l = 0$ at the vertical stability limit where $\Delta\omega_y^2 = 4\left(U_y^2 + V_y^2\right)$. However, when $|U| >> V$, we have seen that the two-dimensional criterion is close to the one-dimensional one, which means that Eq. (3.44) nearly describes the resonance $Q_h - Q_v - l = 0$.

One can verify that, when $\Delta\omega_x$ increases from 0 to the one-dimensional horizontal stability limit $2\sqrt{U_x^2 + V_x^2}$, the required $\Delta\omega_y$ decreases from $\sqrt{4U_y^2 + (16\,V_x U_y^2)^{2/3}}$ to the one-dimensional vertical stability criterion $2\sqrt{U_y^2 + V_y^2}$, which for $|U| >> V$ gives nearly the same value: $\Delta\omega_x$ has thus very little effect in this case.

3.1.4.3 Same distribution function in both planes

If the distribution function is the same in both planes ($\Delta\omega_x = \Delta\omega_y = \Delta\omega$ and $\omega_{x0} = \omega_{y0} + l\Omega_0 = \omega_0$), the dispersion relation writes

$$\begin{aligned}&\left[\omega_c - \omega_0 - j\sqrt{\Delta\omega^2 - \left(\omega_c - \omega_0\right)^2} + 2\left(-U_x + jV_x\right)\right] \times \\ &\left[\omega_c - \omega_0 - j\sqrt{\Delta\omega^2 - \left(\omega_c - \omega_0\right)^2} + 2\left(-U_y + jV_y\right)\right] = \frac{\left|\underline{\hat{K}}_0(l)\right|^2 R^4 \Omega_0^4}{\omega_{x0}\,\omega_{y0}}.\end{aligned} \tag{3.58}$$

This is a second order equation in $X = \omega_c - \omega_0 - j\sqrt{\Delta\omega^2 - \left(\omega_c - \omega_0\right)^2}$ whose solutions are

$$X_{1,2} = \left(U_x + U_y \pm \frac{1}{2}\frac{B}{|B|}\sqrt{\frac{A + \sqrt{A^2 + B^2}}{2}}\right) + j\left(-V_x - V_y \pm \frac{1}{2}\sqrt{\frac{-A + \sqrt{A^2 + B^2}}{2}}\right), \tag{3.59}$$

with

$$\begin{aligned}A &= \frac{4\left|\underline{\hat{K}}_0(l)\right|^2 R^4 \Omega_0^4}{\omega_{x0}\,\omega_{y0}} + 4\left(U_x - U_y\right)^2 - 4\left(V_x - V_y\right)^2, \\ B &= -8\left(U_x - U_y\right)\left(V_x - V_y\right).\end{aligned} \tag{3.60}$$

The solutions $\omega_{c1,2}$ are thus given by

$$\omega_{c1,2} = \omega_0 + X_{\mathrm{R}1,2}\frac{\Delta\omega^2 + X_{\mathrm{R}1,2}^2 + X_{\mathrm{I}1,2}^2}{2\left[X_{\mathrm{R}1,2}^2 + X_{\mathrm{I}1,2}^2\right]} - jX_{\mathrm{I}1,2}\frac{\Delta\omega^2 - X_{\mathrm{R}1,2}^2 - X_{\mathrm{I}1,2}^2}{2\left[X_{\mathrm{R}1,2}^2 + X_{\mathrm{I}1,2}^2\right]}, \tag{3.61}$$

with $X_{\mathrm{R}1,2} = \mathrm{Re}\left(X_{1,2}\right)$ and $X_{\mathrm{I}1,2} = \mathrm{Im}\left(X_{1,2}\right)$, where $\mathrm{Re}(\ )$ and $\mathrm{Im}(\ )$ represent the real and imaginary parts. Since $X_{\mathrm{I}1,2}$ are always negative (for $V_{x,y} > 0$), the stability criterion $\mathrm{Im}\left(\omega_{c1,2}\right) \geq 0$ becomes

$$\Delta\omega \geq \sqrt{X_{\mathrm{R}1,2}^2 + X_{\mathrm{I}1,2}^2}, \tag{3.62}$$

which yields

$$\Delta\omega \geq \left[\left(U_x + U_y \pm \frac{1}{2}\frac{B}{|B|}\sqrt{\frac{A + \sqrt{A^2 + B^2}}{2}}\right)^2 + \left(-V_x - V_y \pm \frac{1}{2}\sqrt{\frac{-A + \sqrt{A^2 + B^2}}{2}}\right)^2\right]^{1/2}. \tag{3.63}$$

In the particular case where $U_x = U_y = U$, the stability criterion takes different forms according to the value of the coupling.

For $\left|\underline{\hat{K}}_0(l)\right| < \frac{\left|V_x - V_y\right|}{R^2\,\Omega_0^2}\sqrt{\omega_{x0}\,\omega_{y0}}$, it reduces to

$$\Delta\omega \geq \left[4U^2 + \left(V_x + V_y + \sqrt{\left(V_x - V_y\right)^2 - \frac{\left|\underline{\hat{K}}_0(l)\right|^2 R^4\,\Omega_0^4}{\omega_{x0}\,\omega_{y0}}}\right)^2\right]^{1/2}. \tag{3.64}$$

For $\left|\underline{\hat{K}}_0(l)\right| = \frac{\left|V_x - V_y\right|}{R^2\,\Omega_0^2}\sqrt{\omega_{x0}\,\omega_{y0}}$, it reduces to

$$\Delta\omega \geq \left[4U^2 + \left(V_x + V_y\right)^2\right]^{1/2}. \tag{3.65}$$

For $\left|\underline{\hat{K}}_0(l)\right| > \frac{\left|V_x - V_y\right|}{R^2\,\Omega_0^2}\sqrt{\omega_{x0}\,\omega_{y0}}$, it reduces to

$$\Delta\omega \geq \left[\left(2\left|U\right| + \sqrt{\frac{\left|\underline{\hat{K}}_0(l)\right|^2 R^4\,\Omega_0^4}{\omega_{x0}\,\omega_{y0}} - \left(V_x - V_y\right)^2}\right)^2 + \left(V_x + V_y\right)^2\right]^{1/2}. \tag{3.66}$$

The optimum coupling is thus $\left|\underline{\hat{K}}_0(l)\right| = \sqrt{\omega_{x0}\,\omega_{y0}}\,\left|V_x - V_y\right| / \left(R^2\,\Omega_0^2\right)$. Equation (3.66) shows the effect of a too strong coupling. It adds to the U - term and thus can shift the coherent frequency outside the spread. If in addition $V_x = V_y = V$, the stability criterion becomes

$$\Delta\omega \geq 2\sqrt{\left(\left|U\right| + \frac{\left|\underline{\hat{K}}_0(l)\right| R^2\,\Omega_0^2}{2\sqrt{\omega_{x0}\,\omega_{y0}}}\right)^2 + V^2}. \tag{3.67}$$

If $\left|\underline{\hat{K}}_0(l)\right| = 0$, the one-dimensional criterion is recovered (see Eq. (2.50)). If $\left|\underline{\hat{K}}_0(l)\right|$ increases, one has to increase the spread according to Eq. (3.67). Therefore, any coupling is bad in that particular case since the stability condition of Eq. (3.67) is more restrictive than the one-dimensional stability criterion.

3.1.4.4 No transverse real frequency shifts

In the absence of horizontal and vertical real frequency shifts ($U_x = U_y = 0$), the dispersion relation writes

$$\begin{aligned}&\left\{\omega_c - \omega_{x0} - j\left[\sqrt{\Delta\omega_x^2 - \left(\omega_c - \omega_{x0}\right)^2} - 2V_x\right]\right\} \times \\ &\left\{\omega_c - \omega_{y0} - l\,\Omega_0 - j\left[\sqrt{\Delta\omega_y^2 - \left(\omega_c - \omega_{y0} - l\,\Omega_0\right)^2} - 2V_y\right]\right\} = \frac{\left|\underline{\hat{K}}_0(l)\right|^2 R^4\,\Omega_0^4}{\omega_{x0}\,\omega_{y0}}.\end{aligned} \tag{3.68}$$

In this case, practically the same result as in the Lorentzian case is found. In fact stability, on the resonance $Q_h - Q_v - l = 0$ and for the coupling $\left|\underline{\hat{K}}_0(l)\right| = \left[-Q_{x0}\,Q_{y0}\left(\Delta\omega_x - 2V_x\right)\left(\Delta\omega_y - 2V_y\right)\right]^{1/2} / \left(R^2\,\Omega_0\right)$, is reached when

$$\Delta\omega_x + \Delta\omega_y \geq 2\left(V_x + V_y\right). \tag{3.69}$$

3.1.4.5 Approximate general stability criterion

An approximate general stability criterion can be expressed as follows. Two cases appear depending on whether the transverse coherent tunes (in the absence of coupling) are "far from" or "near" to the coupling resonances. These two terms will be explained at the end of this section.

1) Q_h "far from" $Q_v + l$:

In this case, the result of coupling is a sharing of the instability growth rates only. There is no transfer of Landau damping since the coherent tunes are too far from each other to share their stabilising spreads. The equation that has to be solved to obtain the stability criterion can be approximated by Eq. (3.29) with $\Delta\omega_{x,y} = 0$. The equation that is obtained is the same as Eq. (3.20) with $\delta\omega_{x,y} = 0$. By analogy with the Lorentzian case, the necessary condition for stability is (see Eq. (3.26))

$$V_x + V_y \leq 0. \tag{3.70}$$

If Eq. (3.70) is true then it is possible to stabilise the beam and the stability criterion is given by Eq. (3.27) with $\delta\omega_{x,y} = 0$.

2) Q_h "near" $Q_v + l$:

In this case, in addition to the sharing of the instability growth rates, there is also a transfer of Landau damping. Equation (3.29) is then approximated by

$$\left\{\omega_c - \omega_{x0} - \frac{\Delta\omega_x^2 + 4U_x^2}{4U_x} - j\left[\mathrm{Re}\left(\sqrt{\Delta\omega_x^2 - 4U_x^2}\right) - 2V_x\right]\right\} \times$$
$$\left\{\omega_c - \omega_{y0} - l\,\Omega_0 - \frac{\Delta\omega_y^2 + 4U_y^2}{4U_y} - j\left[\mathrm{Re}\left(\sqrt{\Delta\omega_y^2 - 4U_y^2}\right) - 2V_y\right]\right\} = \frac{\left|\underline{\hat{K}}_0(l)\right|^2 R^4\,\Omega_0^4}{\omega_{x0}\,\omega_{y0}}. \tag{3.71}$$

Here, the square root has to be omitted if the argument under the root is negative. The necessary condition for stability is thus

$$\mathrm{Re}\left(\sqrt{\Delta\omega_x^2 - 4U_x^2} + \sqrt{\Delta\omega_y^2 - 4U_y^2}\right) \geq 2\left(V_x + V_y\right). \tag{3.72}$$

If Eq. (3.72) is true then it is possible to stabilise the beam and a condition similar to Eq. (3.27) for the stabilising values of the coupling coefficient may be approximated by

$$\left|\underline{\hat{K}}_0(l)\right| \approx \frac{\left\{-Q_{x0}\,Q_{y0}\left[\mathrm{Re}\left(\sqrt{\Delta\omega_x^2-4U_x^2}\right)-2V_x\right]\left[\mathrm{Re}\left(\sqrt{\Delta\omega_y^2-4U_y^2}\right)-2V_y\right]\right\}^{1/2}}{R^2\,\Omega_0}. \quad (3.73)$$

The criterion can be checked numerically. One solution of Eq. (3.29) is always at the stability limit, i.e. $\mathrm{Im}(\omega_c)=0$ whereas the other has generally $\mathrm{Im}(\omega_c)\neq 0$, but the stabilising vertical frequency spread is very close to the solution. The criterion holds exactly in the limiting cases where $\Delta\omega_x = U_y = V_y = 0$ or when $U_x = U_y = 0$ or when $\Delta\omega_x = \Delta\omega_y$ and $U_x = U_y$. In the practical case where $|U| >> V$, the criterion is nearly the one-dimensional one and Eq. (3.72) is an approximate condition for stability in both planes. Therefore, to have an idea of the stability criterion in the general case, this approximate formula, which is always close to the solution to within a few percent, can be used.

Equation (3.72) generalises the one-dimensional stability conditions, which can be written as

$$\mathrm{Re}\left(\sqrt{\Delta\omega_x^2-4U_x^2}\right)\geq 2V_x, \qquad \mathrm{Re}\left(\sqrt{\Delta\omega_y^2-4U_y^2}\right)\geq 2V_y, \quad (3.74)$$

or equivalently (in the more familiar form, for $V_{x,y} > 0$)

$$\Delta\omega_x \geq 2\left|U_x - jV_x\right|, \qquad \Delta\omega_y \geq 2\left|U_y - jV_y\right|. \quad (3.75)$$

The result (Eq. (3.72)) reveals the features mentioned earlier that the imaginary part (U) of the coupling impedance in the unstable plane can be "cancelled" by coupling. The frequency spreads are shared between the two planes and a large tune dispersion becomes effective also in the plane which, without coupling, has little spread.

Coming back to the terms "far from" and "near" to the coupling resonances used above and guided by the results of numerical solutions of Eq. (3.29), it can be concluded that the stability is obtained for coupling values in a range near the value given by Eq. (3.73) and that the tune separation $\left|Q_h - Q_v - l\right|$ should be smaller than the order of magnitude of $\left(\Delta\omega_x + \Delta\omega_y\right)/\Omega_0$ (which seems to be very small) in order to have the transfer of Landau damping.

3.2 Rigid bunched beams

In most accelerators, the RF acceleration mechanism generates azimuthal non-uniformity of particle density and consequently the work of Laslett, Neil and Sessler for continuous beams[26] is not applicable in the case of bunched beams. Courant and Sessler have studied the case of rigid (point-like) bunches, i.e. bunches oscillating as rigid units, and they have shown that the transverse electromagnetic coupling of bunches of particles with each other can lead (due to the effect of imperfectly conducting vacuum chamber walls) to a coherent instability.[40] The physical basis of the instability is that in a resistive vacuum tank, fields due to a particle decay only very slowly in time after the particle has left (long-range interaction). The decay can be so slow that when a bunch returns after one (or more) revolutions it is subject to its own residual wake field which, depending upon its phase relative to the wake field, can lead to damped or undamped transverse motion.

This section extends the results of Courant and Sessler, introducing coupling between the transverse planes into the Landau damping calculation of rigid modes.[38,40] The case of M equally spaced and equally populated (N_b particles per bunch) short rigid bunches is examined.

3.2.1 Equations of motion

The electromagnetic problem is considered first (e.g. in the horizontal plane and without coupling), then the particle dynamics. The horizontal force exerted on itself by a bunched beam is obtained by using the results of Laslett, Neil and Sessler, whose treatment is confined to continuous beams of azimuthally constant density and dimensions, oscillating coherently in such a mode that its horizontal electric dipole moment per unit azimuthal angle ϑ is[41]

$$\frac{dP_x}{d\vartheta} = \frac{dN}{d\vartheta}\Delta_x e^{j\omega t}, \tag{3.76}$$

where $\Delta_x e^{j\omega t}$ describes the rigid horizontal beam oscillations ($\bar{x}$) at a fixed azimuthal position ϑ and $dN/d\vartheta$ is the constant linear density. The interaction between the oscillating beam and the vacuum chamber leads to induced electromagnetic fields and thus to a force F_x acting on each particle of the beam, which has the form

$$F_x = e\left(\vec{E} + \vec{v}\times\vec{B}\right)_x = \frac{dP_x}{d\vartheta}\left(U_{1x} + \sqrt{\frac{-j}{\omega}}\,W_x\right), \tag{3.77}$$

where U_{1x} and W_x are real coefficients proportional to the dispersion relation coefficients U_x and V_x (of Laslett, Neil and Sessler) respectively. Indeed, in the case of coasting beams, $dN/d\vartheta = N/2\pi$, and the wake force exerted on each particle of the beam is given by (see Eqs. (2.6), (2.7) and (2.25))

$$F_x \approx 2\omega_{x0}\left(-U_x - V_x + jV_x\right)\bar{x}, \tag{3.78}$$

using the footnote of page 9. From Eqs. (3.77) and (3.78), one deduces that

$$U_{1x} = -\frac{4\pi\omega_{x0}}{N}U_x, \qquad W_x = \frac{4\pi\omega_{x0}}{N}\sqrt{2\omega}\,V_x. \tag{3.79}$$

To find the fields associated with bunches of arbitrary shape, the somewhat indirect (but transparent) method of first finding the field due to a single particle *r* at the position of another single (test) particle *i*, and then superposing the results, is used. Consider therefore a single particle *r* circulating with the angular frequency Ω_0 (assumed to be the same for all the particles of the beam) and oscillating horizontally with the betatron frequency $Q_{x,r}\,\Omega_0$ and the amplitude $\hat{x}_r$. Its equation of motion is

$$x_r = \hat{x}_r e^{j\left(Q_{x,r}\Omega_0 t + \varphi_{0x,r}\right)}, \qquad \vartheta_r = \vartheta_{0r} + \Omega_0 t. \tag{3.80}$$

The horizontal dipole moment per unit azimuthal angle ϑ of the *r*th particle is thus

$$\frac{dP_{x,r}}{d\vartheta} = \hat{x}_r \, e^{j\left(Q_{x,r}\,\Omega_0\,t+\varphi_{0x,r}\right)}\,\delta_p\left(\vartheta-\vartheta_{0r}-\Omega_0\,t\right), \tag{3.81}$$

where δ_p is the periodic Dirac function

$$\delta_p = \sum_{p=-\infty}^{p=+\infty}\delta\left(\vartheta-\vartheta_{0r}-\Omega_0\,t+2\pi\,p\right) = \frac{1}{2\pi}\sum_{k=-\infty}^{k=+\infty} e^{-j\,k\left(\vartheta-\vartheta_{0r}-\Omega_0\,t\right)}. \tag{3.82}$$

Therefore,

$$\frac{dP_{x,r}}{d\vartheta} = \frac{\hat{x}_r}{2\pi}\,e^{j\,\varphi_{0x,r}}\sum_{k=-\infty}^{k=+\infty} e^{-j\left[k\left(\vartheta-\vartheta_{0r}\right)-\left(k+Q_{x,r}\right)\Omega_0\,t\right]}. \tag{3.83}$$

Each term of the summation in Eq. (3.83) has the form of Eq. (3.76) and thus contributes to the force f_x exerted by the particle *r* on itself and on all the other particles of the beam. Substituting Eq. (3.83) into Eq. (3.77), replacing ω by $\left(k+Q_{x,r}\right)\Omega_0$, yields

$$\begin{aligned} f_x &= \frac{\hat{x}_r}{2\pi}\,e^{j\,\varphi_{0x,r}}\sum_{k=-\infty}^{k=+\infty}\left[U_{1x}+\sqrt{\frac{-\,j}{\left(k+Q_{x,r}\right)\,\Omega_0}}\,W_x\right]e^{-j\left[k\left(\vartheta-\vartheta_{0r}\right)-\left(k+Q_{x,r}\right)\Omega_0\,t\right]} \\ &= U_{1x}\,\frac{dP_{x,r}}{d\vartheta}+\frac{W_x}{2\pi\sqrt{\Omega_0}}\,\hat{x}_r\,e^{j\left(Q_{x,r}\,\Omega_0\,t+\varphi_{0x,r}\right)}\,G\left(\vartheta_{0r}+\Omega_0\,t-\vartheta,Q_{x,r}\right), \end{aligned} \tag{3.84}$$

where

$$G\left(\vartheta_{0r}+\Omega_0\,t-\vartheta,Q_{x,r}\right) = \sum_{k=-\infty}^{k=+\infty}\sqrt{\frac{-\,j}{k+Q_{x,r}}}\,e^{j\,k\left(\vartheta_{0r}+\Omega_0\,t-\vartheta\right)} = \sum_{k=-\infty}^{k=+\infty}\sqrt{\frac{j}{k-Q_{x,r}}}\,e^{-j\,k\left(\vartheta_{0r}+\Omega_0\,t-\vartheta\right)}, \tag{3.85}$$

for $0<\vartheta_{0r}+\Omega_0\,t-\vartheta\le 2\pi$. G is the bunch function, which is defined to be periodic in $\vartheta_{0r}+\Omega_0\,t-\vartheta$ with period 2π. This function takes into account the contribution of the *r*th particle to the horizontal wake field at the place ϑ and at the time t from all its previous turns. It can be shown that[40]

$$G\left(\vartheta_{0r}+\Omega_0\,t-\vartheta,Q_{x,r}\right) = 2\sqrt{\pi}\sum_{s=0}^{s=+\infty}\frac{e^{-j\,Q_{x,r}\left(\vartheta_{0r}+\Omega_0\,t-\vartheta+2\pi\,s\right)}}{\sqrt{\vartheta_{0r}+\Omega_0\,t-\vartheta+2\pi\,s}}. \tag{3.86}$$

The equation of betatron motion of the test particle *i* in the *b*th bunch, subject to the sum of the forces given by Eq. (3.84) for the *r*th particle (evaluated at the position of the *i*th particle $\vartheta_i=\vartheta_{0i}+\Omega_0\,t$), as well as the restoring force of the external focusing field, is thus

$$m_0\,\gamma\left(\ddot{x}_i+\omega_{x,i}^2\,x_i\right) = U_{1x}\left(\sum\frac{dP_{x,r}}{d\vartheta}\right)_b+\frac{W_x}{2\pi\sqrt{\Omega_0}}\sum_r x_r\,G\left(\vartheta_r-\vartheta_i,Q_{x,r}\right). \tag{3.87}$$

Here, $\left(\sum dP_{x,r} / d\vartheta\right)_b$ is the sum of the horizontal dipole moments per unit azimuthal angle ϑ over all the particles of the *b*th bunch, and the second summation of Eq. (3.87) has to be made over all the particles of the beam.

If in addition to the wake fields, the linear coupling forces, represented by the normalised skew gradient (see Section 3.1), are also considered, Eq. (3.87) becomes

$$m_0 \gamma \left(\ddot{x}_i + \omega_{x,i}^2 x_i\right) = U_{1x}\left(\sum \frac{dP_{x,r}}{d\vartheta}\right)_b + \frac{W_x}{2\pi\sqrt{\Omega_0}} \sum_r x_r G\left(\vartheta_r - \vartheta_i, Q_{x,r}\right) + m_0 \gamma \underline{K}_i R_i^2 \Omega_i^2 y_i . \tag{3.88}$$

A similar equation is found for the vertical plane by exchanging the roles of the variables x and y in Eq. (3.88). In the following, the revolution frequency Ω_i is replaced by its average value Ω_0 in the coupling term, the orbit radius R_i is replaced by its average value R, and the skew gradient is supposed to be the same for all the particles, i.e. $\underline{K}_i = \underline{K}_0$.

3.2.2 Two-dimensional dispersion relation

In the following, transverse betatron frequency spreads specified by externally given beam frequency spectra are assumed. The ensemble of particles has spectra with the distribution functions $\rho_x(\omega_{x,i})$ and $\rho_y(\omega_{y,i})$ which are supposed to be uncorrelated and normalised to unity (see Eq. (2.20)). Furthermore, linear coupling is described by Eqs. (3.15) and (3.16). Considering only the dominant Fourier component of the coupling (*l*) and following the standard procedure of identifying normal mode frequencies, yields particular solutions of the form

$$x_i = X_i e^{j\omega_c t}, \qquad y_i = Y_i e^{j(\omega_c - l\Omega_0)t}, \tag{3.89}$$

where ω_c is the coherent betatron frequency to be determined. Substituting Eqs. (3.89) into Eq. (3.88) and dividing by $e^{j\omega_c t}$ in both sides, yields

$$m_0 \gamma X_i = \frac{1}{\omega_{x,i}^2 - \omega_c^2}\left[\begin{array}{l} U_{1x}\left(\sum \frac{dP_{x,r}\, e^{-j\omega_c t}}{d\vartheta}\right)_b + \frac{W_x}{2\pi\sqrt{\Omega_0}} \sum_r X_r G\left(\vartheta_r - \vartheta_i, Q_c\right) \\ + m_0 \gamma R^2 \Omega_0^2 \hat{\underline{K}}_0(l)\, Y_i\, e^{jl\vartheta_{0i}} \end{array}\right]. \tag{3.90}$$

There are as many (horizontal) equations (3.90) as there are particles in the beam ($N_b M$). But this huge amount can be reduced to M by summing over all the particles in a bunch assuming that each bunch oscillates as a rigid unit. The l.h.s of Eq. (3.90) yields

$$\left(\sum_i X_i\right)_b = N_b \overline{\left(X_i\right)_b} = D_x^b . \tag{3.91}$$

Here, D_x^b is the amplitude of the horizontal dipole moment of the *b*th bunch. The r.h.s of Eq. (3.90) leads to

$$\left(\sum_i \frac{1}{\omega_{x,i}^2-\omega_c^2}(\ )\right)_b = N_b \int_{-\infty}^{+\infty} \frac{\rho_x(\omega_{x,i})\,d\omega_{x,i}}{\omega_{x,i}^2-\omega_c^2}\overline{(\ )}\,, \tag{3.92}$$

where the average $\overline{(\ )}$ refers to the particles of the bth bunch. The first term gives

$$\left(\sum \frac{dP_{x,r}\,e^{-j\omega_c t}}{d\vartheta}\right)_b = \frac{N_b\,\overline{(X_r)_b}}{\Delta\vartheta} = \frac{D_x^b}{\Delta\vartheta}, \tag{3.93}$$

where $\Delta\vartheta$ is the common length in angle of the bunches. The second term gives, for $\Delta\vartheta\to 0$,[40]

$$\overline{\sum_r X_r\,G(\vartheta_r-\vartheta_i,Q_c)} = \sum_{b'\neq b} D_x^{b'}G(\vartheta_{b'}-\vartheta_b,Q_c)+D_x^bG(2\pi,Q_c). \tag{3.94}$$

Finally, the third term gives

$$\overline{Y_i\,e^{jl\vartheta_{0i}}} = \frac{D_y^b}{N_b}e^{j2\pi\frac{lb}{M}}\,, \tag{3.95}$$

since the M bunches are equally spaced around the machine. Therefore, one finally obtains

$$m_0\gamma D_x^b = \left[\begin{array}{l} \dfrac{N_b U_{1x}}{\Delta\vartheta}D_x^b + \dfrac{N_b W_x}{2\pi\sqrt{\Omega_0}}D_x^b\,G(2\pi,Q_c) \\ +\dfrac{N_b W_x}{2\pi\sqrt{\Omega_0}}\displaystyle\sum_{b'\neq b} D_x^{b'}\,G(\vartheta_{b'}-\vartheta_b,Q_c) \\ +m_0\gamma R^2\,\Omega_0^2\,\underline{\hat{K}}_0(l)\,D_y^b\,e^{j2\pi\frac{lb}{M}} \end{array}\right] \times \int_{-\infty}^{+\infty}\frac{\rho_x(\omega_{x,i})\,d\omega_{x,i}}{\omega_{x,i}^2-\omega_c^2}. \tag{3.96}$$

Equation (3.96) can be rewritten

$$\begin{aligned} &\left[N_b\left(\frac{U_{1x}}{\Delta\vartheta}+\frac{W_x}{2\pi\sqrt{\Omega_0}}G(2\pi,Q_{x0})\right)-\lambda_x(\omega_c)\right]D_x^b+\frac{N_b W_x}{2\pi\sqrt{\Omega_0}}\sum_{b'\neq b}D_x^{b'}\,G(\vartheta_{b'}-\vartheta_b,Q_{x0}) \\ &=-m_0\gamma R^2\,\Omega_0^2\,\underline{\hat{K}}_0(l)\,D_y^b\,e^{j2\pi\frac{lb}{M}}\,, \end{aligned} \tag{3.97}$$

where

$$\lambda_x(\omega_c)=m_0\gamma\left(\int_{-\infty}^{+\infty}\frac{\rho_x(\omega_{x,i})\,d\omega_{x,i}}{\omega_{x,i}^2-\omega_c^2}\right)^{-1}. \tag{3.98}$$

Here, the approximation $\omega_c\approx\omega_{x0}$ has been made in the bunch function G. The system of equations (3.97) may be cast into the eigensystem

$$\left[A_x-\lambda_x(\omega_c)\,I_M\right]X=-m_0\gamma R^2\,\Omega_0^2\,\underline{\hat{K}}_0(l)\,Y. \tag{3.99}$$

Here, I_M is the $M \times M$ identity matrix. The vectors X, Y and the matrix A_x are of the form

$$X = \left[D_x^0, D_x^1, ..., D_x^{M-1} \right]^t,$$

$$Y = \left[D_y^0, D_y^1 e^{j2\pi \frac{l}{M}}, ..., D_y^b e^{j2\pi \frac{lb}{M}}, ..., D_y^{M-1} e^{j2\pi \frac{l(M-1)}{M}} \right]^t, \tag{3.100}$$

$$A_x = \begin{bmatrix} A_x^0 & A_x^1 & ... & A_x^{M-1} \\ A_x^{M-1} & A_x^0 & ... & A_x^{M-2} \\ ... & ... & ... & ... \\ A_x^1 & A_x^2 & ... & A_x^0 \end{bmatrix}, \tag{3.101}$$

with, for $r = 1,2,..., M-1$,

$$A_x^0 = \frac{N_b U_{1x}}{\Delta \vartheta} + \frac{N_b W_x}{2\pi \sqrt{\Omega_0}} G(2\pi, Q_{x0}), \qquad A_x^r = \frac{N_b W_x}{2\pi \sqrt{\Omega_0}} G\left(\frac{2\pi r}{M}, Q_{x0} \right). \tag{3.102}$$

The vertical equation of motion corresponding to Eq. (3.97) is

$$\begin{aligned} &\left[N_b \left(\frac{U_{1y}}{\Delta \vartheta} + \frac{W_y}{2\pi \sqrt{\Omega_0}} G(2\pi, Q_{y0}) \right) - \lambda_y(\omega_c - l\Omega_0) \right] D_y^b \\ &+ \frac{N_b W_y}{2\pi \sqrt{\Omega_0}} \sum_{b' \neq b} D_y^{b'} G(\vartheta_{b'} - \vartheta_b, Q_{y0}) = -m_0 \gamma R^2 \Omega_0^2 \underline{\hat{K}}_0(-l) D_x^b e^{-j2\pi \frac{lb}{M}}, \end{aligned} \tag{3.103}$$

using also the approximation $\omega_c - l\Omega_0 \approx \omega_{y0}$ in the bunch function G, and with

$$\lambda_y(\omega_c - l\Omega_0) = m_0 \gamma \left(\int_{-\infty}^{+\infty} \frac{\rho_y(\omega_{y,i})\, d\omega_{y,i}}{\omega_{y,i}^2 - (\omega_c - l\Omega_0)^2} \right)^{-1}. \tag{3.104}$$

Multiplying both sides of Eq. (3.103) by $e^{j2\pi \frac{lb}{M}}$, yields

$$\begin{aligned} &\left[N_b \left(\frac{U_{1y}}{\Delta \vartheta} + \frac{W_y}{2\pi \sqrt{\Omega_0}} G(2\pi, Q_{y0}) \right) - \lambda_y(\omega_c - l\Omega_0) \right] D_y^b e^{j2\pi \frac{lb}{M}} \\ &+ \frac{N_b W_y}{2\pi \sqrt{\Omega_0}} \sum_{b' \neq b} D_y^{b'} e^{j2\pi \frac{lb}{M}} G(\vartheta_{b'} - \vartheta_b, Q_{y0}) = -m_0 \gamma R^2 \Omega_0^2 \underline{\hat{K}}_0(-l) D_x^b. \end{aligned} \tag{3.105}$$

Using the fact that

$$D_y^{b'}\, e^{j2\pi\frac{lb}{M}}\, G\left(\vartheta_{b'}-\vartheta_b, Q_{y0}\right)=D_y^{b'}\, e^{j2\pi\frac{lb'}{M}}\, e^{-j2\pi\frac{l(b'-b)}{M}}\, G\left(\vartheta_{b'}-\vartheta_b, Q_{y0}\right)$$
$$=D_y^{b'}\, e^{j2\pi\frac{lb'}{M}}\, G\left(\vartheta_{b'}-\vartheta_b, Q_{y0}+l\right), \tag{3.106}$$

since from the definition of the bunch function given by Eq. (3.85),

$$e^{-jl\vartheta}\, G\left(\vartheta, Q_{y0}\right)= G\left(\vartheta, Q_{y0}+l\right), \tag{3.107}$$

Eq. (3.105) may then be cast into the eigensystem

$$\left[A_y-\lambda_y\left(\omega_c-l\Omega_0\right) I_M\right] Y=-m_0\,\gamma\, R^2\,\Omega_0^2\,\underline{\hat{K}}_0(-l)\, X\,. \tag{3.108}$$

Here, the matrix A_y is given by Eq. (3.101) replacing x by y, with, for $r=1,2,...,M-1$,

$$A_y^0=\frac{N_b\, U_{1y}}{\Delta\vartheta}+\frac{N_b\, W_y}{2\pi\sqrt{\Omega_0}}\, G\left(2\pi, Q_{y0}+l\right), \qquad A_y^r=\frac{N_b\, W_y}{2\pi\sqrt{\Omega_0}}\, G\left(\frac{2\pi r}{M}, Q_{y0}+l\right). \tag{3.109}$$

The coefficient A_y^0 is deduced from Eq. (3.105) using Eq. (3.107) with $\vartheta=2\pi$. From Eqs. (3.99) and (3.108), the following eigensystem must be satisfied

$$\left\{A-\left[m_0\,\gamma\; R^2\,\Omega_0^2\left|\underline{\hat{K}}_0(l)\right|\right]^2 I_M\right\} Y=0, \tag{3.110}$$

where A is the matrix defined by

$$A=\left[A_x-\lambda_x\left(\omega_c\right) I_M\right]\left[A_y-\lambda_y\left(\omega_c-l\Omega_0\right) I_M\right], \tag{3.111}$$

with, for $r=1,2,...,M-1$,

$$A^0=A[1,1]=\left[A_x^0-\lambda_x\left(\omega_c\right)\right]\left[A_y^0-\lambda_y\left(\omega_c-l\Omega_0\right)\right]+A_x^1\, A_y^{M-1}+...+A_x^{M-1}\, A_y^1\,,$$
$$A^r=A[1,r+1]=\left[A_x^0-\lambda_x\left(\omega_c\right)\right] A_y^r+A_x^1\, A_y^{r-1}+...+A_x^r\left[A_y^0-\lambda_y\left(\omega_c-l\Omega_0\right)\right] \tag{3.112}$$
$$+A_x^{r+1}\, A_y^{M-1}+...+A_x^{M-1}\, A_y^{r+1}\,.$$

The matrix A has cyclic coefficients (like A_x and A_y) and the solution is well-known. M relations are obtained

$$\left(m_0\,\gamma\, R^2\,\Omega_0^2\left|\underline{\hat{K}}_0(l)\right|\right)^2=\sum_{r=0}^{M-1} A^r e^{-j2\pi\frac{n_x r}{M}}\,, \qquad n_x=0,1,...,M-1. \tag{3.113}$$

As we will see, n_x is the horizontal coupled-bunch mode number. Equation (3.113) leads to M dispersion relations

$$\left(m_0\,\gamma\,R^2\,\Omega_0^2\left|\underline{\hat{K}}_0(l)\right|\right)^2=\left[\sum_{r=0}^{M-1}A_x^r\,e^{-j\,2\pi\frac{n_x\,r}{M}}-\lambda_x(\omega_c)\right]\left[\sum_{r=0}^{M-1}A_y^r\,e^{-j\,2\pi\frac{n_x\,r}{M}}-\lambda_y(\omega_c-l\,\Omega_0)\right], \tag{3.114}$$

or equivalently

$$\begin{aligned}&\left[\left(\int_{-\infty}^{+\infty}\frac{\rho_x(\omega_{x,i})\,d\omega_{x,i}}{\omega_c-\omega_{x,i}}\right)^{-1}-U_{\mathrm{eq}x}^{n_x}+jV_{\mathrm{eq}x}^{n_x}\right]\times\\&\left[\left(\int_{-\infty}^{+\infty}\frac{\rho_y(\omega_{y,i})\,d\omega_{y,i}}{\omega_c-l\,\Omega_0-\omega_{y,i}}\right)^{-1}-U_{\mathrm{eq}y}^{n_y}+jV_{\mathrm{eq}y}^{n_y}\right]=\frac{\left|\underline{\hat{K}}_0(l)\right|^2R^4\,\Omega_0^4}{4\,\omega_{x0}\,\omega_{y0}},\end{aligned} \tag{3.115}$$

where we have introduced "equivalent" dispersion relation coefficients $U_{\mathrm{eq}x,y}^{n_{x,y}}$ and $V_{\mathrm{eq}x,y}^{n_{x,y}}$, defined by

$$\begin{aligned}U_{\mathrm{eq}x,y}^{n_{x,y}}&=-\mathrm{Re}\left(\sum_{r=0}^{M-1}A_{x,y}^r\,e^{-j\,2\pi\frac{n_x\,r}{M}}\right)/\left(2\,\omega_{x0,y0}\,m_0\,\gamma\right),\\V_{\mathrm{eq}x,y}^{n_{x,y}}&=\mathrm{Im}\left(\sum_{r=0}^{M-1}A_{x,y}^r\,e^{-j\,2\pi\frac{n_x\,r}{M}}\right)/\left(2\,\omega_{x0,y0}\,m_0\,\gamma\right).\end{aligned} \tag{3.116}$$

These coefficients are the transverse real frequency shifts and instability growth rates respectively, for given horizontal and vertical rigid modes, in the absence of both coupling and Landau damping. It can be shown that[40]

$$\left(\sum_{r=0}^{M-1}A_x^r\,e^{-j\,2\pi\frac{n_x\,r}{M}}\right)/\left(2\,\omega_{x0}\,m_0\,\gamma\right)=\frac{N_b}{2\,\omega_{x0}\,m_0\,\gamma}\left[\frac{U_{1x}}{\Delta\vartheta}+\frac{W_x}{2\,\pi\sqrt{\Omega_0}}\sqrt{M}\,G\left(2\,\pi,\frac{Q_{x0}+n_x}{M}\right)\right]. \tag{3.117}$$

Therefore, from Eqs. (3.109) and (3.117), one obtains

$$\left(\sum_{r=0}^{M-1}A_y^r\,e^{-j\,2\pi\frac{n_x\,r}{M}}\right)/\left(2\,\omega_{y0}\,m_0\,\gamma\right)=\frac{N_b}{2\,\omega_{y0}\,m_0\,\gamma}\left[\frac{U_{1y}}{\Delta\vartheta}+\frac{W_y}{2\,\pi\sqrt{\Omega_0}}\sqrt{M}\,G\left(2\,\pi,\frac{Q_{y0}+l+n_x}{M}\right)\right]. \tag{3.118}$$

The vertical coupled-bunch mode number is thus related to the horizontal one by $n_y=n_x+l$. By virtue of Eqs. (3.115) and (3.116), the transverse instability growth rates with neither (horizontal to vertical) coupling nor Landau damping are given by

$$\begin{aligned}V_{\mathrm{eq}x,y}^{n_{x,y}}&=\frac{1}{2\,\omega_{x0,y0}\,m_0\,\gamma}\mathrm{Im}\left(\sum_{r=0}^{M-1}A_{x,y}^r\,e^{-j\,2\pi\frac{n_x\,r}{M}}\right)\\&=\frac{N_b\,W_{x,y}}{4\,\omega_{x0,y0}\,m_0\,\gamma\,\pi\sqrt{\Omega_0}}\sqrt{M}\,\mathrm{Im}\left[G\left(2\,\pi,\frac{Q_{x0,y0}+n_{x,y}}{M}\right)\right].\end{aligned} \tag{3.119}$$

They depend on the function $\mathrm{Im}\left[G(2\pi,x)\right]$, which is a well-known periodic function, with period $\Delta x = 1$, that is plotted in Figure 10. The value of $\mathrm{Im}\left[G(2\pi,x)\right]$ is determined by subtracting an integer from x to obtain a value between 0 and 1. It then remains to read the value on Figure 10.

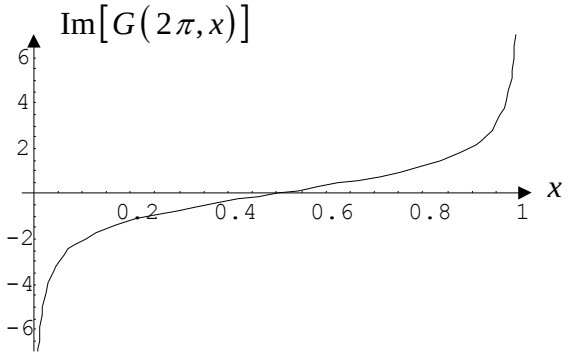

FIGURE 10 Imaginary part of the bunch function $\mathrm{Im}\left[G(2\pi,x)\right]$.

The M dispersion relations of Eq. (3.115) lead to $2M$ coherent oscillation frequencies. Knowing the solutions ω_c, the rigid-bunch (or coupled-bunch, referring here to the coupling between the bunches and not to the horizontal to vertical coupling) vertical modes can be determined by solving the eigensystem (3.110) with respect to Y. In this way, M rigid-bunch modes are found and the relations between the dipole moments of the bunches, in the rigid-bunch mode n_y, are the same for coupled as for uncoupled planes. Indeed, putting Eq. (3.113) into Eq. (3.110), one obtains

$$\frac{D_y^b\, e^{j2\pi\frac{lb}{M}}}{D_y^0} = e^{-j2\pi\frac{bn_x}{M}}, \qquad b = 0,1,...,M-1, \tag{3.120}$$

which leads to

$$\frac{D_y^b}{D_y^0} = e^{-j2\pi\frac{bn_x}{M}}\, e^{-j2\pi\frac{lb}{M}} = e^{-j2\pi\frac{bn_y}{M}} = \frac{\left(D_y^b\right)_{n_y}}{\left(D_y^0\right)_{n_y}}. \tag{3.121}$$

The relation between the vertical dipole moments do correspond to the coupled-bunch mode number n_y. Equation (3.110), deduced from Eqs. (3.99) and (3.108), can also be written with *X* in place of *Y*. The relation between the horizontal dipole moments is obtained in the same way, and do correspond to the coupled-bunch mode number n_x,

$$\frac{D_x^b}{D_x^0} = e^{-2j\pi\frac{bn_x}{M}} = \frac{\left(D_x^b\right)_{n_x}}{\left(D_x^0\right)_{n_x}}, \qquad b = 0,1,...,M-1. \tag{3.122}$$

The two-dimensional dispersion relation for rigid bunched beams, given by Eq. (3.115) for the horizontal and vertical rigid mode numbers $n_{x,y}$ related by $n_x = n_y - l$,

is the same as for coasting beams (see Eq. (3.12)). Using $U_{\mathrm{eq}x,y}^{n_{x,y}}$ and $V_{\mathrm{eq}x,y}^{n_{x,y}}$ (given by Eqs. (3.116)) in the case of rigid bunched beams, instead of the dispersion relation coefficients $U_{x,y}$ and $V_{x,y}$ of Laslett, Neil and Sessler in the case of coasting beams, the same analysis of coupled Landau damping can be made (see Sections 3.1.3 and 3.1.4) and the same results are obtained.

Notice that in the case of coasting beams, the dispersion coefficients $U_{x,y}$ and $V_{x,y}$ also correspond to different azimuthal mode numbers $n_{x,y}$ related by $n_x = n_y - l$. This is perhaps not surprising since the coupled-bunch mode number for bunched beams resembles the azimuthal mode number for coasting beams. Indeed, in the case of coasting beams, a mode, e.g. in the horizontal plane, corresponds to a closed sinusoidal pattern with n_x wavelengths around the machine circumference. The signal is a sinusoid at frequency $\omega = \left(n_x + Q_{x0} \right) \Omega_0$. Its seems legitimate to assume that gathering the beam particles into a large number M of closely spaced bunches should not dramatically change the coherent behaviour of the beam.[25] This is indeed true, although some important differences appear which distinguish a bunched beam from an unbunched beam. For short, well separated bunches it is relatively easy to visualise a transverse coupled-bunch mode: we start from the closed sinusoidal pattern of a continuous beam mode with its n_x wavelengths around the circumference, and we distribute the bunches like beads on top of this wave. For M equispaced bunches, the betatron phase shift from bunch to bunch must therefore be $2\pi n_x / M$, which has been verified above (see Eq. (3.122)). When the bunches are long compared to the wavelength of the continuous beam pattern, we can still play this game but now the bunches must be bent to closely follow the sinusoidal curve: this is possible if we introduce a non-zero chromaticity, which allows different parts of a bunch to oscillate with different phases (see Section 3.3 and Chapter 4).

3.3 Bunched beams with head-tail modes

Pellegrini and, independently, Sands have shown that short-range wake fields (i.e. fields that provide an interaction between the particles of a bunch but have a negligible effect on subsequent passages of the bunch or of other bunches in the beam) together with the internal circulation of the particles in a bunch can cause "internal coherent modes" within the bunch to become unstable.[42-44] The important point here is that the betatron phase advance per unit of time (or betatron frequency) of a particle depends on its instantaneous momentum deviation (from the ideal momentum) in first order through the chromaticity and the slippage factor. Considering a non-zero chromaticity couples the betatron and synchrotron motions, since the betatron frequency varies around a synchrotron orbit. The betatron phase varies linearly along the bunch (from the head) and attains its maximum value at the tail. The total betatron phase shift between head and tail is the physical origin of the head tail instability. It is usually denoted (see Chapter 4), e.g. in the horizontal plane, by $\chi_x = \left(\xi_x / \eta \right) Q_{x0} \, \Omega_0 \, \tau_b$ (radians), where τ_b is the bunch length in seconds. The head and the tail of the bunch oscillate therefore with a phase difference, which reduces to rigid-bunch oscillations only in the limit of zero chromaticity.

This section extends the results of Sands for the short-range interaction, introducing coupling between the transverse planes into the Landau damping calculation of head-tail modes.[38,43]

3.3.1 Equations of motion

The synchrotron motion of a test particle *i* is described in terms of its time-of-arrival τ_i at some azimuth, measured with respect to the time-of-arrival of the synchronous particle of the bunch. A linear restoring force for the synchrotron oscillations is assumed so that τ_i oscillates harmonically at the synchrotron frequency ω_s, (see Appendix B)

$$\tau_i = \hat{\tau}_i \cos\left(\omega_s t + \psi_i\right). \tag{3.123}$$

From Eqs. (2.8) and (2.9), the betatron frequency of the *i*th particle can be written, e.g. in the horizontal plane, as

$$\dot{\varphi}_{x,i} = Q_{x,i}\,\Omega_i = Q_{x0}\,\Omega_0\left[1+\dot{\tau}_i\left(1-\frac{\xi_x}{\eta}\right)\right]+\dot{\varphi}_{x,i}\left(\hat{x}_i\right), \tag{3.124}$$

considering only the dependence on the incoherent betatron amplitudes in the plane of coherent motion, and using the relation $\dot{\tau}_i = -\eta\,\Delta p_i / p_i$. Let's define the parameter

$$\eta_x = 1-\frac{\xi_x}{\eta}, \tag{3.125}$$

so that the varying betatron frequency of Eq. (3.124) can be written (using $\omega_{x0} = Q_{x0}\,\Omega_0$) as

$$\dot{\varphi}_{x,i} = \omega_{x,i} + \omega_{x0}\,\eta_x\,\dot{\tau}_i\,, \tag{3.126}$$

with

$$\omega_{x,i} = \omega_{x0} + \dot{\varphi}_{x,i}\left(\hat{x}_i\right). \tag{3.127}$$

In the absence of perturbation, Eq. (3.126) implies that the betatron motion is described by the differential equation

$$\ddot{x}_i + \left(\omega_{x,i} + \omega_{x0}\,\eta_x\,\dot{\tau}_i\right)^2 x_i = 0, \tag{3.128}$$

which is satisfied by

$$x_i = \hat{x}_i\, e^{j\left(\omega_{x,i}\,t + \omega_{x0}\,\eta_x\,\tau_i\right)}. \tag{3.129}$$

In the presence of both wake fields and linear coupling between the transverse planes (see Section 3.1), the equation of motion, e.g. in the horizontal plane, is given by

$$\ddot{x}_i + \left(\omega_{x,i} + \omega_{x0}\,\eta_x\,\dot{\tau}_i\right)^2 x_i = \sum_r x_r\left(t - \tau_r + \tau_i\right) W_x\left(\tau_r - \tau_i\right) + \underline{K}_i\, R_i^2\,\Omega_i^2\, y_i\,. \tag{3.130}$$

Here, one takes that the horizontal wake force on the *i*th particle (divided by its mass) due to the *r*th particle at the time t is given by the betatron coordinate of the *r*th particle at the earlier time $t-\tau_r+\tau_i$, modified by a wake function $W_x\left(\tau_r-\tau_i\right)$, which describes the transient decay of the wake. The total wake force is obtained by summing over all the particles of the bunch. A similar formula is found for the vertical plane by exchanging the roles of the variables x and y in Eq. (3.130). In the following, the revolution frequency Ω_i is replaced by its average value Ω_0, the orbit radius R_i is

replaced by its average value R, and the skew gradient is supposed to be the same for all the particles, i.e. $\underline{K}_i = \underline{K}_0$.

3.3.2 Two-dimensional dispersion relation

In the following, transverse betatron frequency spreads specified by externally given beam frequency spectra are assumed. The ensemble of particles has spectra with the distribution functions $\rho_x(\omega_{x,i})$ and $\rho_y(\omega_{y,i})$ which are supposed to be uncorrelated and normalised to unity (see Eq. (2.20)). Furthermore, linear coupling is described by Eqs. (3.15) and (3.16). Considering only the dominant Fourier component of the coupling (l), yields particular solutions of the form

$$x_i = X_i\, e^{j(\omega_c t + \omega_{x0}\eta_x \tau_i)}, \qquad y_i = Y_i\, e^{j\left[(\omega_c - l\Omega_0)t + \omega_{y0}\eta_y \tau_i\right]}. \tag{3.131}$$

Here, as opposed to Sands, one considers constant betatron amplitudes X_i and Y_i, and one looks for complex values of the betatron frequency ω_c to be determined. Substituting Eqs. (3.131) into Eq. (3.130), yields

$$\begin{aligned} &X_i\, e^{j(\omega_c t + \omega_{x0}\eta_x \tau_i)}\left[\left(\omega_{x,i} + \omega_{x0}\,\eta_x\,\dot{\tau}_i\right)^2 - \left(\omega_c + \omega_{x0}\,\eta_x\,\dot{\tau}_i\right)^2\right] \\ &= \sum_r X_r\, e^{j\left[\omega_c(t-\tau_r+\tau_i)+\omega_{x0}\eta_x\tau_r\right]} W_x(\tau_r - \tau_i) + R^2\,\Omega_0^2\,\underline{\hat{K}}_0(l)\,Y_i\, e^{j(\omega_c t + \omega_{y0}\eta_y\tau_i + l\Omega_0\tau_i)}, \end{aligned} \tag{3.132}$$

since the azimuthal angle at the position of the ith particle is given by $\vartheta_i = \Omega_0(t+\tau_i)$. Dividing both sides of Eq. (3.132) by $e^{j(\omega_c t + \omega_{x0}\eta_x\tau_i)}$ and using the approximation $\eta_x\,\dot{\tau}_i \approx \eta_x\,\omega_s\,\tau_i << 1$, yields for the horizontal motion

$$X_i = \frac{1}{\omega_{x,i} - \omega_c}\left[\sum_r X_r\, W_{ir}^x(t) + \frac{\underline{\hat{K}}_0(l)\,R^2\,\Omega_0^2}{2\,\omega_{x0}}\,Y_i\, e^{j\tau_i(\eta_y\omega_{y0} - \eta_x\omega_{x0} + l\Omega_0)}\right]. \tag{3.133}$$

Similarly, for the vertical motion, one has

$$Y_i = \frac{1}{\omega_{y,i} - (\omega_c - l\Omega_0)}\left[\sum_r Y_r\, W_{ir}^y(t) + \frac{\underline{\hat{K}}_0(-l)\,R^2\,\Omega_0^2}{2\,\omega_{y0}}\,X_i\, e^{j\tau_i(\eta_x\omega_{x0} - \eta_y\omega_{y0} - l\Omega_0)}\right], \tag{3.134}$$

with

$$W_{ir}^{x,y}(t) = \frac{1}{2\,\omega_{x0,y0}}\, e^{-j\omega_{x0,y0}(1-\eta_{x,y})(\tau_r - \tau_i)}\, W_{x,y}(\tau_r - \tau_i), \tag{3.135}$$

where the approximations $\omega_c \approx \omega_{x0}$ and $\omega_c - l\Omega_0 \approx \omega_{y0}$ have been made in the horizontal and vertical wake field terms respectively.

Since one is generally interested in small perturbations which give only small changes in one synchrotron period, one can for most purposes replace $W_{ir}^{x,y}(t)$ by its average value over one synchrotron period. Let's define

$$\overline{W_{ir}^{x,y}} = \frac{1}{T_s}\int_{T_s} W_{ir}^{x,y}(t)\,dt, \tag{3.136}$$

where $T_s = 2\pi/\omega_s$. The matrices $\overline{W_{ir}^{x,y}}$ are then independent of time and depend only on the two amplitudes $\hat{\tau}_{i,r}$ and the relative phase $\psi_r - \psi_i$,

$$\overline{W_{ir}^{x,y}} = \overline{W^{x,y}}(\hat{\tau}_i, \hat{\tau}_r, \psi_r - \psi_i). \tag{3.137}$$

Following Sands, one takes a particularly simple model for $W_{x,y}(\tau_r - \tau_i)$, namely

$$W_{x,y}(\tau_r - \tau_i) = \begin{cases} 0 & \text{for} \quad \tau_r < \tau_i \\ S_{x,y} & \text{for} \quad \tau_r > \tau_i \end{cases}. \tag{3.138}$$

This wake is zero in front of, and constant (positive) behind, the particle (assuming also that it drops to zero after all the particles of the bunch have passed). Considering $\omega_{x0,y0}\,\tau_i << 1$, the exponent in $W_{ir}^{x,y}$ is then small and Eq. (3.135) takes the simpler form

$$W_{ir}^{x,y}(t) = \frac{1}{2\,\omega_{x0,y0}}\left[1 - j\,\omega_{x0,y0}\left(1-\eta_{x,y}\right)(\tau_r - \tau_i)\right] W_{x,y}(\tau_r - \tau_i). \tag{3.139}$$

Since $\tau_r - \tau_i$ is a sinusoidal function given by

$$\tau_r - \tau_i = R_{ir}\cos(\omega_s\,t + \psi_{ir}), \tag{3.140}$$

where

$$R_{ir}^2 = \hat{\tau}_i^2 + \hat{\tau}_r^2 - 2\,\hat{\tau}_i\,\hat{\tau}_r\cos(\psi_r - \psi_i), \tag{3.141}$$

the mean values (over a full synchrotron period) of $W_{x,y}(\tau_r - \tau_i)$ are just $S_{x,y}/2$, and the mean values of $(\tau_r - \tau_i)\,W_{x,y}(\tau_r - \tau_i)$ are just $S_{x,y}\,R_{ir}/\pi$. Therefore,

$$\overline{W^{x,y}} = \frac{S_{x,y}}{2\,\omega_{x0,y0}}\left[\frac{1}{2} - j\,\omega_{x0,y0}\left(1-\eta_{x,y}\right)\frac{R_{ir}}{\pi}\right]. \tag{3.142}$$

Furthermore, in the coupling terms of Eqs. (3.133) and (3.134), since the arguments in the exponentials are small (in the approximation of Sands, $\omega_{x0,y0}\,\tau_i << 1$), the exponentials can be developed to first order and averaged to 1 over one synchrotron period.

One has now to choose the distribution of particles in synchrotron phase space. Again following Sands, one considers the "hollow-bunch model" in which all the particles (N_b) have the same synchrotron amplitude $\hat{\tau}_i = \hat{\tau}_0$, but uniformly distributed phases ψ of the synchrotron oscillations. Summing over all the particles in the bunch, and replacing the sum in the wake field term by an integral, yields, e.g. for the horizontal plane,

$$\overline{X}(\psi)=\left[\frac{N_b}{2\pi}\int_{-\pi}^{+\pi}\overline{W^x}(\psi-\psi')\,\overline{X}(\psi')\,d\psi'+\frac{\hat{\underline{K}}_0(l)\,R^2\,\Omega_0^2}{2\omega_{x0}}\overline{Y}(\psi)\right]\int_{-\infty}^{+\infty}\frac{\rho_x(\omega_{x,i})\,d\omega_{x,i}}{\omega_{x,i}-\omega_c}. \tag{3.143}$$

Here, the following relations have been used,

$$\sum_i X_i(\psi)=N_b\,\overline{X}(\psi),\qquad \sum_i\frac{1}{\omega_{x,i}-\omega_c}\overline{(\;)}=N_b\int_{-\infty}^{+\infty}\frac{\rho_x(\omega_{x,i})\,d\omega_{x,i}}{\omega_{x,i}-\omega_c}\overline{(\;)}\,. \tag{3.144}$$

The corresponding vertical equation is

$$\overline{Y}(\psi)=\left[\frac{N_b}{2\pi}\int_{-\pi}^{+\pi}\overline{W^y}(\psi-\psi')\,\overline{Y}(\psi')\,d\psi'+\frac{\hat{\underline{K}}_0(-l)\,R^2\,\Omega_0^2}{2\omega_{y0}}\overline{X}(\psi)\right]\int_{-\infty}^{+\infty}\frac{\rho_y(\omega_{y,i})\,d\omega_{y,i}}{\omega_{y,i}-(\omega_c-l\Omega_0)}. \tag{3.145}$$

This equation can be solved by expanding $\overline{X}$ and $\overline{Y}$ into Fourier series in ψ

$$\overline{X}(\psi)=\sum_{k=-\infty}^{k=+\infty}\overline{X}_k\,e^{jk\psi},\qquad\qquad \overline{Y}(\psi)=\sum_{k=-\infty}^{k=+\infty}\overline{Y}_k\,e^{jk\psi}. \tag{3.146}$$

Defining the numbers

$$\Delta\omega_k^{x,y}=-\frac{N_b}{2\pi}\int_{-\pi}^{\pi}\overline{W^{x,y}}(-\phi)\,e^{jk\phi}d\phi, \tag{3.147}$$

one obtains

$$\begin{aligned}&\left(\int_{-\infty}^{+\infty}\frac{\rho_x(\omega_{x,i})\,d\omega_{x,i}}{\omega_{x,i}-\omega_c}\right)^{-1}\sum_{k=-\infty}^{k=+\infty}\overline{X}_k\,e^{jk\psi}\\&=-\sum_{k=-\infty}^{k=+\infty}\Delta\omega_k^x\,\overline{X}_k\,e^{jk\psi}+\frac{\hat{\underline{K}}_0(l)\,R^2\,\Omega_0^2}{2\,\omega_{x0}}\sum_{k=-\infty}^{k=+\infty}\overline{Y}_k\,e^{jk\psi}.\end{aligned} \tag{3.148}$$

Multiplying this equation by $e^{-jm\phi}$ (with $m=...,-2,-1,0,1,2,...$) and integrating over all ϕ, yields

$$\left(\int_{-\infty}^{+\infty}\frac{\rho_x(\omega_{x,i})\,d\omega_{x,i}}{\omega_{x,i}-\omega_c}\right)^{-1}\overline{X}_m=-\Delta\omega_m^x\,\overline{X}_m+\frac{\hat{\underline{K}}_0(l)\,R^2\,\Omega_0^2}{2\,\omega_{x0}}\overline{Y}_m. \tag{3.149}$$

A similar equation is obtained for the vertical plane

$$\left(\int_{-\infty}^{+\infty}\frac{\rho_y(\omega_{y,i})\,d\omega_{y,i}}{\omega_{y,i}-(\omega_c-l\Omega_0)}\right)^{-1}\overline{Y}_m=-\Delta\omega_m^y\,\overline{Y}_m+\frac{\hat{\underline{K}}_0(-l)\,R^2\,\Omega_0^2}{2\,\omega_{y0}}\overline{X}_m. \tag{3.150}$$

Equating the terms $\overline{X}_m$ / $\overline{Y}_m$ of Eqs. (3.149) and (3.150), the following equation must be satisfied

$$\left[\left(\int_{-\infty}^{+\infty}\frac{\rho_x\left(\omega_{x,i}\right)d\omega_{x,i}}{\omega_c-\omega_{x,i}}\right)^{-1}-U_{\mathrm{eq}x}^{m}+jV_{\mathrm{eq}x}^{m}\right]\times$$
$$\left[\left(\int_{-\infty}^{+\infty}\frac{\rho_y\left(\omega_{y,i}\right)d\omega_{y,i}}{\omega_c-l\Omega_0-\omega_{y,i}}\right)^{-1}-U_{\mathrm{eq}y}^{m}+jV_{\mathrm{eq}y}^{m}\right]=\frac{\left|\underline{\hat{K}}_0(l)\right|^2R^4\,\Omega_0^4}{4\,\omega_{x0}\,\omega_{y0}}, \tag{3.151}$$

where we have introduced "equivalent" dispersion relation coefficients $U_{\mathrm{eq}x,y}^{m}$ and $V_{\mathrm{eq}x,y}^{m}$, defined by

$$U_{\mathrm{eq}x,y}^{m}=\mathrm{Re}\left(\Delta\omega_m^{x,y}\right),$$
$$V_{\mathrm{eq}x,y}^{m}=-\mathrm{Im}\left(\Delta\omega_m^{x,y}\right). \tag{3.152}$$

These coefficients are the transverse real frequency shifts and instability growth rates respectively, for a given head-tail mode *m*, in the absence of both coupling and Landau damping. It only remains now to calculate $\Delta\omega_m^{x,y}$ from Eqs. (3.147). For the "hollow-bunch" beam considered here, Eq. (3.141) gives

$$R_{ir}=2\hat{\tau}_0\left|\sin\left(\frac{\psi_r-\psi_i}{2}\right)\right|. \tag{3.153}$$

Then, from Eqs. (3.142) and (3.147), one gets

$$\Delta\omega_m^{x,y}=-\frac{N_b\,S_{x,y}}{4\,\pi\,\omega_{x0,y0}}\int_{-\pi}^{+\pi}\left[\frac{1}{2}-j\,\omega_{x0,y0}\left(1-\eta_{x,y}\right)\frac{2\,\hat{\tau}_0}{\pi}\left|\sin\left(\frac{\phi}{2}\right)\right|\right]e^{jm\phi}\,d\phi, \tag{3.154}$$

which, using Eq. (3.125), finally leads to

$$\Delta\omega_0^{x,y}=-\frac{N_b\,S_{x,y}}{4\,\omega_{x0,y0}}+j\frac{2\,N_b\,S_{x,y}\,\hat{\tau}_0\,\xi_{x,y}}{\pi^2\eta},$$
$$\Delta\omega_m^{x,y}=-j\frac{2\,N_b\,S_{x,y}\,\hat{\tau}_0\,\xi_{x,y}}{\pi^2\eta}\left(4m^2-1\right)^{-1}\qquad\text{for}\qquad m\neq 0. \tag{3.155}$$

The two-dimensional dispersion relation for bunched beams with head-tail modes, given by Eq. (3.151) for the head-tail mode *m*, is the same as for coasting beams (see Eq. (3.12)). Using $U_{\mathrm{eq}x,y}^{m}$ and $V_{\mathrm{eq}x,y}^{m}$ (given by Eqs. (3.152)) in the case of bunched beams with head-tail modes, instead of the dispersion relation coefficients $U_{x,y}$ and $V_{x,y}$ of Laslett, Neil and Sessler in the case of coasting beams, the same analysis of coupled Landau damping can be made (see Sections 3.1.3 and 3.1.4) and the same results are obtained.

For the particular model considered here, $\Delta\omega_m^{x,y}$ are purely imaginary for $m\neq 0$, but other forms of $W_{x,y}$ would, in general, give complex $\Delta\omega_m^{x,y}$ for all modes.

Sands has also considered the case of the fast-wake due to the conventional resistive wall effect in a cylindrical tube. The analysis, as concerns the head-tail instability without Landau damping, leads to the following conclusions. The qualitative features of the head-tail effect for the resistive wall wake are similar to those for a step-function wake except that: (i) the frequency shift, which is purely imaginary for the step-function wake, has, for the resistive wall wake, both real and imaginary parts; (ii) the imaginary part changes from a first power dependence on the bunch length to a square-root dependence. As concerns coupled Landau damping, the same results are obtained with the "equivalent" dispersion relation coefficients given by Eqs. (26) and (27) of Ref. 44.

3.4 Generalised stability criteria for both coasting and bunched beams

It has been shown in Sections 3.1, 3.2 and 3.3, using the single-particle equation formalism, that the two-dimensional dispersion relation is the same for both coasting and bunched beams (see Eqs. (3.12), (3.115) and (3.151)), introducing "equivalent" dispersion relation coefficients U_{eq} and V_{eq}, given by Eqs. (3.116) for rigid bunched beams and by Eqs. (3.152) for bunched beams with head-tail modes. These coefficients are the real betatron frequency shift and instability growth rate respectively, for a given mode, in the absence of both coupling and Landau damping. This is perhaps not surprising because in the three cases (Eqs. (3.1), (3.88) and (3.130)) more or less the same differential equation has to be solved.

In the case of coasting beams, U_{eq} and V_{eq} are equal to the dispersion relation coefficients U, V introduced by Laslett, Neil and Sessler. They are real constants (for the purpose of the dispersion relation analysis without taking into account space-charge non-linearities) that characterise the accelerator (and the beam energy).

In the case of bunched beams, it will be seen in Chapter 4, that the general "equivalent" dispersion relation coefficients can be drawn from the one-dimensional theory of transverse bunched beam instabilities that has been described in its most general form by Sacherer, who combined and extended the results obtained for long and short range interactions.[18,45] These coefficients are real constants that characterise both the accelerator and the beam dynamics.

Using U_{eq} and V_{eq} in the case of bunched beams, instead of U and V in the case of coasting beams, the same analysis of coupled Landau damping can be made (see Sections 3.1.3 and 3.1.4) and the same results are obtained.

3.5 Sharing of both frequency spread and chromaticity

In the case of head-tail instabilities, the transverse betatron frequency shifts, for a given mode m and in the absence of both coupling and Landau damping, are given by Sands for the idealised model in which the wake field of a single particle is zero in front of and constant (positive) behind the particle, and for the "hollow-bunch model" in which all the particles have the same synchrotron amplitude $\hat{\tau}_i = \hat{\tau}_0$ (see Section 3.3.2). It yields

$$U^{0}_{\mathrm{eq}x,y} = -\frac{N_b\, S_{x,y}}{4\,\omega_{x0,y0}}, \qquad U^{m}_{\mathrm{eq}x,y} = 0 \quad \text{for} \quad m \neq 0, \qquad V^{m}_{\mathrm{eq}x,y} = -\,W^{m}_{x,y}\,\xi_{x,y}, \tag{3.156}$$

with

$$W_{x,y}^{m} = -\frac{2 N_b S_{x,y} \hat{\tau}_0}{\pi^2 \eta} \left(4m^2 - 1\right)^{-1}. \tag{3.157}$$

To clearly see the effect of coupling on both Landau damping and chromaticity, it is interesting to look at the stability criteria for zero and optimum coupling.[46] In the following, only the most dangerous mode $m = 0$ (above transition[b]) is considered. In the absence of coupling, the Lorentzian stability criteria in the horizontal and vertical planes respectively, are (see Eqs. (3.25) and (3.156))

$$\delta\omega_x + W_x^0 \xi_x \geq 0, \qquad \delta\omega_y + W_y^0 \xi_y \geq 0. \tag{3.158}$$

In the absence of Landau damping, the condition of Sands, $\xi_{x,y} \geq 0$ for the stability of the head-tail mode $m = 0$, is recovered (above transition, $\eta > 0$ and thus $W_{x,y}^0 > 0$). With full coupling, the two criteria reduce to (see Eq. (3.26))

$$\delta\omega_x + \delta\omega_y + W_x^0 \xi_x + W_y^0 \xi_y \geq 0. \tag{3.159}$$

Equation (3.159) shows the beneficial effect of coupling as concerns both chromaticity compensation and Landau damping. In the absence of a frequency spread, the result obtained by Talman, $W_x^0 \xi_x + W_y^0 \xi_y \geq 0$, is recovered.[47] A negative chromaticity can be maintained in one plane, provided that the other chromaticity is appropriately increased to compensate.[c] In the presence of Landau damping, it is seen that a less restrictive criterion is obtained. Elliptical spectra exhibit the same kind of results. In the absence of coupling, the transverse stability criteria are (see Eqs. (3.74))

$$\mathrm{Re}\left[\sqrt{\Delta\omega_x^2 - \left(2U_{\mathrm{eq}x}^0\right)^2}\,\right] + 2\, W_x^0 \xi_x \geq 0, \quad \mathrm{Re}\left[\sqrt{\Delta\omega_y^2 - \left(2U_{\mathrm{eq}y}^0\right)^2}\,\right] + 2\, W_y^0 \xi_y \geq 0. \tag{3.160}$$

With optimum coupling, these two criteria reduce to (see Eq. (3.72))

$$\mathrm{Re}\left[\sqrt{\Delta\omega_x^2 - \left(2U_{\mathrm{eq}x}^0\right)^2} + \sqrt{\Delta\omega_y^2 - \left(2U_{\mathrm{eq}y}^0\right)^2}\,\right] + 2\left(W_x^0 \xi_x + W_y^0 \xi_y\right) \geq 0. \tag{3.161}$$

In the absence of a frequency spread, the result of Talman is recovered.

The resistive-wall wake field gives similar results with the "equivalent" dispersion relation coefficients given by Eqs. (26) and (27) of Ref. 44.

3.6 Sharing of damping by feedbacks

An electronic feedback system is often used to stabilise a beam in one transverse plane. In the theory of coupled Landau damping, the stabilising effect of a feedback

[b] The natural chromaticities are (usually) negative and then, to eliminate the most dangerous head-tail mode $m = 0$, chromaticity tuning is only necessary above transition energy. The higher head-tail modes, with smaller form factors and wake field coefficients, can be stabilised by Landau damping.

[c] Head-tail modes with linear coupling have also been studied in Ref. 48, introducing a vector quantity called "skew chromaticity".

system can be introduced in the general coefficient V_{eq} (see Section 3.4). Its damping effect in one plane can therefore also be transferred to the other plane using coupling.

3.7 Coupled Landau damping with external non-linearities

Guided by the results of Sections 3.1, 3.2 and 3.3, it is sufficient to consider the case of coasting beams only. Considering "second order" non-linear terms and using Eqs. (3.14) and (3.17), the steady-state response of the l.h.s of the first equation of Eq. (3.1), with $\Omega_i = \Omega_0$, $R_i = R$ and $\underline{K}_i = \underline{K}_0$, to the driving force of the r.h.s, is for $K_x = \left(d\omega_{x,i} / d\hat{x}_i\right) / \left(\omega_{x,i} / \hat{x}_i\right) << 1$,

$$X_i = \left[\left(1 - \frac{K_x}{2}\right)\frac{1}{\omega_{x,i}^2\left(\hat{x}_i, \hat{y}_i, p_i\right) - \left(\omega - n_x \Omega_0\right)^2} - \frac{K_x}{2}\frac{\omega_{x,i}^2\left(\hat{x}_i, \hat{y}_i, p_i\right) + \left(\omega - n_x \Omega_0\right)^2}{\left[\omega_{x,i}^2\left(\hat{x}_i, \hat{y}_i, p_i\right) - \left(\omega - n_x \Omega_0\right)^2\right]^2}\right] \times$$
$$\left[2\omega_{x0}\left(-U_x + jV_x\right)\overline{X} + \hat{\underline{K}}_0(l)\, R^2 \Omega_0^2\, Y_i\right]. \tag{3.162}$$

Using the results of Sections 2.5 and 2.6, calling $h\left(\hat{x}_i^2, \hat{y}_i^2\right)$ the distribution function of the incoherent horizontal and vertical amplitudes, choosing the normalisation

$$\int_{\hat{x}_i^2=0}^{\hat{x}_i^2=+\infty}\int_{\hat{y}_i^2=0}^{\hat{y}_i^2=+\infty} h\left(\hat{x}_i^2, \hat{y}_i^2\right)\frac{d\hat{x}_i^2}{2}\frac{d\hat{y}_i^2}{2} = 1, \tag{3.163}$$

and using the relations equivalent to Eqs. (3.91) and (3.92) for an azimuthal coasting beam slice, the following two-dimensional dispersion relation is obtained

$$\left\{\left[\iiint \frac{1}{\omega_c - \omega_{x,i}\left(\hat{x}_i, \hat{y}_i, p_i\right)}\left(-\frac{1}{4}\frac{\partial h\left(\hat{x}_i^2, \hat{y}_i^2\right)\hat{x}_i^2}{\partial \hat{x}_i^2}\right) g(p_i)\, d\hat{x}_i^2\, d\hat{y}_i^2\, dp_i\right]^{-1} - U_x + jV_x\right\} \times$$
$$\left\{\left[\iiint \frac{1}{\omega_c - l\Omega_0 - \omega_{y,i}\left(\hat{x}_i, \hat{y}_i, p_i\right)}\left(-\frac{1}{4}\frac{\partial h\left(\hat{x}_i^2, \hat{y}_i^2\right)\hat{y}_i^2}{\partial \hat{y}_i^2}\right) g(p_i)\, d\hat{x}_i^2\, d\hat{y}_i^2\, dp_i\right]^{-1} - U_y + jV_y\right\}$$
$$= \frac{\left|\hat{\underline{K}}_0(l)\right|^2 R^4 \Omega_0^4}{4\,\omega_{x0}\,\omega_{y0}}. \tag{3.164}$$

Equation (3.164) is similar to Eq. (3.12) with more involved dispersion integrals. If one approximates the betatron frequency spread in each plane by the square root of the quadratic sum of the spreads induced by the momentum and the octupoles via both horizontal and vertical incoherent betatron amplitudes, then the same analysis of coupled Landau damping can be made.

Notice that for a bunched beam (with instability rise time greater than the synchrotron oscillation period) the momentum spread averages out over one synchrotron period and therefore does not contribute to Landau damping. In the absence of coupling, Eq. (3.164) leads to the one-dimensional result of Ref. 49.

4 COUPLED LANDAU DAMPING USING THE VLASOV FORMALISM

The procedure to find the first order eigensystem describing the coupled Landau damping of transverse bunched beam instabilities is explained in this chapter using the Vlasov formalism, considering uncorrelated incoherent betatron amplitudes distributions and neglecting space-charge non-linearities. A perturbation treatment of the Vlasov equation, including both wake fields and linear coupling between the transverse planes is described, using Laclare's formalism (with sometimes different notations).[17,50-52] A general dispersion relation is derived, describing an eigenvalue problem (see Eq. (4.58)), which generalises Laclare's one-dimensional eigensystem.[17] A simplified two-dimensional dispersion relation (having the same form as in Chapter 3), where the coherent tune shifts are expressed in terms of effective impedances, is then derived, generalising the classical Sacherer's formula (see Eqs. (4.78) and (4.79)).[18]

In this approach, the motion of the beam is described by a superposition of modes, rather than a collection of individual particles. The detailed methods of analysis in the two approaches are different, the particle representation is usually conveniently treated in the time domain, while in the mode representation the frequency domain is more convenient, but in principle they necessarily give the same final results. The advantage of the mode representation is that it offers a formalism that can be used systematically to treat the instability problem.

In the following, we will work in the frequency domain with transverse signals, stationary distributions and perturbations due to both wake fields and linear coupling between the transverse planes. Transverse impedances will be assumed and by means of the Vlasov equation, the transverse coherent motions will be described. We recall that the perturbations consist of slight transverse displacements of the beam, which oscillates from side to side in the external focusing guide field. This creates differential wall currents, which flow in opposite directions on either side of the vacuum chamber. This requires a longitudinal electric field E_z, which varies in strength across the aperture and transverse dipolar magnetic fields $B_{x,y}$. These magnetic fields $B_{x,y}$ deflect the beam and can increase the initial transverse displacements (instability) or decrease them (stability). We will restrict ourselves, as previously, to the study of the effect of the dipolar magnetic fields.

4.1 Single-particle transverse motions

The transverse motions of a test particle *i* in a bunch are described by six coordinates. Two of them are related to the longitudinal phase space. The parameters $(\tau_i, \dot{\tau}_i)$ or $(\hat{\tau}_i, \psi_i)$ will be used. Here, τ_i represents the time interval between the passage of the synchronous particle and the test particle (as opposed to Sands in Section 3.3). A purely linear synchrotron oscillation around the synchronous particle at frequency ω_s is assumed (see Appendix B)

$$\ddot{\tau}_i + \omega_s^2 \tau_i = 0, \tag{4.1}$$

which yields

$$\tau_i = \hat{\tau}_i \cos(\omega_s t + \psi_i). \tag{4.2}$$

The motion in the longitudinal plane is assumed to be stable (no coherent effect). The other four parameters are two pairs of coordinates $(x_i, \dot{x}_i)$ or $(\hat{x}_i, \varphi_{x,i})$, and $(y_i, \dot{y}_i)$ or $(\hat{y}_i, \varphi_{y,i})$. They are related to the transverse phase spaces (horizontal and vertical respectively). Here, x_i and y_i are the betatron coordinates, $\varphi_{x,i}$ and $\varphi_{y,i}$ are the betatron phases at time t. The solution of the equation of unperturbed motion, e.g. in the horizontal plane, is written as[17]

$$x_i = \hat{x}_i \cos(\varphi_{x,i}). \tag{4.3}$$

The horizontal betatron frequency is given by (see Eqs. (2.8) and (2.9))

$$\dot{\varphi}_{x,i} = Q_{x,i}\,\Omega_i = Q_{x0}\,\Omega_0\left[1-\dot{\tau}_i\left(1-\frac{\xi_x}{\eta}\right)\right]+\dot{\varphi}_{x,i}(\hat{x}_i,\hat{y}_i), \tag{4.4}$$

considering external non-linearities (due to octupoles), and using the relation $\dot{\tau}_i = \eta\,\Delta p_i / p_i$. Integrating Eq. (4.4), leads to

$$\varphi_{x,i} = \omega_{x,i}\,t + \left(\omega_{\xi_x} - Q_{x0}\,\Omega_0\right)\tau_i + \varphi_{0x,i}\,, \tag{4.5}$$

where

$$\omega_{x,i} = Q_{x0}\,\Omega_0 + \dot{\varphi}_{x,i}(\hat{x}_i,\hat{y}_i), \tag{4.6}$$

and

$$\omega_{\xi_x} = Q_{x0}\,\Omega_0\,\frac{\xi_x}{\eta} \tag{4.7}$$

is the horizontal chromatic frequency. According to the above definitions, in the absence of perturbation the horizontal coordinate satisfies

$$\ddot{x}_i - \frac{\ddot{\varphi}_{x,i}}{\dot{\varphi}_{x,i}}\dot{x}_i + \dot{\varphi}_{x,i}^2\,x_i = 0. \tag{4.8}$$

In the presence of both electromagnetic fields induced by the beam and linear coupling between the transverse planes, Eq. (4.8), and the corresponding equation for the vertical plane, become

$$\begin{aligned}
&\ddot{x}_i - \frac{\ddot{\varphi}_{x,i}}{\dot{\varphi}_{x,i}}\dot{x}_i + \dot{\varphi}_{x,i}^2\,x_i = \frac{e}{m_0\,\gamma}\left[\vec{E}+\vec{v}\times\vec{B}\right]_x\left(t, \vartheta = \Omega_i(t-\tau_i)\right) + \underline{K}_i\,R_i^2\,\Omega_i^2\,y_i\,,\\
&\ddot{y}_i - \frac{\ddot{\varphi}_{y,i}}{\dot{\varphi}_{y,i}}\dot{y}_i + \dot{\varphi}_{y,i}^2\,y_i = \frac{e}{m_0\,\gamma}\left[\vec{E}+\vec{v}\times\vec{B}\right]_y\left(t, \vartheta = \Omega_i(t-\tau_i)\right) + \underline{K}_i\,R_i^2\,\Omega_i^2\,x_i\,.
\end{aligned} \tag{4.9}$$

Here, $\vec{E}(\vartheta)$ and $\vec{B}(\vartheta)$ are the electromagnetic fields induced by the beam at the azimuthal angle ϑ. The electromagnetic fields must be expressed at $\vartheta = \Omega_i(t-\tau_i)$ when following the particle along its trajectory. In the following, the revolution frequency Ω_i is replaced by its average value Ω_0, the orbit radius R_i is replaced by its

average value R, and the skew gradient is assumed to be the same for all the particles, i.e. $\underline{K}_i = \underline{K}_0$.

4.2 Single-particle transverse signals

The horizontal signal $s_{x,i}(t,\vartheta)$ induced at a perfect pick-up electrode (infinite bandwidth) at angular position ϑ in the ring by the off-centred test particle is given by

$$s_{x,i}(t,\vartheta) = s_{z,i}(t,\vartheta)\, x_i(t) = s_{z,i}(t,\vartheta)\, \hat{x}_i \cos(\varphi_{x,i}), \tag{4.10}$$

where $s_{z,i}(t,\vartheta)$ is the current signal of the particle that moves in the external guide field (no self field and no coupling added). At time $t = 0$, the synchronous particle starts from $\vartheta = 0$ and reaches the pick-up electrode at times t_k^0 satisfying[51]

$$\Omega_0\, t_k^0 = \vartheta + 2k\pi, \qquad -\infty \le k \le +\infty. \tag{4.11}$$

The test particle is delayed by τ_i. It goes through the electrode at times t_k given by

$$t_k = t_k^0 + \tau_i\,. \tag{4.12}$$

The current signal induced by the test particle is a series of impulses delivered on each passage

$$s_{z,i}(t,\vartheta) = e \sum_{k=-\infty}^{k=+\infty} \delta\left(t - \tau_i - \frac{\vartheta}{\Omega_0} - \frac{2k\pi}{\Omega_0}\right). \tag{4.13}$$

In the time domain, $s_{x,i}(t,\vartheta)$ consists of a series of impulses, the amplitude of which x_i changes at each passage through the electrode

$$s_{x,i}(t,\vartheta) = e\,\hat{x}_i \cos(\varphi_{x,i}) \sum_{k=-\infty}^{k=+\infty} \delta\left(t - \tau_i - \frac{\vartheta}{\Omega_0} - \frac{2k\pi}{\Omega_0}\right). \tag{4.14}$$

Developing $\cos(\varphi_{x,i})$ into exponential functions and using the following equation

$$\sum_{k=-\infty}^{k=+\infty} \delta\left(u - \frac{2k\pi}{\Omega_0}\right) = \frac{\Omega_0}{2\pi} \sum_{k=-\infty}^{k=+\infty} e^{jk\Omega_0 u}\,, \tag{4.15}$$

leads to

$$s_{x,i}(t,\vartheta) = \frac{e\Omega_0}{2\pi}\,\hat{x}_i\, \frac{e^{j\varphi_{x,i}} + e^{-j\varphi_{x,i}}}{2} \sum_{k=-\infty}^{k=+\infty} e^{jk[\Omega_0(t-\tau_i)-\vartheta]}. \tag{4.16}$$

Using now

$$e^{-ju\hat{\tau}_i \cos(\omega_s t + \psi_i)} = \sum_{m=-\infty}^{m=+\infty} j^{-m}\, J_m(u\hat{\tau}_i)\, e^{jm(\omega_s t + \psi_i)}\,, \tag{4.17}$$

where J_m is the Bessel function of *m*th order, one finally obtains

$$s_{x,i}(t,\vartheta)=\frac{e\Omega_0}{4\pi}\,\hat{x}_i\,e^{j\left(\omega_{x,i}\,t\,+\,\varphi_{0x,i}\right)}\sum_{m,k} j^{-m}\,J_{m,x}\left(k,\hat{\tau}_i\right)e^{j\left[\left(k\Omega_0+m\omega_s\right)t+m\psi_i-k\vartheta\right]}, \quad (4.18)$$

neglecting the complex conjugate $e^{-j\varphi_{x,i}}$ and with

$$J_{m,x}\left(k,\hat{\tau}_i\right)=J_m\left\{\left[\left(k+Q_{x,i}\right)\Omega_0-\omega_{\xi_x}\right]\hat{\tau}_i\right\}\approx J_m\left\{\left[\left(k+Q_{x0}\right)\Omega_0-\omega_{\xi_x}\right]\hat{\tau}_i\right\}. \quad (4.19)$$

Using the Fourier transform given by

$$s_{x,i}(\omega,\vartheta)=\frac{1}{2\pi}\int_{t=-\infty}^{t=+\infty} s_{x,i}(t,\vartheta)\,e^{-j\omega t}\,dt, \quad (4.20)$$

one can pass on to frequency domain

$$s_{x,i}(\omega,\vartheta)=\frac{e\Omega_0}{4\pi}\,\hat{x}_i\,e^{j\varphi_{0x,i}}\sum_{m,k} j^{-m}\,J_{m,x}\left(k,\hat{\tau}_i\right)\delta\left[\omega-\left(k\Omega_0+\omega_{x,i}+m\omega_s\right)\right]e^{j\left(m\psi_i-k\vartheta\right)}. \quad (4.21)$$

The single particle spectrum is a line spectrum at frequencies $\left(k+Q_{x,i}\right)\Omega_0+m\omega_s$. Around every betatron line $\left(k+Q_{x,i}\right)\Omega_0$, there is an infinite number of synchrotron satellites m, the amplitude of which is given by the Bessel function $J_m\left\{\left[\left(k+Q_{x,i}\right)\Omega_0-\omega_{\xi_x}\right]\hat{\tau}_i\right\}$. The important point here is that the spectrum is centred at the chromatic frequency. A similar equation is obtained for the vertical plane, replacing x by y in Eq. (4.21).

4.3 Distributions of particles

The basic mathematical tool used for the mode representation of the beam motion is the Vlasov equation, which describes the collective behaviour of a multiparticle system under the influence of electromagnetic forces.[8,53] It can be derived from the conservation of the phase-space area (as stated by the Liouville's theorem). To construct the Vlasov equation, one starts with the single-particle equations of motion. The coordinates q_ρ and p_ρ (with $\rho=x,y,z$) should be canonically conjugated, which means that they should be derived from a Hamiltonian $\mathrm{H}\left(q_\rho,p_\rho,t\right)$ by the canonical equations

$$\dot{q}_\rho=\frac{\partial \mathrm{H}\left(q_\rho,p_\rho,t\right)}{\partial p_\rho}, \qquad \dot{p}_\rho=-\frac{\partial \mathrm{H}\left(q_\rho,p_\rho,t\right)}{\partial q_\rho}. \quad (4.22)$$

According to the Liouville's theorem, the particles, in a non-dissipative system of forces, move like an incompressible fluid in phase space. The constancy of the phase space density $\Psi\left(q_\rho,p_\rho,t\right)$ is expressed by the equation

$$\frac{d\,\Psi\left(q_\rho,p_\rho,t\right)}{d\,t}=0, \quad (4.23)$$

where the total differentiation indicates that one follows the particle while measuring the density of its immediate neighbourhood. Equation (4.23), sometimes referred to as the Liouville's theorem, states that the local particle density does not vary with time when following the motion in canonical variables.

Practically, one would like to know the development of this density as seen by a stationary observer (like a beam monitor) which does not follow the particle. It depends now not only directly on the time t but also indirectly through the coordinates q_ρ and p_ρ of the moving particles, which change with time. Therefore, one has to express the total differential with respect to t by the differentiations with respect to time as well as with respect to the coordinates q_ρ and p_ρ multiplied with the time derivative of these coordinates

$$\frac{\partial \Psi\left(q_\rho, p_\rho, t\right)}{\partial t} + \dot{q}_\rho \frac{\partial \Psi\left(q_\rho, p_\rho, t\right)}{\partial q_\rho} + \dot{p}_\rho \frac{\partial \Psi\left(q_\rho, p_\rho, t\right)}{\partial p_\rho} = 0. \tag{4.24}$$

This expression is the Vlasov equation in its most simple form and is nothing else but an expression for the Liouville's conservation of phase-space density seen by a stationary observer.

In Liouville's theorem the phase-space area is only conserved if expressed in canonically conjugated variables q_ρ and p_ρ. The same criterion applies to the validity of the Vlasov equation. However, these variables are often not very practical for accelerator applications, and other coordinates are sometimes used in an approximate manner.

Strictly speaking, $\dot{q}_\rho$ and $\dot{p}_\rho$ are given by external forces. Collisions among discrete particles in the system, for example, are excluded. However, if a particle interacts more strongly with the collective fields of the other particles than with its nearest neighbours, the Vlasov equation still applies if one treats the collective fields on the same footing as the external fields. This in fact forms the basis of treating the collective instabilities using the Vlasov technique.

Let's thus introduce a distribution function $\Psi\left(\hat{x}_i, \varphi_{0x,i}, \hat{y}_i, \varphi_{0y,i}, \hat{\tau}_i, \psi_i, t\right)$ normalised to unity

$$\begin{aligned} &\int_{\hat{x}_i=0}^{\hat{x}_i=+\infty} \int_{\hat{y}_i=0}^{\hat{y}_i=+\infty} \int_{\hat{\tau}_i=0}^{\hat{\tau}_i=\tau_b/2} \int_{\varphi_{0x,i}=0}^{\varphi_{0x,i}=2\pi} \int_{\varphi_{0y,i}=0}^{\varphi_{0y,i}=2\pi} \int_{\psi_i=0}^{\psi_i=2\pi} \Psi\left(\hat{x}_i, \varphi_{0x,i}, \hat{y}_i, \varphi_{0y,i}, \hat{\tau}_i, \psi_i, t\right) \times \\ &\hat{x}_i \, d\hat{x}_i \; \hat{y}_i \, d\hat{y}_i \; \hat{\tau}_i \, d\hat{\tau}_i \, d\varphi_{0x,i} \, d\varphi_{0y,i} \, d\psi_i = 1, \end{aligned} \tag{4.25}$$

where τ_b is the bunch full length. In this case, the Vlasov equation (4.24) becomes

$$\frac{\partial \Psi}{\partial t} + \frac{\partial \Psi}{\partial \hat{x}_i}\dot{\hat{x}}_i + \frac{\partial \Psi}{\partial \varphi_{0x,i}}\dot{\varphi}_{0x,i} + \frac{\partial \Psi}{\partial \hat{y}_i}\dot{\hat{y}}_i + \frac{\partial \Psi}{\partial \varphi_{0y,i}}\dot{\varphi}_{0y,i} + \frac{\partial \Psi}{\partial \hat{\tau}_i}\dot{\hat{\tau}}_i + \frac{\partial \Psi}{\partial \psi_i}\dot{\psi}_i = 0. \tag{4.26}$$

4.3.1 Stationary distributions

In the absence of perturbation, $\hat{x}_i$, $\hat{y}_i$ and $\hat{\tau}_i$ are constant during the motion. Therefore, the stationary distribution is a function of the peak amplitudes only, $\Psi_0\left(\hat{x}_i, \hat{y}_i, \hat{\tau}_i\right)$. No correlation between horizontal, vertical and longitudinal planes is

assumed and the stationary part is thus written as the product of three stationary distributions, one for the longitudinal phase space and one for each transverse phase space

$$\Psi_0 = f_{x0}(\hat{x}_i)\, f_{y0}(\hat{y}_i)\, g_0(\hat{\tau}_i). \tag{4.27}$$

The distribution functions are normalised as follows

$$\int_{\hat{\tau}_i=0}^{\hat{\tau}_i=\tau_b/2} g_0(\hat{\tau}_i)\,\hat{\tau}_i\, d\hat{\tau}_i = \frac{1}{2\pi}, \qquad \int_{\hat{x}_i=0}^{\hat{x}_i=+\infty} f_{x0}(\hat{x}_i)\,\hat{x}_i\, d\hat{x}_i = \frac{1}{2\pi}, \qquad \int_{\hat{y}_i=0}^{\hat{y}_i=+\infty} f_{y0}(\hat{y}_i)\,\hat{y}_i\, d\hat{y}_i = \frac{1}{2\pi}. \tag{4.28}$$

Since on an average, the beam center of mass is on axis, e.g. the horizontal signal as well as the horizontal dipolar magnetic field induced by the stationary distribution are null

$$\begin{aligned} S_x(t,\vartheta) = N_b \int\int\int\int\int\int s_{x,i}(t,\vartheta)\, f_{x0}(\hat{x}_i)\, f_{y0}(\hat{y}_i)\, g_0(\hat{\tau}_i)\,\hat{x}_i\,\hat{y}_i\,\hat{\tau}_i \times \\ d\hat{x}_i\, d\hat{y}_i\, d\hat{\tau}_i\, d\varphi_{0x,i}\, d\varphi_{0y,i}\, d\psi_i = 0, \end{aligned} \tag{4.29}$$

where N_b is the number of particles in the bunch.

4.3.2 Perturbations

Let's define two distribution functions

$$\Psi_x = \Psi_0 + \Delta\Psi_x, \qquad \Psi_y = \Psi_0 + \Delta\Psi_y. \tag{4.30}$$

In order to get some dipolar fields, density perturbations $\Delta\Psi_{x,y}$ that describe beam center-of-mass displacements along the bunch are assumed. The mathematical form of the perturbations is suggested by the single-particle signals. The kind of perturbation we are looking for is the rigid-dipolar mode.[54] This is the mode for which the stationary distributions $f_{x0}(\hat{x}_i)$ and $f_{y0}(\hat{y}_i)$ are displaced from the origin by a small amount and rotate rigidly about the origin. Expanding these distributions to first order and considering a single value of *m* (i.e. considering the case of low intensity coherent modes of oscillation, in which the betatron frequency shift remains small when compared to the incoherent synchrotron frequency ω_s[d]), one then has for the amplitudes of the perturbations

$$\begin{aligned} h_m^x(\hat{x}_i,\hat{y}_i,\hat{\tau}_i) &= \frac{df_{x0}(\hat{x}_i)}{d\hat{x}_i}\,\hat{x}_m(\hat{\tau}_i)\, f_{y0}(\hat{y}_i)\, g_0(\hat{\tau}_i), \\ h_m^y(\hat{x}_i,\hat{y}_i,\hat{\tau}_i) &= \frac{df_{y0}(\hat{y}_i)}{d\hat{y}_i}\,\hat{y}_m(\hat{\tau}_i)\, f_{x0}(\hat{x}_i)\, g_0(\hat{\tau}_i), \end{aligned} \tag{4.31}$$

where $\hat{x}_m(\hat{\tau}_i)$ and $\hat{y}_m(\hat{\tau}_i)$ are the coherent (average) transverse peak betatron amplitudes associated with a given synchrotron orbit $\hat{\tau}_i$. Furthermore, because of the integral over $\varphi_{0x,i}$, $\varphi_{0y,i}$ and ψ_i, the transverse signals induced would be null unless

[d] For a general treatment of bunched beam mode-coupling, see Ref. 55.

one introduces the complex conjugates of $e^{j(\varphi_{0x,i}+m\psi_i)}$ and $e^{j(\varphi_{0y,i}+m\psi_i)}$ in the perturbation terms. The betatron phases and synchrotron phase are chosen in order to satisfy

$$\varphi_{0x,i} + m\psi_i = 0, \qquad \varphi_{0y,i} + m\psi_i = 0. \tag{4.32}$$

Linear coupling is described by Eqs. (3.15) and (3.16). Considering only the dominant Fourier component of the coupling (l), the perturbations are written as follows

$$\Delta\Psi_x = h_m^x(\hat{x}_i, \hat{y}_i, \hat{\tau}_i)\, e^{j\Delta\omega_{c,m}^{x,i} t}, \qquad \Delta\Psi_y = h_m^y(\hat{x}_i, \hat{y}_i, \hat{\tau}_i)\, e^{j\Delta\omega_{c,m}^{y,i} t}, \tag{4.33}$$

with

$$\begin{aligned} \Delta\omega_{c,m}^{x,i} &= \omega_c - \left[\omega_{x,i}(\hat{x}_i, \hat{y}_i) + m\omega_s\right], \\ \Delta\omega_{c,m}^{y,i} &= \omega_c - l\Omega_0 - \left[\omega_{y,i}(\hat{x}_i, \hat{y}_i) + m\omega_s\right], \end{aligned} \tag{4.34}$$

where ω_c is the coherent betatron frequency to be determined. Then in the time domain, e.g. the horizontal signal takes the form (for a single value m)

$$\begin{aligned} &S_x(t,\vartheta) = \frac{e\Omega_0}{4\pi} N_b \int\int\int\int\int\int \hat{x}_i \sum_k j^{-m} J_{m,x}(k, \hat{\tau}_i) \times \\ &h_m^x(\hat{x}_i, \hat{y}_i, \hat{\tau}_i)\, e^{-jk\vartheta}\, e^{j(k\Omega_0+\omega_c)t}\, \hat{x}_i\, \hat{y}_i\, \hat{\tau}_i\, d\hat{x}_i\, d\hat{y}_i\, d\hat{\tau}_i\, d\varphi_{0x,i}\, d\varphi_{0y,i}\, d\psi_i\ . \end{aligned} \tag{4.35}$$

In the frequency domain, the signal is given by

$$S_x(\omega,\vartheta) = \frac{4\pi^2 I_b}{2} \sum_k e^{-jk\vartheta}\, \sigma_{x,m}(k)\, \delta[\,\omega - (k\Omega_0 + \omega_c)], \tag{4.36}$$

with

$$\sigma_{x,m}(k) = j^{-m}\, 2\pi \int\int\int h_m^x(\hat{x}_i, \hat{y}_i, \hat{\tau}_i) J_{m,x}(k, \hat{\tau}_i)\, \hat{x}_i^2\, d\hat{x}_i\, \hat{y}_i\, d\hat{y}_i\, \hat{\tau}_i\, d\hat{\tau}_i, \tag{4.37}$$

where $I_b = N_b\, e\, f_0$ is the bunch current, with f_0 the average revolution frequency. In comparison with the rich spectrum of the test particle, a single synchrotron satellite remains. The perturbation is coherent with respect to the satellite number m. By means of the perturbation, the transverse initial conditions of the particles in the bunch have been arranged. The result of this perturbation is that the position of the center of mass changes along the bunch. The horizontal (resp. vertical) phase space distribution rotates not at incoherent frequency $Q_{x0}\Omega_0 + m\omega_s$ (resp. $Q_{y0}\Omega_0 + m\omega_s$) exactly but at frequency ω_c (resp. $\omega_c - l\Omega_0$), due to the perturbations (wake fields and linear coupling between the transverse planes) and the frequency spreads.

4.4 Transverse coupling impedances

The coupling impedances $Z_{x,y}$, which gather all the characteristics of the electromagnetic response of a machine to a passing particle, allow us to express the transverse fields in terms of transverse signals

$$\left[\vec{E} + \vec{v} \times \vec{B}\right]_{x,y}(t,\vartheta) = \frac{-j\beta}{2\pi R} \int Z_{x,y}(\omega)\, S_{x,y}(\omega,\vartheta)\, e^{j\omega t}\, d\omega. \tag{4.38}$$

The main components of the transverse impedance of a standard circular machine are the resistive wall component, which is peaked at low frequency and is the principal source of transverse instabilities, the parasitic resonators (RF cavities, septum and kicker tanks…), the broad band component, which takes into account the numerous cross section changes of the vaccum chamber and gets larger when the pipe radius is reduced, and the space charge component, which is a negative inductance that can be large for low energy particles.

4.5 Equations of coherent motions

By definition,

$$\Psi_x = f_{y0}\left(\hat{y}_i\right) \int_{\hat{y}_i=0}^{\hat{y}_i=+\infty} \int_{\varphi_{0y,i}=0}^{\varphi_{0y,i}=2\pi} \Psi\, \hat{y}_i\, d\hat{y}_i\, d\varphi_{0y,i}\,,$$

$$\Psi_y = f_{x0}\left(\hat{x}_i\right) \int_{\hat{x}_i=0}^{\hat{x}_i=+\infty} \int_{\varphi_{0x,i}=0}^{\varphi_{0x,i}=2\pi} \Psi\, \hat{x}_i\, d\hat{x}_i\, d\varphi_{0x,i}\,. \tag{4.39}$$

The functions $\Psi_{x,y}$ therefore satisfy the "reduced" Vlasov equations

$$\frac{\partial \Psi_x}{\partial t} + \frac{\partial \Psi_x}{\partial \hat{x}_i}\dot{\hat{x}}_i + \frac{\partial \Psi_x}{\partial \varphi_{0x,i}}\dot{\varphi}_{0x,i} + \frac{\partial \Psi_x}{\partial \hat{\tau}_i}\dot{\hat{\tau}}_i + \frac{\partial \Psi_x}{\partial \psi_i}\dot{\psi}_i = 0,$$

$$\frac{\partial \Psi_y}{\partial t} + \frac{\partial \Psi_y}{\partial \hat{y}_i}\dot{\hat{y}}_i + \frac{\partial \Psi_y}{\partial \varphi_{0y,i}}\dot{\varphi}_{0y,i} + \frac{\partial \Psi_y}{\partial \hat{\tau}_i}\dot{\hat{\tau}}_i + \frac{\partial \Psi_y}{\partial \psi_i}\dot{\psi}_i = 0. \tag{4.40}$$

Dropping the second order terms with respect to the perturbations, the first equation of Eq. (4.40) yields

$$j\,\Delta\omega_{c,m}^{x,i}\, h_m^x\left(\hat{x}_i, \hat{y}_i, \hat{\tau}_i\right) e^{j\,\Delta\omega_{c,m}^{x,i} t} = -\frac{df_{x0}\left(\hat{x}_i\right)}{d\hat{x}_i}\dot{\hat{x}}_i\, f_{y0}\left(\hat{y}_i\right) g_0\left(\hat{\tau}_i\right). \tag{4.41}$$

The expression of $\dot{\hat{x}}_i$ can be drawn from the single-particle horizontal equation of motion (see the first equation of Eqs. (4.9))

$$\dot{\hat{x}}_i = \frac{d}{dt}\left(\hat{x}_i\right) = \frac{d}{dt}\left[x_i^2 + \left(\frac{\dot{x}_i}{\dot{\varphi}_{x,i}}\right)^2\right]^{1/2} = -\frac{\sin\left(\varphi_{x,i}\right)}{\dot{\varphi}_{x,i}} F_x \approx -\frac{j}{2\omega_{x0}} e^{-j\varphi_{x,i}}\, F_x\,. \tag{4.42}$$

Here, $\dot{\varphi}_{x,i}$ has been approximated by ω_{x0} and $\sin\left(\varphi_{x,i}\right)$ by $\left(j/2\right)e^{-j\varphi_{x,i}}$, since the other component can be ignored if the frequency shift is small compared to the betatron frequency. Furthermore, $F_x = F_{x1} + F_{x2}$, with

$$F_{x1} = \frac{e}{m_0 \gamma}\left[\vec{E} + \vec{v} \times \vec{B}\right]_x \left(t, \vartheta = \Omega_0 \left(t - \tau_i \right)\right),$$

$$F_{x2} = \underline{\hat{K}}_0 \left(l \right) e^{j l \Omega_0 \left(t - \tau_i \right)} R^2 \Omega_0^2 \; y_i \,. \tag{4.43}$$

Using Eqs. (4.17), (4.36), (4.37) and (4.38), yields for the first term

$$-\frac{j}{2\omega_{x0}} e^{-j\varphi_{x,i}} \; F_{x1} = -\frac{e\pi I_b}{2 m_0 \, c \, \gamma Q_{x0}} \sum_k Z_x \left(\omega_k^x \right) \sigma_{x,m} \left(k \right) j^m \, J_{m,x} \left(k, \hat{\tau}_i \right) e^{j \Delta\omega_{c,m}^{x,i} t} \,, \tag{4.44}$$

where

$$\omega_k^x = \left(k + Q_{x0} \right) \Omega_0 + m\omega_s \,, \qquad -\infty \le k \le +\infty. \tag{4.45}$$

The second term is given by (for the coherent motion)

$$-\frac{j}{2\omega_{x0}} e^{-j\varphi_{x,i}} \; F_{x2} = -\frac{j}{2\omega_{x0}} \underline{\hat{K}}_0 \left(l \right) e^{j l \Omega_0 t} \, e^{-j l \Omega_0 \tau_i} \; R^2 \, \Omega_0^2 \, \hat{y}_m \left(\hat{\tau}_i \right) e^{j \left(\varphi_{y,i} + \Delta\omega_{c,m}^{y,i} t \, - \, \varphi_{x,i} \right)}. \tag{4.46}$$

This leads to

$$\begin{aligned} j \Delta\omega_{c,m}^{x,i} \; h_m^x \left(\hat{x}_i, \hat{y}_i, \hat{\tau}_i \right) e^{\, j \Delta\omega_{c,m}^{x,i} t} = & \frac{df_{x0} \left(\hat{x}_i \right)}{d\hat{x}_i} \, f_{y0} \left(\hat{y}_i \right) g_0 \left(\hat{\tau}_i \right) \times \\ & \left[\begin{array}{l} \dfrac{e\pi I_b}{2 m_0 \, c \, \gamma Q_{x0}} \sum_k Z_x \left(\omega_k^x \right) \sigma_{x,m} \left(k \right) j^m \, J_{m,x} \left(k, \hat{\tau}_i \right) e^{\, j \Delta\omega_{c,m}^{x,i} t} \\ + \, j \, \dfrac{\underline{\hat{K}}_0 \left(l \right) R^2 \, \Omega_0^2}{2 \, \omega_{x0}} \, \hat{y}_m \left(\hat{\tau}_i \right) e^{\, j \left(\varphi_{y,i} + l \Omega_0 t - l \Omega_0 \tau_i + \Delta\omega_{c,m}^{y,i} t \, - \, \varphi_{x,i} \right)} \end{array} \right]. \end{aligned} \tag{4.47}$$

Multiplying both sides of Eq. (4.47) by $e^{\, j \varphi_{x,i}} \, e^{\, - j \, p \Omega_0 \tau_i}$, where p is an integer, developing it using Eq. (4.17) and retaining only one value m, one obtains

$$\begin{aligned} j \Delta\omega_{c,m}^{x,i} \; h_m^x \left(\hat{x}_i, \hat{y}_i, \hat{\tau}_i \right) J_{m,x} \left(p, \hat{\tau}_i \right) = & \frac{df_{x0} \left(\hat{x}_i \right)}{d\hat{x}_i} \, f_{y0} \left(\hat{y}_i \right) g_0 \left(\hat{\tau}_i \right) \times \\ & \left[\begin{array}{l} \dfrac{e\pi I_b}{2 m_0 \, c \, \gamma Q_{x0}} \sum_k Z_x \left(\omega_k^x \right) \sigma_{x,m} \left(k \right) j^m \, J_{m,x} \left(k, \hat{\tau}_i \right) J_{m,x} \left(p, \hat{\tau}_i \right) \\ + \, j \, \dfrac{\underline{\hat{K}}_0 \left(l \right) R^2 \, \Omega_0^2}{2 \, \omega_{x0}} \, \hat{y}_m \left(\hat{\tau}_i \right) J_{m,y} \left(p + l, \hat{\tau}_i \right) \end{array} \right]. \end{aligned} \tag{4.48}$$

Inserting the first equation of Eqs. (4.31) into Eq. (4.48), multiplying both sides by $\hat{x}_i^2 \, \hat{y}_i$, integrating over $\hat{x}_i$ and $\hat{y}_i$ values and using

$$\int_{\hat{x}_i = 0}^{\hat{x}_i = +\infty} \frac{df_{x0} \left(\hat{x}_i \right)}{d\hat{x}_i} \hat{x}_i^2 \, d\hat{x}_i = -2 \int_{\hat{x}_i = 0}^{\hat{x}_i = +\infty} f_{x0} \left(\hat{x}_i \right) \hat{x}_i \, d\hat{x}_i = -\frac{1}{\pi}, \tag{4.49}$$

one obtains

$$I_x^{-1}\,\hat{x}_m(\hat{\tau}_i)\,J_{m,x}(p,\hat{\tau}_i)\,g_0(\hat{\tau}_i)=-\frac{je\pi I_b}{2m_0\,c\,\gamma\,Q_{x0}}\sum_k Z_x\left(\omega_k^x\right)\sigma_{x,m}(k)\;j^m\times$$
$$J_{m,x}(k,\hat{\tau}_i)\,J_{m,x}(p,\hat{\tau}_i)\,g_0(\hat{\tau}_i)+\frac{\hat{\underline{K}}_0(l)\,R^2\,\Omega_0^2}{2\,\omega_{x0}}\,\hat{y}_m(\hat{\tau}_i)\,J_{m,y}(p+l,\hat{\tau}_i)\,g_0(\hat{\tau}_i), \tag{4.50}$$

with

$$\sigma_{x,m}(k)=j^{-m}\,2\pi\iiint\frac{df_{x0}(\hat{x}_i)}{d\hat{x}_i}\,\hat{x}_m(\hat{\tau}_i)\,J_{m,x}(k,\hat{\tau}_i)\,f_{y0}(\hat{y}_i)g_0(\hat{\tau}_i)\,\hat{x}_i^2\,d\hat{x}_i\,\hat{y}_i\,d\hat{y}_i\;\hat{\tau}_i\,d\hat{\tau}_i$$
$$=-\frac{j^{-m}}{\pi}\int\hat{x}_m(\hat{\tau}_i)\,J_{m,x}(k,\hat{\tau}_i)g_0(\hat{\tau}_i)\,\hat{\tau}_i\;d\,\hat{\tau}_i\,, \tag{4.51}$$

and

$$I_x=\int_{\hat{x}_i=0}^{\hat{x}_i=+\infty}\int_{\hat{y}_i=0}^{\hat{y}_i=+\infty}\frac{-2\pi^2\,\dfrac{df_{x0}(\hat{x}_i)}{d\hat{x}_i}\,\hat{x}_i^2\;f_{y0}(\hat{y}_i)\,\hat{y}_i}{\omega_c-\omega_{x,i}(\hat{x}_i,\hat{y}_i)-m\omega_s}\,d\hat{x}_i\,d\hat{y}_i\,. \tag{4.52}$$

Multiplying both sides of Eq. (4.50) by $\hat{\tau}_i$ and summing over $\hat{\tau}_i$ values, yields

$$I_x^{-1}\,\sigma_{x,m}(p)=\sum_k K_{x,m}^{pk}\,\sigma_{x,m}(k)+\frac{\hat{\underline{K}}_0(l)\,R^2\,\Omega_0^2}{2\,\omega_{x0}}\,\sigma_{y,m}(p+l). \tag{4.53}$$

The corresponding equation for the vertical plane is

$$I_y^{-1}\,\sigma_{y,m}(p+l)=\sum_k K_{y,m}^{(p+l)k}\,\sigma_{y,m}(k)+\frac{\hat{\underline{K}}_0(-l)\,R^2\,\Omega_0^2}{2\,\omega_{y0}}\,\sigma_{x,m}(p). \tag{4.54}$$

Here,

$$K_{x,m}^{pk}=\frac{je\,I_b}{2m_0\,c\,\gamma\,Q_{x0}}Z_x\left(\omega_k^x\right)\int_{\hat{\tau}_i=0}^{\hat{\tau}_i=\tau_b/2}J_{m,x}(k,\hat{\tau}_i)\,J_{m,x}(p,\hat{\tau}_i)\,g_0(\hat{\tau}_i)\,\hat{\tau}_i\,d\hat{\tau}_i\,,$$
$$K_{y,m}^{(p+l)k}=\frac{je\,I_b}{2m_0\,c\,\gamma\,Q_{y0}}Z_y\left(\omega_k^y\right)\int_{\hat{\tau}_i=0}^{\hat{\tau}_i=\tau_b/2}J_{m,y}(k,\hat{\tau}_i)\,J_{m,y}(p+l,\hat{\tau}_i)\,g_0(\hat{\tau}_i)\,\hat{\tau}_i\,d\hat{\tau}_i\,, \tag{4.55}$$

and

$$I_y=\int_{\hat{x}_i=0}^{\hat{x}_i=+\infty}\int_{\hat{y}_i=0}^{\hat{y}_i=+\infty}\frac{-2\pi^2\,\dfrac{df_{y0}(\hat{y}_i)}{d\hat{y}_i}\,\hat{y}_i^2\;f_{x0}(\hat{x}_i)\,\hat{x}_i}{\omega_c-\omega_{y,i}(\hat{x}_i,\hat{y}_i)-l\Omega_0-m\omega_s}\,d\hat{x}_i\,d\hat{y}_i\,. \tag{4.56}$$

This leads to

$$\left[K_{x,m}-I_x^{-1}\,I\right]\Sigma_{x,m}=-\frac{\hat{\underline{K}}_0(l)\,R^2\,\Omega_0^2}{2\,\omega_{x0}}\;\Sigma_{y,m}\,,$$
$$\left[K_{y,m}-I_y^{-1}\,I\right]\Sigma_{y,m}=-\frac{\hat{\underline{K}}_0(-l)\,R^2\,\Omega_0^2}{2\,\omega_{y0}}\;\Sigma_{x,m}\,, \tag{4.57}$$

where I is the identity matrix, $K_{x,m}$ and $K_{y,m}$ are the matrices whose elements are given by Eqs. (4.55), $\Sigma_{x,m}$ and $\Sigma_{y,m}$ are the vectors whose elements are $\sigma_{x,m}(k)$ and $\sigma_{y,m}(k+l)$. From Eqs. (4.57), one thus obtains the general two-dimensional dispersion relation

$$\det\left[\left(K_{x,m}-I_x^{-1}\,I\right)\left(K_{y,m}-I_y^{-1}\,I\right)-\frac{\left|\underline{\hat{K}}_0(l)\right|^2 R^4\,\Omega_0^4}{4\,\omega_{x0}\,\omega_{y0}}\,I\right]=0. \tag{4.58}$$

4.5.1 No coupling and no Landau damping

In the absence of both Landau damping and linear coupling between the transverse planes, the first order one-dimensional eigensystem of Laclare is recovered from Eq. (4.58).[17] It is written, e.g. in the horizontal plane, as

$$\det\left[K_{x,m}-\left(\omega_c-\omega_{x0}-m\omega_s\right)I\right]=0. \tag{4.59}$$

The procedure to obtain first order exact solutions, with realistic modes and a general interaction, thus consists of finding the eigenvalues and eigenvectors of the infinite complex matrix $K_{x,m}$. The result is an infinite number of modes mq $(-\infty<q<+\infty)$ of oscillation. To each mode, one can associate a coherent frequency shift $\left(\omega_c-\omega_{x0}-m\omega_s\right)_q$ (qth eigenvalue of the matrix), a coherent spectrum $\sigma_{x,mq}(k)$ (qth eigenvector of the matrix) and a coherent peak betatron amplitude distribution $\hat{x}_{mq}(\hat{\tau}_i)$ defined by Eq. (4.50) with neither coupling nor Landau damping. For numerical reasons, the matrix needs to be truncated, and thus only a finite frequency domain is explored. Low order eigenvalues and eigenvectors of the matrix $K_{x,m}$ can be found quickly by computation, using the relations

$$\begin{aligned}
&\int_0^X J_m^2(a\,x)\,x\,dx=\frac{X^2}{2}\left[J_m'(a\,X)\right]^2+\frac{1}{2}\left[X^2-\frac{m^2}{a^2}\right]J_m^2(a\,X),\\
&\int_0^X x\,J_m(a\,x)\,J_m(b\,x)\,dx=\frac{X}{a^2-b^2}\left[a\,J_m(b\,X)\,J_{m+1}(a\,X)-b\,J_m(a\,X)\,J_{m+1}(b\,X)\right],
\end{aligned} \tag{4.60}$$

for $a^2\neq b^2$ and where a prime denotes the derivative. It is found that the spectrum of mode mq is peaked near $\omega=(|q|+1)\pi/\tau_b$ and extends over $\pm 2\pi/\tau_b$ (radians/second). The largest eigenvalue $\left(\omega_c-\omega_{x0}-m\omega_s\right)_q$ takes the subscript $q=m$. Usually, only diagonal modes mm are referred to ($m=0$ dipolar mode, $m=1$ quadrupolar mode, etc.). Figure 11 illustrates the results (for the first three diagonal modes) for the "water-bag bunch", $g_0(\hat{\tau}_i)=4/\left(\pi\tau_b^2\right)$, interacting with a very broad band impedance Z_x constant over the mode spectrum (space charge or inductive walls), and for zero and non-zero chromaticity (which shifts the center of the spectra, from 0 to the chromatic frequency, and makes the pick-up signals more complicated).

Finding the eigenvalues and eigenvectors of a complex matrix by computer can be difficult in some cases, and a simple approximate formula for the eigenvalues *mm* (which will be simply written *m* in following) is useful in practice to have a rough estimate. Multiplying both sides of Eq. (4.50), with neither coupling nor Landau damping, by $\hat{x}_m(\hat{\tau}_i)g_0(\hat{\tau}_i)$ and integrating over $\hat{\tau}_i$ values, yields

$$\left(\omega_c - \omega_{x0} - m\omega_s\right)\int_{\hat{\tau}_i=0}^{\hat{\tau}_i=\tau_b/2}\hat{x}_m^2(\hat{\tau}_i)g_0(\hat{\tau}_i)\,\hat{\tau}_i\,d\,\hat{\tau}_i = \frac{je\pi^2 I_b\, j^{2m}}{2m_0\,c\,\gamma Q_{x0}}\sum_{k=-\infty}^{k=+\infty} Z_x\left(\omega_k^x\right)\sigma_{x,m}^2(k). \quad (4.61)$$

Applying the relations (see Appendix C)

$$\pi^{-2}\,j^{-2m}\int_{\hat{\tau}_i=0}^{\hat{\tau}_i=\tau_b/2}\hat{x}_m^2(\hat{\tau}_i)g_0^2(\hat{\tau}_i)\,\hat{\tau}_i\;d\,\hat{\tau}_i = \frac{\Omega_0}{2}\sum_{k=-\infty}^{k=+\infty}\left|\left(k+Q_{x0}\right)\Omega_0 - \omega_{\xi_x}\right|\sigma_{x,m}^2(k), \quad (4.62)$$

Eq. (4.61) becomes

$$\begin{aligned}&\left(\omega_c - \omega_{x0} - m\omega_s\right)\frac{\pi\tau_b^2\,\Omega_0}{8}\sum_{k=-\infty}^{k=+\infty}\left|\left(k+Q_{x0}\right)\Omega_0 - \omega_{\xi_x}\right|\sigma_{x,m}^2(k)\\ &= \frac{je\,I_b}{2m_0\,c\,\gamma Q_{x0}}\sum_{k=-\infty}^{k=+\infty} Z_x\left(\omega_k^x\right)\sigma_{x,m}^2(k).\end{aligned} \quad (4.63)$$

Furthermore, the mode *m* is peaked near the frequency $\left(|m|+1\right)\pi/\tau_b$ and the approximation $\left(k+Q_{x0}\right)\Omega_0 - \omega_{\xi_x} \approx \left(|m|+1\right)\pi/\tau_b$ can be used in Eq. (4.63), which can then be approximately written as

$$\left(\omega_c - \omega_{x0} - m\omega_s\right) = \left(|m|+1\right)^{-1}\frac{je\beta I_b}{2m_0\gamma Q_{x0}\Omega_0 L}\frac{\sum_{k=-\infty}^{k=+\infty} Z_x\left(\omega_k^x\right)\sigma_{x,m}^2(k)}{\sum_{k=-\infty}^{k=+\infty}\sigma_{x,m}^2(k)}, \quad (4.64)$$

where L is the bunch length (in meters). The spectrum $\sigma_{x,m}(k)$ depends on the interaction $Z_x\left(\omega_k^x\right)$. However, for a non exact but realistic set of modes, Eq. (4.64), with $\sigma_{x,m}(k)$ given by Figure 11, can be used to find approximate eigenvalues for any $Z_x\left(\omega_k^x\right)$. A good (proportional) fitting of the power spectrum $\left|\sigma_{x,m}(k)\right|^2$ of Figure 11 is obtained by the function $h_m\left(\omega-\omega_{\xi_x}\right)$, given by

$$h_m\left(\omega-\omega_{\xi_x}\right) = \left(|m|+1\right)^2\frac{1+(-1)^{|m|}\cos\left[\left(\omega-\omega_{\xi_x}\right)\tau_b\right]}{\left[\left(\omega\tau_b/\pi\right)^2-\left(|m|+1\right)^2\right]^2}. \quad (4.65)$$

The power spectrum of mode $|m|$ is peaked near $\omega = \left(|m|+1\right)\pi/\tau_b$ and extends $\pm 2\pi/\tau_b$ (radians/second) as the discrete spectrum found numerically in Figure 11.

Using the fitting function, Sacherer's formula for the transverse coherent frequency shifts of bunched beam modes is obtained[18,45]

$$\Delta\omega_{c,m}^{x} = \left(\omega_c - \omega_{x0} - m\omega_s\right) = \left(|m|+1\right)^{-1} \frac{je\beta I_b}{2m_0\gamma Q_{x0}\Omega_0 L} \frac{\sum_{k=-\infty}^{k=+\infty} Z_x\left(\omega_k^x\right) h_m\left(\omega_k^x - \omega_{\xi_x}\right)}{\sum_{k=-\infty}^{k=+\infty} h_m\left(\omega_k^x - \omega_{\xi_x}\right)}, \tag{4.66}$$

where ω_k^x is given by Eq. (4.45) for a single bunch or several bunches oscillating independently. For coupled motion of M bunches, $k = n_x + k'M$, with $-\infty \le k' \le +\infty$, where n_x is the coupled-bunch mode number. The plot of the fitting function is given in Figure 12 for the first three modes.

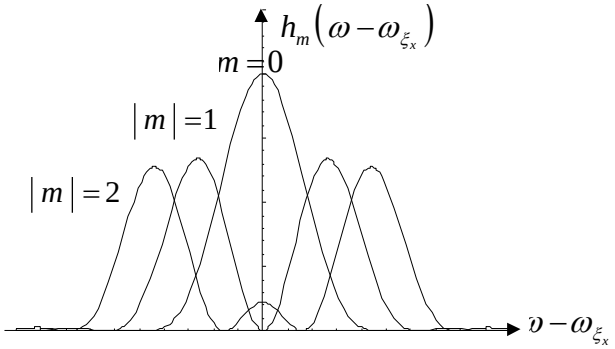

FIGURE 12 Power spectrum (centred at the horizontal chromatic frequency) for the diagonal modes $|m| = 0, 1, 2$.

The function $h_m\left(\omega-\omega_{\xi_x}\right)$ is given by

$$h_m\left(\omega-\omega_{\xi_x}\right) = \frac{2\pi^4}{\tau_b^2} \left| p_m\left(\omega-\omega_{\xi_x}\right)\right|^2, \tag{4.67}$$

where $p_m\left(\omega-\omega_{\xi_x}\right)$ is the Fourier transform of the signal $p_m(t)\, e^{j\omega_{\xi_x} t}$. Here, $p_m(t)$ corresponds to sinusoidal modes given by

$$p_m(t) = \begin{cases} \cos\left[\left(|m|+1\right)\pi t/\tau_b\right], & m \text{ even} \\ \sin\left[\left(|m|+1\right)\pi t/\tau_b\right], & m \text{ odd} \end{cases}. \tag{4.68}$$

The difference signal from a beam position monitor has thus the form[45]

$$\Delta - \text{signal} \propto p_m(t)\, e^{j\left(\chi_x t/\tau_b + 2\pi k Q_{x0}\right)}, \tag{4.69}$$

for the kth revolution, where $\chi_x = \omega_{\xi_x}\tau_b$ (radians) is the total phase shift between head and tail. The frequency (radians/second) of the wiggles along the bunch is determined by the horizontal chromatic frequency ω_{ξ_x}, and the number of nodes on separate

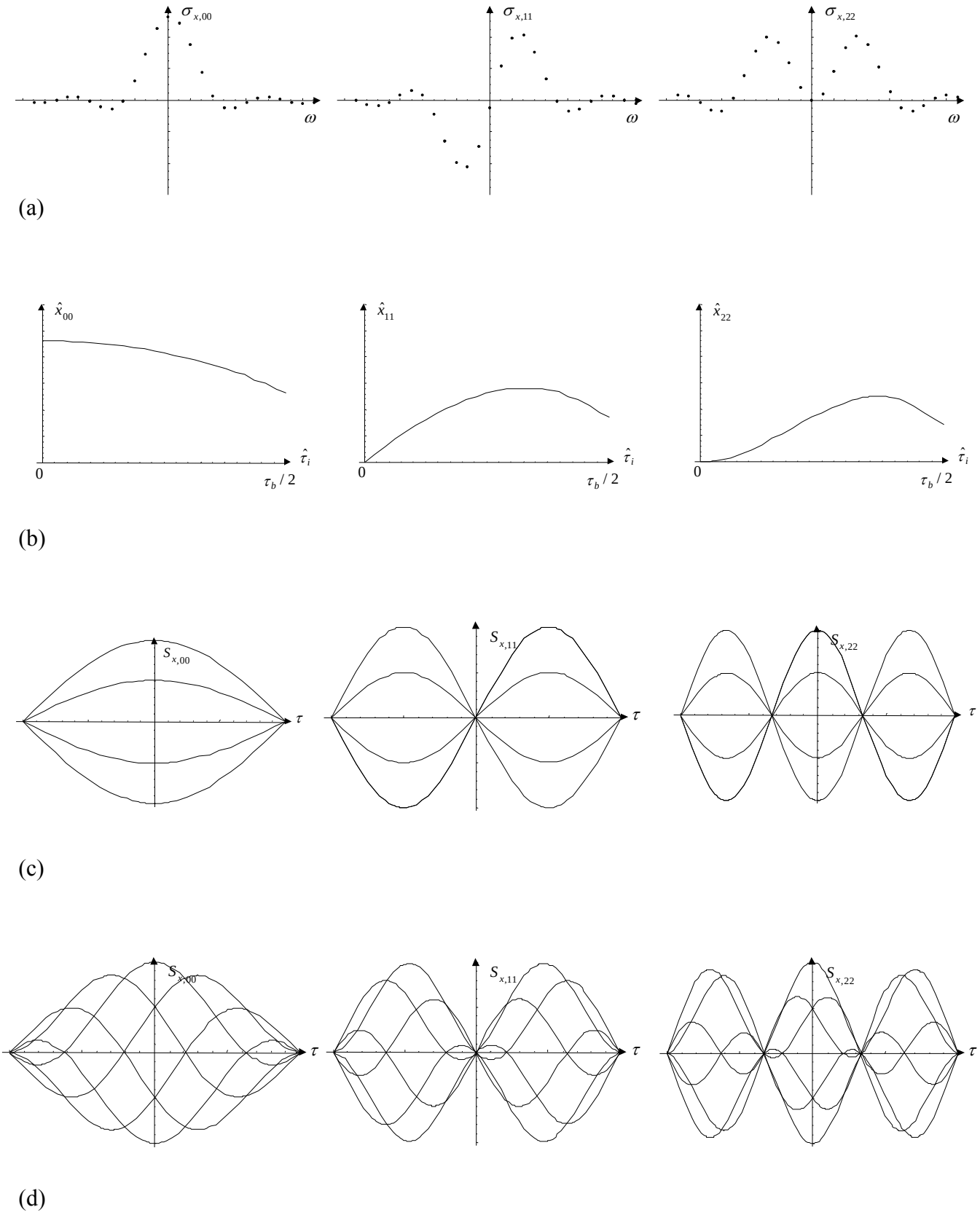

FIGURE 11 Horizontal coherent oscillations of a "water-bag bunch" interacting with a constant inductive impedance, for the first three diagonal modes: (a) Spectra (centred at the horizontal chromatic frequency). (b) Perturbation amplitudes. (c) Several superimposed pick-up signals (for a given tune) with zero chromaticity. (d) Several superimposed pick-up signals (for the given tune) with non-zero chromaticity.

superimposed revolutions gives the modulus of the head-tail mode number $|m|$. The signals (c) and (d) of Figure 11 have been drawn using directly these approximate sinusoidal modes.

4.5.2 No wake fields

In the absence of wake fields, from Eq. (4.58), the two-dimensional dispersion relation is given by

$$I_x^{-1}\, I_y^{-1} = \frac{\left|\underline{\hat{K}}_0(l)\right|^2 R^4\, \Omega_0^4}{4\, \omega_{x0}\, \omega_{y0}}. \tag{4.70}$$

If, in addition, there is no frequency spread, Eq. (4.70) leads to the well-known result of coupling in the smooth approximation

$$\left(\omega_c - \omega_{x0} - m\omega_s\right)\left(\omega_c - \omega_{y0} - l\,\Omega_0 - m\omega_s\right) = \frac{\left|\underline{\hat{K}}_0(l)\right|^2 R^4\, \Omega_0^4}{4\, \omega_{x0}\, \omega_{y0}}. \tag{4.71}$$

4.5.3 Coupled-bunch modes

If only the diagonal terms of the matrices $K_{x,m}$ and $K_{y,m}$ are taken into account, then, from Eq. (4.58), the two-dimensional dispersion relation is given by

$$\begin{aligned}
&\left[I_x^{-1} - \frac{j e I_b}{2 m_0 c \gamma Q_{x0}} Z_x\left(\omega_p^x\right) \int_{\hat{\tau}_i=0}^{\hat{\tau}_i=\tau_b/2} J_m^2 \left\{ \left[\left(p + Q_{x0} \right) \Omega_0 - \omega_{\xi_x} \right] \hat{\tau}_i \right\} g_0\left(\hat{\tau}_i\right) \hat{\tau}_i \, d\hat{\tau}_i \right] \times \\
&\left[I_y^{-1} - \frac{j e I_b}{2 m_0 c \gamma Q_{y0}} Z_y\left(\omega_{p+l}^y\right) \int_{\hat{\tau}_i=0}^{\hat{\tau}_i=\tau_b/2} J_m^2 \left\{ \left[\left(p + l + Q_{y0} \right) \Omega_0 - \omega_{\xi_y} \right] \hat{\tau}_i \right\} g_0\left(\hat{\tau}_i\right) \hat{\tau}_i \, d\hat{\tau}_i \right] \\
&= \frac{\left|\underline{\hat{K}}_0(l)\right|^2 R^4\, \Omega_0^4}{4\, \omega_{x0}\, \omega_{y0}},
\end{aligned} \tag{4.72}$$

where

$$\omega_p^x = \left(p + Q_{x0} \right) \Omega_0 + m\omega_s, \qquad \omega_{p+l}^y = \left(p + l + Q_{y0} \right) \Omega_0 + m\omega_s. \tag{4.73}$$

It corresponds to the case of motions driven by single lines, $\left(p + Q_{x0} \right) \Omega_0 + m\omega_s$ in the horizontal plane and $\left(p + l + Q_{y0} \right) \Omega_0 + m\omega_s$ in the vertical one.

Up to now, a single bunch has been assumed. If M equidistant bunches are present in the ring, M possibilities of coupled-bunch coherent motion exist. The coupled-bunch mode numbers $n_{x,y}$ correspond to phase shifts of $2\pi n_{x,y} / M$ between the coherent perturbations of two successive bunches. Every *M*th line occurs at

$$\omega_{k'}^x = \left(n_x + k' M + Q_{x0} \right) \Omega_0 + m\omega_s, \qquad \omega_{k'}^y = \left(n_y + k' M + Q_{y0} \right) \Omega_0 + m\omega_s, \tag{4.74}$$

but with an amplitude M times larger (see Appendix D). As a consequence, the transverse wake field terms, in Eq. (4.72), must be multiplied by M. The coupled-bunch mode numbers are related by $n_x = n_y - l$.

4.5.4 "Hollow-bunch (or air-bag) model"

In this case, all the particles have the same synchrotron amplitude $\hat{\tau}_i = \hat{\tau}_0$. Equation (4.53) then becomes

$$I_x^{-1}\,\hat{x}_m(\hat{\tau}_0) = \frac{j e I_b}{4\pi m_0 c\,\gamma Q_{x0}} \sum_k Z_x\left(\omega_k^x\right) J_{m,x}^2(k,\hat{\tau}_0)\,\hat{x}_m(\hat{\tau}_0) + \frac{\hat{\underline{K}}_0(l)\,R^2\,\Omega_0^2}{2\,\omega_{x0}}\,\hat{y}_m(\hat{\tau}_0)\,J_{m,y}(p+l,\hat{\tau}_0)\,J_{m,x}^{-1}(p,\hat{\tau}_0). \tag{4.75}$$

A similar equation is obtained for the vertical plane from Eq. (4.54). Equating $\hat{x}_m(\hat{\tau}_0)/\hat{y}_m(\hat{\tau}_0)$ in both equations, leads to

$$\left[I_x^{-1} - \frac{j e I_b}{4\pi m_0 c\,\gamma Q_{x0}} \sum_{k=-\infty}^{k=+\infty} Z_x\left(\omega_k^x\right) J_{m,x}^2(k,\hat{\tau}_0)\right] \times \left[I_y^{-1} - \frac{j e I_b}{4\pi m_0 c\,\gamma Q_{y0}} \sum_{k=-\infty}^{k=+\infty} Z_y\left(\omega_k^y\right) J_{m,y}^2(k,\hat{\tau}_0)\right] = \frac{\left|\hat{\underline{K}}_0(l)\right|^2 R^4\,\Omega_0^4}{4\,\omega_{x0}\,\omega_{y0}}. \tag{4.76}$$

4.5.5 Approximate calculation of the two-dimensional dispersion relation

The starting point is Eqs. (4.53) and (4.54). Equating $\sigma_{x,m}(p)/\sigma_{y,m}(p+l)$ in both equations, leads to

$$\left[I_x^{-1} - \frac{\sum_{k=-\infty}^{k=+\infty} K_{x,m}^{pk}\,\sigma_{x,m}(k)}{\sigma_{x,m}(p)}\right] \times \left[I_y^{-1} - \frac{\sum_{k=-\infty}^{k=+\infty} K_{y,m}^{(p+l)k}\,\sigma_{y,m}(k)}{\sigma_{y,m}(p+l)}\right] = \frac{\left|\hat{\underline{K}}_0(l)\right|^2 R^4\,\Omega_0^4}{4\,\omega_{x0}\,\omega_{y0}}. \tag{4.77}$$

The general two-dimensional dispersion relation (4.58) does not depend on the bunch spectra $\sigma_{x,m}(k)$ and $\sigma_{y,m}(k)$. One can then approximate them in Eq. (4.77) by their uncoupled values (which is quite reasonable for a perturbation treatment). Then,

$$\frac{\sum_{k=-\infty}^{k=+\infty} K_{x,m}^{pk}\,\sigma_{x,m}(k)}{\sigma_{x,m}(p)} \quad \text{and} \quad \frac{\sum_{k=-\infty}^{k=+\infty} K_{y,m}^{(p+l)k}\,\sigma_{y,m}(k)}{\sigma_{y,m}(p+l)}$$

are the horizontal and vertical frequency shifts in the absence of both coupling and Landau damping. These frequency shifts are approximated by the Sacherer's formula (see Eq. (4.66)). One thus finally obtains the following two-dimensional dispersion relation

$$\left[\left(\int_{\hat{x}_i=0}^{\hat{x}_i=+\infty}\int_{\hat{y}_i=0}^{\hat{y}_i=+\infty}\frac{-2\pi^2\dfrac{df_{x0}(\hat{x}_i)}{d\hat{x}_i}\,\hat{x}_i^2\,f_{y0}(\hat{y}_i)\,\hat{y}_i}{\omega_c-\omega_{x,i}(\hat{x}_i,\hat{y}_i)-m\omega_s}\,d\hat{x}_i\,d\hat{y}_i\right)^{-1}-U_{\mathrm{eq}x}^m+jV_{\mathrm{eq}x}^m\right]\times$$

$$\left[\left(\int_{\hat{x}_i=0}^{\hat{x}_i=+\infty}\int_{\hat{y}_i=0}^{\hat{y}_i=+\infty}\frac{-2\pi^2\dfrac{df_{y0}(\hat{y}_i)}{d\hat{y}_i}\,\hat{y}_i^2\,f_{x0}(\hat{x}_i)\,\hat{x}_i}{\omega_c-\omega_{y,i}(\hat{x}_i,\hat{y}_i)-l\Omega_0-m\omega_s}\,d\hat{x}_i\,d\hat{y}_i\right)^{-1}-U_{\mathrm{eq}y}^m+jV_{\mathrm{eq}y}^m\right] \tag{4.78}$$

$$=\frac{\left|\underline{\hat{K}}_0(l)\right|^2R^4\Omega_0^4}{4\,\omega_{x0}\,\omega_{y0}}.$$

Here, the "equivalent" dispersion relation coefficients $U_{\mathrm{eq}x,y}^m$ and $V_{\mathrm{eq}x,y}^m$ are defined by

$$U_{\mathrm{eq}x,y}^m=\mathrm{Re}\left[\left(|m|+1\right)^{-1}\frac{je\beta I_b}{2m_0\gamma Q_{x0,y0}\Omega_0 L}\frac{\displaystyle\sum_{k=-\infty}^{k=+\infty}Z_{x,y}\left(\omega_k^{x,y}\right)h_m\left(\omega_k^{x,y}-\omega_{\xi_{x,y}}\right)}{\displaystyle\sum_{k=-\infty}^{k=+\infty}h_m\left(\omega_k^{x,y}-\omega_{\xi_{x,y}}\right)}\right],$$

$$V_{\mathrm{eq}x,y}^m=-\mathrm{Im}\left[\left(|m|+1\right)^{-1}\frac{je\beta I_b}{2m_0\gamma Q_{x0,y0}\Omega_0 L}\frac{\displaystyle\sum_{k=-\infty}^{k=+\infty}Z_{x,y}\left(\omega_k^{x,y}\right)h_m\left(\omega_k^{x,y}-\omega_{\xi_{x,y}}\right)}{\displaystyle\sum_{k=-\infty}^{k=+\infty}h_m\left(\omega_k^{x,y}-\omega_{\xi_{x,y}}\right)}\right], \tag{4.79}$$

where

$$\omega_k^{x,y}=\left(k+Q_{x0,y0}\right)\Omega_0+m\omega_s. \tag{4.80}$$

In Eqs. (4.79) and (4.80), $-\infty\le k\le+\infty$ for a single bunch or several bunches oscillating independently and $k=n_{x,y}+k'M$, with $-\infty\le k'\le+\infty$ for coupled motion of M bunches, where $n_{x,y}$ are the coupled-bunch mode numbers related by $n_x=n_y-l$.

The two-dimensional dispersion relation (4.78) is similar to Eq. (3.164) with $h\left(\hat{x}_i^2,\hat{y}_i^2\right)=h_x(\hat{x}_i)\,h_y(\hat{y}_i)$, $f_{x0}(\hat{x}_i)=h_x(\hat{x}_i)/2\pi$ and $f_{y0}(\hat{y}_i)=h_y(\hat{y}_i)/2\pi$. Using U_{eq} and V_{eq} (given by Eqs. (4.79)) in the case of bunched beams, instead of U and V in the case of coasting beams, the same analysis of coupled Landau damping can be made (see Sections 3.1.3 and 3.1.4) and the same results are obtained.

In the absence of both Landau damping and linear coupling between the transverse planes, Eqs. (4.78) and (4.79) lead to the Sacherer's formula for transverse bunched beam instabilities (see Eq. (4.66)), as expected.

5 MEASUREMENT OF THE CERN-PS LINEAR COUPLING

In the presence of linear coupling between the transverse planes, any betatron motion can be expressed as a sum of two normal modes of oscillation. On the resonance $Q_h - Q_v =$ integer, the difference in the mode frequencies is proportional to the modulus of the linear coupling coefficient $|C_G|$, which provides a way of measuring it.[56,57] The approach consists in increasing Q_h and reducing Q_v in the vicinity of the resonance, while measuring the normal mode frequencies with a kicker, a pick-up and a FFT (Fast Fourier Transform) analyzer.[58]

In the PS, some skew field exists due to random tilts of the magnet units and for this reason a family of 40 skew quadrupoles have been included in the lattice. Furthermore, there is no axial field and the coupling resonance is $Q_h - Q_v = 0$.

The result of the measurements is the relation between the skew quadrupole current I_{skew} and the linear coupling coefficient $|C_G|$ (or the modulus of the zeroth-order harmonic of the normalised skew gradient $\left|\hat{\underline{K}}_0(0)\right|$ (see Eq. (3.16)), simply written $|\underline{K}_0|$ in the following).[59] An important result is that the minimum of the linear coupling in the PS is obtained for $I_{skew} \approx 0.33\ \text{A}\ (\pm\ 0.1\ \text{A})$.

5.1 Review of the general theory of linear coupling for the particular case of the PS

The exact analysis for linear coupling has been described by Guignard.[56,57] Coupling is treated as a perturbation of the transverse particle oscillations and the exact equations of the perturbed motion are obtained using the Hamiltonian formalism.

In this section we shall give a short review of the theory for the case of the PS. By virtue of the Floquet's theorem,[20,21] the general solutions of the unperturbed transverse motions of a test particle *i* (given by Hill's equations), are

$$x_i = a_1\, u_i(\vartheta)\, e^{jQ_h\vartheta} + a_1^*\, u_i^*(\vartheta)\, e^{-jQ_h\vartheta}, \qquad y_i = a_2\, v_i(\vartheta)\, e^{jQ_v\vartheta} + a_2^*\, v_i^*(\vartheta)\, e^{-jQ_v\vartheta}. \quad (5.1)$$

Here, x_i and y_i are the horizontal and vertical betatron coordinates, a_1, a_2 and their complex conjugates a_1^*, a_2^* are the four constants of the unperturbed motion, $Q_{h,v}$ are the transverse tunes, ϑ is the azimuthal angle and u_i, v_i are the Floquet's functions (u_i^*, v_i^* their complex conjugates) given by

$$u_i(\vartheta) = \left[\frac{\beta_{0x,i}(\vartheta)}{2R}\right]^{1/2} e^{j\int_0^{\vartheta}\left[R/\beta_{0x,i}(\vartheta')-Q_h\right]d\vartheta'}, \qquad v_i(\vartheta) = \left[\frac{\beta_{0y,i}(\vartheta)}{2R}\right]^{1/2} e^{j\int_0^{\vartheta}\left[R/\beta_{0y,i}(\vartheta')-Q_v\right]d\vartheta'}, \quad (5.2)$$

where $\beta_{0x,i}$ and $\beta_{0y,i}$ are the transverse betatron functions, and R the average radius of the machine. The global Hamiltonian H of the perturbed motion is deduced from the transverse equations of motion in the presence of skew quadrupolar fields. Subtracting the unperturbed Hamiltonian H_0 from H, the perturbing Hamiltonian associated with linear coupling is obtained

$$H_1(x_i, y_i, \vartheta) = K_i(\vartheta)\, x_i\, y_i, \quad (5.3)$$

with

$$K_i(\vartheta) = R^2\, \underline{K}_i\,, \tag{5.4}$$

where $\underline{K}_i$ is the normalised skew gradient. Using the canonical equations, given by Eqs.(4.34) for a general Hamiltonian, H_1 can be expressed as a function of the four constants of the unperturbed motion

$$H_1(x_i, y_i, \vartheta) = U_1\left(a_1, a_1^*, a_2, a_2^*, \vartheta\right). \tag{5.5}$$

The perturbation problem is then reduced to the study of the way in which these constants vary with ϑ in agreement with the perturbing Hamiltonian H_1 (or U_1). Since the a_i's are the constants of the unperturbed motion, they verify the Poisson bracket

$$da_i / d\vartheta = [a_i, H_1] = \sum_\rho \left(\frac{\partial a_i}{\partial q_\rho}\frac{\partial H_1}{\partial p_\rho} - \frac{\partial H_1}{\partial q_\rho}\frac{\partial a_i}{\partial p_\rho} \right). \tag{5.6}$$

Using Eq. (5.5), Eq. (5.6) can be written as

$$da_i / d\vartheta = \sum_m [a_i, a_m]\left(\partial U_1 / \partial a_m\right), \tag{5.7}$$

where

$$[a_i, a_m] = \sum_\rho \left(\frac{\partial a_i}{\partial q_\rho}\frac{\partial a_m}{\partial p_\rho} - \frac{\partial a_m}{\partial q_\rho}\frac{\partial a_i}{\partial p_\rho} \right). \tag{5.8}$$

This yields the general equations of the perturbed motion

$$\begin{aligned} da_1 / d\vartheta &= j\left(\partial U_1 / \partial a_1^*\right), & da_1^* / d\vartheta &= -j\left(\partial U_1 / \partial a_1\right), \\ da_2 / d\vartheta &= j\left(\partial U_1 / \partial a_2^*\right), & da_2^* / d\vartheta &= -j\left(\partial U_1 / \partial a_2\right). \end{aligned} \tag{5.9}$$

As the synchrotron is a periodic machine, it is possible to develop in Fourier series the function U_1. Keeping only the dominant terms, we obtain

$$U_1 = h^{(2)}_{1001-0}\, a_1\, a_2^*\, e^{j(Q_h - Q_v)\vartheta} + h^{(2)}_{01100} a_1^*\, a_2\, e^{-j(Q_h - Q_v)\vartheta}, \tag{5.10}$$

with

$$h^{(2)}_{1001-0} = \frac{1}{2\pi}\int_0^{2\pi} h^{(2)}_{1001}(\vartheta)\, d\vartheta, \quad h^{(2)}_{1001}(\vartheta) = K_i(\vartheta)\, u_i(\vartheta)\, v_i^*(\vartheta), \quad h^{(2)}_{01100} = h^{(2)^*}_{1001-0}. \tag{5.11}$$

Equations (5.9), (5.10) and (5.11) give

$$da_1 / d\vartheta = j\, h^{(2)^*}_{1001-0}\, a_2\, e^{-j(Q_h - Q_v)\vartheta}, \qquad da_2 / d\vartheta = j\, h^{(2)}_{1001-0}\, a_1\, e^{j(Q_h - Q_v)\vartheta}. \tag{5.12}$$

Defining a new variable $\tilde{a}_2 = a_2\, e^{-j(Q_h - Q_v)\vartheta}$, putting it into Eq. (5.12) and then differentiating, the equation for $\tilde{a}_2$ becomes a second order differential equation

$$d^2\tilde{a}_2 / d\vartheta^2 + j\left(Q_h - Q_v\right) d\tilde{a}_2 / d\vartheta + h^{(2)}_{1001-0}\, h^{(2)^*}_{1001-0}\, \tilde{a}_2 = 0. \tag{5.13}$$

The general solution of Eq. (5.13) is

$$\tilde{a}_2 = A_+ e^{jQ_+\vartheta} + A_- e^{jQ_-\vartheta}, \tag{5.14}$$

with

$$Q_\pm = -\frac{Q_h - Q_v}{2} \pm \sqrt{\left(\frac{Q_h - Q_v}{2}\right)^2 + \left|h^{(2)}_{1001-0}\right|^2}, \tag{5.15}$$

where $A_{+,-}$ are the constants of the perturbed motion. Finally, the expressions for a_1 and a_2 are

$$\begin{aligned} a_1 &= h^{(2)^*}_{1001-0}\left[\left(A_+ / Q_+\right)e^{jQ_+\vartheta} + \left(A_- / Q_-\right)e^{jQ_-\vartheta}\right], \\ a_2 &= \left(A_+ e^{jQ_+\vartheta} + A_- e^{jQ_-\vartheta}\right)e^{j(Q_h - Q_v)\vartheta}. \end{aligned} \tag{5.16}$$

A linear coupling coefficient is defined by

$$C_G = 2h^{(2)}_{1001-0}. \tag{5.17}$$

Using Eqs. (5.11) and (5.17), yields

$$C_G = \frac{1}{2\pi R}\int_0^{2\pi} \beta^{1/2}_{0x,i}(\vartheta)\,\beta^{1/2}_{0y,i}(\vartheta)\,K_i(\vartheta)\,e^{j\left[\left(\mu_{0x,i} - Q_h\vartheta\right) - \left(\mu_{0y,i} - Q_v\vartheta\right)\right]}d\vartheta, \tag{5.18}$$

where $\mu_{0x,i}$ and $\mu_{0y,i}$ are the phase functions. From Eq. (5.15), one deduces that the difference from the tunes of the two normal modes is given by

$$Q_+ - Q_- = \sqrt{\left(Q_h - Q_v\right)^2 + \left|C_G\right|^2}. \tag{5.19}$$

On the resonance $Q_h = Q_v$, the absolute value of the difference in the normal mode tunes $\left|Q_+ - Q_-\right|$ equals $\left|C_G\right|$ which provides a way of measuring it.

5.2 Coupling measurements from mode frequencies by FFT analysis

The coupling has been measured at 1 GeV, during a 1.2 s long flat bottom, with a low intensity bunched beam ($M = 20$ bunches and $I_{beam} \approx 250\times10^{10}$ protons). The approach is the following: for different skew quadrupole currents, we increase Q_h and reduce Q_v in the vicinity of the coupling resonance and we measure the two normal mode frequencies using a vertical kicker, a vertical pick-up and the FFT analyzer. The vertical pick-up is used because it is more sensitive than the horizontal one due to the elliptical vacuum chamber: it sees indeed the frequencies of the two normal modes.

The working point is thus programmed in such a way that Q_h linearly increases from 6.10 to 6.40 within 300 ms, while Q_v linearly decreases from 6.40 to 6.10. The beam is kicked every 5 ms during the 300 ms and a vertical FFT analysis is made every 4.096 ms during 262.144 ms (64 spectra). This is because a spectrum analysis between

0 and 500 khz (the revolution frequency is $f_0 = 417$ khz) in a time $T_m \leq 5$ ms is required. Indeed, choosing the sampling frequency $F_s = 1$ Mhz (using the Shannon's theorem), the relationships between the different parameters impose the number of channels $N_{ch} = 2048$, the frequency resolution $BW = 0.2441$ khz, the duration of the signal $T_m = 4.096$ ms and the number of consecutive spectra $N_s = 64$.[58] These spectra are then displayed in a "mountain range" display, i.e. they are displayed successively one above the other (Figure 13). For each spectrum, two spectral "lines" appear at the frequencies of the two normal modes. The minimum distance between the two normal mode frequencies (obtained when $Q_h = Q_v$) is equal to $|C_G| \times f_0$. The modulus of the linear coupling coefficient can then be deduced. From Eqs. (5.4) and (5.18), the relation between $|C_G|$ and $|\underline{K}_0|$ in the smooth approximation is

$$|\underline{K}_0| = \frac{Q_0}{R^2}|C_G|. \tag{5.20}$$

Here, Q_0 is the common value of the uncoupled transverse tunes obtained by making the average of the normal mode tunes (whose values are not given here). We obtain $Q_0 = (Q_+ + Q_-)/2 \approx 6.27$.

The plot of the coupled tunes as functions of the distance from the difference

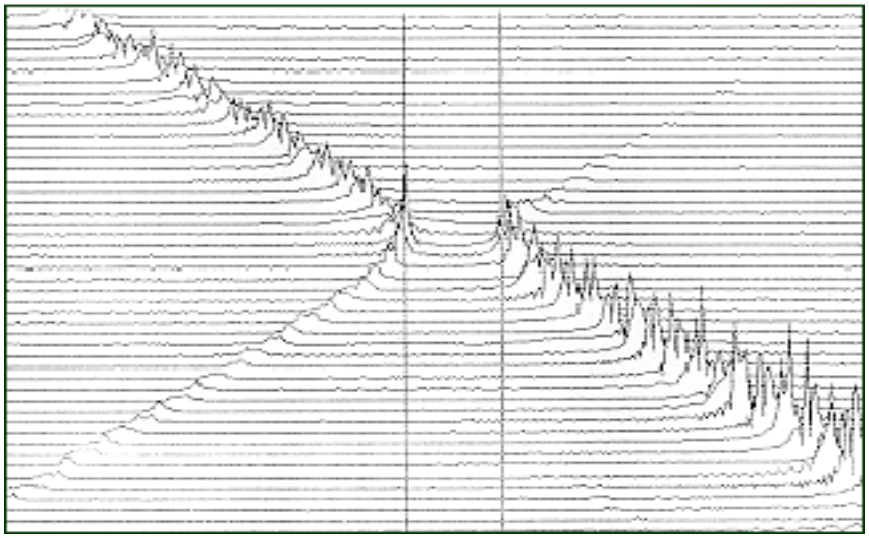

resonance is represented in Figure 13, for the particular case of "natural" coupling.

FIGURE 13 "Mountain range" display of the FFT analysis of the "natural" coupling ($I_{skew} = 0$ A). The horizontal axis is frequency and the vertical one is time.

5.3 Results and conclusions

The results of the measurements are collected in Table 1. For different values of the skew quadrupole current (from -1.5 A to 1.5 A), it exhibits the absolute value of the difference in the mode frequencies $|\Delta f|$, the modulus of the linear coupling coefficient $|C_G|$ and the modulus of the skew gradient $|\underline{K}_0|$ in the smooth approximation.

I_{skew} [A]	$\lvert \Delta f \rvert$ [kHz]	$\lvert C_G \rvert$	$\lvert \underline{K}_0 \rvert$ [m^{-2}]
-1.5	50	0.120	7.5E-05
-1.25	44	0.106	6.6E-05
-1	37	0.089	5.6E-05
-0.75	30	0.072	4.5E-05
-0.5	23	0.055	3.4E-05
-0.25	16	0.038	2.4E-05
0	9	0.022	1.4E-05
0.5	5	0.012	7.5E-06
0.75	11	0.026	1.6E-05
1	19	0.046	2.8E-05
1.25	25	0.060	3.8E-05
1.5	32	0.077	4.8E-05

TABLE 1 Measured values of $\lvert \Delta f \rvert$, $\lvert C_G \rvert$ and $\lvert \underline{K}_0 \rvert$ for different skew quadrupole currents.

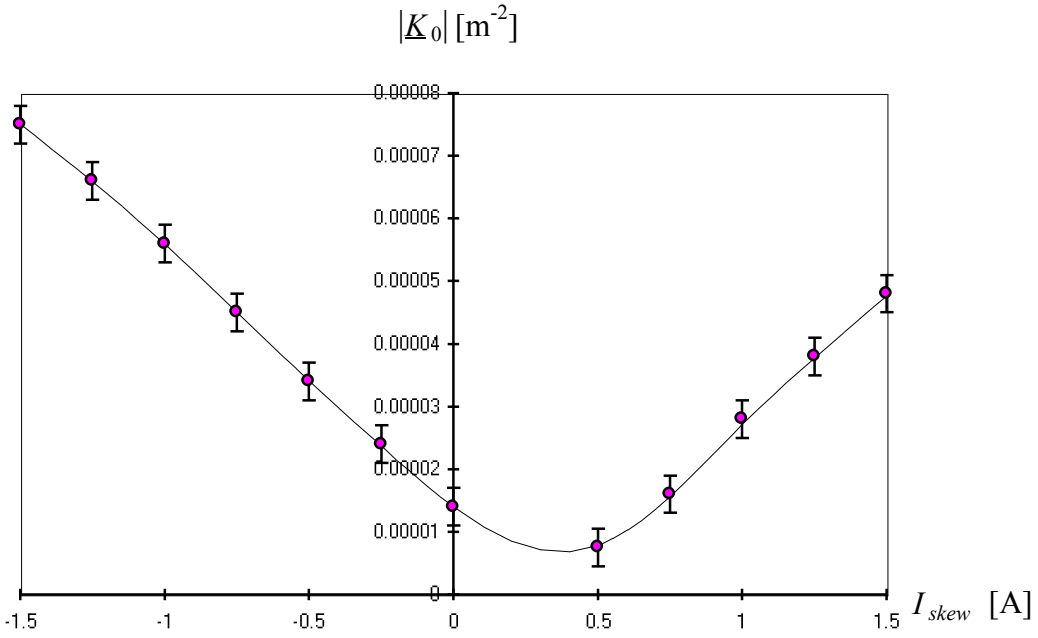

The plot of $\lvert \underline{K}_0 \rvert$ as a function of I_{skew} is represented in Figure 14.

FIGURE 14 Modulus of the normalised skew gradient (in the smooth approximation) vs. skew quadrupole current.

The error bar of the measured data depends on two different errors. The first one is the frequency resolution $BW = 0.2441\,\text{khz}$ that comes from the fact that the signal is observed only during $T_m = 1/BW = 4.096\,\text{ms}$. The second one is a reading error due to the tune spreads introduced by the transverse natural chromaticities ($\zeta_x \approx -1$ and $\zeta_y \approx -1.5$). The error in measuring a frequency is estimated to be $\pm 1\,\text{khz}$ and thus, the error in measuring Δf is $\pm 2\,\text{khz}$. The precision on $\lvert C_G \rvert$ is then

$\pm$ 2 khz $/f_0 = \pm$ 4.8$\times 10^{-3}$ and the precision on $\left|\underline{K}_0\right|$ is $\pm 3\times 10^{-6}$. Better accuracy could be obtained setting the chromaticities to zero.

The minimum of the linear coupling in the PS can not be determined exactly due to the tune spreads but the value of the current in the skew quadrupoles that corresponds to this minimum of coupling can be obtained by fitting the discrete data. The result is $I_{skew} \approx 0.33$ A (± 0.1 A, taking into account the error bar of the measured data).

6 MEASUREMENTS OF COUPLED LANDAU DAMPING OF THE PS COHERENT RESISTIVE INSTABILITY

Measurements have been performed to verify the theory of coupled Landau damping. One family of 8 octupoles located at large β_y (D-octupoles) is used in the PS to suppress transverse coherent instabilities. However, the main stabilising effect is produced in the vertical plane, whereas instabilities always occur in the horizontal one. The idea is therefore to transfer Landau damping from the stable vertical to the unstable horizontal plane, in order to minimise the amount of external non-linearities. This chapter reports measurements made on the damping of the horizontal coherent resistive instability of a 1 GeV PS bunched proton beam ($M = 20$ bunches and $I_{beam} \approx 1.5\times10^{13}$ protons) using octupoles, skew quadrupoles and tune separation.[60]

6.1 Horizontal coherent resistive instability in the PS

Using Sacherer's formula, given by Eq. (4.66) for the horizontal plane, a coherent instability occurs if, by the beam spectrum-impedance spectrum interaction, the imaginary part of the coherent frequency shift is negative.

The transverse bunch spectra of mode $|m|$ are given (see Eq. (4.65)) by $h_m(\omega)$. The plot of the horizontal bunch spectrum is represented in Figure 15 for modes $|m| = 0$ to 5 (see Appendix).

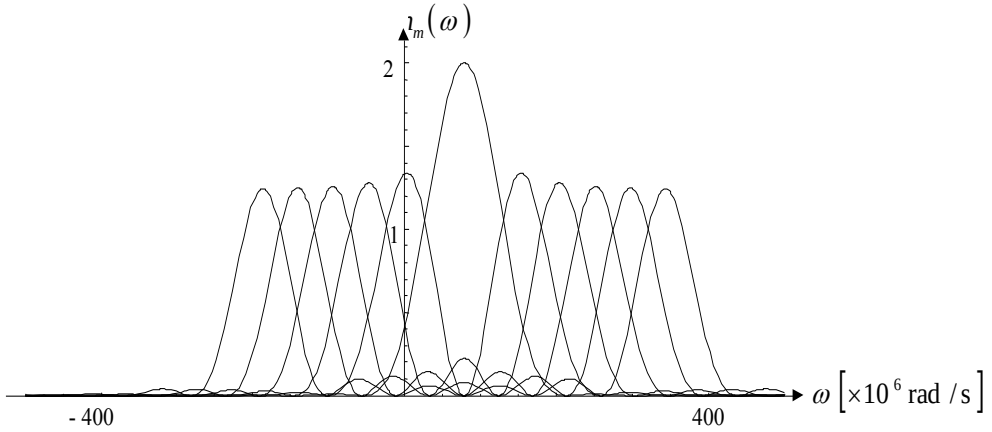

FIGURE 15 Horizontal power-spectrum envelopes for modes $|m| = 0$ to 5, with the natural horizontal chromaticity ($\xi_x \approx -1$).

The same kind of spectrum exists for the vertical motion, with the natural vertical chromaticity $\xi_y \approx -1.5$.

The PS transverse coupling impedances $Z_{x,y}(\omega)$ are approximated by the sum of the resistive wall and broad band impedances[16,61,62]

$$Z_c^{RW}(\omega) = [\,Sgn(\omega) + j\,]\,\frac{R}{b_w^3}\sqrt{\frac{2\rho_w}{\varepsilon_0|\omega|}}, \quad Z_{x,y}^{BB}(\omega) = \frac{\omega_r}{\omega}R_{x,y} \Big/ \left[\,1 - jQ\left(\frac{\omega_r}{\omega} - \frac{\omega}{\omega_r}\right)\right]. \quad (6.1)$$

Here, $Z_c^{RW}(\omega)$ is the resistive wall impedance of a circular beam pipe of radius b_w. The plot of the real part of the circular resistive wall impedance is represented in Figure 16.

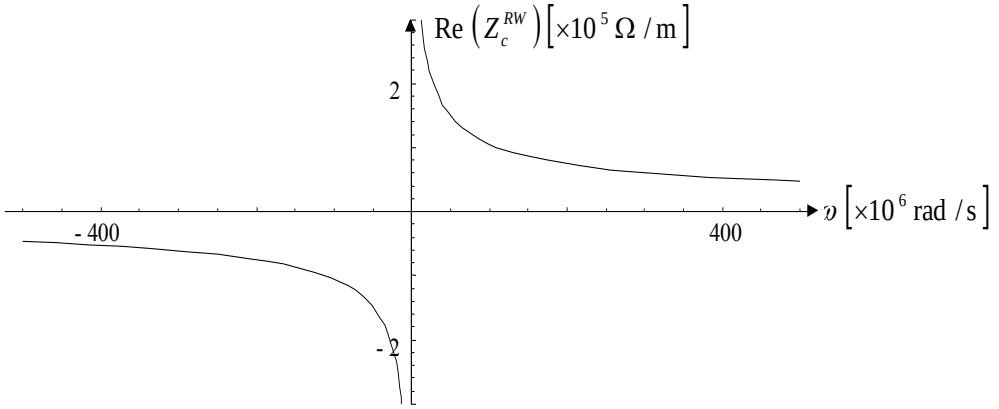

FIGURE 16 Real part of the circular resistive wall impedance.

For an elliptical vacuum chamber, the transverse resistive wall impedances can be found in the ultrarelativistic limit.[63] In the case of the PS ($a_w = 2\,b_w$), this yields

$$Z_x^{RW}(\omega) \approx Z_c^{RW}(\omega)\times 0.45, \qquad Z_y^{RW}(\omega) \approx Z_c^{RW}(\omega)\times 0.85. \qquad (6.2)$$

As concerns Landau damping, octupoles cure either single-bunch or coupled-bunch instability if they produce enough frequency spread within the bunch to prevent its coherent motion. The transverse betatron frequency spreads are given analytically by (see Appendix E)

$$\Delta\omega_{\mathrm{HWHH}}^{x,y} \approx \frac{3\,f_0\,N_{\mathrm{oct}}}{8}\left[\left(\beta_{\mathrm{octx},y}^2\,\varepsilon_{x,y}^{\mathrm{rms}}\right)^2+\left(2\,\beta_{\mathrm{octx}}\,\beta_{\mathrm{octy}}\,\varepsilon_{y,x}^{\mathrm{rms}}\right)^2\right]^{1/2}\int_0^{l_{mag}} K_{\mathrm{oct}}\,dl, \qquad (6.3)$$

using the approximation $\Delta\omega_{\mathrm{HWHH}}^{x,y} \approx \Delta\omega_{\mathrm{rms}}^{x,y}$, where $\Delta\omega_{\mathrm{HWHH}}^{x,y}$ are the half widths at half height of the transverse spectra. The simplified stability criterion, which is drawn from dispersion relation analysis considering elliptical betatron frequency distributions, is given (see Eq. (2.51)), without taking into account space-charge non-linearities, by

$$\Delta\omega_{\mathrm{HWHH}}^{x,y} \geq \sqrt{3}\,\left|\Delta\omega_{c,m}^{x,y}\right|. \qquad (6.4)$$

6.1.1 Theoretical predictions

Applying Sacherer's formula, transverse coupled-bunch instabilities should appear. The first unstable transverse betatron lines are such that $n_{x,y}+k'M$ are just below $-Q_{x0,y0}$. During the experiment, the working point was $Q_h = 6.14$ and $Q_v = 6.22$, which corresponds to the coupled-bunch mode numbers $n_{x,y}$ =13. Making the numerical computations, the following results, collected in Table 2, are obtained.

Head-tail mode m	0	1	2	3	4	5
Horizontal growth rate [s^{-1}]	-104	121	35	0	2	-3
Vertical growth rate [s^{-1}]	-423	-40	142	18	-13	-11
Horizontal frequency shift [rad/s]	-3708	-1945	-1234	-896	-716	-592
Vertical frequency shift [rad/s]	-10491	-5376	-3669	-2650	-2090	-1738

TABLE 2 Transverse instability growth rates and real frequency shifts for modes $m = 0$ to 5.

One concludes therefore that the theory, based on the above impedance model, predicts transverse coupled-bunch instabilities ($n_{x,y} = 13$) with the most critical head-tail mode numbers $m = 1$ for the horizontal plane and $m = 2$ for the vertical one. Furthermore, the spread $\Delta\omega^{x}_{\mathrm{HWHH}} \approx 3400$ rad/s should damp the horizontal instability $m = 1$.

6.1.2 Observations

To insure the validity of the one-dimensional theory, the skew quadrupole current must be set such as to have the minimum of linear coupling between the horizontal and vertical planes, i.e. $I_{skew} \approx 0.33$ A (see Chapter 5). Setting the octupole current to zero, an instability appeared.

6.1.2.1 Growth rate measurement and determination of the mode numbers

The instability was observed to happen only in the horizontal plane. The measured values of the horizontal growth rate (rise time ~ 10 ms) on the first unstable betatron line confirm the validity of the resistive wall instability theory (Figure 17(a)).

The modulus of the head tail mode number can be determined by looking the contortions of a single bunch on separate superimposed revolutions. The number of nodes along the bunch corresponds to $|m|$. It is thus inferred from Figure 17(b) that the head-tail mode number is indeed $|m| = 1$. This is in perfect agreement with theory.

A regular pattern which is the signature of coupled motion has not been clearly observed. However, the instability was sensitive to inequalities in bunch intensities, which demonstrates the existence of some coupled motion.

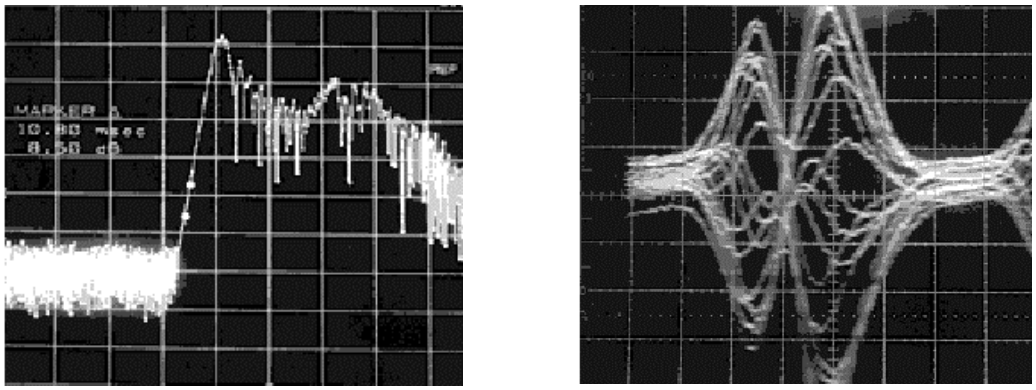

(a) (b)

FIGURE 17 (a) Measured horizontal instability growth rate on the first unstable betatron line (spectrum analyzer operating in zero frequency span). Vertical scale: 10 dB/div. (b) ΔR signal from a radial beam-position monitor during 20 consecutive turns. Time scale: 20 ns/div.

6.1.2.2 Stabilisation by Landau damping

Tuning the octupole current, the instability could be damped. From the numerical computations, the relations between the transverse betatron frequency spreads and the octupole current are given by

$$\Delta\omega^{x}_{\mathrm{HWHH}}\left[\mathrm{rad/s}\right] \approx 320\, I_{oct}\left[\mathrm{A}\right], \qquad \Delta\omega^{y}_{\mathrm{HWHH}}\left[\mathrm{rad/s}\right] \approx 630\, I_{oct}\left[\mathrm{A}\right]. \quad (6.5)$$

The octupole current required for (one-dimensional) stabilisation was $I_{oct} = 3.5\,\mathrm{A}$, which corresponds to the spread $\Delta\omega^{x}_{\mathrm{HWHH}} \approx 1100$ rad/s. This is less than required by the stability criterion of Eq. (6.4) by a factor three (but without taking into account space-charge non-linearities).[23]

Notice that, for a given octupole current, the vertical tune spread produced was approximately two times greater than the horizontal one.

6.2 Stabilisation by coupled Landau damping

To verify the two-dimensional theory of Landau damping, two series of measurements have been undertaken.

6.2.1 Constant tune separation

In this first measurement campaign (with the same conditions as in Section 6.1), the working point was fixed and coupling was changed using the skew quadrupole family. The stabilising effect of coupling through Landau damping has been studied for different octupole currents between 0.5 and 3 A. The results of the measurements compared to theory are collected in Table 3. For different values of the octupole current, it exhibits the measured stabilising skew quadrupole current, its corresponding normalised skew gradient (from Chapter 5), the theoretical normalised skew gradient and the ratio between the two.

I_{oct} [A]	I_{skew} [A]	$\lvert\underline{K}_0\rvert^{\mathrm{exp}}(\times 10^{-5})$ [m^{-2}]	$\lvert\underline{K}_0\rvert^{\mathrm{theory}}(\times 10^{-5})$ [m^{-2}]	Ratio = $\lvert\underline{K}_0\rvert^{\mathrm{exp}}$ / $\lvert\underline{K}_0\rvert^{\mathrm{theory}}$
0.5	-1.2	6.4	8.8	0.7
1	-1	5.6	5.1	1.1
1.5	-0.8	4.7	4.0	1.2
2	-0.5	3.4	3.3	1.0
2.5	0	1.4	2.9	0.5
3	0.5	0.8	2.6	0.3

TABLE 3 Measured and theoretical stabilising normalised skew gradients.

The theoretical stabilising skew gradient is given by (see Eq. (3.27))

$$\left|\underline{K}_0\right|^{\mathrm{theory}} = \frac{2\left[Q_{x0}\,Q_{y0}\,V_{\mathrm{eq}x}\left(\Delta\omega^{y}_{\mathrm{HWHH}} - V_{\mathrm{eq}y}\right)\right]^{1/2}}{R^2\,\Omega_0} \times \frac{\left[\left(\Delta\omega^{y}_{\mathrm{HWHH}} - V_{\mathrm{eq}x} - V_{\mathrm{eq}y}\right)^2 + \Omega_0^2\left(Q_h - Q_v\right)^2\right]^{1/2}}{\Delta\omega^{y}_{\mathrm{HWHH}} - V_{\mathrm{eq}x} - V_{\mathrm{eq}y}}, \quad (6.6)$$

where $V_{\mathrm{eq}x,y}$ are the transverse instability growth rates in the absence of both coupling and Landau damping (see Table 2). Here, the following assumptions are made: (i) the horizontal tune spread is approximated by zero since the coherent tunes are "far from"

each other; (ii) a Lorentzian distribution function is assumed in the vertical plane since it seems to better describe the "reality" of the PS than an elliptical spectrum.

The plot of the experimental and theoretical stabilising skew gradients vs. octupole current is represented in Figure 18.

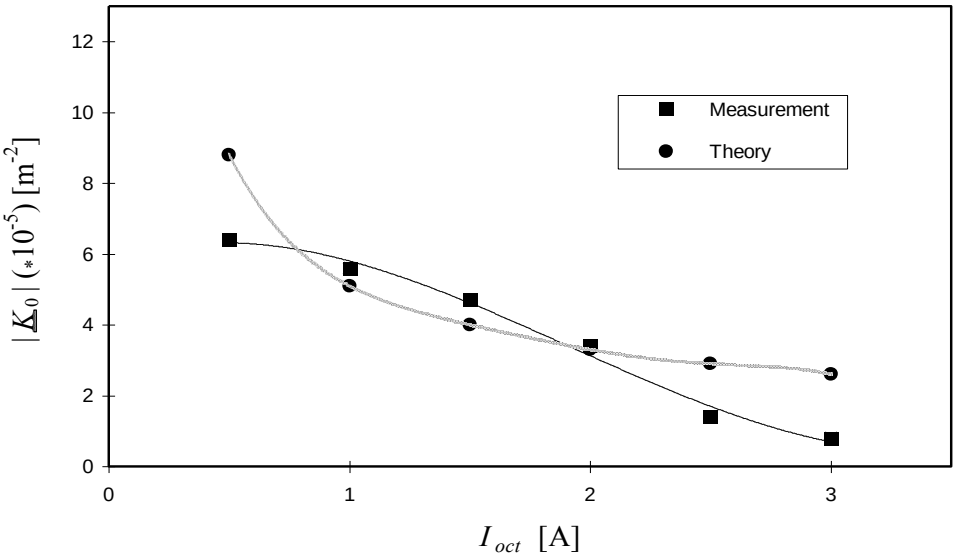

FIGURE 18 Measured and theoretical stabilising skew gradients vs. octupole current.

6.2.2 Constant octupole strength

In this second measurement campaign, the octupole strength was fixed and coupling was changed using the tune separation. The conditions were slightly different from those of Section 6.1 and the octupole current required for one-dimensional stabilisation was $I_{oct} = 5$ A. The value of the octupole current has been set to 2 A, for instance. Furthermore, the vertical tune has been set to 6.22 and the instability was damped by approaching the horizontal one. The results of the measurements compared to theory are collected in Table 4. For different values of the skew quadrupole current (with the corresponding skew gradient given in Chapter 5), it exhibits the measured stabilising tune separation, the theoretical tune separation (which is drawn from Eq. (6.6)) and the ratio between the two.

I_{oct} [A]	I_{skew} [A]	$\lvert Q_h\text{-}Q_v\rvert^{exp}$	$\lvert Q_h\text{-}Q_v\rvert^{theory}$	Ratio = $\lvert Q_h\text{-}Q_v\rvert^{exp}$ / $\lvert Q_h\text{-}Q_v\rvert^{theory}$
2	0	0.09	0.03	3.0
2	-0.5	0.10	0.08	1.2
2	-1	0.11	0.13	0.8

TABLE 4 Measured and theoretical stabilising tune separations.

The plot of the experimental and theoretical stabilising tune separations vs. skew quadrupole current is represented in Figure 19.

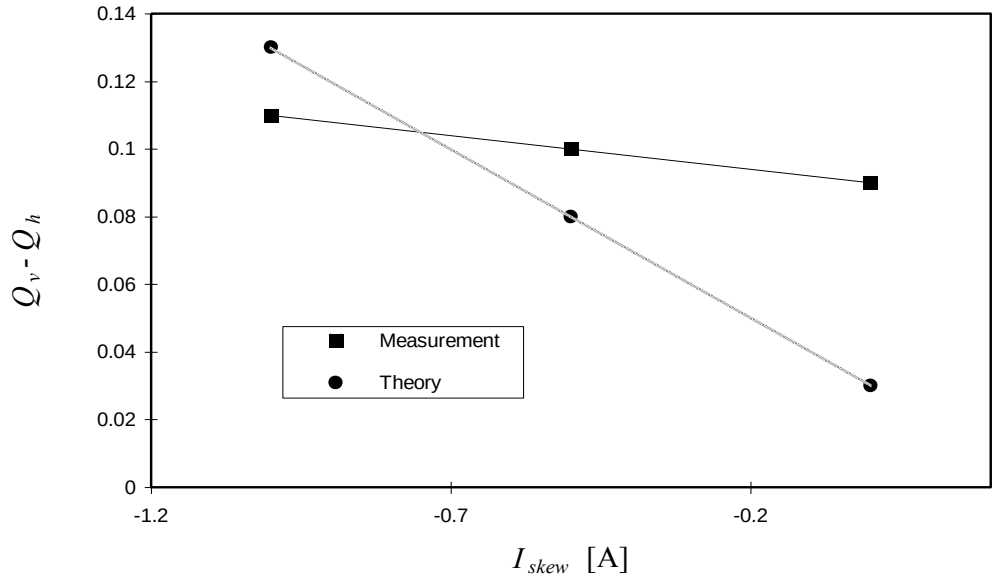

FIGURE 19 Measured and theoretical stabilising tune separations vs. skew quadrupole current.

6.3 Conclusions

The predicted beneficial effect of coupling on Landau damping is confirmed. The PS horizontal coherent resistive instability can be Landau-damped, in the presence of a sufficient tune spread in the vertical plane, by tuning the skew quadrupole current and/or the tune separation. A major assumption (a Lorentzian vertical tune spread) has however been made here to correlate theory with observations. The difference between theoretical predictions and experiments (by a factor 3) could partly be explained by the stabilising effect of space-charge non-linearities, which have not been taken into account in the theory. Further work should be made to investigate the "stability" of the vertical plane. Probably more detailed impedance and frequency spread models of the PS are required to make a more precise quantitative comparison possible.

Appendix: List of PS and beam parameters during the experiment

$a_w = 7$ cm	Half major axis of the elliptical beam pipe
$b_w = 3.5$ cm	Half minor axis of the elliptical beam pipe
$c = 3\times10^8$ ms^{-1}	Velocity of light
$e = 1.6\times10^{-19}$ C	Elementary charge
$E_0 = 0.938$ Gev	Proton rest energy
$E_c = 1$ Gev	Proton kinetic energy
$f_0 = 417$ khz	Average revolution frequency of the particles
$f_r = 1.4$ Ghz	Vacuum chamber cut-off frequency (resonance frequency describing the broadband impedances)
$f_s = 1.7$ khz	Synchrotron frequency of the particles
$I_{beam} \approx 1.5\times10^{13}$ protons	Beam intensity
$l_{mag} = 220$ mm	Equivalent octupolar magnetic length
$M = 20$	Number of bunches of the beam
$N_b \approx 7.5\times10^{11}$ protons	Bunch intensity

$N_{\mathrm{oct}} = 8$	Number of octupoles
$Q \approx 1$	Quality factor of the resonators describing the broadband impedances
$R = 100$ m	Average radius of the machine
$R_x \approx 1$ MΩ/m	Shunt resistance describing the horizontal broadband impedance
$R_y \approx 3$ MΩ/m	Shunt resistance describing the vertical broadband impedance
$\alpha_p = \gamma_{tr}^{-2} = 0.027$	Momentum compaction factor
$\beta = 0.875$	Relativistic velocity factor
$\beta_{\mathrm{oct}x} \approx 12.4$ m	Horizontal betatron function at the locations of the octupoles
$\beta_{\mathrm{oct}y} \approx 22.6$ m	Vertical betatron function at the locations of the octupoles
$\gamma = E_t / E_0 = 2.066$	Relativistic mass factor
$\varepsilon_x^{\mathrm{rms}} = 6.5 \times 10^{-6}$ m	R.m.s horizontal emittance (horizontal phase space area divided by π)
$\varepsilon_y^{\mathrm{rms}} = 3.1 \times 10^{-6}$ m	R.m.s vertical emittance (vertical phase space area divided by π)
$\eta = \alpha_p - \gamma^{-2} = -0.207$	Slippage (or off-momentum) factor
$\xi_x \approx -1$	Horizontal chromaticity, defined by $\xi_x = \left(d Q_{0x,i} / Q_{0x,i} \right) / \left(dp_i / p_i \right)$
$\xi_y \approx -1.5$	Vertical chromaticity, defined by $\xi_y = \left(d Q_{0y,i} / Q_{0y,i} \right) / \left(dp_i / p_i \right)$
$\rho_w = 9 \times 10^{-7}$ Ωm	Vacuum chamber resistivity
$\tau_b = 70$ ns	Total bunch length
$B_y \rho_x = 5.66$ Tm	Beam rigidity
$\int_0^{l_{mag}} K_{oct}\, dl\, [\mathrm{m}^{-3}] = \frac{4.33}{6 B_y \rho_x} \times I_{oct}\, [\mathrm{A}]$	Integrated octupole strength

7 CONCLUSION

Beam brightness (i.e. normalised transverse phase space density or intensity to emittance ratio) conservation is a major concern in the LHC injector chain, as in the design and operation of high energy hadron colliders. Many sources of brightness deterioration exist, such as space charge effects, matching, injection or extraction errors. Furthermore, instabilities of many kinds can also blow-up and even destroy the beam. In the CERN-PS, for example, the total emittance blow-up must be less than 20%, which imposes a rigorous handling of all possible sources of blow-up along the injector chain.

The present work on collective instabilities reveals that linear coupling between the horizontal and vertical planes together with the tune distance from the linear coupling resonances $Q_h - Q_v =$ integer can have a stabilising effect against transverse coherent instabilities through Landau damping. Indeed, if, after applying damping via tune spreads from octupoles, a coherent instability remains in one of the two planes, then linear coupling together with tune separation can be used to transfer Landau damping from the stable to the unstable plane. This result could therefore be used to minimise the amount of external non-linearities required for Landau damping.

In the case of Lorentzian distributions, if the sum of the betatron frequency spreads $\delta\omega_{x,y}$ (half widths at half maximum of the distribution functions) is greater than the sum of the instability growth rates $V_{\mathrm{eq}x,y}$ (given by Eq. (2.25) for a coasting beam or Eq. (4.79) for a bunched beam), then it is possible to stabilise the beam in the two planes by increasing the skew gradient and/or by getting closer to the coupling resonances. The necessary condition $\delta\omega_x + \delta\omega_y \geq V_{\mathrm{eq}x} + V_{\mathrm{eq}y}$ becomes sufficient for full coupling.

However, in practice the coupling has to be optimised because realistic frequency distributions have finite tails. The stability is obtained for coupling values of a certain range. For elliptical spectra, an approximate criterion, valid for optimum coupling, can be expressed as $\mathrm{Re}\left(\sqrt{\Delta\omega_x^2 - 4U_{\mathrm{eq}x}^2} + \sqrt{\Delta\omega_y^2 - 4U_{\mathrm{eq}y}^2}\right) \geq 2\left(V_{\mathrm{eq}x} + V_{\mathrm{eq}y}\right)$, where $\mathrm{Re}(\ )$ stands for real part, indicating that the square root has to be omitted if the argument under the root is negative. Here, $\Delta\omega_{x,y}$ are the half widths at the bottom of the distribution functions and $U_{\mathrm{eq}x,y}$ (real betatron frequency shifts), $V_{\mathrm{eq}x,y}$ are given by Eq. (2.25) for a coasting beam or Eq. (4.79) for a bunched beam.

The instability growth rate (which depends on chromaticity for a bunched beam) and damping by feedbacks are "always" transferred between the transverse planes in the presence of coupling. Several parameters could therefore be used to damp transverse coherent instabilities and fix the best working point.

The theory of coupled Landau damping gives a possible explanation of the phenomenon observed in Ref. 16, where a single-bunch instability of the head-tail type has been damped by adjusting $Q_h \approx Q_v$. Furthermore, experiments in the PS have been performed on a 1 GeV flat bottom, varying the distance from the resonance $Q_h - Q_v = 0$, and the excitation of the skew quadrupoles and octupoles lenses, observing the threshold of a coupled-bunch instability. The results confirm the general behaviour predicted by the theory, considering a Lorentzian distribution in the vertical plane.

The results of coupled Landau damping can be used to find optimum values of tune split and linear coupling strength for the PS beam with the LHC characteristics, for which coupling is not harmful since the horizontal and vertical emittances are equal. The low-energy head-tail instabilities can indeed be damped using this method, and the result is that the octupole current can be reduced by a factor 2 or 3. Further work is planned to better correlate theory with observations.

APPENDIX A: BEAM OPTICS

The motion of a charged particle in a beam transport channel or a circular accelerator is governed by the Lorentz force equation

$$\vec{F} = e\left(\vec{E} + \vec{v} \times \vec{B}\right). \tag{A.1}$$

The Lorentz forces are applied as bending forces to guide the particles along a predefined ideal path, the "design orbit", on which -ideally- all particles should move, and as focusing forces to confine the particles in the vicinity of the ideal path, from which most particles will unavoidably deviate. The motion of particle beams under the influence of these Lorentz forces is called "beam optics".

To express deviations of individual particle trajectories from the design orbit, a right-handed orthogonal system $\left[\vec{e}_x(s), \vec{e}_y, \vec{e}_z(s)\right]$, that follows an ideal particle travelling along the design orbit, is used.

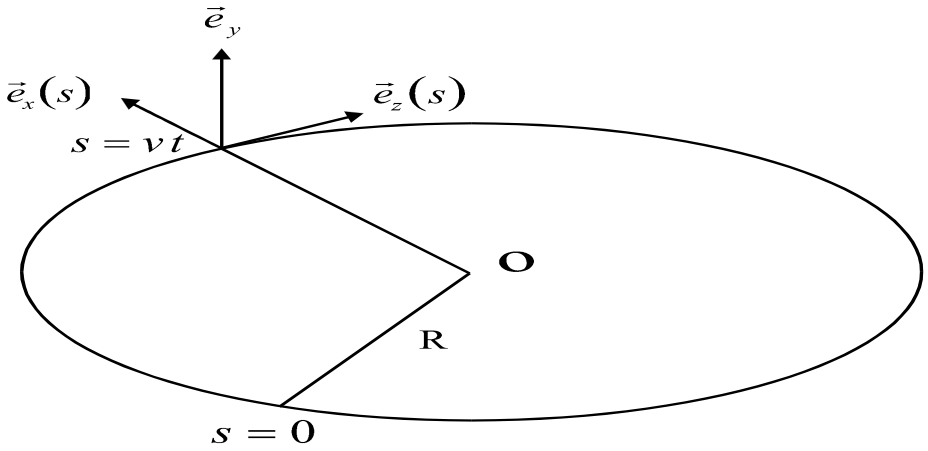

FIGURE 20 Circular design orbit in the horizontal plane and Frenet-Serret coordinate system $\left[\vec{e}_x(s), \vec{e}_y, \vec{e}_z(s)\right]$ used to describe particle trajectories.

Let's consider the horizontal motion (the same analysis applies for the vertical one). The linear unperturbed horizontal equation of motion of a test particle *i* having the design momentum $p_i = p_0$ (and thus the revolution frequency $\Omega_i = \Omega_0$, the average orbit radius $R_i = R$, and the azimuthal coordinate $s_i = R_i\,\Omega_i\,t = s$) is[20,21]

$$\frac{d^2 x_i}{ds^2} + K_{x,i}(s)\,x_i = 0, \tag{A.2}$$

where x_i is the horizontal coordinate. Here, the bending and focusing forces have been combined in one periodic function of the *s*-coordinate, $K_{x,i}(s + L_c) = K_{x,i}(s)$, due to the orbit being a closed curve. The period L_c may be the accelerator circumference $C = 2\pi R$ or the length of a "cell" repeated N_{cell} times around the machine. Equation (A.2), with periodic coefficient $K_{x,i}(s)$, is called "Hill's equation". The solution of the Hill's equation is a pseudo-harmonic oscillation with varying amplitude and frequency, called "betatron oscillation"

$$x_i(s) = a_{0x,i}\beta_{0x,i}^{1/2}(s)\cos\left[\mu_{0x,i}(s) + \varphi_{0x,i}\right], \tag{A.3}$$

where

$$\mu_{0x,i}(s) = \int_0^s \frac{dt}{\beta_{0x,i}(t)}, \qquad \mu_{0x,i} = \int_0^{L_c} \frac{dt}{\beta_{0x,i}(t)} \tag{A.4}$$

are the "phase function" and "phase advance per period". The number of betatron oscillations executed by the particle travelling once around the machine circumference is the single-particle (incoherent) tune $Q_{0x,i}$. It is related to the phase advance by

$$Q_{0x,i} = \frac{N_{cell}\,\mu_{0x,i}}{2\pi} = \frac{1}{2\pi}\int_0^C \frac{dt}{\beta_{0x,i}(t)}. \tag{A.5}$$

The function $\beta_{0x,i}(s)$ is called the "betatron function" and is solution of the differential equation

$$\frac{1}{2}\beta_{0x,i}\,\beta''_{0x,i} - \frac{1}{4}\beta'^2_{0x,i} + K_{x,i}(s)\beta^2_{0x,i} = 1. \tag{A.6}$$

In practice, particle beams have a finite dispersion of momenta about the ideal momentum p_0. A particle i with the momentum $p_i \neq p_0$ will perform betatron oscillations about a different closed orbit from that of the reference particle. For small deviations in momentum $\Delta p_i = p_i - p_0$, the equation of motion is

$$\frac{d^2x_i}{ds_i^2} + K_{x,i}(s_i)\,x_i = \frac{\Delta p_i}{p_0}\rho_x^{-1}(s_i), \tag{A.7}$$

where $\rho_x(s_i)$ stands for the local bending radius. The individual particle deviation from the design orbit can be regarded as being the sum of two parts

$$x_i(s_i) = x_{\beta,i}(s_i) + x_{\delta,i}(s_i), \tag{A.8}$$

where $x_{\delta,i}(s_i)$ is the displacement at the closed orbit for the off-momentum particle from that of the reference particle, and $x_{\beta,i}(s_i)$ is the betatron oscillation around this off-momentum orbit

$$\frac{d^2x_{\beta,i}}{ds_i^2} + K_{x,i}(s_i)\,x_{\beta,i} = 0. \tag{A.9}$$

The particular solution $x_{\delta,i}(s_i)$ of the inhomogeneous equation (A.7) is generally re-expressed as

$$x_{\delta,i}(s_i) = D_i(s_i)\frac{\Delta p_i}{p_0}, \tag{A.10}$$

where $D_i(s_i)$ is called the "dispersion function", which evidently satisfies the equation

$$\frac{d^2 D_i}{ds_i^2} + K_{x,i}(s_i)\, D_i = \rho_x^{-1}(s_i). \tag{A.11}$$

In the presence of extra forces, Eq. (A.7) takes the general form

$$\frac{d^2 x_i}{ds_i^2} + K_{x,i}(s_i)\, x_i = P_{x,i}\,, \tag{A.12}$$

where $P_{x,i}$ stands for any perturbation. By an appropriate transformation of variables, the equation of motion (A.12) can be expressed in the form of a perturbed harmonic oscillator with constant frequency. To this end, the normalised (Courant-Snyder) coordinate and angle are introduced

$$\eta_i = x_i\, \beta_{0x,i}^{-1/2}(s), \qquad \phi_i = Q_{0x,i}^{-1} \int_0^s \beta_{0x,i}^{-1}(t)\, dt. \tag{A.13}$$

The perturbed Hill's equation is thus transformed into

$$\frac{d^2 \eta_i}{d\phi_i^2} + Q_{0x,i}^2\, \eta_i = Q_{0x,i}^2\, \beta_{0x,i}^{3/2}\, P_{x,i}\,. \tag{A.14}$$

When the perturbation vanishes, Eq. (A.14) reduces to a harmonic oscillator with constant frequency $Q_{0x,i}$, whose solution is

$$\eta_i(\phi_i) = a_{0\eta,i} \cos\left[\mu_{0\eta,i}(\phi_i) + \varphi_{0\eta,i}\right], \tag{A.15}$$

where the phase advance is

$$\mu_{0\eta,i}(\phi_i) = Q_{0x,i}\, \phi_i\,. \tag{A.16}$$

This leads to

$$\eta_i^2 + \left(\frac{d\eta_i}{d\mu_{0\eta,i}}\right)^2 = a_{0\eta,i}^2\,. \tag{A.17}$$

Therefore, in the absence of perturbation, the particle trajectory in the phase plane $(\eta_i\,, d\eta_i / d\mu_{0\eta,i})$ is a circle of radius equal to the amplitude $a_{0\eta,i}$ of the oscillation. The phase $\mu_{0\eta,i}(\phi_i)$ advances 2π every betatron oscillation (i.e. the trajectory describes a full phase circle) or by $2\pi Q_{0x,i}$ every machine revolution.

In the smooth approximation, the betatron function is approximated by a constant

$$\beta_{0x,i}(s_i) \approx \overline{\beta}_{0x,i}\,. \tag{A.18}$$

Equations (A.4), (A.5) and (A.6) then give

$$K_{x,i}(s_i) \approx \frac{1}{\overline{\beta}_{0x,i}^2}, \qquad \overline{\beta}_{0x,i} \approx \frac{R_i}{Q_{0x,i}}. \tag{A.19}$$

Using $\phi_i = \Omega_i t$, Eq. (A.14) finally leads to the differential equation

$$\ddot{x}_i + Q_{0x,i}^2 \Omega_i^2 x_i = R_i^2 \Omega_i^2 P_{x,i}, \tag{A.20}$$

where a point denotes the derivative with respect to time.

APPENDIX B: RF ACCELERATION

The voltage across the gap of an accelerating cavity can be expressed as[65]

$$V = \hat{V}_{\mathrm{RF}} \sin \phi_{\mathrm{RF}}(t). \tag{B.1}$$

The accelerating frequency f_{RF} is an integral multiple h (which is called the harmonic number, and which defines the maximum number of bunches in a machine) of the revolution frequency f_0 of the synchronous particle

$$f_{\mathrm{RF}} = h\, f_0 = h\, \frac{v_0}{2\pi R}, \tag{B.2}$$

where v_0 is the velocity and R the average orbit radius of the synchronous particle, which experiences a constant RF phase

$$\phi_{\mathrm{RF}}(t) = \phi_{\mathrm{RF},0} = \text{const.} \tag{B.3}$$

In a synchrotron, the energy of the synchronous particle changes during the acceleration. If one wishes to keep this particle on the same orbit R, the magnetic field must change with time. The average bending field $\overline{B}_0$ around the synchronous orbit is given by

$$\overline{B}_0 = \frac{p_0}{e\,R}, \tag{B.4}$$

where p_0 is the synchronous particle momentum and e the elementary charge. During acceleration at constant radius, one thus has

$$\dot{p}_0 = e\,R\,\dot{\overline{B}}_0 . \tag{B.5}$$

The momentum gain per revolution for the synchronous particle is then

$$\left(\Delta p_0\right)_{\mathrm{revolution}} = e\,R\,\dot{\overline{B}}_0\, T_0 , \tag{B.6}$$

where $T_0 = 1 / f_0$ is the revolution period. Using the relativistic kinematic formula between energy deviation and momentum deviation, yields, for the (total) energy gain of the synchronous particle,

$$\left(\Delta E_{t,0}\right)_{\mathrm{revolution}} = v_0 \left(\Delta p_0\right)_{\mathrm{revolution}}. \tag{B.7}$$

Furthermore, from Eq. (B.1), the energy gain in one revolution is also given by

$$\left(\Delta E_{t,0}\right)_{\mathrm{revolution}} = e\hat{V}_{\mathrm{RF}} \sin \phi_{\mathrm{RF},0} . \tag{B.8}$$

The phase of the synchronous particle can then be deduced. If Eq. (B.8) is satisfied for $\phi_{\mathrm{RF},0}$, it is also satisfied for $\pi - \phi_{\mathrm{RF},0}$. However, only one possibility corresponds to a stable dynamical equilibrium (see Eq. (B.24)).

Working to first order in the deviations given by

$$\begin{aligned} f_i &= f_0 + \Delta f_i \,, \\ \phi_{\mathrm{RF},i} &= \phi_{\mathrm{RF},0} + \Delta\phi_{\mathrm{RF},i} \,, \\ p_i &= p_0 + \Delta p_i \,, \\ E_{t,i} &= E_{t,0} + \Delta E_{t,i} \,, \\ \vartheta_i &= \vartheta_0 + \Delta\vartheta_i \,, \end{aligned} \tag{B.9}$$

the motion of a non-synchronous test particle *i* can be deduced. One then has

$$\Delta\phi_{\mathrm{RF},i} = -h\,\Delta\vartheta_i \,, \tag{B.10}$$

where the minus sign comes from the fact that a particle that lags behind the synchronous particle ($\Delta\vartheta_i < 0$) arrives later in the RF cavity ($\Delta\phi_{\mathrm{RF},i} > 0$). Using the definition of the azimuthal angle,

$$\vartheta_i(t) = \int_{t_0}^{t} \Omega_i \, dt' \,, \tag{B.11}$$

yields

$$\Delta\Omega_i = -\frac{1}{h}\,\dot{\phi}_{\mathrm{RF},i} \,, \tag{B.12}$$

since $\dot{\phi}_{\mathrm{RF},0} = 0$ by definition, where $\Omega_i = 2\pi f_i$. From the definition of the slippage (or off-momentum) factor η, one has

$$\Delta p_i = -\frac{p_i}{\eta\Omega_i}\Delta\Omega_i = \frac{p_i}{h\eta\Omega_i}\dot{\phi}_{\mathrm{RF},i} \,. \tag{B.13}$$

On each revolution, a particle gains an energy

$$\left(\Delta E_{t,i}\right)_{\mathrm{revolution}} = e\hat{V}_{\mathrm{RF}} \sin\phi_{\mathrm{RF},i} \,, \tag{B.14}$$

which, using Eq. (B.7) for a non-synchronous particle, corresponds to a momentum increment of

$$\left(\Delta p_i\right)_{\mathrm{revolution}} = \frac{e\hat{V}_{\mathrm{RF}}}{R_i\,\Omega_i} \sin\phi_{\mathrm{RF},i} \,. \tag{B.15}$$

The average rate of momentum gain over one revolution is

$$\dot{p}_i = \frac{e\hat{V}_{\mathrm{RF}}}{2\pi R_i} \sin\phi_{\mathrm{RF},i} \,, \tag{B.16}$$

and so

$$R_i\ \dot{p}_i = \frac{e\hat{V}_{\mathrm{RF}}}{2\pi}\sin\phi_{\mathrm{RF},i}\,. \tag{B.17}$$

For the synchronous particle, Eq. (B.17) reads

$$R\,\dot{p}_0 = \frac{e\hat{V}_{\mathrm{RF}}}{2\pi}\,\sin\phi_{\mathrm{RF},0}\,. \tag{B.18}$$

From Eq. (B.17) and (B.18), the following equation is obtained

$$R_i\ \dot{p}_i - R\,\dot{p}_0 = \Delta\left(R_i\ \dot{p}_i\right) = \frac{e\hat{V}_{\mathrm{RF}}}{2\pi}\left(\sin\phi_{\mathrm{RF},i} - \sin\phi_{\mathrm{RF},0}\right). \tag{B.19}$$

Expanding $\Delta\left(R_i\ \dot{p}_i\right)$ to first order, yields

$$\Delta\left(R_i\ \dot{p}_i\right) = \frac{d}{dt}\left(\frac{\Delta E_{t,i}}{\Omega_0}\right). \tag{B.20}$$

From Eq. (B.19) and (B.20), a first equation of motion is given by

$$\frac{d}{dt}\left(\frac{\Delta E_{t,i}}{\Omega_0}\right) = \frac{e\hat{V}_{\mathrm{RF}}}{2\pi}\left(\sin\phi_{\mathrm{RF},i} - \sin\phi_{\mathrm{RF},0}\right). \tag{B.21}$$

A second equation of motion is obtained from Eq. (B.13), using Eq. (B.7),

$$\dot{\phi}_{\mathrm{RF},i} = \frac{h\eta\Omega_0}{p_0\,R}\left(\frac{\Delta E_{t,i}}{\Omega_0}\right). \tag{B.22}$$

Here, Ω_i, p_i and R_i have been evaluated for the synchronous particle, which is permissible to first order. Also, p_0 is considered to be constant in time, which is valid for storage rings or for accelerators over a limited range of energy. The two-first order differential equations (B.21) and (B.22) can be combined into one second-order equation (eliminating $\Delta E_{t,i}$ in both equations)

$$\frac{d}{dt}\left(\frac{p_0\,R}{h\eta\Omega_0}\,\dot{\phi}_{\mathrm{RF},i}\right) - \frac{e\hat{V}_{\mathrm{RF}}}{2\pi}\left(\sin\phi_{\mathrm{RF},i} - \sin\phi_{\mathrm{RF},0}\right) = 0. \tag{B.23}$$

Replacing $\phi_{\mathrm{RF},i}$ by $\phi_{\mathrm{RF},0} + \Delta\phi_{\mathrm{RF},i}$, approximating for $\Delta\phi_{\mathrm{RF},i} << 1$ and for constant coefficients, yields the linearised equation of small-amplitude synchrotron oscillations

$$\frac{d^2}{dt^2}\left(\Delta\phi_{\mathrm{RF},i}\right) - \frac{e\hat{V}_{\mathrm{RF}}\,h\Omega_0\,\eta\cos\phi_{\mathrm{RF},0}}{2\pi\,p_0\,R}\,\Delta\phi_{\mathrm{RF},i} = 0. \tag{B.24}$$

Equation (B.24) has stable oscillatory solutions if $\eta \cos\phi_{\mathrm{RF},0} < 0$. The frequency of small-amplitude synchrotron (or energy) oscillations is then given by

$$\omega_s = \left(-\frac{e\hat{V}_{\mathrm{RF}}\, h\Omega_0\, \eta \cos\phi_{\mathrm{RF},0}}{2\pi\, p_0\, R} \right)^{1/2}. \tag{B.25}$$

Equation (B.24), with Eq. (B.25), describes the motion of a harmonic oscillator. Using the parameter τ_i, which represents the time interval between the passage of the test particle and the synchronous particle at some azimuth (as in Section 3.3), or the opposite (as in Chapter 4), instead of the RF phase deviation $\Delta\phi_{\mathrm{RF},i}$, Eq. (B.24) can be written as

$$\ddot{\tau}_i + \omega_s^2\, \tau_i = 0, \tag{B.26}$$

which yields

$$\tau_i = \hat{\tau}_i \cos\left(\omega_s\, t + \psi_i \right). \tag{B.27}$$

APPENDIX C

In this appendix, the detailed calculations to obtain Eq. (4.62) are recalled.[50] From Eq. (4.51) one has

$$\frac{1}{2}\int_{\omega=-\infty}^{\omega=+\infty}|\omega|\sigma_{x,m}^2\left(\omega+\omega_{\xi_x}+m\omega_s\right)d\omega=\frac{\pi^{-2}\,j^{-2m}}{2}\int_{\hat{\tau}_i=0}^{\hat{\tau}_i=\tau_b/2}\int_{\hat{\tau}_i'=0}^{\hat{\tau}_i'=\tau_b/2}\left[\int_{\omega=-\infty}^{\omega=+\infty}|\omega|J_m\left(\omega\hat{\tau}_i\right)J_m\left(\omega\hat{\tau}_i'\right)d\omega\right]$$
$$\times\hat{x}_m\left(\hat{\tau}_i\right)g_0\left(\hat{\tau}_i\right)\hat{\tau}_i\;d\hat{\tau}_i\;\hat{x}_m\left(\hat{\tau}_i'\right)g_0\left(\hat{\tau}_i'\right)\hat{\tau}_i'\;d\hat{\tau}_i'. \tag{C.1}$$

Using the relation[8]

$$\int_{\omega=-\infty}^{\omega=+\infty}|\omega|J_m\left(\omega\hat{\tau}_i\right)J_m\left(\omega\hat{\tau}_i'\right)d\omega=\frac{2}{\hat{\tau}_i}\delta\left(\hat{\tau}_i-\hat{\tau}_i'\right), \tag{C.2}$$

one obtains

$$\begin{aligned}&\frac{1}{2}\int_{\omega=-\infty}^{\omega=+\infty}|\omega|\sigma_{x,m}^2\left(\omega+\omega_{\xi_x}+m\omega_s\right)d\omega\\&=\pi^{-2}\,j^{-2m}\int_{\hat{\tau}_i=0}^{\hat{\tau}_i=\tau_b/2}\int_{\hat{\tau}_i'=0}^{\hat{\tau}_i'=\tau_b/2}\hat{x}_m\left(\hat{\tau}_i\right)g_0\left(\hat{\tau}_i\right)d\,\hat{\tau}_i\;\hat{x}_m\left(\hat{\tau}_i'\right)g_0\left(\hat{\tau}_i'\right)\hat{\tau}_i'\;d\,\hat{\tau}_i'\,\delta\left(\hat{\tau}_i-\hat{\tau}_i'\right).\end{aligned} \tag{C.3}$$

Integrating over $\hat{\tau}_i'$ values, yields

$$\frac{1}{2}\int_{\omega=-\infty}^{\omega=+\infty}|\omega|\sigma_{x,m}^2\left(\omega+\omega_{\xi_x}+m\omega_s\right)d\omega=\pi^{-2}\,j^{-2m}\int_{\hat{\tau}_i=0}^{\hat{\tau}_i=\tau_b/2}\hat{x}_m^2\left(\hat{\tau}_i\right)g_0^2\left(\hat{\tau}_i\right)\hat{\tau}_i\,d\hat{\tau}_i. \tag{C.4}$$

Sampling the function $|\omega|\sigma_{x,m}^2\left(\omega+\omega_{\xi_x}+m\omega_s\right)$ at frequencies $\omega=\left(k+Q_{x0}\right)\Omega_0-\omega_{\xi_x}$, one has

$$\begin{aligned}&\left[|\omega|\sigma_{x,m}^2\left(\omega+\omega_{\xi_x}+m\omega_s\right)\right]_{sampled}=\Omega_0\sum_{k=-\infty}^{k=+\infty}|\omega|\sigma_{x,m}^2\left(\omega+\omega_{\xi_x}+m\omega_s\right)\times\\&\delta\left[\omega-\left(k+Q_{x0}\right)\Omega_0+\omega_{\xi_x}\right].\end{aligned} \tag{C.5}$$

Then,

$$\begin{aligned}&\frac{1}{2}\int_{\omega=-\infty}^{\omega=+\infty}\left[|\omega|\sigma_{x,m}^2\left(\omega+\omega_{\xi_x}+m\omega_s\right)\right]_{sampled}d\omega\\&=\frac{\Omega_0}{2}\sum_{k=-\infty}^{k=+\infty}\left|\left(k+Q_{x0}\right)\Omega_0-\omega_{\xi_x}\right|\sigma_{x,m}^2\left[\left(k+Q_{x0}\right)\Omega_0+m\omega_s\right].\end{aligned} \tag{C.6}$$

Equation (4.62) is finally obtained from Eqs. (C.4) and (C.6), using the approximation

$$\int_{\omega=-\infty}^{\omega=+\infty}\left[|\omega|\sigma_{x,m}^2\left(\omega+\omega_{\xi_x}+m\omega_s\right)\right]_{sampled}d\omega\approx\int_{\omega=-\infty}^{\omega=+\infty}|\omega|\sigma_{x,m}^2\left(\omega+\omega_{\xi_x}+m\omega_s\right)d\omega. \tag{C.7}$$

APPENDIX D: COUPLED-BUNCH COHERENT MOTION

If one considers M equidistant bunches and a sample of M particles (one per bunch, e.g. the *i*th of each bunch) on the same synchrotron orbit $\hat{\tau}_i$ and betatron orbit $\hat{x}_i$, the resulting signal of the sample, induced at a perfect pick-up electrode (infinite bandwidth) at angular position ϑ in the ring, can be written, e.g. in the horizontal plane,[50] (see Section 4.2)

$$s_{x,sample}(t,\vartheta) = e \sum_{r=1}^{r=M} \hat{x}_i \cos\left[\omega_{x,i}\, t + \left(\omega_{\xi_x} - Q_{x0}\,\Omega_0\right)\hat{\tau}_i \cos\left(\omega_s\, t + \psi_r\right) + \varphi_{0x,r}\right] \times$$
$$\sum_{k=-\infty}^{k=+\infty} \delta\left(t - \hat{\tau}_i \cos\left(\omega_s\, t + \psi_r\right) - \frac{\vartheta}{\Omega_0} - \frac{2k\pi}{\Omega_0} - \frac{2\pi r}{\Omega_0 M}\right). \tag{D.1}$$

Following the same procedure as in Section 4.2 leads to

$$s_{x,sample}(t,\vartheta) = \frac{e\Omega_0}{4\pi}\hat{x}_i\, e^{j\omega_{x,i}t} \sum_{m,k} j^{-m} J_m\left\{\left[\left(k + Q_{x,i}\right)\Omega_0 - \omega_{\xi_x}\right]\hat{\tau}_i\right\} \times$$
$$e^{j\left[\left(k\Omega_0 + m\omega_s\right)t - k\vartheta\right]} \sum_{r=1}^{r=M} e^{j\left(m\psi_r + \varphi_{0x,r} - \frac{2\pi r k}{M}\right)}. \tag{D.2}$$

The maximum of $\sum_{r=1}^{r=M} e^{j\left(m\psi_r + \varphi_{0x,r} - \frac{2\pi r k}{M}\right)}$ is obtained when $m\psi_r + \varphi_{0x,r} = 2\pi r k / M$. This requires $k = n_x + k' M$, where $0 \le n_x \le M - 1$ is called the horizontal coupled-bunch mode number. Every *M*th line occurs with an amplitude *M* times larger, and the phase shift between the coherent perturbations of two adjacent bunches is $2\pi n_x / M$.

APPENDIX E: TUNE SPREADS BY OCTUPOLES

The classical calculation of the tune spreads due to octupoles is recalled here.[23] The betatron equation of a test particle *i* in the presence of octupolar field is given, e.g. in the horizontal plane, by

$$\frac{d^2 x_i}{ds_i^2} + K_{x,i}(s_i)\, x_i + \frac{e}{p_i} B_y^{\mathrm{oct}}(x_i, y_i) = 0, \tag{E.1}$$

where

$$\frac{e}{p_i} B_y^{\mathrm{oct}}(x_i, y_i) = K_{\mathrm{oct}}\left(x_i^3 - 3 x_i y_i^2\right). \tag{E.2}$$

Here, x_i, y_i are the transverse coordinates of the particle, s_i is the azimuthal coordinate, $K_{x,i}$ represents the linear focusing, e is the elementary charge, p_i is the momentum, $B_y^{\mathrm{oct}}(x_i, y_i)$ is the vertical octupolar magnetic field and K_{oct} is the octupolar strength. Inserting for x_i and y_i, the free betatron oscillations, given by

$$\begin{aligned} x_i &= \hat{x}_i \cos(\varphi_{x,i}), \\ y_i &= \hat{y}_i \cos(\varphi_{y,i}), \end{aligned} \tag{E.3}$$

using the formulae $\sin^3\varphi = (3/4)\sin\varphi - (1/4)\sin 3\varphi$, $\sin^2\varphi = 1/2 - (1/2)\cos 2\varphi$, and neglecting the influence of the harmonics higher than one (averaging method), one obtains

$$\frac{e}{p_i} B_y^{\mathrm{oct}}(x_i, y_i) \approx K_{\mathrm{oct}}\left(\frac{3}{4}\hat{x}_i^2 - \frac{3}{2}\hat{y}_i^2\right)\hat{x}_i \cos(\varphi_{x,i}). \tag{E.4}$$

This term is equivalent to a linear (quadrupolar) focusing term $\Delta K_{x,i}(s_i)\, x_i$ in Eq. (E.1), with

$$\Delta K_{x,i}(s_i)\, x_i = K_{\mathrm{oct}}\left(\frac{3}{4}\hat{x}_i^2 - \frac{3}{2}\hat{y}_i^2\right). \tag{E.5}$$

The corresponding tune shift is given by the classical tune-shift formula[21]

$$\Delta Q_{shift}^x = \frac{1}{4\pi}\int_0^{2\pi R} \Delta K_{x,i}(s_i)\beta_{0x,i}(s_i)\, ds_i = \frac{1}{4\pi}\int_0^{2\pi R} K_{\mathrm{oct}}\left(\frac{3}{4}\hat{x}_i^2 - \frac{3}{2}\hat{y}_i^2\right)\beta_{0x,i}(s_i)\, ds_i, \tag{E.6}$$

where R is the average radius of the machine and $\beta_{0x,i}(s_i)$ the horizontal betatron function. In a similar way, the vertical tune shift is given by

$$\Delta Q_{shift}^y = \frac{1}{4\pi}\int_0^{2\pi R} \Delta K_{y,i}(s_i)\beta_{0y,i}(s_i)\, ds_i = -\frac{1}{4\pi}\int_0^{2\pi R} K_{\mathrm{oct}}\left(\frac{3}{4}\hat{y}_i^2 - \frac{3}{2}\hat{x}_i^2\right)\beta_{0y,i}(s_i)\, ds_i. \tag{E.7}$$

As the incoherent amplitudes $\hat{x}_i$ and $\hat{y}_i$ change with the betatron functions, one will use the "single-particle emittances" $\varepsilon_{x,i} = \hat{x}_i^2 / \beta_{0x,i}$ and $\varepsilon_{y,i} = \hat{y}_i^2 / \beta_{0y,i}$, which are constant around the ring. The r.m.s tune spreads can then be written as

$$\Delta Q_{\mathrm{rms}}^{x,y} \approx \frac{3}{16\pi} \int_0^{2\pi R} K_{\mathrm{oct}} \left[\left(\beta_{\mathrm{octx},y}^2 \, \varepsilon_{x,y}^{\mathrm{rms}} \right)^2 + \left(2 \beta_{\mathrm{octx}} \, \beta_{\mathrm{octy}} \, \varepsilon_{y,x}^{\mathrm{rms}} \right)^2 \right]^{1/2} ds, \qquad \text{(E.8)}$$

where $\beta_{\mathrm{octx},y}$ are the betatron functions at the positions of the octupoles and $\varepsilon_{x,y}^{\mathrm{rms}}$ are the r.m.s beam emittances.

For a family of octupoles located at the same betatron functions, Eq. (E.8) becomes

$$\Delta Q_{\mathrm{rms}}^{x,y} \approx \frac{3 N_{\mathrm{oct}}}{16\pi} \left[\left(\beta_{\mathrm{octx},y}^2 \, \varepsilon_{x,y}^{\mathrm{rms}} \right)^2 + \left(2 \beta_{\mathrm{octx}} \, \beta_{\mathrm{octy}} \, \varepsilon_{y,x}^{\mathrm{rms}} \right)^2 \right]^{1/2} \int_0^{l_{mag}} K_{\mathrm{oct}} \, dl, \qquad \text{(E.9)}$$

where N_{oct} is the number of octupoles and l_{mag} the equivalent octupolar magnetic length.

APPENDIX F: LIST OF FIGURES

APPENDIX G: LIST OF TABLES

APPENDIX H: LIST OF SYMBOLS

a_w	Half major axis of the elliptical beam pipe
b_w	Half minor axis of the elliptical beam pipe
$\vec{B}$	Magnetic field vector
$\overline{B}_0$	Average bending field around the synchronous orbit
c	Velocity of light
$C = 2\pi R$	Circumference of the machine
C_G	Linear coupling coefficient of Guignard[56]
$D_i(s_i)$	Dispersion function of the *i*th particle in the external focusing field
$D_x^b,\ D_y^b$	Amplitudes of the horizontal and vertical dipole moments of the *b*th rigid bunch
e	Elementary charge
$e^{(\ )}$	Exponential function
$\vec{E}$	Electric field vector
$E_0 = 0.938\ \text{Gev}$	Proton rest energy
E_c	Proton kinetic energy
$E_t = E_0 + E_c$	Proton total energy
$E_{t,0}$	Total energy of the synchronous particle
$E_{t,i}$	Total energy of the *i*th particle
f_0	Average revolution frequency of the particles (revolution frequency of the synchronous particle)
f_i	Revolution frequency of the *i*th particle
f_r	Vacuum chamber cut-off frequency (resonance frequency describing the broadband impedances)
$f_{\text{RF}} = h\, f_0$	Accelerating (RF) frequency
f_s	Synchrotron frequency of the particles
$f_{x0}(\hat{x}_i),\ f_{y0}(\hat{y}_i)$	Horizontal and vertical distribution functions of the incoherent betatron amplitudes of the particles
$\vec{F} = e\left(\vec{E} + \vec{v} \times \vec{B}\right)$	Electromagnetic (Lorentz) force
$g(p_i)$	Distribution function of the momenta of the particles
$g_0(\hat{\tau}_i)$	Distribution function of the synchrotron amplitudes of the particles
$G(\vartheta_r - \vartheta, Q_c)$	Bunch function (for rigid bunched beams) that takes into account the contribution of the *r*th particle to the horizontal wake-field at the place ϑ and at the time t from all its previous turns
h	Harmonic number, which defines the maximum number of bunches in a machine
$h(\hat{x}_i^2, \hat{y}_i^2)$	Distribution function of the transverse incoherent betatron amplitudes of the particles

$h_m(\omega)$	Bunch spectrum of head-tail mode $\lvert m \rvert$
$h_x(\hat{x}_i),\ h_y(\hat{y}_i)$	Horizontal and vertical distribution functions of the incoherent betatron amplitudes of the particles. They are related to $f_{x0}(\hat{x}_i)$ and $f_{y0}(\hat{y}_i)$ by $h_x(\hat{x}_i) = 2\pi\, f_{x0}(\hat{x}_i)$ and $h_y(\hat{y}_i) = 2\pi\, f_{y0}(\hat{y}_i)$
$\mathrm{H}(q_\rho, p_\rho, t)$	Function called Hamiltonian, with q_ρ and p_ρ two families of canonically conjugated coordinates. If the system is non-dissipative, the equations of motion can be obtained from the Hamiltonian through the canonical equations (see Eq. (4.34))
I	Circulating beam current in a coasting beam or infinite identity matrix
I_b	Current in one bunch
I_{beam}	Number of particles in a beam (beam intensity)
$\mathrm{Im}(\ )$	Imaginary part
I_M	$M \times M$ identity matrix
I_{oct}	Octupole current
I_{skew}	Skew quadrupole current
$j = \sqrt{-1}$	Imaginary unit
J_m	Bessel function of *m*th order
$k_{x,y} = n_{x,y} / R$	Horizontal and vertical wave numbers for a coasting beam
K_{oct}	Normalised octupole gradient, defined by $K_{\mathrm{oct}} = \left(\partial^3 B_y / \partial x^3\right) / \left(6 B_y \rho_x\right)$
$K_{x,i},\ K_{y,i}$	Horizontal and vertical functions including the bending and focusing forces exerted on the *i*th particle
$\underline{K}_0$	Average normalised skew gradient, defined by $\underline{K}_0 = \left(e / p_0\right)\left(\partial B_x / \partial x\right)$
$\hat{\underline{K}}_0(l)$	*l*th Fourier component of the linear coupling $\underline{K}_0$
$\underline{K}_i$	Normalised skew gradient of the *i*th particle, defined by $\underline{K}_i = \left(e / p_i\right)\left(\partial B_{x,i} / \partial x_i\right)$
l	Integer describing the linear coupling resonance $Q_h - Q_v = l$
l_{mag}	Equivalent octupolar magnetic length
l.h.s	Left-hand side
L	Total bunch length (in meters)
L_c	Length of a "cell" repeated N_{cell} times around the machine. If $N_{cell} = 1,\ L_c = C$
$m = \ldots, -1, 0, 1, \ldots$	Head-tail (or within-bunch) mode number
m_0	Proton rest mass
M	Number of bunches of a beam
$n_{x,y}$	Horizontal and vertical azimuthal mode numbers for a coasting beam, $n_{x,y} = \ldots, -2, -1, 0, 1, 2, \ldots$; horizontal and vertical

	coupled-bunch mode numbers for a bunched beam, $n_{x,y} = 0,1,2,\ldots,M-1$
N	Number of particles in a coasting beam
N_b	Number of particles per bunch (bunch intensity)
N_{cell}	Number of periodic "cells" around the machine
N_{oct}	Number of octupoles
p_0	Ideal momentum, corresponding to a particle travelling on the design orbit
p_i	Momentum of the *i*th particle
P.V.	Principal value
$P_{x,i}$, $P_{y,i}$	Any horizontal and vertical perturbations (on the r.h.s of the horizontal and vertical Hill's equations)
Q	Quality factor of the resonators describing the broadband impedances
$Q_{0x,i}$, $Q_{0y,i}$	Horizontal and vertical tunes of the *i*th particle in the external focusing field
Q_{0x0}, Q_{0y0}	Averages of the tunes $Q_{0x,i}$, $Q_{0y,i}$
Q_c	Coherent tune
$Q_{h,v}$	Horizontal and vertical coherent tunes
$Q_{x0,y0}$	Centres of the distribution functions of the tunes $Q_{x,i}$, $Q_{y,i}$
$Q_{x,i}$, $Q_{y,i}$	Horizontal and vertical tunes of the *i*th particle, taking into account the incoherent tune shifts
r.h.s	Right-hand side
R	Average radius of the machine (average orbit radius of the synchronous particle)
$\mathrm{Re}(\ )$	Real part
R_i	Orbit radius of the *i*th particle
R.m.s	Root mean square
R_x, R_y	Shunt resistances describing the horizontal and vertical broadband impedances
s	Azimuthal coordinate
s_0	Azimuthal coordinate of the synchronous particle
s_i	Azimuthal coordinate of the *i*th particle
$Sgn(\omega) = 1$ if $\omega > 0, -1$ if $\omega < 0$	
t	Time
$T_0 = f_0^{-1}$	Average revolution period of the particles
$T_i = f_i^{-1}$	Revolution period of the *i*th particle
$T_s = f_s^{-1}$	Synchrotron oscillation period of the particles
$U_{x,y}$, $V_{x,y}$	Horizontal and vertical dispersion relation coefficients of Laslett, Neil and Sessler[26]
$U_{1x,y}$, $W_{x,y}$	Real horizontal and vertical coefficients proportional to $U_{x,y}$ and $V_{x,y}$ respectively

$\vec{v}$	Particle velocity vector
v_0	Velocity of the synchronous particle
v_i	Velocity of the *i*th particle
$V = \hat{V}_{\mathrm{RF}} \sin \phi_{\mathrm{RF}}(t)$	Voltage across the gap of an accelerating cavity
$\hat{V}_{\mathrm{RF}}$	Amplitude of the voltage across the gap of an accelerating cavity
$W_{x,y}(\tau_r - \tau_i)$	Horizontal and vertical wake functions, which describe the transient decay of the wake forces on the *i*th particle due to the *r*th particle at the time t
x_i, y_i	Horizontal and vertical betatron coordinates of the *i*th particle
$\hat{x}_i$, $\hat{y}_i$	Horizontal and vertical incoherent betatron amplitudes of the *i*th particle
$\hat{x}_m(\hat{\tau}_i)$, $\hat{y}_m(\hat{\tau}_i)$	Horizontal and vertical coherent (average) betatron amplitudes associated with the synchrotron orbit $\hat{\tau}_i$, for the head-tail mode $\lvert m \rvert$
$\bar{x}$, $\bar{y}$	Horizontal and vertical betatron coordinates of the beam centre
z	Longitudinal coordinate
$Z_{x,y}(\omega)$	Horizontal and vertical coupling impedances
$Z_{x,y}^{BB}$	Horizontal and vertical broadband impedances
Z_c^{RW}	Resistive wall impedance of a circular beam pipe of radius b_w
$Z_{x,y}^{RW}$	Horizontal and vertical resistive wall impedances
$\alpha_p = \gamma_{tr}^{-2}$	Momentum compaction factor, defined by $\alpha_p = (dR_i / R_i) / (dp_i / p_i)$
β	Relativistic velocity factor
$\beta_{0x,i}$, $\beta_{0y,i}$	Horizontal and vertical betatron functions of the *i*th particle in the external focusing field
β_{octx}, β_{octy}	Horizontal and vertical betatron functions at the locations of the octupoles
γ	Relativistic mass factor
γ_{tr}	Relativistic mass factor at transition energy
$\delta(\ )$	Dirac function
$\delta_p(\ )$	Periodic Dirac function
$\delta\omega_{x,y}$	Half widths at half maximum of the Lorentzian betatron frequency spectra
$\Delta_{x,y}\, e^{j\omega t}$	Rigid horizontal and vertical beam oscillations of a coasting beam at a fixed azimuthal position
$\Delta E_{t,i}$	Total energy deviation (from the synchronous particle) of the *i*th particle
Δf_i	Frequency revolution deviation (from the synchronous particle) of the *i*th particle

Δp_i	Momentum deviation (from the synchronous particle) of the *i*th particle
$\Delta Q_{coh,x}$, $\Delta Q_{coh,y}$	Horizontal and vertical coherent tune shifts
$\Delta Q_{inc,x}$, $\Delta Q_{inc,y}$	Horizontal and vertical incoherent tune shifts
$\Delta\vartheta$	Common length (in angle) of the rigid bunches
$\Delta\vartheta_i$	Azimuthal angle deviation (from the synchronous particle) of the *i*th particle
$\Delta\phi_{\mathrm{RF},i}$	Accelerating (RF) phase deviation (from the synchronous particle) of the *i*th particle
$\Delta\omega_{x,y}$	Half widths at the bottom of the elliptical betatron frequency spectra
$\Delta\omega_{\mathrm{HWHH}}^{x,y}$	Half widths at half maximum of the horizontal and vertical betatron frequency distributions
$\varepsilon_0 = 8.84\times10^{-12}$ Fm^{-1}	Permittivity of free space
$\varepsilon_{x,i} = \hat{x}_i^2 / \beta_{0x,i}$	"Single-particle horizontal emittance"
$\varepsilon_{y,i} = \hat{y}_i^2 / \beta_{0y,i}$	"Single-particle vertical emittance"
$\varepsilon_x^{\mathrm{rms}}$, $\varepsilon_y^{\mathrm{rms}}$	R.m.s horizontal and vertical emittances (horizontal and vertical phase space areas divided by π)
$\zeta_i = y_i\,\beta_{0y,i}^{-1/2}(s)$	Normalised (Courant-Snyder) vertical coordinate of the *i*th particle
$\overline{\zeta}$	Normalised (Courant-Snyder) vertical coordinate of the beam centre
$\eta = \gamma_{tr}^{-2} - \gamma^{-2}$	Slippage (or off-momentum) factor, defined by $\eta = -(d\Omega_i/\Omega_i)/(dp_i/p_i)$
$\eta_i = x_i\,\beta_{0x,i}^{-1/2}(s)$	Normalised (Courant-Snyder) horizontal coordinate of the *i*th particle
$\overline{\eta}$	Normalised (Courant-Snyder) horizontal coordinate of the beam centre
ϑ	Azimuthal angle defined by $\vartheta = s/R$
ϑ_0	Azimuthal angle of the synchronous particle
ϑ_i	Azimuthal angle of the *i*th particle
$\mu_{0x,i}$, $\mu_{0y,i}$	Horizontal and vertical phase advances per period of the *i*th particle in the external focusing field, defined by $\mu_{0x,i} = \int_0^{L_c} \beta_{0x,i}^{-1}(t)\,dt$ and $\mu_{0y,i} = \int_0^{L_c} \beta_{0y,i}^{-1}(t)\,dt$
$\mu_{0x,i}(s)$, $\mu_{0y,i}(s)$	Horizontal and vertical phase functions of the *i*th particle in the external focusing field, defined by $\mu_{0x,i}(s) = \int_0^{s} \beta_{0x,i}^{-1}(t)\,dt$ and $\mu_{0y,i}(s) = \int_0^{s} \beta_{0y,i}^{-1}(t)\,dt$

$\xi_{x,y}$ Horizontal and vertical chromaticities, defined by $\xi_x = \left(d\,Q_{0x,i} / Q_{0x,i} \right) / \left(dp_i / p_i \right)$, $\xi_y = \left(d\,Q_{0y,i} / Q_{0y,i} \right) / \left(dp_i / p_i \right)$

$\rho_{x,y}$ Average horizontal and vertical bending radii

$\rho_{x,y}(s)$ Local horizontal and vertical bending radii

$\rho_x(\omega_{x,i})$, $\rho_y(\omega_{y,i})$ Externally given distribution functions of the horizontal and vertical betatron (angular) frequencies

$\rho_x(\hat{x}_i)$ Horizontal distribution function of the incoherent betatron amplitudes of the particles. It is related to $h_x(\hat{x}_i)$ by

$$h_x'(\hat{x}_i) = 2\,\omega_{x0}\,\frac{\pi}{N}\,\rho_x'(\hat{x}_i)$$

ρ_w Vacuum chamber resistivity

τ_b Total bunch length (in seconds)

τ_i Synchrotron oscillation coordinate: (i) time-of-arrival of the *i*th particle of a bunch at some azimuth measured with respect to the time-of-arrival of the synchronous particle (in Section 3.3); (ii) time interval between the passage of the synchronous particle and the test particle (in Chapter 4)

$\hat{\tau}_i$ Synchrotron amplitude

$\varphi_{0x,i}$, $\varphi_{0y,i}$ Initial horizontal and vertical betatron phases of the *i*th particle

$\varphi_{x,i}$, $\varphi_{y,i}$ Horizontal and vertical betatron phases of the *i*th particle at time *t*

ϕ_i Normalised (Courant-Snyder) angle, defined by

$$\phi_i = Q_{0x,i}^{-1} \int_0^s \beta_{0x,i}^{-1}(t)\,dt \approx Q_{0y,i}^{-1} \int_0^s \beta_{0y,i}^{-1}(t)\,dt$$

$\phi_{\mathrm{RF}}(t)$ Accelerating (RF) phase at time *t*

$\phi_{\mathrm{RF},0}$ Constant accelerating (RF) phase experienced by the synchronous particle

$\phi_{\mathrm{RF},i}$ Accelerating (RF) phase experienced by the *i*th particle

χ_x, χ_y Total horizontal and vertical betatron phase shifts between the head and the tail of a bunch, defined by $\chi_x = \left(\xi_x / \eta \right) Q_{x0}\,\Omega_0\,\tau_b$ and $\chi_y = \left(\xi_y / \eta \right) Q_{y0}\,\Omega_0\,\tau_b$

ψ_i Initial synchrotron phase of the *i*th particle

ω Local collective (angular) frequency (seen by a stationary observer at a fixed location ϑ around the accelerator)

$\omega_{0x,i}$, $\omega_{0y,i}$ Horizontal and vertical betatron (angular) frequencies of the *i*th particle in the external focusing field

$\omega_c = Q_c\,\Omega_0$ Coherent betatron (angular) frequency

$\omega_r = 2\pi\,f_r$ Vacuum chamber cut-off (angular) frequency

$\omega_s = 2\pi\,f_s$ Synchrotron oscillation (angular) frequency

$\omega_{x0,y0}$ Centres of the distribution functions of the betatron (angular) frequencies $\omega_{x,i}$, $\omega_{y,i}$

$\omega_{x,i}$, $\omega_{y,i}$	Horizontal and vertical betatron (angular) frequencies of the *i*th particle, taking into account the incoherent betatron frequency shifts
ω_{ξ_x}, ω_{ξ_y}	Horizontal and vertical chromatic (angular) frequencies, defined by $\omega_{\xi_x} = \left(\xi_x / \eta\right) Q_{x0}\, \Omega_0$ and $\omega_{\xi_y} = \left(\xi_y / \eta\right) Q_{y0}\, \Omega_0$
$\Omega_0 = 2\pi f_0$	Average revolution (angular) frequency of the particles
$\Omega_i = 2\pi f_i$	Revolution (angular) frequency of the *i*th particle
$B_y \rho_x$	Beam rigidity
$dN / d\vartheta$	Linear density of the particles
$(dP_x / d\vartheta)$, $(dP_y / d\vartheta)$	Horizontal and vertical dipole moments per unit azimuthal angle ϑ
$\left[\vec{e}_x(s), \vec{e}_y, \vec{e}_z(s)\right]$	Frenet-Serret coordinate system used to describe particle trajectories
$\dot{}$	Derivative with respect to time t
$\left\| \right\|$	Complex module
$( )^t$	Transpose
$( )^*$	Complex conjugated
$\sqrt{}$	Square root (positive value)

APPENDIX I: RESUME DE LA THESE

AMORTISSEMENT DE LANDAU COUPLE DES INSTABILITES COHERENTES TRANSVERSALES DANS LES ACCELERATEURS DE PARTICULES

RESUME

L'effet du couplage linéaire entre les plans transversaux d'un accélérateur circulaire sur l'amortissement de Landau des instabilités cohérentes est étudié en considérant deux distributions caractéristiques de fréquences (Lorentzienne et "elliptique"). Celles-ci correspondent à des cas limites modélisant des spectres avec et sans longues queues.

Un critère général de stabilité, où interviennent la force du couplage (dû aux quadrupôles[a] tournés) et la distance des nombres d'ondes bétatroniques aux résonances de couplage, est obtenu dans les deux cas. Ce dernier révèle la possibilité de partager les dispersions de fréquences stabilisatrices entre les deux plans, ce qui peut considérablement améliorer la stabilité cohérente du faisceau, en particulier dans les cas où la situation est plus critique dans un plan. Une seconde observation importante est que l'effet d'une grande partie imaginaire de l'impédance de couplage, qui normalement requiert une dispersion de fréquences équivalente pour l'amortissement de Landau, peut être compensé (du moins dans un plan) par un choix judicieux du couplage.

Les résultats d'expériences effectuées au Synchrotron à Protons (PS) du CERN confirment le comportement général prédit par la théorie. Le mécanisme de l'amortissement de Landau couplé pourrait donc expliquer pourquoi une machine comme le PS peut être stabilisée en rapprochant le point de fonctionnement près d'une résonance de couplage. Il peut par conséquent être utilisé pour déterminer des valeurs optimales du point de fonctionnement et de la force du couplage linéaire.

[a] La langue française exige "quadripôle" mais l'usage impose "quadrupôle".

I.1 Introduction

Le transfert d'énergie entre les degrés de liberté d'un oscillateur multi-dimensionnel est un phénomène très répandu en physique. Un fort couplage entre les plans transversaux d'un accélérateur de particules conduit à une "équi-partition" de l'énergie d'oscillation, et du "taux de croissance" dans le cas d'instabilités cohérentes. Le but de ce papier est de montrer qu'en présence d'une dispersion de fréquences, l'amortissement de Landau peut aussi être partagé entre les deux plans pour un couplage "optimum". Ce résultat pourrait donc être utilisé pour minimiser les non-linéarités externes nécessaires pour l'amortissement de Landau.

La Section I.2 traite des faisceaux dégroupés. Les résultats obtenus sont ensuite étendus au cas de faisceaux groupés dans la Section I.3. Le partage de l'amortissement de Landau et de la chromaticité est illustré dans le cas d'une instabilité "head-tail" en utilisant le modèle "hollow-bunch" (paquet creux), et le transfert d'amortissement par "feedbacks" est aussi discuté. La mesure du couplage linéaire du PS est décrite dans la Section I.4, et les mesures d'amortissement de Landau couplé sont analysées dans la Section I.5.

I.2 Faisceaux dégroupés

I.2.1 Equations du mouvement

Quatre forces sont prises en compte pour décrire les mouvements bétatroniques horizontal et vertical d'une particule de référence i :[38]

1) les forces de focalisation externes qui dépendent de la déviation horizontale x_i (déviation verticale y_i) de la particule par rapport à une référence fixe (e.g. le centre de la chambre). Le nombre d'ondes correspondant est $Q_{0x,i}$ ($Q_{0y,i}$) ;
2) les forces de charges d'espace cohérentes qui dépendent de la déviation $\bar{x}$ ($\bar{y}$) du centre du faisceau par rapport au centre de la chambre. Le déplacement du nombre d'ondes correspondant est $\Delta Q_{coh,x}$ ($\Delta Q_{coh,y}$) ;
3) les forces de charges d'espace incohérentes qui dépendent de la déviation $x_i - \bar{x}$ ($y_i - \bar{y}$) de la particule par rapport au centre de la chambre. Le déplacement du nombre d'ondes correspondant est $\Delta Q_{inc,x}$ ($\Delta Q_{inc,y}$) ;
4) les forces de couplage, représentées par le gradient normalisé des quadrupôles tournés $\underline{K}_i = \left(e / p_i\right)\left(\partial B_{x,i} / \partial x_i\right)$, qui font apparaître la déviation verticale (horizontale) dans l'équation du mouvement horizontale (verticale) de la particule. On obtient

$$\frac{d^2 x_i}{d t^2} + \Omega_i^2 \left(Q_{0x,i}^2 + 2 Q_{0x,i}\, \Delta Q_{inc,x}\right) x_i = -2\Omega_i^2\, Q_{0x,i} \left(\Delta Q_{coh,x} - \Delta Q_{inc,x}\right) \bar{x} + \underline{K}_i\, R_i^2\, \Omega_i^2\, y_i \,,$$

$$\frac{d^2 y_i}{d t^2} + \Omega_i^2 \left(Q_{0y,i}^2 + 2 Q_{0y,i}\, \Delta Q_{inc,y}\right) y_i = -2\Omega_i^2\, Q_{0y,i} \left(\Delta Q_{coh,y} - \Delta Q_{inc,y}\right) \bar{y} + \underline{K}_i\, R_i^2\, \Omega_i^2\, x_i \,. \qquad \text{(I.1)}$$

Ici, e est la charge élémentaire, p_i la quantité de mouvement de la particule, $B_{x,i}$ l'induction magnétique à la position de la particule, t le temps, Ω_i la fréquence

angulaire de révolution de la particule et R_i le rayon de l'orbite décrite par la particule (approximé par la suite par le rayon moyen R de la machine). Les déplacements des nombres d'ondes cohérents et incohérents de Laslett sont généralisés ici pour inclure les champs de sillage. Les trois premières forces peuvent être traitées en utilisant l'approximation douce. En considérant les coordonnées normalisées (de Courant et Snyder) $\eta_i = x_i\,\beta_{0x,i}^{-1/2}(s)$, $\zeta_i = y_i\,\beta_{0y,i}^{-1/2}(s)$ et $\phi_i = Q_{0x,i}^{-1}\int \beta_{0x,i}^{-1}(s)\,ds \approx Q_{0y,i}^{-1}\int \beta_{0y,i}^{-1}(s)\,ds$, où les fonctions bétatroniques sont données par $\beta_{0x,i} \approx R_i / Q_{0x,i} \approx R/Q_{0x0}$ et $\beta_{0y,i} \approx R_i / Q_{0y,i} \approx R/Q_{0y0}$ dans l'approximation douce (avec Q_{0x0} et Q_{0y0} les nombres d'ondes moyens), les Eqs. (I.1) s'écrivent

$$\begin{aligned}
\frac{d^2\eta_i}{d\phi^2} + Q_{x,i}^2\,\eta_i &= -j\,\frac{e\beta I Z_x}{2\pi R m_0 \gamma \Omega_0^2}\,\overline{\eta} + R^2\left(\frac{Q_{0x0}}{Q_{0y0}}\right)^{1/2}\underline{K}_0\,\zeta_i\,, \\
\frac{d^2\zeta_i}{d\phi^2} + Q_{y,i}^2\,\zeta_i &= -j\,\frac{e\beta I Z_y}{2\pi R m_0 \gamma \Omega_0^2}\,\overline{\zeta} + R^2\left(\frac{Q_{0y0}}{Q_{0x0}}\right)^{1/2}\underline{K}_0\,\eta_i\,.
\end{aligned} \tag{I.2}$$

Ici, s est la coordonnée azimuthale, $Q_{x,i} = Q_{0x,i} + \Delta Q_{inc,x}$ et $Q_{y,i} = Q_{0y,i} + \Delta Q_{inc,y}$ sont les nouveaux nombres d'ondes incohérents, $j = \sqrt{-1}$ est l'unité imaginaire, β et γ sont les facteurs relativistes de vitesse et de masse, I est le courant du faisceau circulant, m_0 est la masse du proton au repos, $\overline{\eta}$ et $\overline{\zeta}$ sont les coordonnées normalisées du centre du faisceau. De plus, dans l'Eq. (I.2), la fréquence angulaire de révolution Ω_i et le gradient des quadrupôles tournés $\underline{K}_i$ ont été remplacés par leurs valeurs moyennes, Ω_0 ($\phi_i = \Omega_0\,t = \phi$) et $\underline{K}_0$. Enfin, les déplacements des nombres d'ondes cohérents et incohérents ont été exprimés en fonction des impédances de couplage transversales qui sont données, e.g. dans le plan horizontal, par[23]

$$Z_x(\omega) = \frac{j}{e\beta I \Delta_x}\int_0^{2\pi R} \overline{F}_{x,i}\,ds = -j\,\frac{2\pi R\gamma m_0}{e\beta I}\,2\Omega_i^2\,Q_{0x,i}\left(\Delta Q_{coh,x} - \Delta Q_{inc,x}\right)_{(\omega)}, \tag{I.3}$$

où $\Delta_x\,e^{j\omega t}$ décrit les oscillations horizontales du faisceau et $\overline{F}_{x,i}\,e^{j\omega t}$ représente la force horizontale cohérente exercée sur la particule *i* ("moyennée" sur toute la section).

I.2.2 Relation de dispersion

Les fréquences bétatroniques transversales sont données par $\omega_{x,i} = \Omega_0\,Q_{x,i}$ et $\omega_{y,i} = \Omega_0\,Q_{y,i}$. Dans un premier temps, les dispersions de fréquences betatroniques sont spécifiées par des distributions externes données. Les fonctions de répartition, $\rho_x(\omega_{x,i})$ et $\rho_y(\omega_{y,i})$, sont supposées non-corrélées et normalisées à l'unité. De plus, dans une machine circulaire, le couplage linéaire est périodique en ϕ, de période 2π. Sa série de Fourier s'écrit

$$\underline{K}_0(\phi) = \sum_{l=-\infty}^{l=+\infty} \hat{\underline{K}}_0(l)\,e^{jl\phi}, \tag{I.4}$$

avec

$$\underline{\hat{K}}_0(l) = \frac{1}{2\pi}\int_0^{2\pi} \underline{K}_0(\phi)\, e^{-jl\phi}\, d\phi. \tag{I.5}$$

Si on ne considère que la composante de Fourier dominante (l) du couplage et qu'on cherche des modes propres d'oscillation, on obtient des solutions particulières de la forme

$$\eta_i = \mathrm{H}_i\, e^{jQ_c\phi}, \qquad \zeta_i = \mathrm{Z}_i\, e^{j(Q_c - l)\phi}, \tag{I.6}$$

où Q_c est le nombre d'ondes cohérent (nombre complexe) recherché. Si on substitue les Eqs. (I.6) dans les Eqs. (I.2) et qu'on intègre sur les spectres transversaux, on obtient alors la relation de dispersion bi-dimensionnelle avec pour inconnue la fréquence bétatronique cohérente $\omega_c = \Omega_0 Q_c$

$$\begin{aligned}&\left[\left(\int_{-\infty}^{+\infty} \frac{\rho_x(\omega_{x,i})\, d\omega_{x,i}}{\omega_c - \omega_{x,i}}\right)^{-1} - U_x + jV_x\right]\times \\ &\left[\left(\int_{-\infty}^{+\infty} \frac{\rho_y(\omega_{y,i})\, d\omega_{y,i}}{\omega_c - l\Omega_0 - \omega_{y,i}}\right)^{-1} - U_y + jV_y\right] = \frac{\left|\underline{\hat{K}}_0(l)\right|^2 R^4 \Omega_0^4}{4\,\omega_{x0}\,\omega_{y0}}.\end{aligned} \tag{I.7}$$

Les approximations $\omega_{x,i} \approx \omega_c \approx \omega_{x0}$ et $\omega_{y,i} \approx \omega_c - l\Omega_0 \approx \omega_{y0}$, où $\omega_{x0} = \Omega_0 Q_{x0}$ et $\omega_{y0} = \Omega_0 Q_{y0}$ représentent les centres des distributions, ont été faites pour obtenir l'Eq. (I.7). De plus, les coefficients de dispersion $U_{x,y}$ [b] et $V_{x,y}$ de Laslett, Neil et Sessler[26] ont été utilisés. Ces derniers sont reliés aux impédances de couplage transversales par[19]

$$\left(U_{x,y} - jV_{x,y}\right)_{(\omega)} = \frac{je\beta I Z_{x,y}(\omega)}{4\pi R m_0 \gamma \omega_{x0,y0}}. \tag{I.8}$$

Rappelons que les termes de champs de sillage doivent être évalués aux fréquences collectives locales (fréquences observées à des endroits fixes autour de l'accélérateur), données par

$$\omega_1 \approx (n_x + Q_{x0})\,\Omega_0, \qquad \omega_2 \approx (n_y + Q_{y0})\,\Omega_0, \tag{I.9}$$

où $n_{x,y}$ représentent les modes azimuthaux décrivant les oscillations collectives transversales, et sont reliés par $n_x = n_y - l$.

En réalité, le traitement de l'amortissement de Landau par les non-linéarités est plus compliqué. En effet, dans le plan du mouvement cohérent, c'est en fait la dérivée de la fonction de répartition par rapport à l'amplitude d'oscillation incohérente qui apparait dans l'intégrale de dispersion à la place de la fonction de répartition elle-même. Une méhode pour obtenir directement ce résultat consiste à utiliser l'équation de Vlasov.[26,32] Avec le formalisme de l'équation du mouvement d'une particule, Hereward a obtenu le même résultat en considérant les termes non-linéaires du "second ordre".[37] Ce résultat (Eq. (5.4) de la Réf. 37) peut aussi être généralisé en présence de couplage,

[b] Quelques fois $U + V$ est écrit à la place du U utilisé ici.

et l'équation de dispersion bi-dimensionnelle obtenue est similaire à l'Eq. (I.7). En effet, si les distributions des amplitudes bétatroniques incohérentes et des quantités de mouvement sont décrites par les fonctions de répartition $h\left(\hat{x}_i^2, \hat{y}_i^2\right)$ et $g\left(p_i\right)$, normalisées par

$$\int_{\hat{x}_i^2=0}^{\hat{x}_i^2=+\infty} \int_{\hat{y}_i^2=0}^{\hat{y}_i^2=+\infty} h\left(\hat{x}_i^2, \hat{y}_i^2\right) \frac{d\hat{x}_i^2}{2} \frac{d\hat{y}_i^2}{2} = 1, \qquad \int_0^{+\infty} g\left(p_i\right) dp_i = 1, \tag{I.10}$$

la relation de dispersion bi-dimensionnelle s'écrit

$$\left\{ \left[\iiint \frac{1}{\omega_c - \omega_{x,i}\left(\hat{x}_i, \hat{y}_i, p_i\right)} \left(-\frac{1}{4} \frac{\partial h\left(\hat{x}_i^2, \hat{y}_i^2\right) \hat{x}_i^2}{\partial \hat{x}_i^2} \right) g\left(p_i\right) d\hat{x}_i^2 \, d\hat{y}_i^2 \, dp_i \right]^{-1} - U_x + jV_x \right\} \times$$

$$\left\{ \left[\iiint \frac{1}{\omega_c - l\Omega_0 - \omega_{y,i}\left(\hat{x}_i, \hat{y}_i, p_i\right)} \left(-\frac{1}{4} \frac{\partial h\left(\hat{x}_i^2, \hat{y}_i^2\right) \hat{y}_i^2}{\partial \hat{y}_i^2} \right) g\left(p_i\right) d\hat{x}_i^2 \, d\hat{y}_i^2 \, dp_i \right]^{-1} - U_y + jV_y \right\}$$

$$= \frac{\left|\underline{\hat{K}}_0(l)\right|^2 R^4 \Omega_0^4}{4\, \omega_{x0}\, \omega_{y0}}. \tag{I.11}$$

Par la suite, seule l'Eq. (I.7) est étudiée mais la même analyse s'applique pour l'Eq. (I.11), en approximant la dispersion des fréquences bétatroniques dans chaque plan par la racine carrée de la somme quadratique des dispersions introduites par la quantité de mouvement et les amplitudes bétatroniques incohérentes.

I.2.3 Critère de stabilité pour des spectres Lorentziens

Dans ce cas, la fonction de répartition, e.g. dans le plan horizontal, s'écrit[8]

$$\rho_x\left(\omega_{x,i}\right) = \frac{\delta\omega_x}{\pi} \left[\left(\omega_{x,i} - \omega_{x0}\right)^2 + \delta\omega_x^2 \right]^{-1}, \tag{I.12}$$

où $\delta\omega_x$ est la demi-largeur à mi-hauteur du spectre. L'intégrale de dispersion correspondante est[8]

$$\int_{-\infty}^{+\infty} \frac{\rho_x\left(\omega_{x,i}\right) d\omega_{x,i}}{\omega_c - \omega_{x,i}} = \frac{1}{\omega_c - \omega_{x0} - j\,\delta\omega_x}. \tag{I.13}$$

Si on substitue l'Eq. (I.13), et l'équation similaire pour le plan vertical, dans l'Eq. (I.7), la relation de dispersion devient

$$\begin{aligned} &\left[\omega_c - \omega_{x0} - U_x - j\left(\delta\omega_x - V_x\right)\right] \times \\ &\left[\omega_c - \omega_{y0} - l\Omega_0 - U_y - j\left(\delta\omega_y - V_y\right)\right] = \frac{\left|\underline{\hat{K}}_0(l)\right|^2 R^4 \Omega_0^4}{4\, \omega_{x0}\, \omega_{y0}}. \end{aligned} \tag{I.14}$$

Cette équation a deux solutions pour ω_c décrivant les deux modes d'oscillation cohérents du système couplé. Les mouvements cohérents considérés sont de la forme

$e^{j\omega_c t}$; par conséquent, pour chaque solution ω_c, $\mathrm{Re}(\omega_c)$ décrit la fréquence d'oscillation cohérente et $-\mathrm{Im}(\omega_c)$ représente le taux de croissance de l'instabilité. Ainsi, pour être stable, un mode d'oscillation cohérent doit satisfaire $\mathrm{Im}(\omega_c) \geq 0$.

Les parties imaginaires des deux fréquences cohérentes sont données par

$$\mathrm{Im}(\omega_{c1,2}) = (\delta\omega_{x,y} - V_{x,y}) \pm \frac{(\delta\omega_y - V_y - \delta\omega_x + V_x)}{2} C(a,\delta). \qquad \text{(I.15)}$$

Ici, $C(a,\delta)$ est une fonction de couplage (partage) donnée par

$$C(a,\delta) = 1 - \frac{1}{\sqrt{2}} \sqrt{1 - 4a^2 - \delta^2 + \sqrt{(-1 + 4a^2 + \delta^2)^2 + 4\delta^2}}\,, \qquad \text{(I.16)}$$

avec

$$a = \frac{\left|\underline{\hat{K}}_0(l)\right| R^2 \Omega_0^2}{2\sqrt{\omega_{x0}\,\omega_{y0}}\left|\delta\omega_y - V_y - \delta\omega_x + V_x\right|}, \qquad \delta = \frac{\Omega_0 \left|Q_h - Q_v - l\right|}{\left|\delta\omega_y - V_y - \delta\omega_x + V_x\right|}, \qquad \text{(I.17)}$$

où

$$Q_{h,v} = (\omega_{x0,y0} + U_{x,y}) / \Omega_0 \qquad \text{(I.18)}$$

représentent les nombres d'ondes cohérents horizontal et vertical en présence de champs de sillage ($U_{x,y}$), mais en l'absence de couplage.

Trois graphes de $C(a)$ sont représentés sur la Figure 7 pour $\delta = 1$, $\delta = 0.25$ et $\delta = 0$.

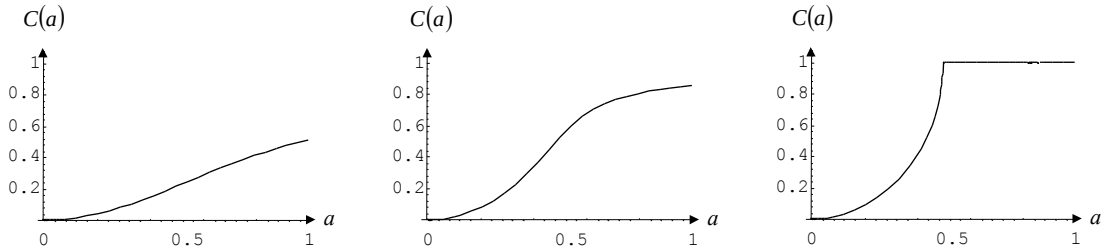

FIGURE 7 Fonction de partage $C(a)$ pour : (a) $\delta = 1$; (b) $\delta = 0.25$; (c) $\delta = 0$.

Quelque soit la valeur de δ, la fonction de partage varie entre $C = 0$ et $C = 1$. Cependant, plus δ est petit et plus $C(a)$ croit rapidement. Le partage peut être choisi en ajustant la séparation des nombres d'ondes et/ou la force du couplage.

Pour $C = 0$ (couplage nul), le critère de stabilité dans les plans horizontal et vertical s'écrit

$$\delta\omega_x \geq V_x\,, \qquad \delta\omega_y \geq V_y\,. \qquad \text{(I.19)}$$

Pour $C = 1$ (couplage total), en utilisant l'Eq. (I.15), les deux critères précédents se reduisent en un seul

$$\delta\omega_x + \delta\omega_y \geq V_x + V_y\,. \qquad \text{(I.20)}$$

L'Equation (I.20) montre clairement l'effet bénéfique du couplage. Même en l'absence d'une dispersion de fréquences dans un plan, une instabilité cohérente peut être amortie grâce à l'autre plan : l'amortissement de Landau est transféré du plan stable au plan instable. Dans le cas d'un couplage total, chaque plan dispose de la dispersion de fréquences bétatroniques transversales $(\delta\omega_x + \delta\omega_y)/2$ pour amortir l'instabilité représentée par le taux de croissance moyen $(V_x + V_y)/2$. Lorsque les dispersions de nombres d'ondes transversaux sont égaux, il n'y a pas de redistribution de l'amortissement de Landau mais il reste un partage des taux de croissance. Par conséquent, le faisceau peut être stabilisé si $\delta\omega_x = \delta\omega_y \geq (V_x + V_y)/2$. Le résulat du couplage est donc un transfert de l'amortissement de Landau du plan stable au plan instable et dans un même temps un transfert du taux de croissance du plan instable au plan stable jusqu'à un partage égal d'amortissement et de croissance. On peut conclure de l'Eq. (I.20) que si les deux plans sont stables sans couplage, alors ils restent stables pour un couplage total. De même, si les deux plans sont instables sans couplage, ils restent instables pour un couplage total.

Considérons le cas intéressant d'un plan transversal instable en l'absence de couplage. Si la condition nécessaire de l'Eq. (I.20) est remplie, alors il est possible de stabiliser le faisceau dans les deux plans en choisissant une paire (a, δ) qui satisfasse $\mathrm{Im}(\omega_{c1,2}) \geq 0$ (cf. Eq. (I.15)). Les valeurs stabilisatrices du module du coefficient de Fourier du gradient des quadrupôles tournés sont

$$\left|\underline{\hat{K}}_0(l)\right| \geq \frac{2\left[-Q_{x0}\,Q_{y0}\left(\delta\omega_x - V_x\right)\left(\delta\omega_y - V_y\right)\right]^{1/2}}{R^2\,\Omega_0} \times \frac{\left[\left(\delta\omega_x + \delta\omega_y - V_x - V_y\right)^2 + \Omega_0^2\left(Q_h - Q_v - l\right)^2\right]^{1/2}}{\delta\omega_x + \delta\omega_y - V_x - V_y}. \tag{I.21}$$

Le graphe de la frontière de stabilité (donnée par le signe égal dans l'Eq. (I.21)) est une courbe symétrique par rapport à l'axe vertical (Figure 8). Une région de stabilité est obtenue pour le module du coefficient de Fourier du gradient des quadrupôles tournés et la séparation des nombres d'ondes $Q_h - Q_v - l$.

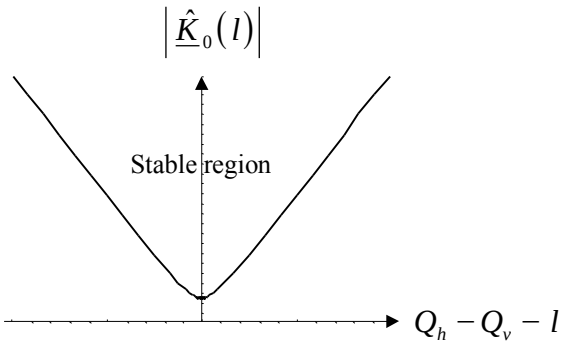

FIGURE 8 Forme de la frontière de stabilité dans le plan ($Q_h - Q_v - l$, $\left|\underline{\hat{K}}_0(l)\right|$).

I.2.4 Critère de stabilité pour des spectres "elliptiques"

Du fait de ses queues infinies, la distribution Lorentzienne de fréquences tend à sous-estimer deux points importants. Le premier est l'effet du déplacement réel de la

fréquence bétatronique. L'importance de U émerge déjà dans le cas non couplé où, pour des distributions à queues finies, l'amortissement de Landau disparaît si le déplacement $|U|$ est plus grand que la dispersion de fréquences $\Delta\omega$. Ceci s'explique par le fait que la fréquence cohérente déplacée (en présence de champ de sillage) $\omega_0 + U$ se trouve à l'extérieur du spectre $\omega_0 \pm \Delta\omega$.

Le second point, qui est en fait lié au premier, est qu'un fort couplage peut aussi être nuisible en déplaçant la fréquence cohérente à l'extérieur du spectre, empêchant à nouveau l'amortissement de Landau. Pour étudier ces deux effets, des spectres "elliptiques" sont considérés, sachant que les spectres Lorentzien et "elliptique" sont des cas limites et que les distributions réelles peuvent probablement être décrites par des situations intermédiaires.[8,34-36]

Dans ce cas, la fonction de répartition, e.g. dans le plan horizontal, s'écrit[8]

$$\rho_x\left(\omega_{x,i}\right) = \begin{cases} \dfrac{2}{\pi\,\Delta\omega_x^2}\sqrt{\Delta\omega_x^2 - \left(\omega_{x,i} - \omega_{x0}\right)^2} & , \quad \left|\omega_{x,i} - \omega_{x0}\right| \le \Delta\omega_x \\ 0 & , \quad \left|\omega_{x,i} - \omega_{x0}\right| > \Delta\omega_x \end{cases}, \tag{I.22}$$

où $\Delta\omega_x$ est la demi-largeur au pied de la distribution. L'intégrale de dispersion correspondante est donnée par[8]

$$\int_{-\infty}^{+\infty} \frac{\rho_x\left(\omega_{x,i}\right) d\omega_{x,i}}{\omega_c - \omega_{x,i}} = 2\left[\,\omega_c - \omega_{x0} - j\sqrt{\Delta\omega_x^2 - \left(\omega_c - \omega_{x0}\right)^2}\,\right]^{-1}, \tag{I.23}$$

avec

$$\begin{aligned} -j\sqrt{\Delta\omega_x^2 - \left(\omega_c - \omega_{x0}\right)^2} &= \sqrt{\left(\omega_c - \omega_{x0}\right)^2 - \Delta\omega_x^2} \qquad \text{for} \quad \omega_c > \omega_{x0} + \Delta\omega_x\,, \\ -j\sqrt{\Delta\omega_x^2 - \left(\omega_c - \omega_{x0}\right)^2} &= -\sqrt{\left(\omega_c - \omega_{x0}\right)^2 - \Delta\omega_x^2} \qquad \text{for} \quad \omega_c < \omega_{x0} - \Delta\omega_x\,. \end{aligned} \tag{I.24}$$

Si on substitue l'Eq. (I.23), et l'équation similaire pour le plan vertical, dans l'Eq. (I.7), la relation de dipersion devient

$$\begin{aligned} &\left\{\omega_c - \omega_{x0} - 2U_x - j\left[\sqrt{\Delta\omega_x^2 - \left(\omega_c - \omega_{x0}\right)^2} - 2V_x\right]\right\} \times \\ &\left\{\omega_c - \omega_{y0} - l\,\Omega_0 - 2U_y - j\left[\sqrt{\Delta\omega_y^2 - \left(\omega_c - \omega_{y0} - l\,\Omega_0\right)^2} - 2V_y\right]\right\} = \frac{\left|\underline{\hat{K}}_0(l)\right|^2 R^4\,\Omega_0^4}{\omega_{x0}\,\omega_{y0}}. \end{aligned} \tag{I.25}$$

Cette équation semble être difficile à résoudre dans le cas général. Cependant, un critère de stabilité approximatif, qui peut être vérifié numériquement et qui est toujours proche de la solution à quelques pourcents près, peut être exprimé comme suit. Deux cas apparaissent selon que les nombres d'ondes cohérents (en l'absence de couplage) soient "loins" ou "proches" de résonances de couplage. Ces deux termes sont expliqués à la fin de la section.

1) Q_h "loin" de $Q_v + l$:

Dans ce cas, le résultat du couplage est un partage des taux de croissance uniquement. Il n'y pas de transfert d'amortissement de Landau car les nombres d'ondes cohérents sont trop éloignés pour qu'un partage de leurs dispersions stabilisatrices puisse avoir lieu. L'équation qui doit être résolue pour obtenir le critère de stabilité peut être approximée par l'Eq. (I.25) avec $\Delta\omega_{x,y} = 0$. L'équation ainsi obtenue est la même que l'Eq. (I.14) avec $\delta\omega_{x,y} = 0$. Par analogie avec le cas Lorentzien, la condition nécessaire de stabilité est (cf. Eq. (I.20))

$$V_x + V_y \le 0. \tag{I.26}$$

Si l'Eq. (I.26) est vérifiée alors il est possible de stabiliser le faisceau dans les deux plans et le critère de stabilité est donné par l'Eq. (I.21) avec $\delta\omega_{x,y} = 0$.

2) Q_h "proche" de $Q_v + l$:

Dans ce cas, en plus du partage des taux de croissance, un transfert de l'amortissement de Landau a lieu. L'équation (I.25) est alors approximée par

$$\left\{ \omega_c - \omega_{x0} - \frac{\Delta\omega_x^2 + 4U_x^2}{4U_x} - j\left[\mathrm{Re}\left(\sqrt{\Delta\omega_x^2 - 4U_x^2}\right) - 2V_x\right]\right\} \times$$
$$\left\{ \omega_c - \omega_{y0} - l\,\Omega_0 - \frac{\Delta\omega_y^2 + 4U_y^2}{4U_y} - j\left[\mathrm{Re}\left(\sqrt{\Delta\omega_y^2 - 4U_y^2}\right) - 2V_y\right]\right\} = \frac{\left|\underline{\hat{K}}_0(l)\right|^2 R^4\,\Omega_0^4}{\omega_{x0}\,\omega_{y0}}, \tag{I.27}$$

où $\mathrm{Re}(\ )$ représente la partie réelle, ce qui implique que la racine carrée doit être omise si l'argument sous la racine est négatif. La condition nécessaire de stabilité est donnée par

$$\mathrm{Re}\left(\sqrt{\Delta\omega_x^2 - 4U_x^2} + \sqrt{\Delta\omega_y^2 - 4U_y^2}\ \right) \ge 2\left(V_x + V_y\right). \tag{I.28}$$

Si l'Eq. (I.28) est vérifiée alors il est possible de stabiliser le faisceau dans les deux plans et une condition similaire à l'Eq. (I.21) pour les valeurs stabilisatrices du coefficient de couplage peut être approximée par

$$\left|\underline{\hat{K}}_0(l)\right| \approx \frac{\left\{-Q_{x0}\,Q_{y0}\left[\mathrm{Re}\left(\sqrt{\Delta\omega_x^2 - 4U_x^2}\ \right) - 2V_x\right]\left[\mathrm{Re}\left(\sqrt{\Delta\omega_y^2 - 4U_y^2}\ \right) - 2V_y\right]\right\}^{1/2}}{R^2\,\Omega_0}. \tag{I.29}$$

L'équation (I.28) généralise ainsi les conditions de stabilité uni-dimensionnelles qui s'écrivent

$$\mathrm{Re}\left(\sqrt{\Delta\omega_x^2 - 4U_x^2}\right) \ge 2V_x, \qquad \mathrm{Re}\left(\sqrt{\Delta\omega_y^2 - 4U_y^2}\right) \ge 2V_y, \tag{I.30}$$

ou de manière équivalente (sous la forme plus familière, pour $V_{x,y} > 0$)

$$\Delta\omega_x \ge 2\left|U_x - jV_x\right|, \qquad \Delta\omega_y \ge 2\left|U_y - jV_y\right|. \tag{I.31}$$

Le résultat (Eq. (I.28)) révèle les caractéristiques mentionnées précédemment, i.e. que la partie imaginaire (U) de l'impédance de couplage du plan instable peut être "compensée" par couplage. Les dispersions de fréquences sont réparties entre les deux plans et une dispersion importante dans un plan devient effective aussi dans l'autre plan qui, sans couplage, disposait d'une faible dispersion.

Revenons aux termes "loin" et "proche" de résonances de couplage utilisés ci-dessus. Guidé par les résultats de solutions numériques de l'Eq. (I.25), on peut conclure que la stabilité est obtenue pour une gamme de valeurs de couplage proches de la valeur donnée par l'Eq. (I.29) et que la séparation des nombres d'ondes $\left| Q_h - Q_v - l \right|$ doit être inférieure à l'ordre de grandeur de $\left(\Delta\omega_x + \Delta\omega_y \right) / \Omega_0$ (ce qui semble être très petit) pour qu'un transfert de l'amortissement de Landau puisse avoir lieu.

I.3 Extension aux faisceaux groupés

I.3.1 Equations du mouvement

Dans le cas de faisceaux groupés rigides,[40] l'équation du mouvement bétatronique de la particule *i* du paquet *b*, e.g. dans le plan horizontal et en présence de champs de sillage et de couplage linéaire entre les plans transversaux, est[38]

$$m_0 \gamma \left(\frac{d^2 x_i}{d t^2} + \omega_{x,i}^2 \, x_i \right) = U_{1x} \left(\sum \frac{dP_{x,r}}{d\vartheta} \right)_b + \frac{W_x}{2\pi \sqrt{\Omega_0}} \sum_r x_r \, G\left(\vartheta_r - \vartheta_i, Q_{x,r} \right) + m_0 \gamma \, \underline{K}_i \, R_i^2 \, \Omega_i^2 \, y_i \, . \tag{I.32}$$

Ici, U_{1x} et W_x sont des coefficients réels proportionnels aux coefficients de dispersion U_x et V_x respectivement, et $\left(\sum dP_{x,r} / d\vartheta \right)_b$ est la somme des moments dipolaires horizontaux par unité d'angle azimuthal ϑ de toutes les particules du paquet *b*. La fonction G prend en compte la contribution de la particule *r* au champ de sillage horizontal à la place ϑ_i et au temps t de tous ses tours précédents. La seconde sommation dans l'Eq. (I.32) doit être effectuée sur toutes les particules du faisceau. Une formule similaire est obtenue pour le plan vertical en échangeant les rôles des variables x et y dans l'Eq. (I.32).

Dans le cas de faisceaux groupés avec des modes "head-tail",[43,44] l'équation du mouvement bétatronique de la particule *i* d'un paquet unique, e.g. dans le plan horizontal et en présence de champs de sillage et de couplage linéaire entre les plans transversaux, est[38]

$$\frac{d^2 x_i}{d t^2} + \left[\omega_{x,i} + \omega_{x0} \left(1 - \frac{\xi_x}{\eta} \right) \frac{d \tau_i}{d t} \right]^2 x_i = \sum_r x_r \left(t - \tau_r + \tau_i \right) W_x \left(\tau_r - \tau_i \right) + \underline{K}_i \, R_i^2 \, \Omega_i^2 \, y_i \, . \tag{I.33}$$

Ici, $\xi_x = \left(d Q_{0x,i} / Q_{0x,i} \right) / \left(dp_i / p_i \right)$ est la chromaticité horizontale et $\eta = \gamma_{tr}^{-2} - \gamma^{-2} = -\left(d\Omega_i / \Omega_i \right) / \left(dp_i / p_i \right)$ le facteur de dispersion des fréquences de révolution. Le temps d'arrivée de la particule *i* à une certaine position azimuthale mesuré par rapport au temps d'arrivée de la particule synchrone du paquet est τ_i, et $x_r \left(t - \tau_r + \tau_i \right) W_x \left(\tau_r - \tau_i \right)$ représente la force horizontale du champ de sillage exercée

sur la particule *i* (divisée par sa masse) due à la particule *r*. Une formule similaire est obtenue pour le plan vertical en échangeant les rôles des variables x et y dans l'Eq. (I.33).

I.3.2 Critère de stabilité généralisé

Il a été montré dans les Réfs. 38 et 39 que la relation de dispersion bi-dimensionnelle pour des faisceaux dégroupés et groupés (avec les deux champs de sillage particuliers considérés ci-dessus) est la même, en introduisant des coefficients de dispersion "équivalents" U_{eq} et V_{eq}, qui représentent le déplacement réel de la fréquence bétatronique et le taux de croissance respectivement, pour un mode donné, et en l'absence de couplage et d'amortissement de Landau. Ce n'est peut être pas surprenant puisque dans les trois cas (Eqs. (I.1), (I.32) et (I.33)), c'est plus ou moins la même équation différentielle qui doit être résolue.

Dans le cas de faisceaux dégroupés, U_{eq} et V_{eq} sont donnés par les coefficients U, V introduits par Laslett, Neil et Sessler (cf. Eq. (I.8)). Dans le cas de faisceaux groupés, U_{eq} et V_{eq} peuvent être déduits de la théorie uni-dimensionnelle des instabilités transversales de faisceaux groupés. Celle-ci a été décrite sous sa forme la plus générale par Sacherer, qui a combiné et étendu les résultats obtenus pour des interactions à courte et longue distances.[18,45] Les résultats de l'amortissement de Landau couplé des instabilités cohérentes transversales de faisceaux groupés (dues à des impédances de couplage transversales $Z_{x,y}$) peuvent être résumés en utilisant la formule générale de Sacherer pour les modes dipolaires[18]

$$\Delta\omega_{c,m}^{x,y} = \left(|m|+1\right)^{-1} \frac{j e \beta I_b}{2 m_0 \gamma Q_{x0,y0} \Omega_0 L} \frac{\sum_{k=-\infty}^{k=+\infty} Z_{x,y}\left(\omega_k^{x,y}\right) h_m\left(\omega_k^{x,y} - \omega_{\xi_{x,y}}\right)}{\sum_{k=-\infty}^{k=+\infty} h_m\left(\omega_k^{x,y} - \omega_{\xi_{x,y}}\right)}, \quad \text{(I.34)}$$

avec

$$\omega_k^{x,y} = \left(k + Q_{x0,y0}\right)\Omega_0 + m\omega_s . \quad \text{(I.35)}$$

Dans l'Eq. (I.34), $-\infty \le k \le +\infty$ pour un paquet unique ou pour plusieurs paquets oscillants de manière indépendante et $k = n_{x,y} + k'M$ avec $-\infty \le k' \le +\infty$ pour des oscillations couplées de M paquets. Ici, $m = ...,-1,0,1,...$ est le mode "head-tail", $n_{x,y} = 0,1,...,M-1$ représentent les modes couplés reliés par $n_x = n_y - l$, I_b est le courant dans un paquet, L est la longueur d'un paquet (en mètres) et ω_s est la fréquence angulaire synchrotronique. Les fonctions $h_m\left(\omega - \omega_{\xi_{x,y}}\right)$, centrées aux fréquences angulaires chromatiques $\omega_{\xi_{x,y}} = \left(\xi_{x,y}/\eta\right) Q_{x0,y0}\,\Omega_0$, décrivent les spectres transversaux de mode m d'un bunch, et sont données par

$$h_m\left(\omega - \omega_{\xi_{x,y}}\right) = \left(|m|+1\right)^2 \frac{1 + (-1)^{|m|}\cos\left[\left(\omega - \omega_{\xi_{x,y}}\right)\tau_b\right]}{\left[\left(\omega\tau_b/\pi\right)^2 - \left(|m|+1\right)^2\right]^2}. \quad \text{(I.36)}$$

Ici, τ_b est la longueur totale (en seconde) d'un paquet. Les relations entre les coefficients " équivalents" et les déplacements en fréquences (pour le mode m) sont

$$U^m_{\mathrm{eq}x,y} = \mathrm{Re}\left(\Delta\omega^{x,y}_{c,m}\right), \qquad V^m_{\mathrm{eq}x,y} = -\mathrm{Im}\left(\Delta\omega^{x,y}_{c,m}\right), \tag{I.37}$$

où $\mathrm{Im}(\ )$ représente la partie imaginaire. Par conséquent, dans le cas de faisceaux groupés, ces coefficients sont des constantes réelles (en omettant les non-linéarités de charges d'espace) qui caractérisent à la fois l'accélérateur et la dynamique du faisceau.

Avec quelques hypothèses simplificatrices, ces résultats ont été vérifiés dans la Réf. 52 en utilisant l'équation de Vlasov. Si les distributions des amplitudes bétatroniques incohérentes (supposées non corrélées) sont décrites par les fonctions de répartition $f_{x0}(\hat{x}_i)$ and $f_{y0}(\hat{y}_i)$, normalisées par

$$\int_{\hat{x}_i=0}^{\hat{x}_i=+\infty} f_{x0}(\hat{x}_i)\,\hat{x}_i\,d\hat{x}_i = \frac{1}{2\pi}, \qquad \int_{\hat{y}_i=0}^{\hat{y}_i=+\infty} f_{y0}(\hat{y}_i)\,\hat{y}_i\,d\hat{y}_i = \frac{1}{2\pi}, \tag{I.38}$$

la relation de dispersion bi-dimensionnelle s'écrit

$$\begin{aligned}
&\left[\left(\int_{\hat{x}_i=0}^{\hat{x}_i=+\infty}\int_{\hat{y}_i=0}^{\hat{y}_i=+\infty} \frac{-2\pi^2\,\dfrac{df_{x0}(\hat{x}_i)}{d\hat{x}_i}\,\hat{x}_i^2\,f_{y0}(\hat{y}_i)\,\hat{y}_i}{\omega_c-\omega_{x,i}(\hat{x}_i,\hat{y}_i)-m\omega_s}\,d\hat{x}_i\,d\hat{y}_i\right)^{-1} - U^m_{\mathrm{eq}x} + j\,V^m_{\mathrm{eq}x}\right]\times \\
&\left[\left(\int_{\hat{x}_i=0}^{\hat{x}_i=+\infty}\int_{\hat{y}_i=0}^{\hat{y}_i=+\infty} \frac{-2\pi^2\,\dfrac{df_{y0}(\hat{y}_i)}{d\hat{y}_i}\,\hat{y}_i^2\,f_{x0}(\hat{x}_i)\,\hat{x}_i}{\omega_c-\omega_{y,i}(\hat{x}_i,\hat{y}_i)-l\Omega_0-m\omega_s}\,d\hat{x}_i\,d\hat{y}_i\right)^{-1} - U^m_{\mathrm{eq}y} + j\,V^m_{\mathrm{eq}y}\right] \\
&= \frac{\left|\underline{\hat{K}}_0(l)\right|^2 R^4\,\Omega_0^4}{4\,\omega_{x0}\,\omega_{y0}}.
\end{aligned} \tag{I.39}$$

En utilisant U_{eq} et V_{eq} dans le cas de faisceaux groupés, à la place de U et V pour des faisceaux dégroupés, la même équation de dispersion bi-dimensionnelle est obtenue (cf. Eq. (I.7) ou (I.11)) et les résultats précédents restent valables (cf. Eqs. (I.20), (I.21), (I.26) et (I.28)), en approximant la dispersion des fréquences bétatroniques dans chaque plan par la racine carrée de la somme quadratique des dispersions introduites par les amplitudes bétatroniques incohérentes.

I.3.3 Partage des dispersions de fréquences et des chromaticités

Dans le cas d'instabilités "head-tail", les déplacements des fréquences bétatroniques transversales, pour le mode m et en l'absence de couplage et d'amortissement de Landau, sont donnés par Sands pour le modèle idéal où le champ de sillage d'une particule est zéro devant et constant derrière la particule[43] ($W_{x,y}(\tau_r-\tau_i)\equiv S_{x,y}$ (const. positive) pour $\tau_r>\tau_i$ dans l'Eq. (I.33) et l'équation similaire pour le plan vertical). On obtient alors

$$U^0_{\mathrm{eq}x,y} = -\frac{N_b\, S_{x,y}}{4\,\omega_{x0,y0}}, \qquad U^m_{\mathrm{eq}x,y} = 0 \quad \text{for} \quad m \neq 0, \qquad V^m_{\mathrm{eq}x,y} = -\,W^m_{x,y}\,\xi_{x,y}, \quad \text{(I.40)}$$

avec

$$W^m_{x,y} = -\frac{2\,N_b\, S_{x,y}\,\hat{\tau}_0}{\pi^2\,\eta}\left(4m^2-1\right)^{-1}. \qquad \text{(I.41)}$$

Ici, N_b est le nombre de particules du paquet et $\hat{\tau}_0$ est l'amplitude (en temps) des oscillations synchrotroniques dans le modèle "hollow-bunch" où $\hat{\tau}_i = \hat{\tau}_0$.

Pour voir clairement l'effet du couplage sur l'amortissement de Landau et la chromaticité, il est intéressant d'examiner les critères de stabilité pour un couplage nul et pour un couplage optimum. Dans ce qui suit, seul le mode le plus dangereux $m = 0$ (au dessus de la transition[c]) est considéré. En l'absence de couplage, les critères de stabilité Lorentziens pour les plans horizontal et vertical respectivement, sont (cf. Eqs. (I.19) et (I.40))

$$\delta\omega_x + W^0_x\,\xi_x \geq 0, \qquad \delta\omega_y + W^0_y\,\xi_y \geq 0. \qquad \text{(I.42)}$$

En l'absence d'amortissement de Landau, la condition de Sands, $\xi_{x,y} \geq 0$ pour la stabilité du mode "head-tail" $m = 0$, est retrouvée (au dessus de la transition, $\eta > 0$ et donc $W^0_{x,y} > 0$). Pour un couplage optimum, les deux critères se réduisent en un seul (cf. Eq. (I.20))

$$\delta\omega_x + \delta\omega_y + W^0_x\,\xi_x + W^0_y\,\xi_y \geq 0. \qquad \text{(I.43)}$$

L'équation (I.43) montre clairement l'effet bénéfique du couplage sur la compensation de la chromaticité et l'amortissement de Landau. En l'absence d'une dispersion de fréquences, le résultat obtenu par Talman,[47] $W^0_x\,\xi_x + W^0_y\,\xi_y \geq 0$, est retrouvé. Une chromaticité négative peut être maintenue dans un plan à condition que l'autre chromaticité soit suffisamment augmentée pour compenser. En présence d'amortissement de Landau, un critère moins restrictif est obtenu. Le même genre de résultats est obtenu avec des spectres elliptiques. En l'absence de couplage, les critères de stabilité pour les plans horizontal et vertical respectivement sont (cf. Eqs. (I.30))

$$\mathrm{Re}\left[\sqrt{\Delta\omega_x^2 - \left(2U^0_{\mathrm{eq}x}\right)^2}\,\right] + 2\,W^0_x\,\xi_x \geq 0, \quad \mathrm{Re}\left[\sqrt{\Delta\omega_y^2 - \left(2U^0_{\mathrm{eq}y}\right)^2}\,\right] + 2\,W^0_y\,\xi_y \geq 0. \quad \text{(I.44)}$$

Pour un couplage optimum, ces deux critères se réduisent en un seul (cf. Eq. (I.28))

$$\mathrm{Re}\left[\sqrt{\Delta\omega_x^2 - \left(2U^0_{\mathrm{eq}x}\right)^2} + \sqrt{\Delta\omega_y^2 - \left(2U^0_{\mathrm{eq}y}\right)^2}\,\right] + 2\left(W^0_x\,\xi_x + W^0_y\,\xi_y\right) \geq 0. \qquad \text{(I.45)}$$

En l'absence de dispersion de fréquences, le résultat de Talman est retrouvé.

[c] Les chromaticités naturelles sont (en général) négatives. Ainsi, pour éliminer le mode "head-tail" le plus dangereux $m = 0$, un changement de signe de la chromaticité n'est nécessaire qu'au dessus de l'énergie de transition. Les modes "head-tail" plus élevés, avec des facteurs de forme et des valeurs de champs de sillage plus petits, peuvent être stabilisés par amortissement de Landau.

Le champ de sillage correspondant à la paroi resistive donne des résultats similaires avec les coefficients de dispersion “équivalents” donnés par les Eqs. (26) et (27) de la Réf. 44.

I.3.4 Partage de l’amortissement par “feedbacks”

Un système électronique de “feedback” est souvent utilisé pour stabiliser un faisceau dans un plan. Dans la théorie de l’amortissement de Landau couplé, l’effet stabilisateur d’un système de “feedback” peut être introduit dans le coefficient général V_{eq} (cf. Section I.3.2). L’effet d’amortissement dans un plan peut donc aussi être transféré dans l’autre plan en utilisant le couplage.

I.4 Mesure du couplage linéaire du PS

L’analyse exacte du couplage linéaire a été décrite par Guignard.[56,57] Le couplage est traité comme une perturbation des oscillations transversales d’une particule et les équations exactes du mouvement perturbé sont obtenues en utilisant le formalisme Hamiltonien.

Dans cette section, les résultats principaux de la théorie sont donnés et utilisés pour mesurer le couplage linéaire du PS. Le résultat des mesures est la relation entre le courant dans les quadrupôles tournés I_{skew} et le coefficent de couplage linéaire $\left|C_G\right|$ (ou le module de l’harmonique zéro du gradient normalisé des quadrupôles tournés $\left|\hat{\underline{K}}_0(0)\right|$ (cf. Eq. (I.5)), écrit $\left|\underline{K}_0\right|$ par la suite pour simplifier).[59]

I.4.1 Résultat de la théorie générale du couplage linéaire dans le cas du PS

Dans le PS, un champ magnétique tourné existe en raison des inclinaisons aléatoires des unités d’aimants, et pour cette raison une famille de 40 quadrupôles tournés a été inclue dans la maille. De plus, il n’y pas de champ axial et la résonance de couplage est $Q_h - Q_v = 0$.

En présence de couplage linéaire entre les plans transversaux, chaque mouvement bétatronique peut être exprimé par une somme de deux modes normaux d’oscillation, dont la différence des nombres d’ondes est donnée par

$$Q_+ - Q_- = \sqrt{\left(Q_h - Q_v\right)^2 + \left|C_G\right|^2}\,. \tag{I.46}$$

Ici, C_G est le coefficient de couplage linéaire de Guignard, défini par

$$C_G = \frac{R}{2\pi}\int_0^{2\pi} \beta_{0x,i}^{1/2}(\vartheta)\,\beta_{0y,i}^{1/2}(\vartheta)\,\underline{K}_i(\vartheta)\,e^{j\left[\left(\mu_{0x,i}-Q_h\vartheta\right)-\left(\mu_{0y,i}-Q_v\vartheta\right)\right]}\,d\vartheta, \tag{I.47}$$

où $\mu_{0x,i}$ et $\mu_{0y,i}$ représentent les fonctions de phase. On déduit de l’Eq. (I.46) que sur la résonance de couplage $Q_h = Q_v$, la valeur absolue de la différence des deux nombres d’ondes normaux $\left|Q_+ - Q_-\right|$ est égal à $\left|C_G\right|$, ce qui permet de mesurer ce dernier.

I.4.2 Mesures de couplage par analyse FFT des fréquences normales

Le couplage a été mesuré à 1 GeV, sur un long palier de 1.2 s, avec un faisceau groupé de basse intensité ($M = 20$ paquets et $I_{beam} \approx 250 \times 10^{10}$ protons). L'approche adoptée est la suivante: pour différents courants dans les quadrupôles tournés, la valeur de Q_h est augmentée et celle de Q_v est diminuée au voisinage de la résonance de couplage, et les deux fréquences normales sont mesurées en utilisant un "kicker" (élément provoquant une déflection rapide du faisceau) vertical, une "pick-up" (moniteur de position) verticale et un analyseur FFT (Fast Fourier Transform).[58] La "pick-up" verticale est utilisée car elle est plus sensible que la "pick-up" horizontale en raison de la forme elliptique de la chambre à vide, et elle voit les fréquences des deux modes.

Le point de fonctionnement est donc programmé de telle sorte que Q_h augmente linéairement de 6.10 à 6.40 en 300 ms, alors que Q_v décroit linéairement de 6.40 à 6.10. Le faisceau est "kické" toutes les 5 ms pendant les 300 ms et une FFT verticale est effectuée toutes les 4.096 ms pendant 262.144 ms (64 spectres). Ceci parce qu'une analyse spectrale entre 0 et 500 khz (la fréquence de révolution étant $f_0 = 417$ khz) dans un temps $T_m \leq 5$ ms est requise. En effet, en choisissant la fréquence d'échantillonnage $F_s = 1\,\text{Mhz}$ (en utilisant le théorème de Shannon), les relations entre les différents paramètres imposent le nombre de canaux $N_{ch} = 2048$, la fréquence de résolution $BW = 0.2441\,\text{khz}$, la durée du signal $T_m = 4.096\,\text{ms}$ et le nombre de spectres consécutifs $N_s = 64$.[58] Ces spectres sont alors affichés en "mountain range", i.e. affichés successivement les uns au dessus des autres (Figure 13). Pour chaque spectre, deux "lignes" spectrales apparaissent aux fréquences d'oscillation des deux modes normaux. La distance minimum entre les deux fréquences normales (obtenue pour $Q_h = Q_v$) est égale à $|C_G| \times f_0$.

Le graphe des nombres d'ondes couplés en fonction de la distance à la

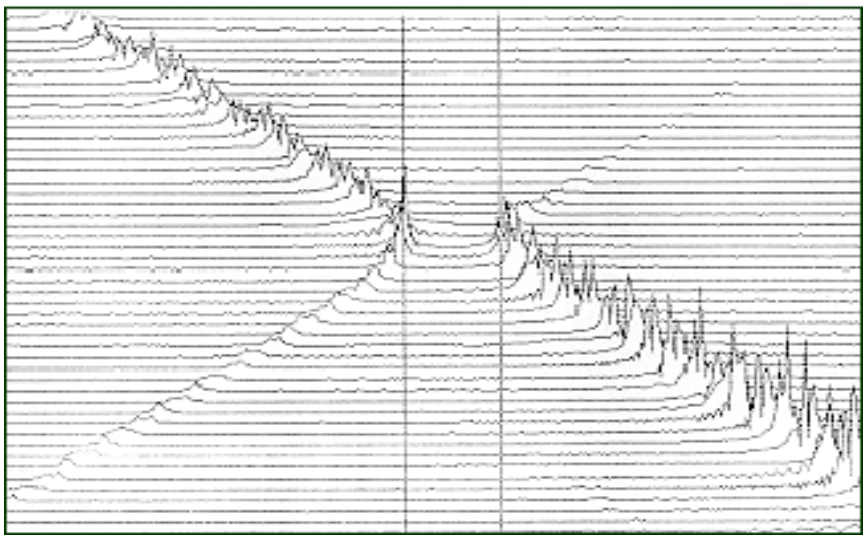

résonance de couplage est reprenté sur la Figure 13, dans le cas du couplage "naturel".

FIGURE 13 Affichage en "Mountain range" de l'analyse FFT du couplage "naturel" ($I_{skew} = 0\,\text{A}$). L'axe horizontal et vertical représentent la fréquence et le temps respectivement.

La relation entre $|C_G|$ et $|\underline{K}_0|$ dans l'approximation douce est obtenue à l'aide de l'Eq. (I.47),

$$|\underline{K}_0| = \frac{Q_0}{R^2}|C_G|. \tag{I.48}$$

Ici, $Q_0 = (Q_+ + Q_-)/2 \approx 6.27$ est la valeur commune des nombres d'ondes transversaux non couplés déduite en faisant la moyenne des nombres d'ondes normaux.

I.4.3 Résultats et conclusion

Les résultats des mesures sont regroupés dans le Tableau 1. Pour différents courants dans les quadrupôles tournés (de -1.5 A à 1.5 A), on y trouve la valeur absolue de la différence des fréquences normales $|\Delta f|$, les modules du coefficient de couplage linéaire $|C_G|$ et du gradient des quadrupôles tournés $|\underline{K}_0|$ dans l'approximation douce.

I_{skew} [A]	$\|\Delta f\|$ [kHz]	$\|C_G\|$	$\|\underline{K}_0\|$ [m^{-2}]
-1.5	50	0.120	7.5E-05
-1.25	44	0.106	6.6E-05
-1	37	0.089	5.6E-05
-0.75	30	0.072	4.5E-05
-0.5	23	0.055	3.4E-05
-0.25	16	0.038	2.4E-05
0	9	0.022	1.4E-05
0.5	5	0.012	7.5E-06
0.75	11	0.026	1.6E-05
1	19	0.046	2.8E-05
1.25	25	0.060	3.8E-05
1.5	32	0.077	4.8E-05

TABLEAU 1 Valeurs mesurées de $|\Delta f|$, $|C_G|$ et $|\underline{K}_0|$ pour différents courants dans les quadrupôles tournés.

Le graphe de $|\underline{K}_0|$ en fonction de I_{skew} est reprenté sur la Figure 14.

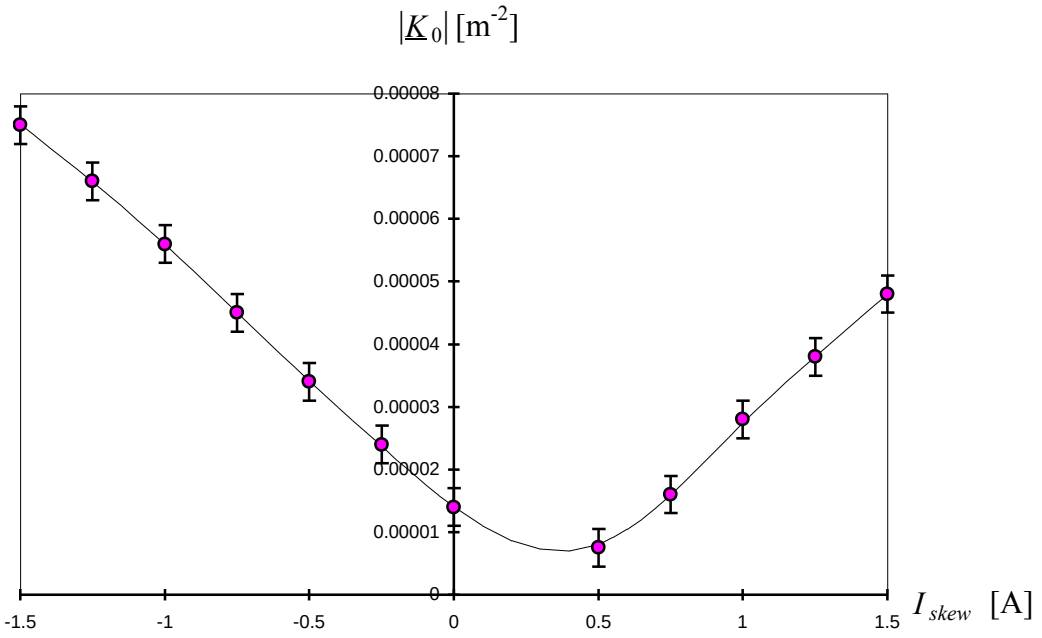

FIGURE 14 Module du gradient normalisé des quadrupôles tournés (dans l'approximation douce) en fonction du courant dans les quadrupôles tournés.

La barre d'erreur des valeurs mesurées dépend de deux erreurs différentes. La première est due à la résolution en fréquence $BW = 0.2441\,\text{khz}$ qui découle du fait que le signal est observé uniquement pendant la durée $T_m = 1/BW = 4.096\,\text{ms}$. La seconde est une erreur de lecture : les dispersions des nombres d'ondes introduites par les chromaticités naturelles transversales ($\zeta_x \approx -1$ et $\zeta_y \approx -1.5$) élargissent les raies, rendant ainsi la lecture plus difficile. L'erreur de mesure d'une fréquence est estimée à $\pm 1\,\text{khz}$ et par conséquent, l'erreur sur Δf est de $\pm 2\,\text{khz}$. La précision sur $|C_G|$ est alors de $\pm 2\,\text{khz}/f_0 = \pm 4.8\times10^{-3}$ et la précision sur $|\underline{K}_0|$ est de $\pm 3\times10^{-6}$. Une meilleure précision pourrait être obtenue en annulant les chromaticités.

Le minimum de couplage linéaire dans le PS ne peut pas être déterminé exactement en raison des dispersions des nombres d'ondes mais la valeur du courant dans les quadrupôles tournés correspondant à ce minimum de couplage peut être obtenue en lissant les données mesurées discrètes. Le résultat est $I_{skew} \approx 0.33\,\text{A}$ ($\pm 0.1\,\text{A}$, en prenant en compte la barre d'erreur).

I.5 Mesures d'amortissement de Landau couplé de l'instabilité résistive cohérente du PS

Des mesures ont été effectuées pour vérifier la théorie de l'amortissement de Landau couplé. Une famille de 8 octupoles, situés à large fonction bétatronique verticale, est utilisée au PS pour supprimer les instabilités cohérentes transversales. Cependant, l'effet stabilisateur principal est produit dans le plan vertical, alors que les instabilités apparaissent toujours dans le plan horizontal. L'idée est donc de transférer de l'amortissement de Landau du plan vertical stable au plan horizontal instable. Cette section rapporte les mesures faites sur l'amortissement de l'instabilité résistive cohérente horizontale d'un faisceau groupé de protons à 1 GeV au PS ($M = 20$ paquets et $I_{beam} \approx 1.5\times10^{13}$ protons) en utilisant les octupoles, les quadrupôles tournés et la

séparation des nombres d'ondes.[60] Les paramètres du faisceau et du PS pendant l'expérience se trouvent en annexe de cette section.

I.5.1 Instabilité résistive cohérente horizontale du PS

D'après la formule de Sacherer, une instabilité cohérente apparaît si, par l'interaction entre le spectre du faisceau et le spectre de l'impédance de couplage, la partie imaginaire du déplacement de la fréquence cohérente est négative.

Les spectres transversaux de mode $|m|$ d'un paquet sont donnés par $h_m(\omega)$ (cf. Eq. (I.36)). Le graphe du spectre horizontal d'un paquet est reprenté sur la Figure 15 pour les modes $|m| = 0$ à 5. Le même type de spectre existe pour le mouvement vertical, avec la chromaticité verticale naturelle $\xi_y \approx -1.5$.

Les impédances de couplage transversales $Z_{x,y}(\omega)$ du PS sont approximées par la somme des impédances de paroi résistive et larges bandes[16,61,62]

$$Z_c^{RW}(\omega) = [\,Sgn(\omega) + j\,]\,\frac{R}{b_w^3}\sqrt{\frac{2\rho_w}{\varepsilon_0|\omega|}},\quad Z_{x,y}^{BB}(\omega) = \frac{\omega_r}{\omega}R_{x,y} \Big/ \left[\,1 - jQ\left(\frac{\omega_r}{\omega} - \frac{\omega}{\omega_r}\right)\right]. \quad \text{(I.49)}$$

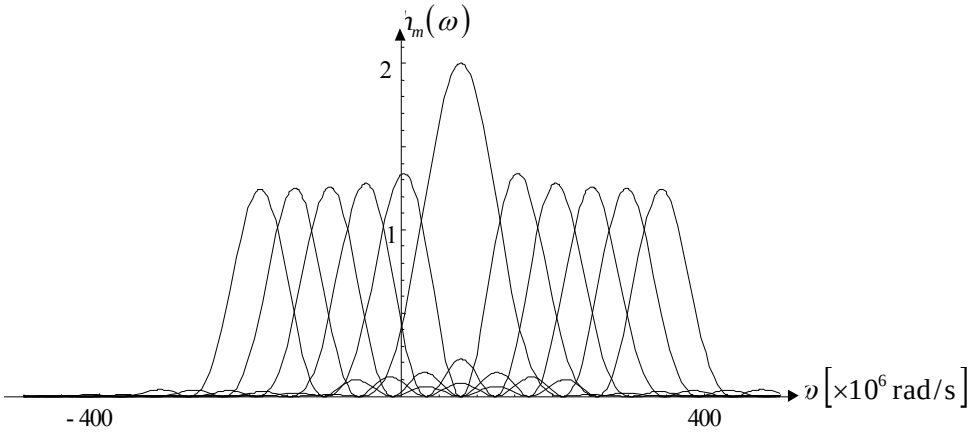

FIGURE 15 Enveloppes du spectre horizontal d'un paquet pour les modes $|m| = 0$ à 5, et pour la chromaticité horizontale naturelle ($\xi_x \approx -1$).

Dans L'équation (I.49), $Z_c^{RW}(\omega)$ représente l'impédance de couplage de paroi resistive pour une chambre circulaire de rayon b_w. Pour une chambre à vide elliptique, les impédances de paroi résistive transversales peuvent être déterminées dans la limite ultra-relativiste.[63] Dans le cas du PS ($a_w = 2\,b_w$), on trouve

$$Z_x^{RW}(\omega) \approx Z_c^{RW}(\omega)\times 0.45, \qquad Z_y^{RW}(\omega) \approx Z_c^{RW}(\omega)\times 0.85. \quad \text{(I.50)}$$

Le graphe de la partie réelle de l'impédance circulaire de paroi resistive est représenté sur la Figure 16.

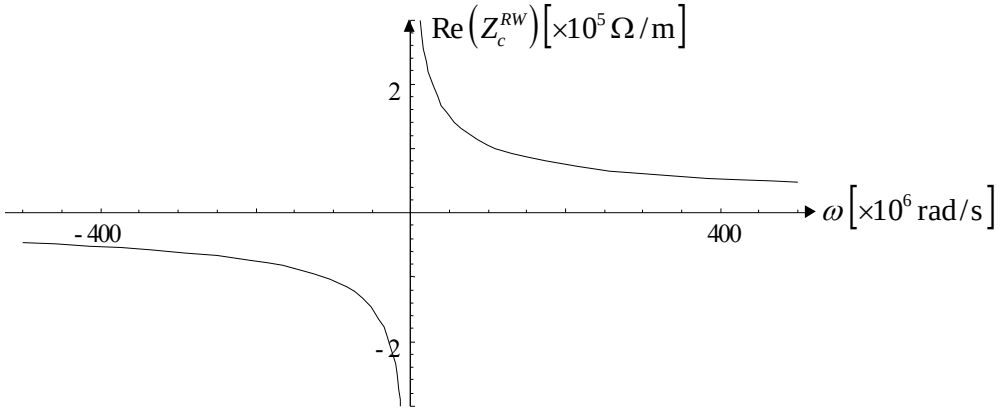

FIGURE 16 Partie réelle de l'impédance circulaire de paroi résistive.

En ce qui concerne l'amortissement de Landau, les octupoles amortissent les instabilités de paquet unique ou de paquets couplés si ces derniers produisent une dispersion de fréquences à l'intérieur des paquets suffisante pour empêcher le mouvement cohérent de se développer. Les dispersions de fréquences bétatroniques transversales sont données analytiquement par[23]

$$\Delta\omega_{\mathrm{HWHH}}^{x,y} \approx \frac{3\,f_0\,N_{\mathrm{oct}}}{8}\left[\left(\beta_{\mathrm{oct}x,y}^2\,\varepsilon_{x,y}^{\mathrm{rms}}\right)^2+\left(2\,\beta_{\mathrm{oct}x}\,\beta_{\mathrm{oct}y}\,\varepsilon_{y,x}^{\mathrm{rms}}\right)^2\right]^{1/2}\int_0^{l_{mag}} K_{\mathrm{oct}}\,dl\,, \quad \text{(I.51)}$$

en utilisant l'approximation $\Delta\omega_{\mathrm{HWHH}}^{x,y} \approx \Delta\omega_{\mathrm{rms}}^{x,y}$, où $\Delta\omega_{\mathrm{HWHH}}^{x,y}$ représentent les demi-largeurs à mi-hauteur des spectres transversaux. Le critère de stabilité uni-dimensionnel simplifié, déduit de l'analyse de la relation de dispersion en considérant une distribution de fréquences bétatroniques elliptique, est donné, sans tenir compte des non-linéarités de charges d'espace, par

$$\Delta\omega_{\mathrm{HWHH}}^{x,y} \geq \sqrt{3}\,\left|\Delta\omega_{c,m}^{x,y}\right|. \quad \text{(I.52)}$$

I.5.1.1 Prédictions théoriques

La formule de Sacherer prédit des instabilités transversales de paquets couplés. Les premières raies bétatroniques transversales instables sont telles que $n_{x,y}+k'M$ correspondent aux premiers entiers inférieurs à $-Q_{x0,y0}$. Durant l'expérience, le point de fonctionnement était donné par $Q_h = 6.14$ et $Q_v = 6.22$, ce qui correspond aux modes couplés $n_{x,y}$ =13. Les résultats numériques obtenus sont regroupés dans le Tableau 2.

Mode "head-tail" *m*	0	1	2	3	4	5
$V_{\mathrm{eq}x}^{m}$ [s^{-1}]	-104	121	35	0	2	-3
$V_{\mathrm{eq}y}^{m}$ [s^{-1}]	-423	-40	142	18	-13	-11
$U_{\mathrm{eq}x}^{m}$ [rad/s]	-3708	-1945	-1234	-896	-716	-592
$U_{\mathrm{eq}y}^{m}$ [rad/s]	-10491	-5376	-3669	-2650	-2090	-1738

TABLEAU 2 Taux de croissance des instabilités transversales et déplacements réels des fréquences cohérentes pour les modes $m = 0$ à 5.

En conclusion, la théorie basée sur le modèle d'impédance précédent, prédit des instabilités transversales de paquets couplés ($n_{x,y} = 13$) avec le mode "head-tail" le plus critique $m = 1$ pour le plan horizontal et $m = 2$ pour le plan vertical. De plus, la dispersion $\Delta\omega^{x}_{\mathrm{HWHH}} \approx 3400$ rad/s devrait être suffisante pour amortir l'instabilité horizontale $m = 1$.

I.5.1.2 Observations

Pour vérifier la théorie uni-dimensionelle, le courant dans les quadrupôles tournés doit être ajusté au minimum de couplage linéaire entre les plans transversaux, i.e. $I_{skew} \approx 0.33$ A (cf. Section I.4). Dans ces conditions, si le courant dans les octupoles est nul alors une instabilité apparaît.

I.5.1.2.1 Mesure du taux de croissance de l'instabilité et détermination des modes

L'instabilité a été observée uniquement dans le plan horizontal. Les valeurs mesurées du taux de croissance (temps de montée ~ 10 ms) sur la première raie bétatronique instable confirment la validité de la théorie de l'instabilité de paroi resistive (Figure 17(a)).

Le module du mode "head-tail" peut être déterminé en regardant les contorsions d'un paquet sur plusieurs traces superposées. Le nombre de noeuds le long du paquet correspond à $|m|$. On peut donc conclure de la Figure 17(b) que le mode "head-tail" est $|m| = 1$, ce qui est en parfait accord avec la théorie.

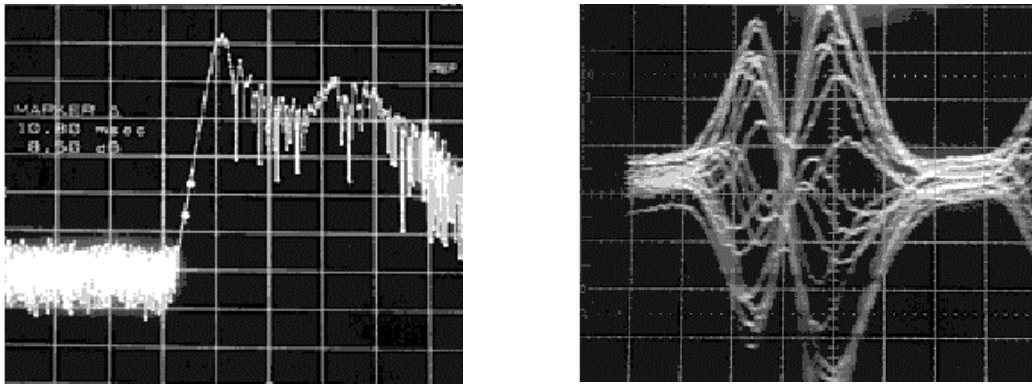

(a) (b)

FIGURE 17 (a) Taux de croissance mesuré de l'instabilité horizontale (analyseur de spectre fonctionnant en temps). Echelle verticale : 10 dB/div. (b) Signal ΔR d'un moniteur de position radiale pendant 20 tours consécutifs. Echelle de temps : 20 ns/div.

Une figure régulière décrivant le mouvement couplé n'a pas été clairement observée. Cependant, l'instabilité était sensible à des inégalités dans les intensités des paquets, ce qui démontre l'existence de mouvements couplés.

I.5.1.2.2 Stabilisation par amortissement de Landau

En jouant sur les octupoles l'instabilité pouvait être amortie. Les relations numériques entre les dispersions de fréquences bétatroniques transversales et le courant dans les octupoles sont données par

$$\Delta\omega^{x}_{\mathrm{HWHH}}\left[\mathrm{rad/s}\right] \approx 320\, I_{oct}\left[\mathrm{A}\right], \qquad \Delta\omega^{y}_{\mathrm{HWHH}}\left[\mathrm{rad/s}\right] \approx 630\, I_{oct}\left[\mathrm{A}\right]. \quad \text{(I.53)}$$

Le courant requis pour la stabilisation (uni-dimensionnelle) était $I_{oct} = 3.5\,\mathrm{A}$, ce qui correspond à la dispersion $\Delta\omega^{x}_{\mathrm{HWHH}} \approx 1100$ rad/s. C'est inférieur d'un facteur 3 aux prévisions du critère de stabilité de l'Eq. (I.52) (sans tenir compte des non-linéarités de charges d'espace).[23]

Remarquons que, pour un courant dans les octupoles donné, la dispersion verticale des nombres d'ondes était approximativement deux fois plus grande que celle du plan horizontal.

I.5.2 Stabilisation par amortissement de Landau couplé

Deux séries de mesure ont été réalisées pour vérifier la théorie bi-dimensionnelle de l'amortissement de Landau.

I.5.2.1 Distance constante des nombres d'ondes

Dans cette première campagne de mesures (avec les mêmes conditions que celles de la Section I.5.1), le point de fonctionnement était fixé et le couplage était modifié en utilisant la famille des quadrupôles tournés. L'effet stabilisateur du couplage sur l'amortissement de Landau a éte étudié pour différents courants dans les octupoles entre 0.5 et 3 A. Les résultats des mesures comparés à la théorie sont regroupés dans le Tableau 3. Pour différents courants dans les octupoles, on y trouve la valeur mesurée du courant stabilisateur dans les quadrupôles tournés, le gradient normalisé correspondant (cf. Section I.4), le gradient normalisé théorique et le rapport entre les deux.

I_{oct} [A]	I_{skew} [A]	$\lvert\underline{K}_0\rvert^{\mathrm{exp}}(\times 10^{-5})$ [m^{-2}]	$\lvert\underline{K}_0\rvert^{\mathrm{theory}}(\times 10^{-5})$ [m^{-2}]	Ratio = $\lvert\underline{K}_0\rvert^{\mathrm{exp}}$ / $\lvert\underline{K}_0\rvert^{\mathrm{theory}}$
0.5	-1.2	6.4	8.8	0.7
1	-1	5.6	5.1	1.1
1.5	-0.8	4.7	4.0	1.2
2	-0.5	3.4	3.3	1.0
2.5	0	1.4	2.9	0.5
3	0.5	0.8	2.6	0.3

TABLEAU 3 Gradients normalisés stabilisateurs théorique et mesuré des quadrupôles tournés.

Le gradient stabilisateur théorique des quadrupôles tournés est donné par (cf. Eq. (I.21))

$$\left|\underline{K}_0\right|^{\mathrm{theory}} = \frac{2\left[Q_{x0}\,Q_{y0}\,V_{\mathrm{eq}x}\left(\Delta\omega^{y}_{\mathrm{HWHH}} - V_{\mathrm{eq}y}\right)\right]^{1/2}}{R^2\,\Omega_0}\times \frac{\left[\left(\Delta\omega^{y}_{\mathrm{HWHH}} - V_{\mathrm{eq}x} - V_{\mathrm{eq}y}\right)^2 + \Omega_0^2\left(Q_h - Q_v\right)^2\right]^{1/2}}{\Delta\omega^{y}_{\mathrm{HWHH}} - V_{\mathrm{eq}x} - V_{\mathrm{eq}y}}, \tag{I.54}$$

où $V_{\mathrm{eq}x,y}$ correspondent aux taux de croissance des instabilités transversales en l'absence de couplage et d'amortissement de Landau (cf. Tableau 2). Ici, les approximations suivantes ont été faites: (i) la dispersion horizontale des nombres d'ondes est approximée par zéro puisque le point de fonctionnement est loin de la résonance de couplage ; (ii) une fonction de répartition Lorentzienne est supposée dans le plan vertical puisque cela semble mieux décrire la "réalité" du PS qu'un spectre elliptique.

Le graphe des gradients stabilisateurs théorique et expérimental des quadrupôles tournés en fonction du courant dans les octupoles est représenté sur la Figure 18.

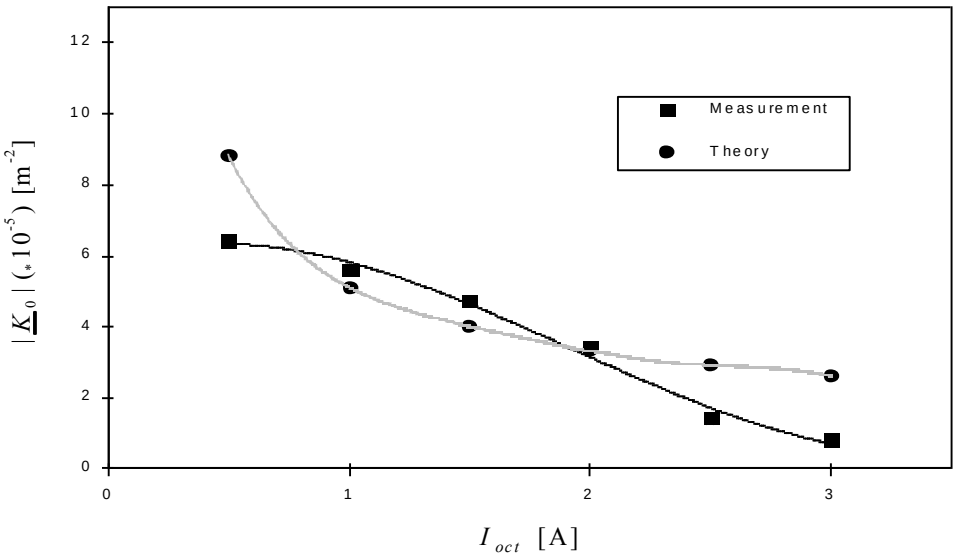

FIGURE 18 Gradients stabilisateurs théorique et mesuré des quadrupôles tournés en fonction du courant dans les octupoles.

I.5.2.2 Force octupolaire constante

Dans cette seconde campagne de mesures, le courant dans les octupoles était fixé et le couplage était modifié en utilisant la séparation des nombres d'ondes. Les conditions étaient légèrement différentes de celles de la Section I.5.1 et le courant dans les octupoles requis pour la stabilisation uni-dimensionnelle était $I_{oct} = 5\,\mathrm{A}$. La valeur du courant dans les octupoles a été fixée arbitrairement à $2\,\mathrm{A}$. De plus, le nombre d'ondes vertical a été fixé à 6.22, et l'instabilité était amortie en rapprochant le nombre d'ondes horizontal. Les résultats des mesures comparés à la théorie sont regroupés dans le Tableau 4. Pour différentes valeurs de courants dans les quadrupôles tournés (avec le gradient correspondant donné en Section I.4), on y trouve la valeur mesurée de la séparation stabilisatrice des nombres d'ondes, la séparation stabilisatrice théorique (cf. Eq. (I.54)) et le rapport entre les deux.

I_{oct} [A]	I_{skew} [A]	$\lvert Q_h\text{-}Q_v\rvert^{exp}$	$\lvert Q_h\text{-}Q_v\rvert^{theory}$	Ratio = $\lvert Q_h\text{-}Q_v\rvert^{exp}$ / $\lvert Q_h\text{-}Q_v\rvert^{theory}$
2	0	0.09	0.03	3.0
2	-0.5	0.10	0.08	1.2
2	-1	0.11	0.13	0.8

TABLEAU 4 Séparations stabilisatrices théorique et mesurée des nombres d'ondes.

Le graphe des séparations stabilisatrices théorique et expérimentale des nombres d'ondes en fonction du courant dans les quadrupôles tournés est représenté sur la Figure 19.

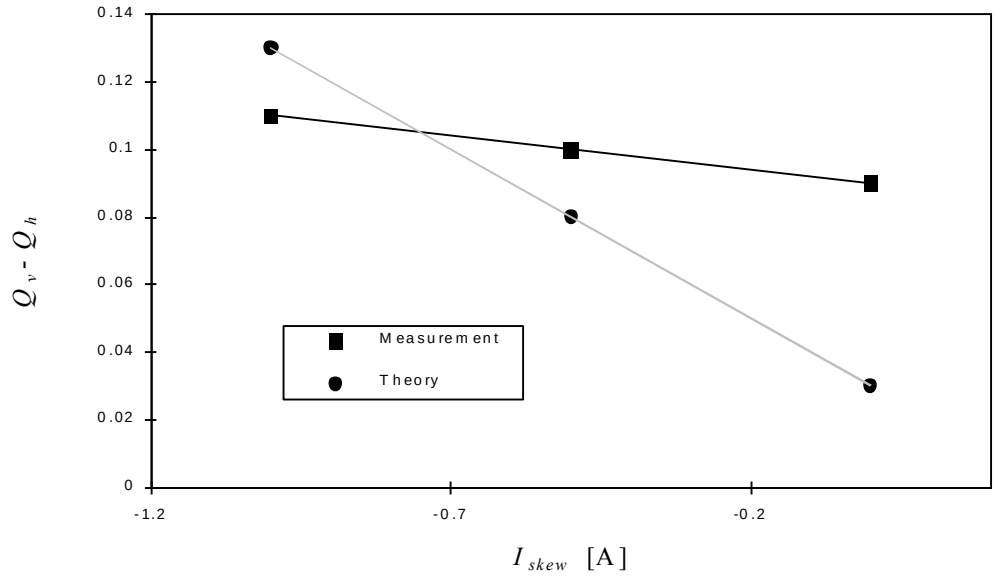

FIGURE 19 Séparations stabilisatrices théorique et mesurée des nombres d'ondes en fonction du courant dans les quadrupôles tournés.

I.5.3 Conclusions

L'effet bénéfique du couplage sur l'amortissement de Landau prédit par la theorie est confirmé. L'instabilité horizontale cohérente de paroi résistive du PS peut être amortie par effet de Landau, en présence d'une dispersion de nombres d'ondes suffisamment grande dans le plan vertical, en jouant sur le courant dans les quadrupôles tournés et/où la séparation des nombres d'ondes. Une hypothèse majeure (à savoir une dispersion de nombres d'ondes verticale Lorentzienne) a cependant été faite ici pour corréler la théorie avec l'observation. L'écart entre les prévisions théoriques et l'expérience (d'un facteur 3), pourrait être expliqué en partie par l'effet stabilisateur des non- linéarités de charge d'espace qui n'ont pas été prises en compte dans la théorie. D'autres études devraient être faites pour analyser la "stabilité" du plan vertical. Il est probable que des modèles d'impédances de couplage et de dispersions des nombres d'ondes plus détaillés soient nécessaires pour pouvoir faire des comparaisons quantitatives plus précises.

Annexe: Liste des paramètres du faisceau et du PS pendant l'expérience

$a_w = 7$ cm	Demi grand axe de la chambre à vide elliptique
$b_w = 3.5$ cm	Demi petit axe de la chambre à vide elliptique
$c = 3\times10^8$ ms^{-1}	Vitesse de la lumière
$e = 1.6\times10^{-19}$ C	Charge élémentaire
$E_0 = 0.938$ Gev	Energie au repos d'un proton
$E_c = 1$ Gev	Energie cinétique d'un proton
$f_0 = 417$ khz	Fréquence de révolution moyenne des particules
$f_r = 1.4$ Ghz	Fréquence de coupure de la chambre à vide (fréquence de résonance décrivant les impédances de couplage larges bandes)
$f_s = 1.7$ khz	Fréquence synchrotronique des particules

$I_{beam} \approx 1.5\times10^{13}$ protons	Intensité du faisceau
$l_{mag} = 220$ mm	Longueur magnétique octupolaire équivalente
$M = 20$	Nombre de paquets du faisceau
$N_b \approx 7.5\times10^{11}$ protons	Intensité d'un paquet
$N_{\mathrm{oct}} = 8$	Nombre d'octupoles
$Q \approx 1$	Facteur de qualité des résonateurs décrivant les impédances de couplage larges bandes
$R = 100$ m	Rayon moyen de la machine
$R_x \approx 1$ MΩ/m	Résistance de shunt décrivant l'impédance de couplage large bande horizontale
$R_y \approx 3$ MΩ/m	Résistance de shunt décrivant l'impédance de couplage large bande verticale
$\alpha_p = \gamma_{tr}^{-2} = 0.027$	Facteur de compaction
$\beta = 0.875$	Facteur relativiste de vitesse
$\beta_{\mathrm{octx}} \approx 12.4$ m	Fonction bétatronique horizontale aux positions des octupoles
$\beta_{\mathrm{octy}} \approx 22.6$ m	Fonction bétatronique verticale aux positions des octupoles
$\gamma = E_t / E_0 = 2.066$	Facteur relativiste de masse
$\varepsilon_x^{\mathrm{rms}} = 6.5\times10^{-6}$ m	Emittance horizontale r.m.s (aire de l'espace de phase horizontal divisée par π)
$\varepsilon_y^{\mathrm{rms}} = 3.1\times10^{-6}$ m	Emittance verticale r.m.s (aire de l'espace de phase vertical divisée par π)
$\eta = \alpha_p - \gamma^{-2} = -0.207$	Facteur de dispersion des fréquences de révolution
$\xi_x \approx -1$	Chromaticité horizontale, définie par $\xi_x = \left(d\,Q_{0x,i} / Q_{0x,i}\right) / \left(dp_i / p_i\right)$
$\xi_y \approx -1.5$	Chromaticité verticale, définie par $\xi_y = \left(d\,Q_{0y,i} / Q_{0y,i}\right) / \left(dp_i / p_i\right)$
$\rho_w = 9\times10^{-7}$ Ωm	Résistivité de la chambre à vide
$\tau_b = 70$ ns	Longueur totale d'un paquet
$B_y\rho_x = 5.66$ Tm	Rigidité du faisceau
$\int_0^{l_{mag}} K_{oct}\,dl\,[\mathrm{m}^{-3}] = \frac{4.33}{6\,B_y\rho_x} \times I_{oct}\,[\mathrm{A}]$	Force octupolaire intégrée

I.6 Conclusion

La conservation de la brillance (i.e. le rapport intensité sur émittance) des faisceaux est un problème majeur pour la chaine d'injection du LHC comme pour la conception et l'opération des collisionneurs de hadrons de haute énergie. Plusieurs sources de détérioration de la brillance existent, e.g. l'effet de charges d'espace, l'adaptation et les erreurs d'injection ou d'extraction. De plus, des instabilités de toutes sortes peuvent aussi faire grossir et même détruire le faisceau. Dans le Synchrotron à

Protons (PS) du CERN, par exemple, le grossissement total de l'émittance doit être inférieur à 20%, ce qui impose un traitement rigoureux de toutes les sources possibles de grossissement le long de la chaine d'injection.

L'étude précédente sur les instabilités collectives a révélé que le couplage linéaire entre les plans horizontal et vertical et la distance des nombres d'ondes aux résonances de couplage $Q_h - Q_v =$ entier peut avoir un effet stabilisateur sur les instabilités cohérentes transversales par amortissement de Landau. En effet, si, après avoir introduit des dispersions de nombres d'ondes à l'aide d'octupoles, une instabilité cohérente persiste dans un des deux plans, le couplage linéaire et la séparation des nombres d'ondes peuvent alors être utilisés pour transférer de l'amortissement de Landau du plan stable au plan instable. Ce résultat pourrait donc être utilisé pour minimiser les non-linéarités externes requises pour l'amortissement de Landau.

Dans le cas de distributions Lorentziennes, si la somme des dispersions de fréquences bétatroniques $\delta\omega_{x,y}$ (demi-largeurs à mi-hauteur des fonctions de répartition) est plus grande que la somme des taux de croissance $V_{\mathrm{eq}x,y}$ (donnés par l'Eq. (I.8) pour un faisceau dégroupé ou l'Eq. (I.37) pour un faisceau groupé), alors il est possible de stabiliser le faisceau dans les deux plans en augmentant le gradient des quadrupôles tournés et/ou en rapprochant le point de fonctionnement près d'une résonance de couplage. La condition nécessaire de stabilité $\delta\omega_x + \delta\omega_y \geq V_{\mathrm{eq}x} + V_{\mathrm{eq}y}$ devient suffisante pour un couplage total.

Cependant, en pratique le couplage doit être optimisé car les distributions réelles de fréquences ont des queues finies. La stabilité est alors obtenue pour une certaine bande de valeurs du couplage. Pour des spectres elliptiques, un critère de stabilité approximatif général, obtenu pour le couplage optimum, s'écrit $\mathrm{Re}\left(\sqrt{\Delta\omega_x^2 - 4U_{\mathrm{eq}x}^2} + \sqrt{\Delta\omega_y^2 - 4U_{\mathrm{eq}y}^2}\right) \geq 2\left(V_{\mathrm{eq}x} + V_{\mathrm{eq}y}\right)$, où $\mathrm{Re}(\ )$ représente la partie réelle, indiquant que la racine carrée doit être omise si l'argument sous la racine est négatif. Ici, $\Delta\omega_{x,y}$ sont les demi-largeurs aux pieds des distributions et $U_{\mathrm{eq}x,y}$ (déplacements réels des fréquences bétatroniques), $V_{\mathrm{eq}x,y}$ sont donnés par l'Eq. (I.8) pour un faisceau dégroupé ou l'Eq. (I.37) pour un faisceau groupé.

Le taux de croissance d'une instabilité (qui dépend de la chromaticité pour un faisceau groupé) et l'amortissement par "feedbacks" sont "toujours" transférés entre les plans transversaux en présence de couplage. Plusieurs paramètres pourraient donc être utilisés pour amortir des instabilités cohérentes transversales et fixer le meilleur point de fonctionnement.

La théorie de l'amortissement de Landau couplé donne une explication possible du phénomène observé dans la Réf. 16, où une instabilité de paquet unique de type "head-tail" a été amortie en ajustant $Q_h \approx Q_v$. De plus, des expériences ont été effectuées au PS sur un long palier à 1 GeV, en variant la distance à la résonance $Q_h - Q_v = 0$ et l'excitation des lentilles octupolaires et quadrupôlaires tournées, et en observant le seuil d'une instabilité de paquets couplés. Les résultats confirment l'allure générale prédite par la théorie, en considérant une distribution Lorentzienne dans le plan vertical.

Les résultats de l'amortissement de Landau couplé peuvent être utilisés pour déterminer des valeurs optimales de séparation des nombres d'ondes et de force du couplage linéaire pour le faisceau de type LHC du PS, pour qui le couplage n'est pas dangereux puisque les émittances horizontale et verticale sont égales. Les instabilités "head-tail" de basse énergie peuvent être en effet amorties en utilisant cette méthode, et

le résultat est que le courant dans les octupoles peut être réduit par un facteur 2 ou 3. D'autres études sont prévues pour mieux corréler la théorie avec l'observation.

REMERCIEMENTS

Je remercie le Ministère français de l'Education Nationale, de la Recherche et de la Technologie, de m'avoir accordé une bourse doctorale, et j'exprime ma profonde gratitude au CERN pour m'avoir accueilli au sein de son organisation et avoir co-financé ce travail.

Je tiens à exprimer ma plus vive reconnaissance à Monsieur J.P. Riunaud qui m'a accueilli dans son groupe et m'a donné les moyens de mener à bien cette étude.

Je remercie Monsieur J.M. Loiseaux pour avoir accepté d'être directeur de thèse auprès de l'université Joseph Fourier.

J'adresse mes plus vifs remerciements à Monsieur M. Martini pour avoir accepté la lourde charge de directeur de thèse au CERN. Je le remercie très chaleureusement pour sa grande disponibilité et pour tout ce qu'il m'a appris dans le domaine de la physique des accélérateurs. Son aide et ses conseils pour la rédaction et la présentation de rapports m'ont été, de plus, fort utiles. Qu'il trouve dans ces lignes toute ma reconnaissance.

Pour réaliser la partie théorique de cette thèse, j'ai eu la chance et l'honneur d'être dirigé par Monsieur D. Möhl. Ses qualités humaines, sa patience infinie et sa très grande compétence dans le domaine des instabilités de faisceaux ont rendu ces deux années et demie extrêmement enrichissantes. Je lui adresse toute ma reconnaissance pour m'avoir proposé un sujet aussi fascinant, ainsi que pour les nombreuses discussions fructueuses que nous avons eues.

Pour réaliser mes expériences, j'ai eu là aussi la chance et l'honneur d'être dirigé par Monsieur R. Cappi. Je le remercie vraiment beaucoup pour tout ce qu'il m'a appris, avec patience, sur les instabilités et les instruments de diagnostic du PS. C'est grâce à lui que j'ai pu effectuer mes premiers pas d'expérimentateur et réaliser mes mesures.

Je veux aussi exprimer ma gratitude à Monsieur D. Manglunki ainsi qu'aux personnes de l'opération, en particulier Monsieur G. Métral, pour leur disponibilité et leur aide dans la salle de contrôle.

Je remercie Madame M. Rey-Campagnolle, organisatrice du JUAS (Joint Universities Accelerator School), où j'ai été étudiant, d'avoir accepté de présider ce jury.

Messieurs J. Le Duff et F. Ruggiero m'ont fait l'honneur de juger cette thèse. Je les remercie très sincèrement pour avoir accepté cette charge de rapporteurs auprès de l'université, ainsi que pour les commentaires constructifs qu'ils ont apportés.

Je tiens à remercier aussi Madame M. Blanc, secrétaire du DEA, pour son aide et sa sympathie.

Je voudrais enfin ne pas oublier dans mes remerciements ma famille et mes amis, qui ont tous joué un rôle de près ou de loin dans cet aboutissement.

Enfin, je dédie cette thèse à ma mère pour m'avoir permis d'étudier, à ma femme Emmanuelle, pour sa patience, son soutien constant et ses nombreux commentaires toujours très à propos, à ma fille Johanna, dont je suis déjà si fier, et à mes futurs enfants.

REFERENCES

[1] P.J. Bryant, *A Brief History and Review of Accelerators*, CERN Accelerator School, CERN 94-01, p. 1, 1994.

[2] Waldemar Scharf, *Particle Accelerators and their Uses*, Harwood Academic Publishers, 1050 p, 1996.

[3] O. Barbalat, *Applications of Particle Accelerators*, CERN Accelerator School, CERN 94-01, p. 841, 1994.

[4] http://www.cern.ch/Public/.

[5] F. Ruggiero, *Theoretical Aspects of Some Collective Instabilities in High-Energy Particle Storage Rings*, CERN 86-06, 1986.

[6] Y. Baconnier, *How to Reach High Luminosity?*, Joint US-CERN School on Particle Accelerators, Benalmádena, Spain, 1992.

[7] R. Cappi, *CERN PS High Brightness Operation for LHC*, CERN/PS 97-09 (CA), 1997.

[8] A.W. Chao, *Physics of Collective Beam Instabilities in High Energy Accelerators*, New York: Wiley, 371 p, 1993.

[9] R. Cappi *et al.*, *Production and Measurements in the PS Complex of a High-Brilliance Proton Beam in View of the LHC*, CERN/PS 92-52 (PA), 1992.

[10] R. Cappi, *PS for LHC-Emittance Conservation at Low Energy*, CERN/PS 93-09 (PA), 1993.

[11] R. Cappi, *Emittance Issues in the CERN-PS*, CERN/PS 95-05 (PA), 1995.

[12] R. Cappi, *The PS in the LHC Injector Chain*, CERN/PS 97-16 (CA), 1997.

[13] J. Gareyte, J.P. Koutchouk and F. Ruggiero, *Landau Damping, Dynamic Aperture and Octupoles in LHC*, LHC Project Report 91, 1997.

[14] G. Garron *et al.*, *Observation of Transverse Quadrupole Mode Instability in Intense Cooled Antiproton Beams in the AA*, CERN/PS/89-18 (AR) and Proc. 1989 Part. Acc. Conf., Chicago, March 20-23.

[15] Rui Alves-Pires and Dieter Möhl, *Landau Damping of Coupled Quadrupole Modes*, CERN/PS/AR/Note 90-09, 1990.

[16] R. Cappi, *Observations of High-Order Head-Tail Instabilities at the CERN-PS*, CERN/PS 95-02 (PA), 1995.

[17] J.L. Laclare, *Bunched Beam Coherent Instabilities*, CERN Accelerator School, Oxford, CERN 87-03, p. 264, 1987.

[18] F. Sacherer, *Transverse Bunched-Beam Instability-Theory*, Proc. 9th Int. Conf. on High Energy Accelerators, Stanford 1974 (CONF 740522, US Atomic Energy Commission, Washington D.C., 1974), p. 347.

[19] B. Zotter, *Single Beam Collective Phenomena-Transverse (Coasting Beams),* Proc. First Course Int. School on Accelerators, Erice, 1976: Theoretical Aspects of the Behaviour of Beams in Accelerators and Storage Rings, CERN 77-13, p. 176, 1977.

[20] E. Keil, *Linear Theory of Perfect Machines*, CERN 77-13, p. 11, 1977.

[21] M. Martini, *An Introduction to Transverse Beam Dynamics in Accelerators*, CERN/PS 96-11 (PA).

[22] P. Bryant and K. Johnsen, *The Principles of Circular Accelerators and Storage Rings*, Cambridge University Press, 1993.

[23] D. Möhl, *On Landau Damping of Dipole Modes by Non-Linear Space Charge and Octupoles*, CERN/PS 95-08 (DI), 1995.

[24] D. Möhl and H. Schönauer, *Landau Damping by Non-Linear Space-Charge Forces and Octupoles*, Proc. IX Int. Conf. High Energy Acc., Stanford, 1974 (AEC, Washington, D.C., 1974), [CONF 740522] p. 380.
[25] J. Gareyte, *Beam Observations and the Nature of Instabilities*, CERN SPS/87-18 (AMS), 1987.
[26] L.J. Laslett, V.K. Neil, A.M. Sessler, *Transverse Resistive Instabilities of Intense Coasting Beams in Particle Accelerators*, R.S.I, Vol. 36, No. 4, 436-448, 1965.
[27] D. Möhl and A.M. Sessler, *The Use of RF Knockout for Determination of the Characteristics of the Transverse Coherent Instability of an Intense Beam*, Proc. 8th Int. Conf. on High Energy Accelerators, CERN 1971, p. 334.
[28] L.D. Landau, *On the Vibrations of the Electronic Plasma*, J. Phys. USSR 10, 25 (1946).
[29] H.G. Hereward, *The Elementary Theory of Landau Damping*, CERN/PS 65-20, 1965.
[30] D. Sagan, *On the Physics of Landau Damping*, CLNS-93-1185, 1993.
[31] R.D. Kohaupt, *What is Landau Damping? Plausibilities, Fundamental Thoughts, Theory*, DESY M-86-02, 1986.
[32] H.G. Hereward, *Landau Damping*, CERN 77-13, p. 219, 1977.
[33] A. Hofmann, *Landau Damping*, CERN 89-01, p. 40, 1989.
[34] K. Hübner, A.G. Ruggiero and V.G. Vaccaro, *Stability of the Coherent Transverse Motion of a Coasting Beam for Realistic Distribution Functions and any Given Coupling with its Environment*, CERN-ISR-TH-RF/69-23.
[35] K. Hübner, P. Strolin, V.G. Vaccaro, B. Zotter, *Concerning the Stability of the ISR Beam Against Coherent Dipole Oscillations*, CERN/ISR-RF-TH/70-2.
[36] K. Hübner and V.G. Vaccaro, *Dispersion Relations and Stability of Coasting Particle Beams*, CERN-ISR-TH/70-44.
[37] H.G. Hereward, *Landau Damping by Non-Linearity*, CERN/MPS/DL 69-11, 1969.
[38] E. Métral, *Coupled Landau Damping*, CERN/PS 97-33 (CA), 1997.
[39] E. Métral, *Coupled Landau Damping with Elliptical Spectra*, CERN/PS 98-004 (CA), 1998.
[40] E.D. Courant and A.M. Sessler, *Transverse Coherent Resistive Instabilities of Azimuthally Bunched Beams in Particle Accelerators*, R.S.I, Vol. 37, No. 11, 1579-1588, 1966.
[41] H. Bruck, *Accélérateurs Circulaires de Particules*, Presses universitaires de France, Paris, 358 p, 1966.
[42] C. Pellegrini, Nuovo Cimento 64A, 477, 1969.
[43] M. Sands, *The Head-Tail Effect: An Instability Mechanism in Storage Rings*, SLAC-TN-69-8, 1969.
[44] M. Sands, *Head-Tail Effect II: From a Resistive-Wall Wake*, SLAC-TN-69-10, 1969.
[45] F. Sacherer, *Single Beam Collective Phenomena-Transverse (Bunched Beams),* Proc. First Course Int. School on Accelerators, Erice, 1976: Theoretical Aspects of the Behaviour of Beams in Accelerators and Storage Rings, CERN 77-13, p. 210, 1977.
[46] E. Métral, *Coupled Landau Damping of Head-Tail Modes Revisited*, CERN/PS/CA/Note 98-05, 1998.
[47] R. Talman, *Theory of Head-Tail Chromaticity Sharing*, CBN-97-16, 1997.

[48] S. Peggs and G.F. Dell, *Skew Chromaticity*, Part. Accelerators, Vol. 50, p. 189, 1995.
[49] J. Scott Berg and F. Ruggiero, *Landau Damping with Two-Dimensional Betatron Tune Spread*, CERN/SL-AP-96-71 (AP), 1996.
[50] J. L. Laclare, LNS/GT-043, Saclay, 1980.
[51] J.L. Laclare, *Introduction to Coherent Instabilities-Coasting Beam Case*, CERN Accelerator School, Paris, CERN 85-19, p. 377, 1985.
[52] E. Métral, *On Coupled Landau Damping of Transverse Bunched Beam Instabilities*, CERN/PS/CA/Note 98-15, 1998.
[53] A. Hofmann, *Kinetic Theory*, CERN 89-01, p. 25, 1989.
[54] F. Sacherer, *Methods for Computing Bunched-Beam Instabilities*, CERN/SI-BR/72-5, 1972.
[55] J. Scott Berg, *Coherent Modes for Multiple Non-Rigid Bunches in a Storage Ring*, SLAC-R-478, 1996.
[56] G. Guignard, *The General Theory of All Sum and Difference Resonances in a Three-Dimensional Magnetic Field in a Synchrotron*, CERN 76-06, March 1976.
[57] G. Guignard, *A General Treatment of Resonances in Accelerators*, CERN 78-11, November 1978.
[58] R. Cappi, *Beam Dynamics Measurements with a "Local Intelligent Device"*, CERN/PS/87-48 (PSR), May 1987.
[59] E. Métral, *Measurement of the PS Linear Coupling using FFT Analysis*, CERN PS/CA/Note 97-24, 1997.
[60] E. Métral, *Measurements of Coupled Landau Damping of the PS Coherent Resistive Instability*, CERN/PS/CA/Note 98-16, 1998.
[61] D. Möhl, *Equipment Responsible for Transverse Beam Instability in the PS*, MPS/DL/Note 74-6, 1974.
[62] R. Cappi, M. Martini, T. Risselada, J.P. Riunaud, D. Trione, *Recent Studies on Transverse Beam Behaviour at the CERN PS*, CERN/PS 89-39 (PA), 1989.
[63] R.L. Gluckstern, J. van Zeijts and B. Zotter, *Coupling Impedance of Beam Pipes of General Cross Section*, Phys. Rev. E, 47, 1993.
[64] R. Cappi, G. Métral, *Observation of e-p Instabilities at CERN-PS?*, http://www.cern.ch/PSdoc/ppc/md/md980716/epinstab.html, 1998.
[65] B.W. Montague, *RF Acceleration*, CERN 77-13, p. 63, 1977.